

Synthesis and Biological Evaluation of 2-
Aminothiophene and Benzothiazole Derivatives as
Isoprenoid Biosynthesis Inhibitors

By

Adrienne M. Langille

A thesis submitted to McGill University in partial fulfillment of the
requirements of the degree of Master of Science

Department of Chemistry

McGill University

Montreal, Quebec

Fall 2012

© Adrienne Langille 2012

Table of Contents

| | |
|--|------|
| Abstract | iv |
| Résumé | iv |
| Acknowledgements | v |
| Contribution to Knowledge | vi |
| List of Figures | viii |
| List of Schemes | viii |
| List of Tables | ix |
| List of Symbols and Abbreviations | xi |
| 1. Modular Assembly of Thieno[2,3- <i>d</i>]pyrimid-4-amines via Condensation of a Trimethylsilyl Ylidene..... | 1 |
| 1.1 Introduction | 1 |
| 1.1.1 Designing Molecular ‘Tools’ with Drug-like Properties | 1 |
| 1.1.2 Biological Activities of Thienopyrimidines | 3 |
| 1.1.3 Synthesis of Thieno[2,3- <i>d</i>]pyrimid-4-amines | 8 |
| 1.2 Results and Discussion | 14 |
| 1.3 Conclusions | 32 |
| 1.4 Experimental | 32 |
| 1.4.1 General Information | 32 |
| 1.4.2 Synthesis of Key Fragments | 33 |
| 1.5 Acknowledgements | 58 |

| | |
|---|-----|
| 1.6 References | 59 |
| 2. Nitrogen-Containing Bisphosphonates and the Mevalonate Pathway ... | 77 |
| 2.1 Introduction | 77 |
| 2.1.1 History of Bisphosphonates | 77 |
| 2.1.2 Bisphosphonate Mechanism of Action: ATP Analogs and the Mevalonate Pathway | 79 |
| 2.1.3 <i>N</i> -BPs and Isoprenylation in Non-Bone Related Therapeutics | 84 |
| 2.1.4 Synthesis and Structure Activity Relationships (SAR) of <i>N</i> -BPs | 88 |
| 2.2 Results and Discussion | 100 |
| 2.2.1 Synthetic Studies | 101 |
| 2.2.2 Biological Activity | 107 |
| 2.3 Conclusions | 112 |
| 2.4 Experimental | 112 |
| 2.4.1 General Information | 112 |
| 2.4.2 Synthesis of Key Compounds | 113 |
| 2.4.3 Biological Assays | 129 |
| 2.5 Acknowledgements | 131 |
| 2.6 References | 133 |
| Appendix – Spectral Data | 148 |

Abstract

The condensation of stable 2-(1-(trimethylsilyl)ethylidene)malononitrile with elemental sulfur was explored in the parallel-synthesis of a small library of structurally diverse 2-aminothiophenes and thieno[2,3-*d*]pyrimidines. Bromination and *ipso*-iododesilylation of these heterocyclic scaffolds provided synthetic methods to efficiently generate key intermediates, allowing for great versatility. Bisphosphonic acid derivatives of thieno[2,3-*d*]pyrimidine and benzothiazole scaffolds, with favourable physicochemical properties, were evaluated for their ability to inhibit isoprenoid biosynthesis and potentially modulate the function of small G-proteins implicated in a range of human diseases. Preliminary biological activities and selectivity will be presented.

Résumé

La condensation de 2-(1-(triméthylsilyl)éthylidène)malononitrile avec du soufre élémentaire a été explorée dans le parallèle synthèse d'une petite group de structures diverses de 2-aminothiophenes et thieno[2,3-*d*]pyrimidines. Bromation et *ipso*-iododesilylation de ces échafaudages hétérocyclique fourni des méthodes de synthèse pour générer efficacement des intermédiaires clés, ce qui permet une grande polyvalence. Dérivés d'acide bisphosphonique de thieno[2,3-*d*]pyrimidines et échafaudages benzothiazole, avec de bonnes propriétés physico-chimiques, ont été évalués pour leur capacité à inhiber la biosynthèse des isoprénoïdes et potentiellement moduler la fonction des petites protéines G impliquées dans un assortiment de maladies humaines. Les activités préliminaires biologiques et la sélectivité sera présenté.

Acknowledgements

First and foremost, I would like to thank my supervisor and mentor, Prof. Youla S. Tsantrizos. I am so grateful for all the support and guidance that I received over the course of my degree. In addition to gaining valuable scientific knowledge under her leadership, I learned how important it is to follow your passions in life and career. I would also like to thank past group members (John and Olivier) for showing me the synthetic ropes and countless fruitful discussions. To my comrades in OM300, thank you for all the help, suggestions, and advice in all things chemistry. I am particularly indebted to my lab counselors and great friends, Joris, Daniel, and Rodrigo. I have many great memories of my time in Montreal, filled with many great people, especially the Dudes crew (Katie, Graham, and Chris) and roomies (Katerina and Matt).

My family has always supported and encouraged me through all of my goals, dreams, and plans. I am so grateful for all that they have done to help me fulfill them.

Contribution to Knowledge

A novel synthetic methodology was developed for the preparation of 2-aminothiophenes and thienopyrimidines. This methodology addresses some of the limitations of previously reported procedures for the preparation of such compounds. Our methodology was then employed in the preparation of a small library of highly substituted and structurally diverse 2-aminothiophene and thienopyrimidine derivatives, which were subsequently converted to inhibitors of the human FPPS. Some of the work described in this thesis was carried out in collaboration with Dr. John Mancuso, and Mr. Chun Yuen Leung, and under the supervision of Prof. Youla S. Tsantrizos. The research discussed in this thesis has been presented in a recent publication as well as two conference proceedings.

Publications:

a) Leung, C.-Y.; **Langille, A. M.**; Mancuso, J.; Tsantrizos, Y. S. Discovery of thienopyrimidine-based inhibitors of the human farnesyl pyrophosphate synthase – Parallel synthesis of analogs via trimethylsilyl ylidene intermediate. *Bioorg. Med. Chem.* **2013**, *21*, 2229-2240.

Conference Proceedings:

a) Oral Presentation: Gewald-type synthesis and structure-activity relationship studies of novel 2-aminothiophene derivatives as isoprenoid biosynthesis inhibitors. **Langille, A. M.**; Lin, Y.-S.; Mancuso, J.; *Tsantrizos, Y. S.

Canadian Society for Chemistry, 94th Canadian Chemistry Conference and Exhibition, Montreal, QC, Canada, June 5-9th, 2011

b) Poster: Novel Two-Step Synthesis for 2-Aminopyridine and 2-Aminothiophene Synthons. Mancuso, J.; Lin, Y.-S.; **Langille, A. M.**; *Tsantrizos, Y. S.

Canadian Society for Chemistry, 93rd Canadian Chemistry Conference and Exhibition, Toronto, ON, Canada, May 29th- June 2nd, 2010

List of Figures

| | |
|--|----|
| Figure 1.1 Drug development timeline | 2 |
| Figure 1.2 Structures of thienopyrimidine kinase inhibitors | 4 |
| Figure 1.3 Development of thienopyrimidine γ -secretase modulators from benzimidazole compounds | 6 |
| Figure 1.4 Structures of Istradefylline and thienopyrimidine $A_{2A}R$ antagonists ... | 7 |
| Figure 2.1 Structures of bisphosphonates and inorganic pyrophosphate | 75 |
| Figure 2.2 Structures of ATP and AppCR ₁ R ₂ p metabolites | 78 |
| Figure 2.3 The mevalonate pathway | 79 |
| Figure 2.4 Structures of ApppI and ApppD metabolites | 81 |
| Figure 2.5 Direct and indirect antitumor effects of <i>N</i> -BPs | 82 |
| Figure 2.6 Binding affinities of BPs with hydroxyapatite (HAP) and carbonated hydroxyapatite (CAP) | 86 |
| Figure 2.7 hFPPS (PDB 2F8Z) crystallized with IPP and ZOL in active site | 94 |

List of Schemes

| | |
|---|----|
| Scheme 1.1 Gewald reaction mechanism with elemental sulfur | 8 |
| Scheme 1.2 Gewald synthesis of 2-aminothiophenes | 9 |
| Scheme 1.3 Gewald-type synthesis with α -mercaptoketones and aldehydes (5).. | 10 |
| Scheme 1.4 Classical synthesis of thieno[2,3- <i>d</i>]pyrimidines (9) from 2-aminothiophenes (3) | 11 |
| Scheme 1.5 Dimroth rearrangement mechanism | 12 |
| Scheme 1.6 Bromination reactions with thienopyrimidine intermediates | 13 |
| Scheme 1.7 Bromination via base-catalyzed halogen dance (BCHD) | 14 |
| Scheme 1.8 Mechanism of classical base-catalyzed halogen dance | 14 |
| Scheme 1.9 Synthesis of highly substituted 2-aminothiophene intermediates for thieno[2,3- <i>d</i>]pyrimidin-4-amine preparation | 15 |
| Scheme 1.10 Di-substituted thienopyrimidine library synthesis | 18 |
| Scheme 1.11 Proposed mechanism of cyclization | 21 |

| | |
|---|-----|
| Scheme 1.12 Attempted cyclization of 14b with Dean Stark apparatus | 23 |
| Scheme 1.13 Decomposition hypothesis to explain cyclization results | 28 |
| Scheme 1.14 Thermal or photochemical degradation of AIBN | 31 |
| Scheme 1.15 Thermal or photochemical degradation of DCP | 31 |
| Scheme 2.1 Metabolism of non-nitrogen-containing BPs | 77 |
| Scheme 2.2 Isoprenoid biosynthesis | 80 |
| Scheme 2.3 Key compounds from the library | 93 |
| Scheme 2.4 General mechanism of α -amino <i>N</i> -BP synthesis | 99 |
| Scheme 2.5 Mono-substituted thieno[2,3- <i>d</i>]pyrimidin-4-ylamine <i>N</i> -BPs | 100 |
| Scheme 2.6 Attempted bromination of <i>N</i> -BP 36a | 101 |
| Scheme 2.7 Synthesis of di-substituted thieno[2,3- <i>d</i>]pyrimidin-4-ylamine <i>N</i> -BPs | 102 |
| Scheme 2.8 Synthesis of 2-aminobenzothiazole <i>N</i> -BPs | 103 |

List of Tables

| | |
|--|----|
| Table 1.1 Lithium halogen exchange conditions | 19 |
| Table 1.2 Cyclization reaction with ammonia | 21 |
| Table 1.3 Cyclization reaction under light and dark conditions | 23 |
| Table 1.4 Cyclization reaction with radical quenchers | 24 |
| Table 1.5 Various reaction conditions for the synthesis of 15b from 14c | 26 |
| Table 1.6 Attempted synthesis of 19g via bromination of 15a | 29 |
| Table 2.1 Farnesyltransferase and geranylgeranyltransferase I inhibitors in clinical trials | 83 |
| Table 2.2 Effect of modifying nitrogen orientation in RIS on FPPS inhibition .. | 87 |
| Table 2.3 Relative bone affinity and hFPPS inhibition of RIS analogs 20a-d | 88 |
| Table 2.4 Relative bone affinity, hFPPS and GGPII inhibition of phosphono- carboxylate RIS analogues (21a-e) | 89 |
| Table 2.5 Comparison of <i>N</i> -BP inhibition activities (IC ₅₀) against hFPPS and hGGPII | 90 |
| Table 2.6 Comparison of key lipophilic <i>N</i> -BP properties and activities to ZOL .. | 92 |

| | |
|---|-----|
| Table 2.7 Biological activities of key 2-aminopyridine <i>N</i> -BPs | 95 |
| Table 2.8 Biological activity of mono- and di-substituted isoprenoid BPs | 96 |
| Table 2.9 Trial Suzuki cross-coupling reaction conditions with 2-amino-5-bromobenzothiazole <i>N</i> -BPs | 104 |
| Table 2.10 Inhibition data for hFPPS | 105 |
| Table 2.11 Inhibition data for hGGPPS | 107 |

List of Symbols and Abbreviations

°C = Degrees Celsius

ACN = acetonitrile

AcOH = acetic acid

Ar = Aryl

dba = dibenzylidene acetone

Bn = benzyl

BP = bisphosphonate

br = broad

CAP = carbonated hydroxyapatite

DCM = dichloromethane

DMAPP = dimethylallyl pyrophosphate

DME = 1,2-dimethoxyethane

DMF = *N,N*-dimethylformamide

DMSO = *N,N*-dimethylsulfoxide

Dppf = (diphenylphosphino)ferrocene

DPPS = decaprenyl diphosphate synthase

eq. = molar equivalence

Et = ethyl

Ether = diethylether

EtOAc = ethyl acetate

EtOH = ethanol

FPP = farnesyl pyrophosphate

FPPS = farnesyl pyrophosphate synthase
GGPP = geranylgeranyl pyrophosphate
GGPPS = geranylgeranyl pyrophosphate synthase
GPP = geranyl pyrophosphate
GTPases = small guanine triphosphate binding proteins
h = hours
HAP = hydroxyapatite
hex = hexanes
HPLC = high-performance liquid chromatography
IC₅₀ = half maximal inhibitory concentration
IPP = isopentenyl pyrophosphate
K_i = inhibition constant
LCMS = liquid chromatography-mass spectrometry
LDA = lithium diisopropylamide
M = molar
Me = methyl
MeOH = methanol
min = minutes
MHz = megahertz
MS = mass spectrometry
m/z = mass-to-charge ratio
NBS = *N*-bromosuccinimide
*n*BuLi = butyl lithium
NCS = *N*-chlorosuccinimide

NMR = nuclear magnetic resonance

Ph = phenyl

PhH = benzene

PhMe = toluene

PPh₃ = triphenylphosphine

Py = pyridine

R = proton or variable organic group

R.T. = room temperature

SAR = structure activity relationship

SM = starting material

SPR = structure property relationship

SQS = squalene synthase

TBAF = tetrabutylammonium fluoride

*t*BuLi = *tert*-butyl lithium

TNF α = tumor necrosis factor- α

THF = tetrahydrofuran

THP = tetrahydropyran

TMS = trimethylsilyl

UV = ultraviolet light

uW = microwave irradiation

XantPhos = 4,5-bis(diphenylphosphino)-9,9-dimethylxanthene

XPhos = 2-dicyclohexylphosphino-2',4',6'-triisopropylbiphenyl

1. Modular Assembly of Thieno[2,3-*d*]pyrimid-4- amines via Condensation of a Trimethylsilyl Ylidene

1.1 Introduction

1.1.1 Designing Molecular ‘Tools’ with Drug-like Properties

The development of molecular ‘tools’ to study biological systems is crucial for the identification and investigation of novel biochemical targets and mechanisms of action for the treatment of disease.¹ Advances in the fields of molecular genetics, molecular biology, and bioinformatics as well as techniques such as high-throughput screening (HTS) and animal models of disease have provided much needed insight into disease mechanisms. This information can help accelerate drug design², which is expensive (over a billion dollars)³, lengthy (12 - 15 years to reach the market; Figure 1.1),⁴ and suffers from low success rates.¹ The design of small molecular ‘tools’ incorporating both structure-activity (SAR) and structure-property (SPR) relationships in order to optimize biological activity, pharmacokinetic ADME (adsorption, distribution, metabolism, and excretion) and toxicity properties, structural diversity, and synthetic tractability have been shown to help ease the challenges and costs of drug discovery even at its earliest stages.^{5,6,7}

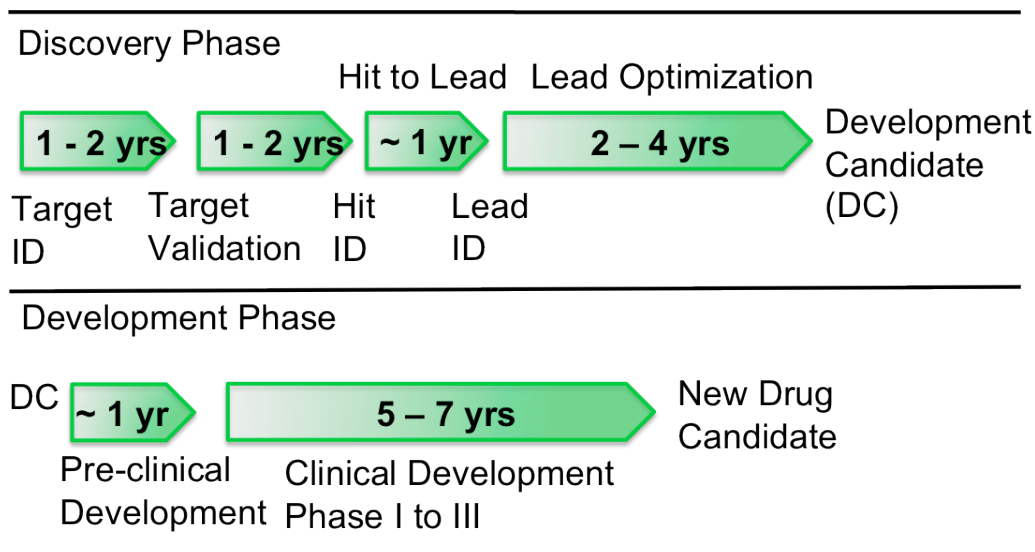


Figure 1.1 Drug development timeline.

Potency, specificity and efficient delivery to the target are required to successfully study and address medical needs. Biopharmaceutical and pharmacokinetic properties such as ADME, stability, transporter effects, and extent of target binding contribute to the overall success of candidate compounds.⁸ The importance of incorporating SPR into small molecules with the potential for disease modification was demonstrated by the seminal work by Lipinski and colleagues⁹ from Pfizer. The results of their assessment of physicochemical properties of orally bioavailable drugs and candidates has become known as Lipinski's "rule of five" (Ro5), which describes the SPR properties important for drug-like pharmacokinetics. In general, the Ro5 states that an orally available drug does not violate more than two of the outlined criteria: (a) molecular weight less than 500 Da; (b) octanol-water partition coefficient (logP) less than 5; (c) no more than 5 hydrogen bond donors; and (d)

less than 10 hydrogen bond acceptors.¹⁰ Although these and other complementary guidelines¹¹ may not describe all drugs available on the market, they are nevertheless helpful to illustrate drug-like chemical space in the age of high-throughput screening.¹²

In light of these observations and guidelines, focus has shifted to designing and tailoring libraries of structurally diverse small molecules while simultaneously incorporating physicochemical properties important for optimal ADMET and bioactivity.¹³ A parallel and divergent synthetic approach allows the generation of diverse libraries of compounds containing heterocycles and side-chains common to drug-like molecules, such as thienopyrimidines and benzothiazoles, with synthetic ease.^{14,15}

1.1.2 Biological Activities of Thienopyrimidines

The thienopyrimidine scaffold, which adheres to the Ro5 guidelines, has played a key role in numerous biologically active compounds such as agrochemicals¹⁶ and human therapeutics (*e.g.* antifungal¹⁷ and antiviral¹⁸ agents). The ability of thienopyrimidines to serve as bioisosteres of adenine nucleobases¹⁹ may explain its usefulness as the core to a variety of kinase inhibitors (Figure 1.2), including phosphoinositide 3-kinase α (PI3K α),²⁰ Aurora kinase,²¹ epidermal growth factor receptor (EGFR/ErbB-2),²² receptor tyrosine kinases (RTKs),²³ Protein kinase R (PKR)-like endoplasmic reticulum kinase (PERK),²⁴ and cyclin-dependent kinase (CDK),²⁵ and LIM-kinase (LIMK).²⁶ Human protein kinases regulate many signal transduction pathways responsible for cellular functions such as growth, division, differentiation, metabolism, motility, and death.²⁷

Aberrant activation of kinases has been implicated in cancer²⁸ as well as metabolic,²⁹ inflammatory,³⁰ autoimmune,³¹ and neurodegenerative diseases.³² Therefore, designing inhibitors targeting human kinases may be useful as therapeutics. Although several kinase inhibitors have advanced into clinical trials, many are nonselective for kinase-related proteins, which could be a therapeutic disadvantage leading to toxicity due to the ubiquitous nature of kinases. Selective inhibitors are also useful as biochemical tools for investigating the mechanisms of complex regulatory biochemical pathways.³³

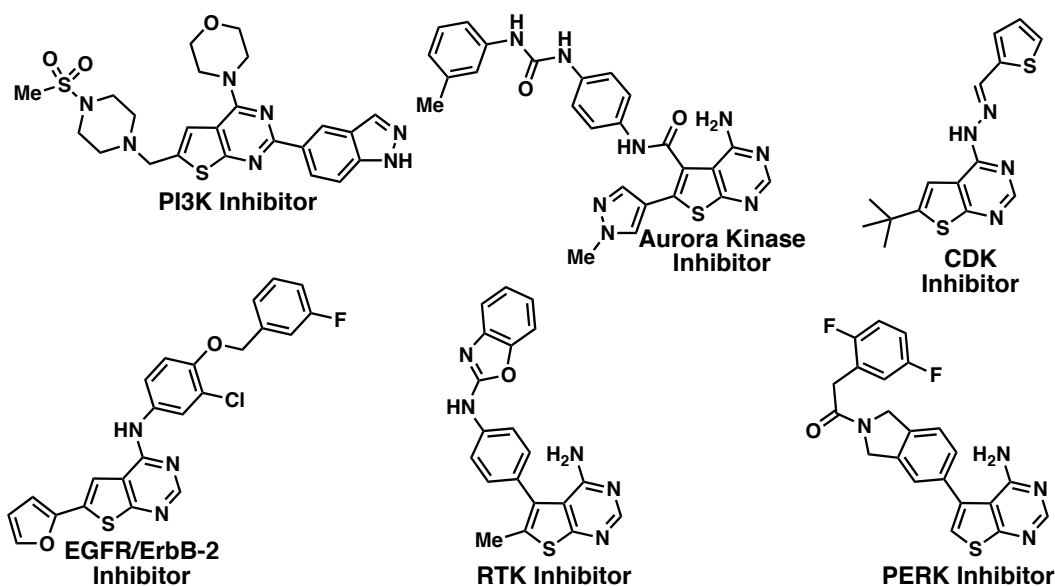


Figure 1.2 Structures of thienopyrimidine kinase inhibitors.

Furthermore, the design of thienopyrimidine-based γ -secretase modulators³⁴ and antagonists of the adenosine A_{2A} receptor³⁵ have demonstrated the potential impact of this scaffold towards modulating neurodegenerative diseases, including Alzheimer's and Parkinson's. The most common form of dementia, Alzheimer's

disease (AD),³⁶ for which there are no effective treatments, is characterized by the presence of neurofibrillary tangles (NFTs) composed of hyperphosphorylated tau protein and extracellular protein plaques.³⁷ Although the relationship between these two hallmarks and AD remains unclear, both pathologies provide targets for treatment.³⁸ Of the most extensively studied are the secretase proteases (α , β , and γ), potentially responsible for generating toxic plaque-causing amyloid- β (A β) protein through misprocessing.³⁹ γ -Secretase inhibitors, such as Semagacestat (Eli-Lilly)⁴⁰ and Begacestat (Wyeth),⁴¹ decreased brain A β concentration in preclinical studies but did not lower A β levels as well as expected in the clinic and have been linked to toxicity. The results of these studies may indicate that the ratio of ‘non-aggregating’ A β 40 to ‘aggregating’ A β 42, not total A β , requires modulation by decreasing the amount of A β 42 while increasing A β 40.⁴² As such, thienopyrimidine γ -secretase modulators were designed to investigate this approach.³⁴

As a testament to the favorable physicochemical properties of the thienopyrimidine core, the thienopyrimidine γ -secretase modulators (Figure 1.3) exhibited improved solubility with a slight loss in potency over the initial benzimidazole compounds. They also demonstrated similar selectivity for A β 42 inhibition over A β 40 production and weaker hERG binding. Blockage of human ether-a-go-go related gene (hERG) channels as a drug side effect can induce cardiac arrhythmia and sudden death. Quantifying hERG binding has become a common component of early drug development as a way to improve the toxicity profile.^{5-8,43}

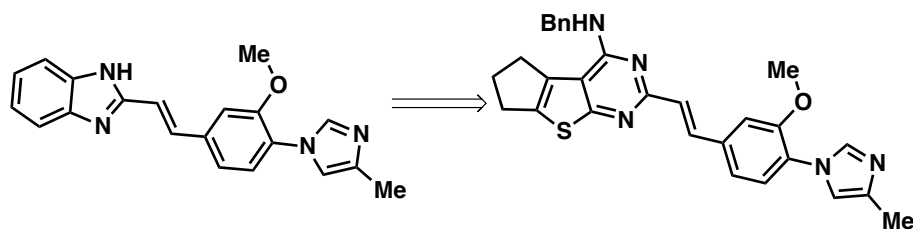


Figure 1.3 Development of thienopyrimidine γ -secretase modulators from benzimidazole compounds.

Parkinson's disease (PD) is a neurodegenerative disease characterized by motor disabilities such as tremors at rest, rigidity, and slowness/absence of voluntary movement. One of the hallmark pathologies of PD, is the loss of dopaminergic neurons resulting in dopamine depletion.⁴⁴ Current PD treatment involves dopaminergic replacement therapy for symptom management. However, long term treatment with Levodopa, an orally available dopamine precursor, commonly results in complications and side effects, including involuntary movements (dyskinesias).⁴⁵ Since PD currently affects 10 million people worldwide and the number of afflicted people is expected to double by 2030,⁴⁶ there is considerable need to investigate alternative targets, such as adenosine A_{2A} receptors ($A_{2A}Rs$), for effective, long-term disease-modifying treatments.⁴⁷

Adenosine A_{2A} receptors ($A_{2A}Rs$), of the G protein coupled receptor (GPCR) family, display a range of activities in the brain, including neurotransmitter modulation, dopamine D_2 receptor affinity regulation, and motor control.⁴⁸ Observation of an abundance of $A_{2A}Rs$ as well as their close proximity to dopamine D_2 receptors in neurons that are overactive in PD lead to interest in the development of $A_{2A}R$ antagonists for PD treatment. Preclinical studies with antagonists, revealed that blocking activity of $A_{2A}Rs$ improved symptoms of

tremors and rigidity, reduced dyskinesias, and protected against neuronal degradation. However, in the clinic, a well-studied $A_{2A}R$ antagonist Istradefylline (Kyowa Hakko Kogyo)⁴⁹ generated conflicting results in phase III trials, where a reduction in motor deficits was not consistently observed in all trials.⁵⁰ Furthermore, although oral Istradefylline (Figure 1.4) was well tolerated in the clinic, xanthine derivatives have found limited biological use to investigate $A_{2A}R$ modulation due to unfavorable physicochemical properties such as poor solubility and stability. Such xanthine-based compounds can photoisomerize when a dilute solution is exposed to light, although not necessarily relevant for solids administered orally, nevertheless demonstrates poor stability.⁵¹ To address these drawbacks of solubility and stability, thienopyrimidine compounds (Figure 1.4) are under development as potent and selective $A_{2A}R$ antagonists.³⁵

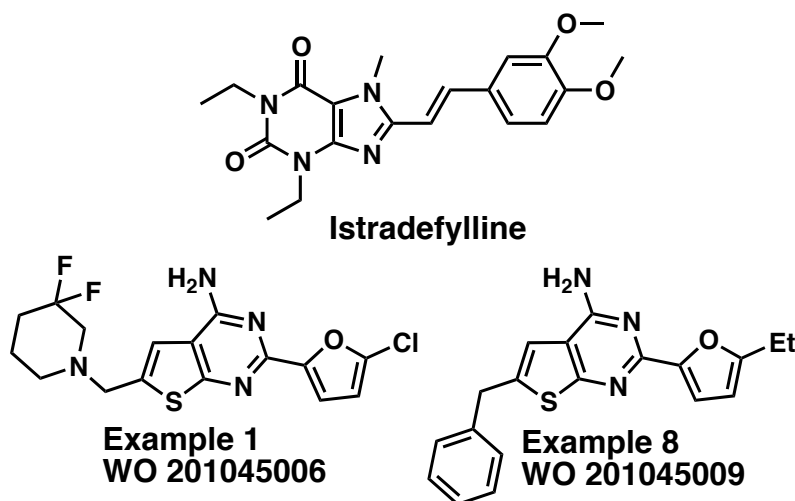


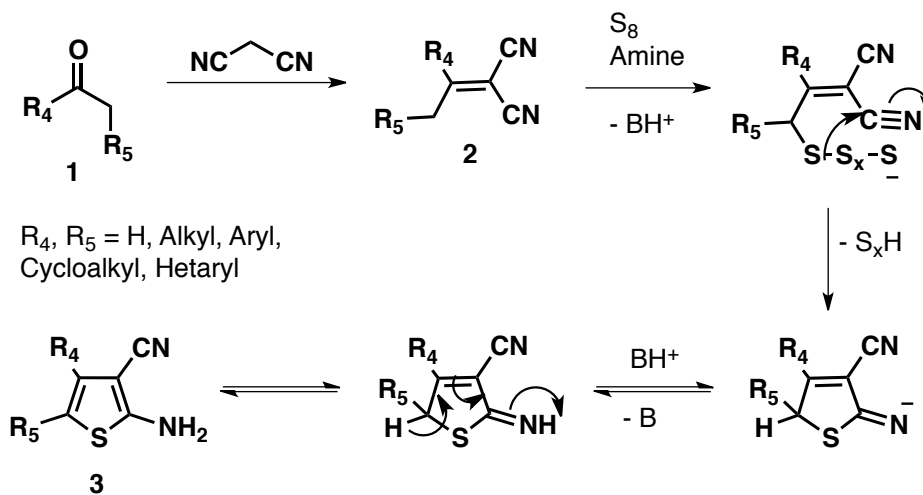
Figure 1.4 Structures of Istradefylline and thienopyrimidine $A_{2A}R$ antagonists.

As demonstrated by the variety of applications, the development of synthetic methodologies for the efficient preparation of structurally diverse

libraries of thienopyrimidines is an important pursuit for modern synthetic chemistry.

1.1.3 Synthesis of Thieno[2,3-*d*]pyrimid-4-amines

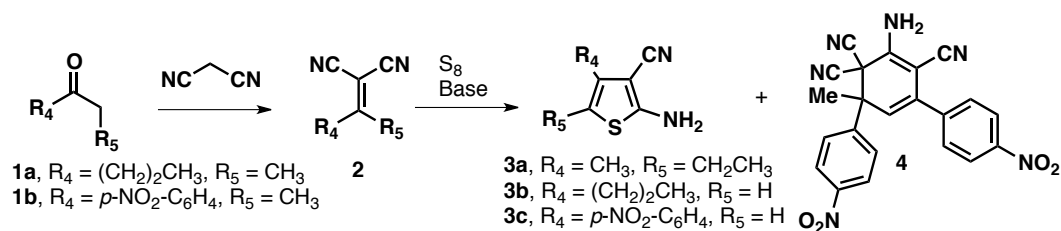
Traditionally, thieno[2,3-*d*]pyrimid-4-amines have been synthesized in a multistep process from 2-aminothiophenes. The Gewald method, which was first described in the 1960s (Scheme 1.1) is a very convenient approach to build the 2-aminothiophene core.⁵² Various optimizations, including one-step and two-step procedures under either thermal or microwave conditions, have been reported for the condensation of the Knoevenagel ylidene **2** with elemental sulfur to give the thiophene core **3**.



Scheme 1.1 Gewald reaction mechanism with elemental sulfur.

A few drawbacks to this versatile protocol are: (a) structural diversity must be generated early on in the library synthesis in a non-divergent manner with the selection of ketone **1** starting materials; (b) poor regioselectivity in the cyclization step. For example, when non-symmetrical ketones **1** with an alkyl or a benzylic

substituent, such as pentane-2-one **1a** (Scheme 1.2) are used in a one-pot condensation with malononitrile, sulfur, and catalytic amounts of imidazole, a mixture of thiophenes **3a** and **3b** was produced in a 3.4:1 ratio with modest yields (Scheme 1.2);⁵³ and (c) ylidene **2** can be chemically unstable due to the presence of an enolizable methyl group. Likewise, under standard Gewald reaction conditions, acetophenones bearing electron withdrawing substituents on the phenyl ring (e.g. **1b**) often produce very low yields of the desired 2-aminothiophene (Scheme 1.2). These low yields can be attributed, to some extent, to the decomposition of ylidene **2** under high temperatures and basic conditions and dimerization of the ylidene to compounds such as **4** (Scheme 1.2).⁵⁴

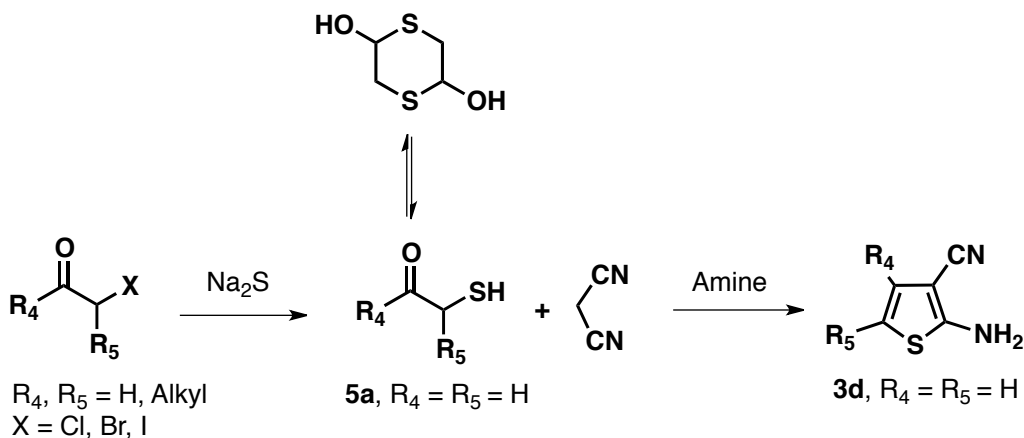


Scheme 1.2 Gewald synthesis of 2-aminothiophenes.

Alternatively, the condensation of an aliphatic α -mercaptoketone (or aldehyde) **5** with malononitrile also yields the 2-amino-thiophene-3-carbonitrile core **3** (Scheme 1.3). This is a much less versatile and convenient version of Gewald-type reactions with several shortcomings, such as the poor stability and difficult preparation of **5**. Most α -mercapto-compounds (**5**) must be generated *in situ* by, for example, reaction of α -halocarbonyl compounds with sodium sulfide. Likewise, a more stable and commercially available dimer form of mercaptoacetaldehyde, 1,4-dithiane-2,5-diol, is used to generate **5a**, where $R_4 =$

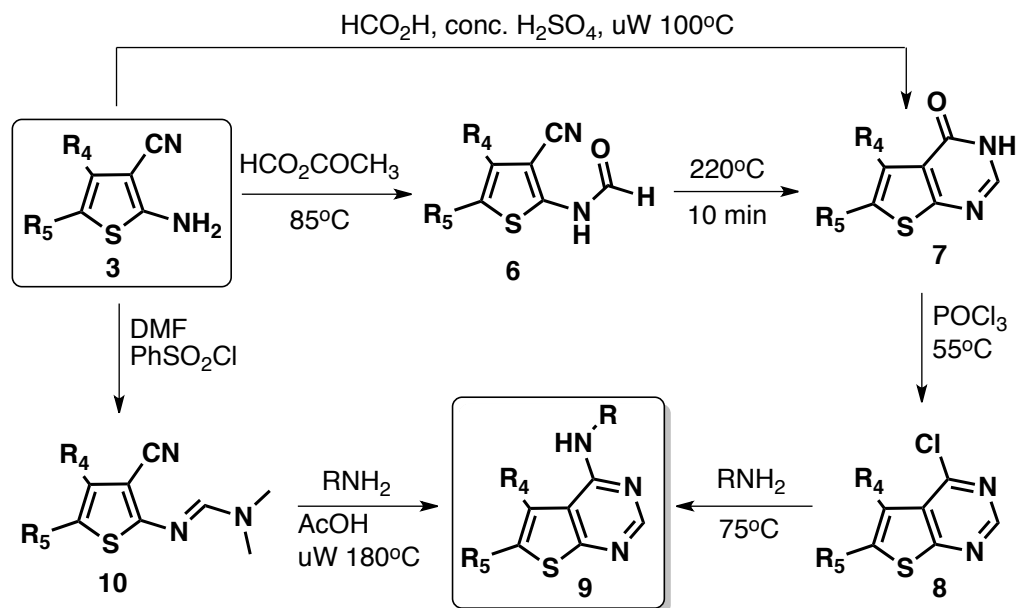
$R_5 = H$, which upon treatment with an activated nitrile and a basic amine produces

3d (Scheme 1.3).^{52a,55}



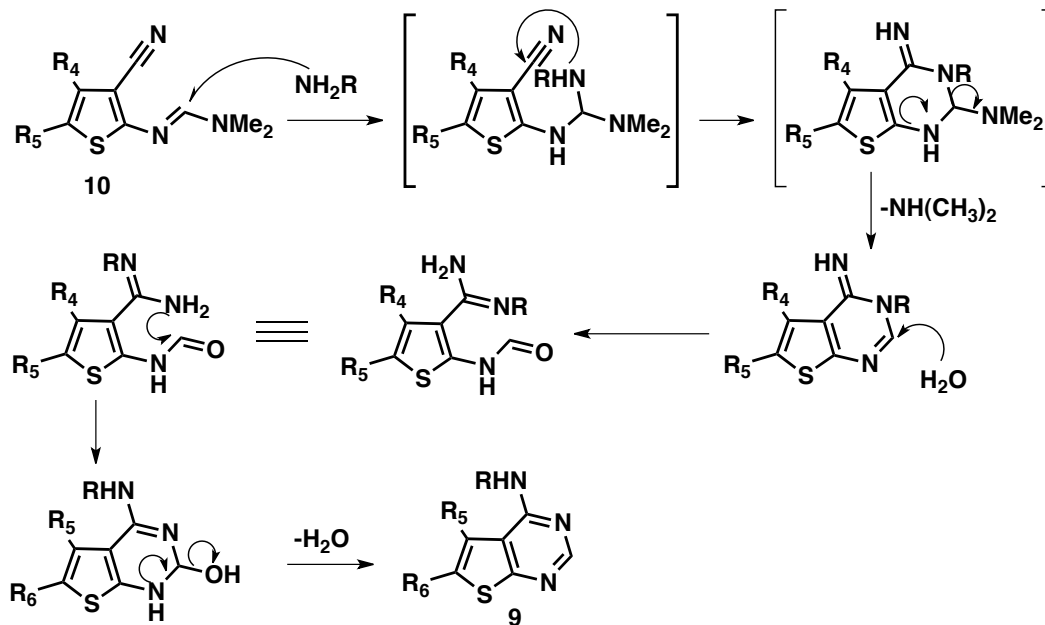
Scheme 1.3 Gewald-type synthesis with α -mercaptoketones and aldehydes (**5**).

The 2-aminothiophene scaffold can then be further elaborated to give rise to substituted thieno[2,3-*d*]pyrimidines **9** in a few ways (Scheme 1.4).⁵⁶ The most common method involves the formation of an *N*-formyl derivative **6** either by reaction with *in situ* generated acetic formic anhydride or formic acid. Ring closure to give the pyrimidone **7** may be accomplished under harshly acidic conditions and/or extremely high temperatures. The pyrimidone **7** is typically chlorinated with phosphorus oxychloride to produce **8**, which is then displaced by an amine (**9**).⁵⁷ This multistep route (Scheme 1.4) requires harsh reaction conditions and reagents, therefore, potentially limiting the accessibility of library synthesis of thieno[2,3-*d*]pyrimidines.⁵⁸



Scheme 1.4 Classical synthesis of thieno[2,3-*d*]pyrimidines (9) from 2-aminothiophenes (3).

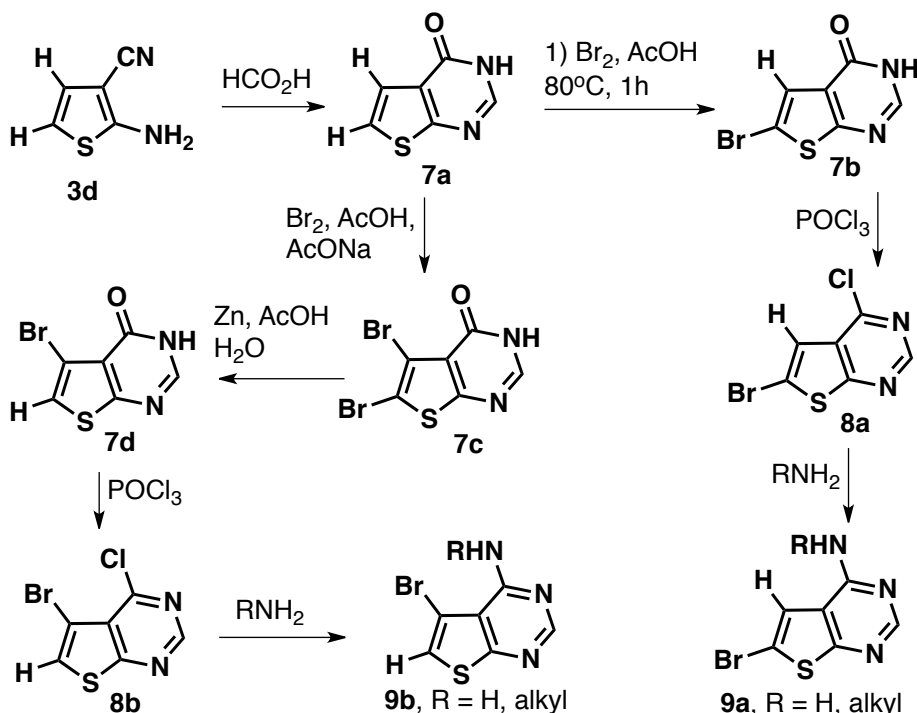
More recently, a two-step protocol via formamidine **10** (Scheme 1.4) was reported for the synthesis of thieno[2,3-*d*]pyrimidines (9) under microwave irradiation.⁵⁸ The formamidine **10** was synthesized from the corresponding 2-aminothiophenes, DMF, and phenylsulfonyl chloride as a condensation reagent.⁵⁹ Upon optimization, the synthesis of a library of thienopyrimidines (9) was accomplished in the microwave at 180°C for 35 min with 1.5 eq. of amine in acetic acid via a Dimroth rearrangement mechanism (Scheme 1.5).⁶⁰ Interestingly, either the amine or the imine derivatives could be synthesized depending on the reaction temperature. Although this approach is selective (imine v.s. amine) and efficient, the highly acidic environment may limit the applicability of this method towards library synthesis.



Scheme 1.5 Dimroth rearrangement mechanism.

With the goal of a divergent synthetic approach to library synthesis, bromination at C-6 (α -C) of the thiophene moiety in thienopyrimidinone scaffolds (**8a**) can be achieved with elemental bromine under acidic conditions (Scheme 1.6). The corresponding pyrimidine (**9a**) could then be prepared according to the traditional means of chlorination followed by displacement with an amine (Scheme 1.4 and 1.6).⁶¹ However, a direct and regiospecific protocol for halogenation at the β -carbon (C-5), or the equivalent carbon on any thiophene-containing bicyclic heterocycle, is unknown. Recent reports of indirect multi-step C-5 brominations include the 5,6-dibromination of thieno[2,3-*d*]pyrimidin-4-one (**7a**) with elemental bromine under acidic conditions to give **7c** (Scheme 1.6). Dehalogenation at the more reactive C-6 position with zinc in aqueous acetic acid gives the C-5 mono-brominated pyrimidinone **7d**, followed by another 2 steps to

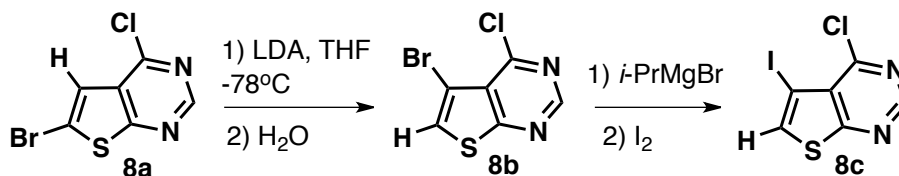
generate **9b** (Scheme 1.6).^{26,62} These pyrimidines (**8a,b** and **9a,b**) can then be used to prepare mono-substituted analogs.



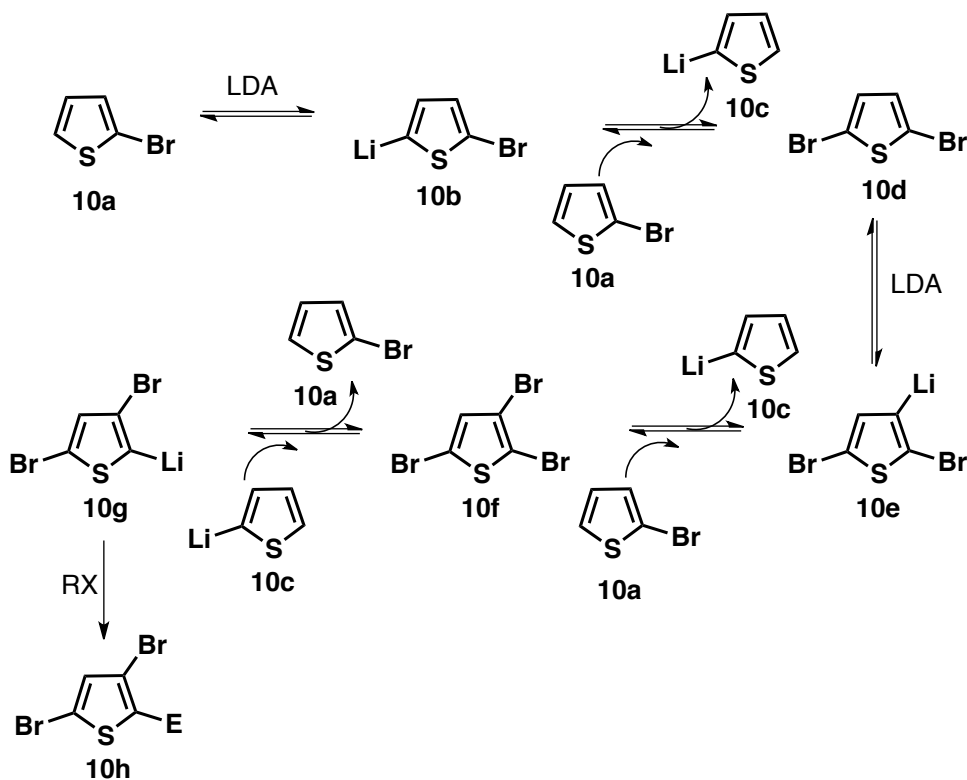
Scheme 1.6 Bromination reactions with thienopyrimidine intermediates.

Alternatively, the preparation of 3-bromothiophenes and 5-bromothiopyrimidines have been described via generation of an α -lithium- β -bromothiophene species (Scheme 1.7) from 2-bromothiophenes (**10a**) and 6-bromothiopyrimidines, respectively, using the so-called base-catalyzed halogen dance (BCHD) reaction (Scheme 1.8).⁶³ This approach has also been used in the synthesis of 4-chloro-5-iodothieno[2,3-*d*]pyrimidine (**8c**) from an LDA-mediated BCHD rearrangement of 6-bromo-4-chloropyrimidine (**8a**) to the 5-bromo analog **8b** (Scheme 1.6 and 1.7). Treatment of **8b** with a Grignard reagent and quenching

the generated anion with iodine produced **8c**, which was potentially more reactive to future cross-coupling reactions than **8a** (Scheme 1.7).^{16a,c}



Scheme 1.7 Bromination via base-catalyzed halogen dance (BCHD).

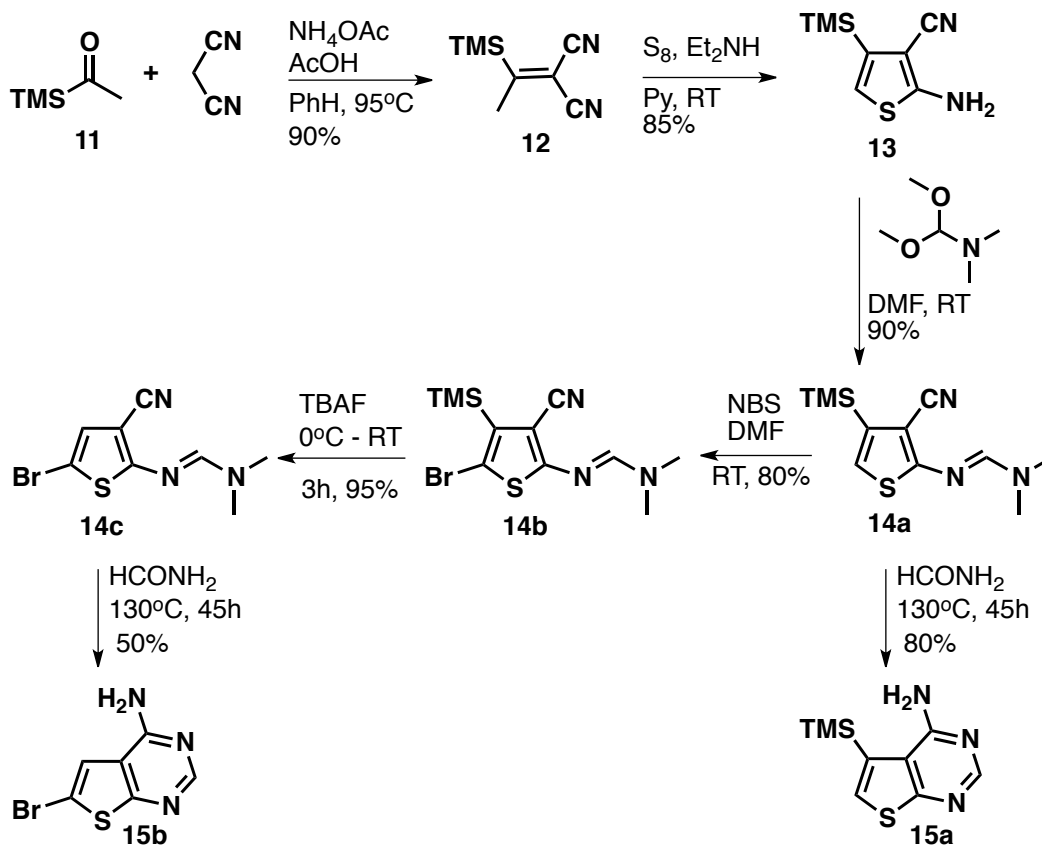


Scheme 1.8 Mechanism of classical base-catalyzed halogen dance.

1.2 Results and Discussion

As part of our continued interest in developing efficient, robust methodologies that are amenable to high throughput parallel synthesis of

structurally diverse libraries of compounds,⁶⁴ we modified the classical Knoevenagel/Gewald approach incorporating the trimethylsilyl ylidene **11** (Scheme 1.9) as the precursor to the 2-amino-thiophene-3-carbonitrile scaffold. We first decided to focus on the synthesis of 2-amino-5-bromo-4-(trimethylsilyl)-thiophene-3-carbonitrile (**14b**) in order to explore its direct use in cross-coupling reactions, taking advantage of the enhanced reactivity of the C-5 thiophene position as well as the dual capabilities of TMS at C-4, both preventing and conferring reactivity (Scheme 1.9). Efficiency, atom economy, and structural diversity were the key elements that we were looking to explore in this synthetic protocol.



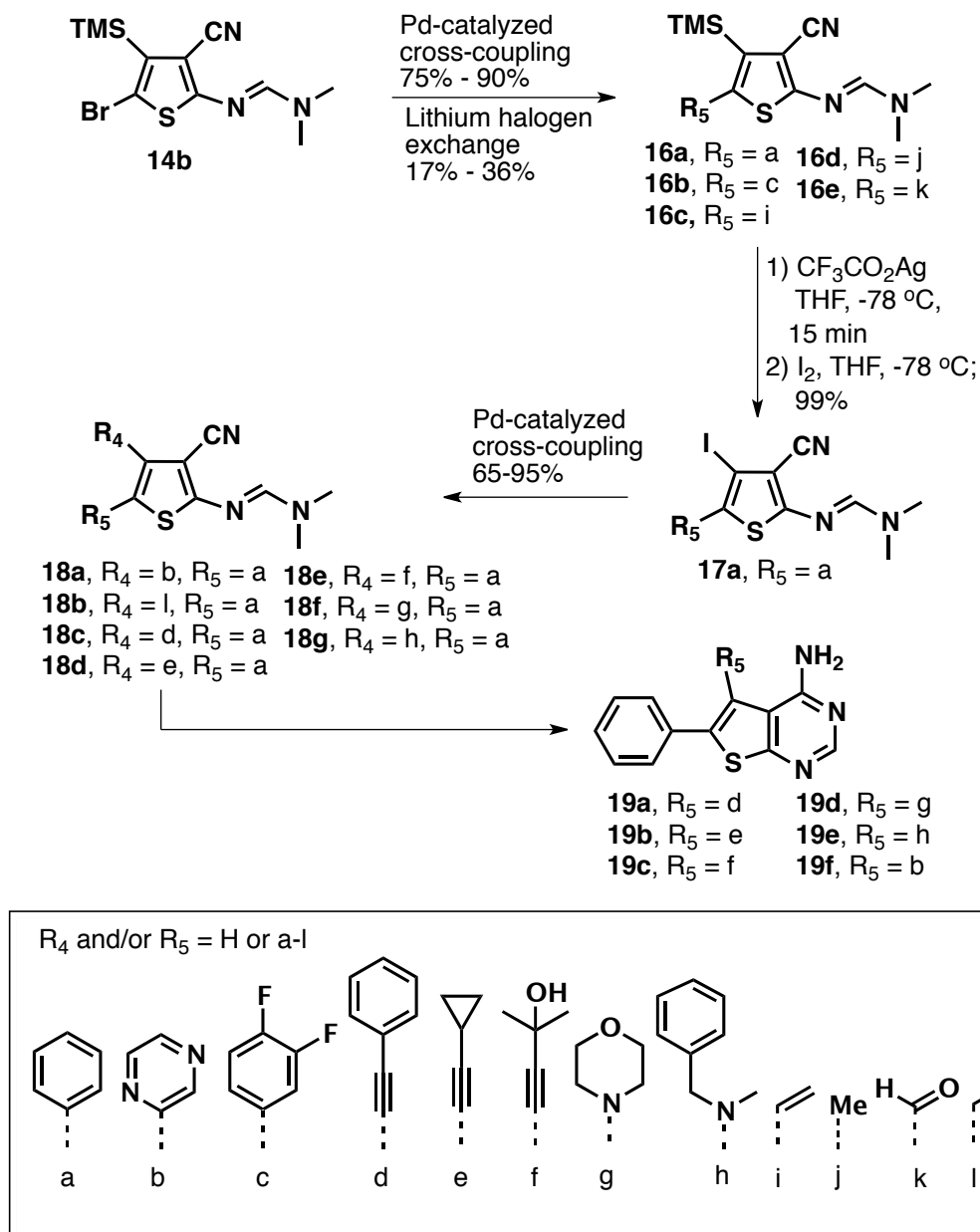
Scheme 1.9 Synthesis of highly substituted 2-aminothiophene intermediates for thieno[2,3-*d*]pyrimidin-4-amine preparation.

The 2-(1-(trimethylsilyl)ethylidene)malononitrile ylidine (**12**) was easily prepared in nearly quantitative yield *via* condensation of acetyltrimethylsilane (**11**) with malononitrile under slightly acidic conditions (Scheme 1.9). Ylidine **12** was found to be stable at -20 °C for several months and at RT for weeks without any evidence of decomposition. Condensation of **12** with elemental sulfur in pyridine provided the 2-amino-4-(trimethylsilyl)-thiophene-3-carbonitrile (**13**) as a dark orange/brown solid in >85% yield. Initial efforts to transform intermediate **13** to the desired C-4 iodo derivative, using silver trifluoroacetate and elemental iodine,⁶⁵ lead to decomposition of the starting material at temperatures ranging from 0 °C to -78 °C. In the past, examples of *ipso*-iododesilylation of thiophenes under these conditions were reported to give modest or poor yields when the TMS was adjacent to substituents with *sp* character.^{65b} In general, thiophene **13** was found to be chemically unstable, thus unsuitable as building-blocks in a library synthesis. Interestingly, protection of the 2-amino moiety with *N,N*-dimethylformamide-dimethylacetal, provided an intermediate (**14a**) that was much more stable and easy to prepare in high yield and purity (Scheme 1.9).

Cyclization of **14a** with formamide produced the 5-(trimethylsilyl)thieno[2,3-*d*]pyrimidin-4-amine (**15a**) in 76% yield (Scheme 1.9). Mindful of the facile decomposition of thiophenes upon exposure to light, this reaction was usually carried out in the dark. Due to the availability of the C-5 TMS to undergo *ipso*-substitution,⁶⁶ this methodology provides significant atom economy and efficiency in preparing C-5 mono-substituted thieno[2,3-*d*]pyrimidin-4-amines as compared to procedures described previously (Scheme 1.6 and 1.7).

Bromination at C-5 of the protected thiophene **14a** was then carried-out in >80% yield, providing intermediate **14b** (Scheme 1.9). The highly functionalized compound **14b** is a suitable building block for a variety of reactions. Access to C-5 mono-substituted thienopyrimidines may be gained through TMS removal under standard TBAF conditions to give intermediate **14c** (Scheme 1.9). Cyclization of **14c** generated 6-bromothieno[2,3-*d*]pyrimidin-4-amine (**15b**) in a moderate 50% yield (Scheme 1.9). This mono-substituted thienopyrimidine (**15b**) was generated in good yields over four steps (from **13**; Scheme 1.9) without the use of harsh acidic conditions common to classical synthetic methods (Scheme 1.6).

Selective cross-coupling was explored at C-5 with a few boronic acids or boronate esters to obtain intermediates of general structure **16a-c** ($R_4 = \text{TMS}$, $R_5 = \text{a, c, i}$) (Scheme 1.10). Whereby *ipso*-iododesilylation at C-4, followed by cross-coupling of the iodide **17a** *via* Suzuki, Buchwald-Hartwig, Sonogashira, Stille or other cross-coupling reactions, followed by cyclization of **18**, provided a mini-library of novel and structurally diverse C-5/C-6 di-substituted thieno[2,3-*d*]pyrimidin-4-amines (Scheme 1.10) in good overall yields. For example, analogs **19b** and **19d**, involving sequential cross coupling under typical Suzuki, followed by either Sonogashira (for **19b**) or Buchwald-Hartwig amination (for **19d**) conditions were obtained in an overall isolated yield of 50% and 30%, respectively, for the last 7 steps (*i.e.* from **13** to **19b** or **19d**).



Scheme 1.10 Di-substituted thienopyrimidine library synthesis.

Lithium-halogen exchange (LHE) reactions, discovered simultaneously by Wittig⁶⁷ and Gilman⁶⁸ in the 1930s, have regained popularity in recent years due to advancements in methods and the availability of exchange reagents.^{63d} Thiophenes have been employed extensively as substrates of LHE reactions. They are, however, notorious for participating in one of the potential complications of

LHE reactions, the base catalyzed lithium-halogen dance (BCHD), leading to scrambling of halogen atoms.^{63c,69} The versatility of precursor **14b**, was further demonstrated through use of the LHE reaction to install alkyl groups at the C5 position (Scheme 1.10 and Table 1.1).

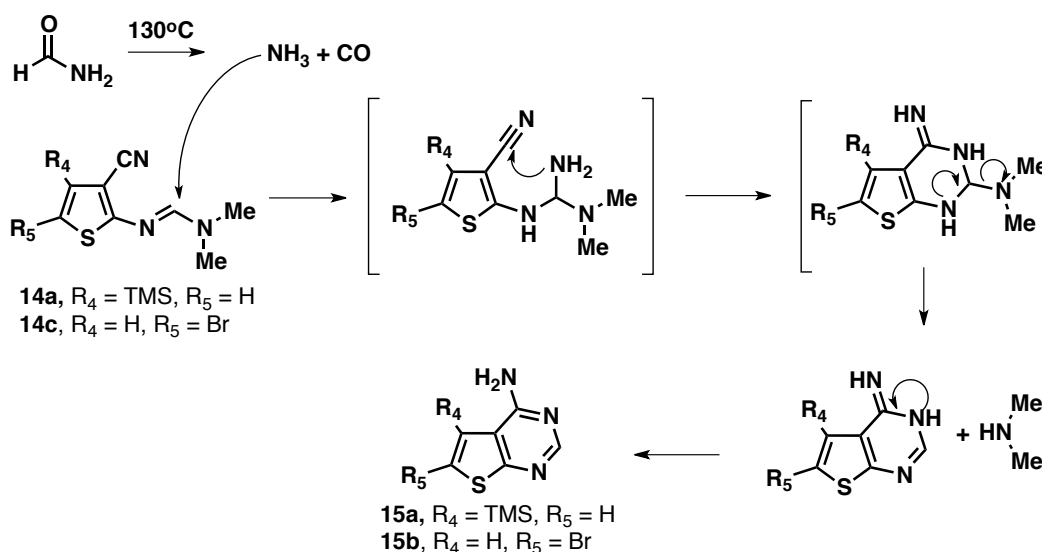
Table 1.1 Lithium halogen exchange conditions.

| Entry | R'Li | Time @ Temp (°C) | RX | Time @ Temp (°C) | Products |
|--|---------------|------------------|------------------|------------------------|--|
| 1 | <i>n</i> BuLi | 30 min @ -78 | MeI | 30 min @ -78 | 14a (70%) + degradation (20%) ^b |
| 2 | <i>n</i> BuLi | 15 min @ -78 | MeI ^a | 25h @ -78 | 16d (10%) + 14a (40%) + 13 (15%) + degradation (22%) ^b |
| 3 | <i>t</i> BuLi | 15 min @ -78 | MeI ^a | 15h @ -78 | SM (14b , 80%) ^b + 14a (15%) ^b |
| 4 | <i>t</i> BuLi | 13 min @ -78 | MeI ^a | 1.5h @ -78 2h @ -41 | 14a (95%) ^b |
| 5 | <i>t</i> BuLi | 5 min @ -78 | MeI ^a | 2h @ -78 | 16d (17%) ^c + degradation (60%) ^b |
| 6 | <i>t</i> BuLi | 5 min @ -78 | MeI ^a | 30 min @ -78 | 16d (36%) ^c + 14a (20%) ^c + degradation (21%) ^b |
| 7 | <i>t</i> BuLi | 5 min @ -78 | DMF | 1h @ -78 15h @ RT | 16e (31%) ^c + degradation (22%) ^b |
| ^a Filtered through basic alumina ^b Suggested by LCMS ^c Isolated yield SM = Starting material | | | | | |

Although the use of trialkylsilyl groups have been explored in LHE reactions with benzene and pyridine, they have not been explored with a 2-aminothiophene scaffold.⁷⁰ A variety of LHE reaction conditions demonstrated (Table 1.1) that the introduction of the trimethylsilyl group at C4 blocked the problematic BCHD reaction, thereby fulfilling its role as a dual protecting group/handle. These TMS groups have been used to deactivate the *ortho*-position of aromatic rings to hydrogen-metal exchange by blocking access to the base and can play a similar role in LHE reactions.^{63d} In our case, it appears that the LHE occurs faster than the subsequent attack of the electrophile (RX), leading to a protonated by-product **14a** (Table 1.1, entries 1-4, 6). The less nucleophilic base *t*BuLi was used to eliminate the formation of the deprotected thiophene (**13**) by-product (Table 1.1, entries 3-7). The best results were obtained when *t*BuLi was used in combination with short reaction times (Table 1.1, entries 5-7). Less degradation and by-product formation also occurred when shorter reaction times were employed upon electrophile addition (Table 1.1, entries 6). Longer reaction times and warmer conditions were required, however, for DMF due its less electrophilic character (Table 1.1, entry 7). The yields (Table 1.1, entries 6 and 7) were comparable with LHE reactions with thiophenes reported in the literature.⁶⁹

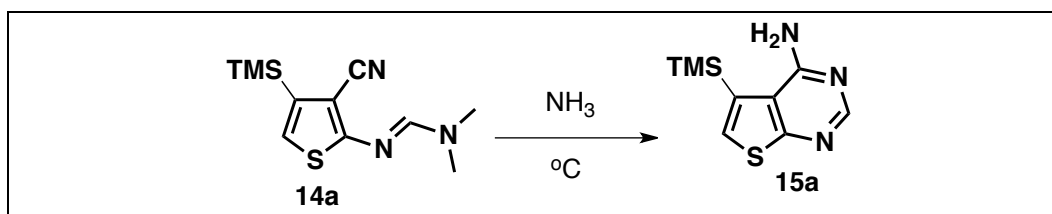
Thienopyrimidine formation was achieved via cyclization of formamidine protected 2-aminothiophenes (**14a**, **14c**, and **18a-g**) with formamide (Scheme 1.9 and 1.10). We attempted to elucidate the mechanism of this cyclization, with curious results. A similar cyclization reaction was reported in the literature to occur according to a mechanism similar to that of a Dimroth rearrangement (Scheme 1.5).⁵⁸ We initially proposed that the cyclization occurred in a

comparable manner whereby formamide breaks down to ammonia, which then closes the pyrimidine ring (Scheme 1.11).⁷¹ We tested our hypothesis by attempting the reaction with ammonia (Table 1.2). Interestingly, only starting material was isolated in both cases (Table 1.2, entries 1-2) without any indication of degradation. Perhaps the reaction required the addition of acid, common to the traditional methods of thienopyrimidine synthesis, or microwave irradiation in sealed reactors.^{26,58} Further synthetic studies towards elucidating the mechanistic details of this reaction with ammonia were not undertaken.



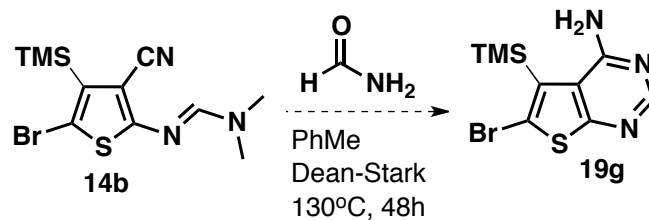
Scheme 1.11 Proposed mechanism of cyclization.

Table 1.2 Cyclization reaction with ammonia.



| Entry | NH ₃ Source | Temperature (°C) | Time | Products ^a |
|---|------------------------|------------------|------|-----------------------|
| 1 | Liquid | -78 - RT | 15h | SM (14a) |
| 2 | 1M in EtOH | 50 -100 | 36h | SM (14a) |
| ^a Determined by ¹ H NMR SM = Starting material | | | | |

To assess the scope of the cyclization reaction, we tried to synthesize the corresponding thienopyrimidine (**19g**, Scheme 1.12) from **14b** in formamide with toluene and a Dean Stark apparatus, and under light and dark conditions (Table 1.3). The reaction with the Dean Stark apparatus to drive water out of the reaction mixture did not proceed to give the desired product **19g** and only 50% of the starting material was recovered, which could indicate a stability problem. Interestingly, product formation appeared to demonstrate a dependence on the presence or absence of light. The di-substituted thienopyrimidine (**19g**) was not generated under any conditions, however (Table 1.3, entries 1-2). In the presence of light, only **15a** was isolated (Table 1.3, entry 1) whereas, in the dark both **15a** and **15b** were generated (Table 1.3, entry 2). This could be due to a radical based mechanism of cyclization or a problem with the stability of the starting material, intermediates, and/or products.



Scheme 1.12 Attempted cyclization of **14b** with Dean Stark apparatus.

Table 1.3 Cyclization reaction under light and dark conditions.

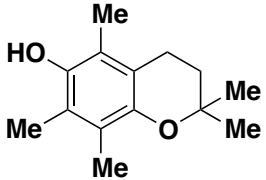
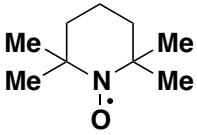
| Entry | Light/ Dark | Yield 19g (%) ^a | Yield 15a (%) ^a | Yield 15b (%) ^a |
|-------|-------------|--------------------------------------|--------------------------------------|--------------------------------------|
| 1 | Light | 0 | 23 | 0 |
| 2 | Dark | 0 | 18 | 21 |

^a Isolated yields

Reaction of **14b** with formamide was further investigated with the addition of radical quenchers (Table 1.4). We proposed that if the reaction proceeds via radical mechanism, the addition of radical quenchers should prevent any cyclization reaction from taking place. Two quenchers were used, 2,2,5,7,8-pentamethyl-6-chromanol (Table 1.4, entry 1) and TEMPO (Table 1.4, entry 2). The reactions were carried out in the absence of light and afforded similar results to the cyclization reaction in the absence of both light and radical quenchers (Table 1.3, entry 2). The desired product **19g** was not synthesized whereas both

15a and **15b** were generated in a 1 : 1 ratio (Table 1.4, entries 1-2). Neither radical quencher made a difference to the result of the reaction, suggesting that the reaction did not involve a radical mechanism.

Table 1.4 Cyclization reaction with radical quenchers.

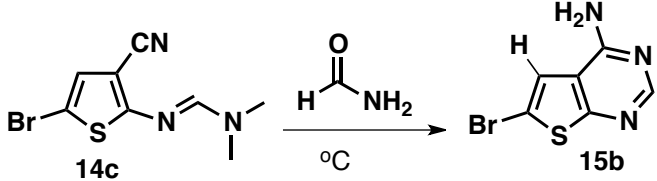
| Entry | Radical Quencher | Ratio 19g : 15a : 15b ^a |
|-------|---|---|
| 1 |  | 0 : 1 : 1 |
| 2 |  | 0 : 1 : 1 |

^a Suggested by LCMS

The unusual results of previous cyclization reactions with **14b** (Tables 1.3 and 1.4) may be due to chemical instability or insolubility of the products and/or reactants. To probe this theory, pyrimidine **15b** was synthesized via **14c** in formamide under various reaction conditions and work-up procedures (Table 1.5). Interestingly, the reaction proceeded with a moderate yield of **16b** (35%) in the presence of light. Starting material (**14c**) remained upon heating to 100°C for 20

hours, therefore, the temperature was increased to 130°C and the reaction continued to stir for another 10 hours, such that starting material (**14c**) was no longer observed. However, a degradation by-product (debrominated thiophene) and complete decomposition was also observed, which may indicate starting material instability (entry 1, Table 1.6). When the reaction was shielded from light and heated to 130°C for 15 hours, the yield of **15b** (entry 2) was slightly less than the yield of the reaction in light conditions (entry 1, Table 1.5). Less degradation by-product was isolated (10%), however, suggesting that the reaction may be photochemically unstable. After 40 hours in the dark, **15b** was isolated in the modest yield, 50% (entry 3, Table 1.5). The thienopyrimidine **15b** was only moderately soluble in EtOAc, consequently, the extraction was done with *n*-butanol and salted water to try to maximize compound recovery. Purification by trituration, instead of column chromatography, was carried out to investigate whether **15b** precipitated out on silica gel, leading to only moderate yields. The change in purification method did not increase the yield of the desired product and the same degradation by-product (common to all previous reactions) was not isolated (entry 4, Table 1.5). In conclusion, the highest yield we were able to obtain with this reaction (Table 1.5) was 50% and the modest yield was not caused by the product's poor solubility.

Table 1.5 Various reaction conditions for the synthesis of **15b** from **14c**.

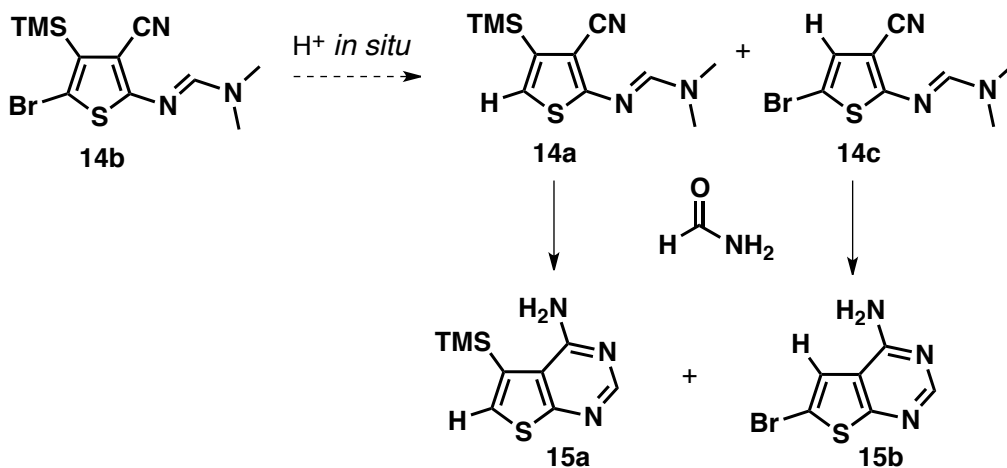
|  | | | | | | |
|--|--------------|------------|---------------|--|--|---|
| Entry | °C | Time (h) | Light or Dark | Extraction | Purification | Products ^a |
| 1 | 100 then 130 | 20 then 10 | Light | EtOAc H ₂ O, brine | Column: DCM EtOAc/Hex | 15b (35%) + degradation by-product (15%) + 50% decomposition |
| 2 | 130 | 15 | Dark | EtOAc H ₂ O, brine | Column: EtOAc/Hex | 15b (25%) + degradation by-product (10%) + 65% decomposition |
| 3 | 130 | 40 | Dark | EtOAc H ₂ O, brine | Column: EtOAc/Hex | 15b (50%) + degradation by-product (15%) + 35% decomposition |
| 4 | 130 | 24 | Dark | <i>n</i> Butanol salted H ₂ O, brine | Trituration: MeOH, DMSO Ether | 15b (50%) + 50% decomposition |
| ^a Isolated yield | | | | | | |

Although the above studies (Table 1.5) evaluated the potential insolubility of **15b**, they did not probe the role that instability may have in the outcome of this reaction. To test the chemical stability of both the starting material (**14c**) and product(s), an NMR sample of **14c** and the desired thienopyrimidine product (**15b**) were exposed to light at ambient temperature. Degradation of **14c**, but not

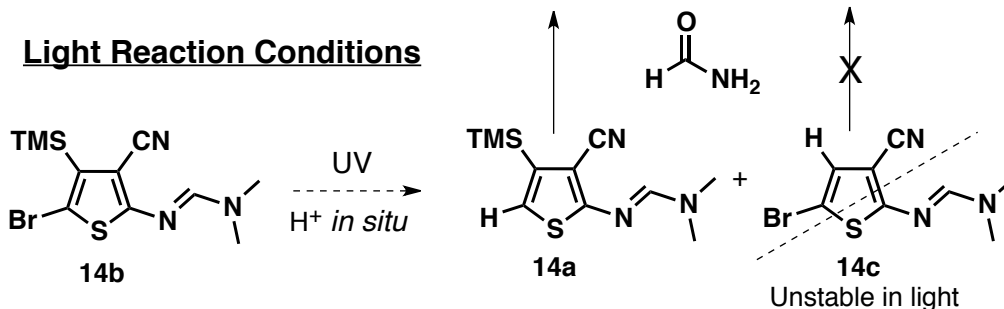
thienopyrimidine **15b**, was observed with ^1H NMR after 4 days of exposure to light. This indicated that the instability of thiophene **14c** could affect the yields of the reaction carried out in the presence or absence of light and at high temperatures. Perhaps this finding helps to explain the unexpected results of the attempted thienopyrimidine **15b** synthesis in Tables 1.3, 1.4, and 1.5.

After these efforts to optimize the reaction conditions, we attempted to explain the unusual results by hypothesizing that if an acid was generated *in situ* at high temperature, **14b** (Scheme 1.9) could lose either the TMS group at C4 to generate **14a** or the bromine at C5, generating **14c** (Scheme 1.9), prior to cyclization (Scheme 1.13). This degradation may occur because thiophene derivatives can be acid labile and/or to relieve the steric strain that is generated by two neighboring bulky groups on a 5-membered ring.^{72, 73, 74} If **14b** decomposes to **14a** and **14c** prior to cyclization, the two products generated would be **15a** and **15b**, respectively (Table 1.3, entry 2). However, in the light, thiophene **14c** is unstable and could decompose, thereby prohibiting the formation of **15b** (Table 1.3, entry 1), while **15a** is formed via **14a** (Scheme 1.13).

Dark Reaction Conditions



Light Reaction Conditions

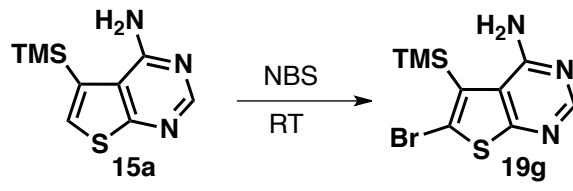


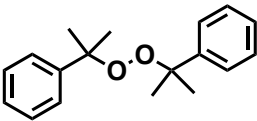
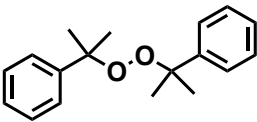
Scheme 1.13 Decomposition hypothesis to explain cyclization results.

Following these studies, it became obvious that a different synthetic route was required to synthesize thienopyrimidine (**19g**), an interesting branching point for the divergent synthesis of our library. A potential solution to circumvent the problems associated with the thiophene instability would be to brominate the stable thienopyrimidine **15a**. Both non-radical and radical bromination reaction conditions were investigated (Table 1.6). Only starting material was isolated using standard electrophilic aromatic substitution conditions, which was successfully employed for thiophene **14a** (Scheme 1.9), with N-bromosuccinimide (NBS) in DMF at RT even after 48 hours (entry 1, Table 1.6). This was likely due to the decreased reactivity of the C6 (C- α) position of thieno[2,3-*d*]pyrimidines

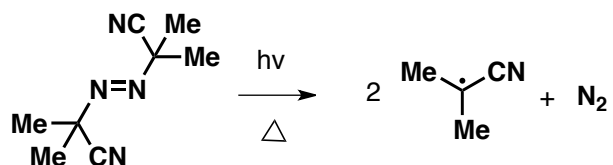
compared to the C5 (C- α) position of thiophenes due to the influence of annulation with the pyrimidine ring.⁷⁵ Although, elemental bromine is commonly chosen for reaction with thienopyrimidines, the use of NBS as the brominating agent has several advantages, including a slow and steady release of molecular bromine over the course of the reaction and the lack of strong acid formation, which can lead to the degradation of thiophenes and TMS-containing derivatives. Heat was not applied to the electrophilic aromatic substitution reaction (entry 1, Table 1.6) because selectivity may decrease as the reaction temperature is increased with thiophene scaffolds.⁷⁶ In our case, the *ipso*-substitution of the C5 TMS group with bromine was a potential side reaction of bromination that we hoped to avoid.^{73,77}

Table 1.6 Attempted synthesis of **19g** via bromination of **15a**.

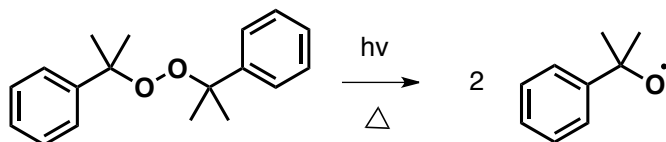
|  | | | | | |
|--|---------|------|------|---------------------|-----------------------|
| Entry | Solvent | Time | UV | Additional Reagents | Products ^a |
| 1 | DMF | 48 h | Dark | - | SM |

| | | | | | |
|--|-------------------|-------|--------|---|--|
| 2 | CHCl ₃ | 4 min | 257 nm |  DCP | 19g (25% + impurities) + SM (70%) |
| 3 | CHCl ₃ | 6 min | 257 nm |  DCP | 19g (10% + impurities) + SM (50%) |
| ^a Suggested by LCMS SM = Starting material | | | | | |

Radical initiated electrophilic aromatic substitution reactions have also been employed in bromination reactions with olefins, benzylic positions, and heterocycles. NBS was again a suitable bromine source for radical initiated substitutions.⁷⁸ A commonly used radical initiator is azobisisobutyronitrile (AIBN), which upon thermal or photochemical initiation decomposes to generate two cyanoisopropyl radicals and N₂ (Scheme 1.14). Complications may arise, however, as these cyanoisopropyl radicals can produce several by-products by disproportionation, dimerization, and chain reactions.⁷⁹ To minimize potential complications and side-products, dicumyl peroxide (DCP) was chosen as the radical initiator in the radical bromination reaction of **15a** (Table 1.6, entries 2-3). DCP was photochemically cleaved to generate two cumyloxyl radicals at room temperature (Scheme 1.15), which are very stable and mainly reactive towards hydrogen atom transfer, thereby minimizing potential by-products.



Scheme 1.14 Thermal or photochemical degradation of AIBN.



Scheme 1.15 Thermal or photochemical degradation of DCP.

A solution of **15a**, NBS, and DCP in chloroform at RT was exposed to UV light at 257 nm for 4 minutes (entry 2, Table 1.6) and 6 minutes (entry 3, Table 1.6). After 4 minutes, **19g** was generated (according to LCMS) in poor yield with poor conversion. After 6 minutes, conversion of starting material was greater but the product yield was less, indicating that **19g** may not have been stable under these conditions with longer reaction times. Perhaps **19g** was not photochemically stable in a manner similar to thiophene **14c** (Table 1.5 and Scheme 1.13). Alternatively, **19g** was perhaps consumed in a radical chain mechanism leading to degradation products, which were difficult to isolate and identify.

These initial reactions have demonstrated that although challenging, synthesis of **19g** is possible. The reaction conditions could be optimized with the wide variety of available solvents, radical initiators and brominating agents.

1.3 Conclusions

In summary, the traditional Knoevenagel/Gewald methodology is not easily amenable to divergent parallel synthesis of structurally diverse libraries of thieno[2,3-*d*]pyrimid-4-amines (**19**). Structural diversity is dictated by the starting aldehydes or ketones **1** (Scheme 1.1), thus the synthesis is linear and does not allow preparation of structurally diverse permutation libraries.

Furthermore, selective substitution at the C- β of the thiophene moiety (from a halide precursor) is challenging due to the inherent higher reactivity of the C- α carbon. We developed a modular methodology, which employs 2-(1-(trimethylsilyl)-ethylidene)-malononitrile (**12**) as a novel synthon in the preparation of building blocks that are amenable to high throughput library synthesis of thieno[2,3-*d*]pyrimid-4-amines (Schemes 1.9 and 1.10; **15a,b** and **19**). Preparation of 2-amino-4-(trimethylsilyl)thiophene-3-carbonitrile derivatives **13**, **14a-c**, **16a-e**, **17a**, **18a-h**, and thieno[2,3-*d*]pyrimid-4-amines (**15a,b** and **19a-f**) can be achieved easily, with high yields and significant atom economy.

1.4 Experimental

1.4.1 General Information

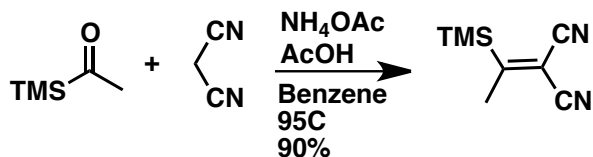
All intermediate and final compounds were purified by normal phase flash column chromatography on silica gel using an automated CombiFlash flash column chromatography instrument and the solvent gradient indicated. The purified compounds were analyzed for homogeneity by HPLC; homogeneity was confirmed by C18 reversed phase HPLC, using a Waters ALLIANCE[®] instrument

(e2695 with 2489 UV detector and 3100 mass spectrometer), equipped with a Waters Atlantis T3 C18 5 μm column using the following conditions: Solvent A: H_2O , 0.1% formic acid; Solvent B: CH_3CN , 0.1% formic acid; Mobile phase: linear gradient from 95% A and 5% B to 5% A and 95% B in 13 min, then 2 min at 100% B; Flow rate: 1 mL/min

Key intermediates and all final products were characterized by ^1H and ^{13}C NMR, as well as MS; final compounds were further characterized by HRMS. Chemical shifts (δ) are reported in ppm relative to the internal deuterated solvent, unless indicated otherwise. High-Resolution MS spectra (HRMS) were recorded at the McGill University, MS facilities using electrospray ionization ($\text{ESI}^{+/-}$) and Fourier transform ion cyclotron resonance mass analyzer (FTMS).

1.4.2 Synthesis of Key Fragments

2-(1-(Trimethylsilyl)ethyl)malononitrile (12):



Acetyltrimethylsilane (1.46 g, 12.56 mmol), malononitrile (1.14 g, 12.56 mmol) and ammonium acetate (262.1 mg, 2.39 mmol) were dissolved in acetic acid (0.58 mL, 10.0 mmol) and benzene (30 mL) in a 100 mL round bottom flask attached to a Dean-Stark trap and filled with benzene. The reaction mixture was stirred and heated to 95°C for 24 h. The resulting orange solution was cooled and diluted with EtOAc (20 mL). The organic layer was washed with saturated sodium bicarbonate solution (15 mL), water (45 mL), brine (15 mL) and dried over MgSO_4 . The

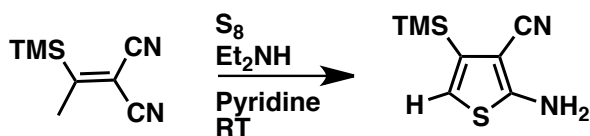
product was purified by column chromatography (25% EtOAc/hex) to give the desired product as clear pale yellow oil in 90% yield (1.97 g).

^1H NMR (400 MHz, CDCl_3) δ 2.34 (s, 3H), 0.35 (s, 9H)

^{13}C NMR (75 MHz, CDCl_3) δ 188.0, 113.0, 111.2, 94.3, 24.1, -2.3

HRMS (ESI-) calculated for $\text{C}_8\text{H}_{11}\text{N}_2\text{Si}$ m/z $[\text{M} - \text{H}]^-$: 163.06970, found m/z 163.06875 and HRMS (ESI-) calculated for $\text{C}_{16}\text{H}_{23}\text{N}_4\text{Si}_2$ m/z $[2\text{M} - \text{H}]^-$: 327.14667, found m/z 327.14695

2-Amino-4-(trimethylsilyl)thiophene-3-carbonitrile (13):



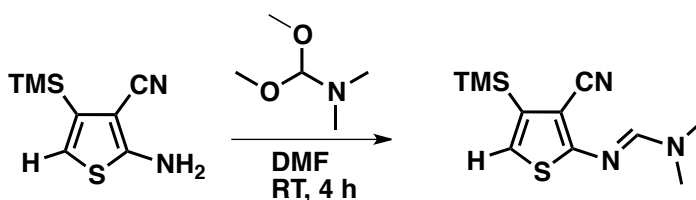
2-(1-(trimethylsilyl)ethyl)malononitrile (**12**, 1.21 g, 7.37 mmol) and sulfur (248.0 mg, 7.73 mmol) were dissolved in pyridine (25 mL) at room temperature. To this, diethylamine (0.76 mL, 7.37 mmol) was added dropwise. The reaction mixture stirred at room temperature for 18 h. Evaporation of pyridine afforded the crude thiophene, which was dissolved in EtOAc (20 mL) and washed with water (45 mL), brine (15 mL), and dried over MgSO_4 . Purification by column chromatography (25% EtOAc/hex, R_f = 0.58) afforded the desired product as an orange oil in 85% yield (803 mg).

^1H NMR (400 MHz, CDCl_3) δ 6.37 (s, 1H), 4.73 (bs, 2H), 0.31 (s, 9H)

^{13}C NMR (75 MHz, CDCl_3) δ 164.2, 141.0, 116.6, 116.5, 92.1, -1.5

HRMS (ESI+) calculated for $\text{C}_8\text{H}_{13}\text{N}_2\text{SSi}$ m/z $[\text{M} + \text{H}]^+$: 197.05632, found m/z 197.05615

3-Cyano-4-(trimethylsilyl)thiophen-2-yl)-N, N-dimethylformimidamide (14a):



To a solution of 2-amino-4-(trimethylsilyl)thiophene-3-carbonitrile (**13**, 372.40 mg, 1.90 mmol) in DMF (20 mL) was added DMF-DMA (2.5 mL, 18.97 mmol). After stirring at room temperature for 4 h, the reaction mixture was diluted with EtOAc, washed with water (60 mL), brine (20 mL), and dried over MgSO₄. Solvent was removed *in vacuo* to afford the desired product as a brown-yellow solid in 90% yield (440 mg; R_f = 0.3, 25% EtOAc/Hex).

¹H NMR (400 MHz, CDCl₃) δ 7.72 (s, 1H), 6.63 (s, 1H), 3.10 (s, 3H), 3.09 (s, 3H), 0.32 (s, 9H)

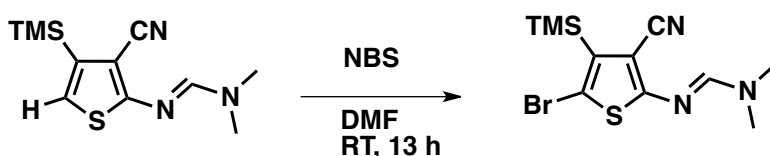
¹³C NMR (125 MHz, CDCl₃) δ 168.9, 154.8, 141.6, 120.7, 117.5, 101.2, 40.7, 35.15, -1.3

²⁹Si NMR (99 MHz, CDCl₃) δ -6.688

HRMS (ESI⁺) calculated for C₁₁H₁₈N₃SSi *m/z* [M + H]⁺: 252.09852, found *m/z* 252.09781

5-Bromo-3-cyano-4-(trimethylsilyl)thiophen-2-yl)-N,N-dimethylformimidamide

(14b):



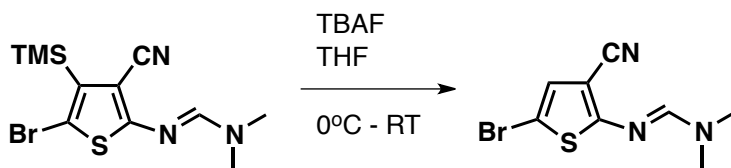
N-Bromosuccinimide (121.2 mg, 0.68 mmol) was added to a solution of **14a** (163.0 mg, 0.648 mmol) in DMF (7 mL). The yellow solution was stirred in the absence of light at room temperature for 13 h. The mixture was diluted with EtOAc, washed with water (25 mL), brine (10 mL), and dried over MgSO₄. Solvent was removed *in vacuo* to afford the desired product as a brown-orange solid in 80% yield (177 mg; R_f = 0.61, 25% EtOAc/Hex).

¹H NMR (400 MHz, CDCl₃) δ 7.63 (s, 1H), 3.09 (s, 6H), 0.44 (s, 9H)

¹³C NMR (125 MHz, CDCl₃) δ 168.4, 154.6, 138.9, 116.7, 106.2, 101.9, 40.8, 35.3, 0.24

HRMS (ESI+) calculated for C₁₁H₁₇N₃BrSSi *m/z* [M + H]⁺: 330.00903, found *m/z* 330.00926

5-Bromo-3-cyanothiophen-2-yl-N,N-dimethylformimidamide (14c):



A 1M solution of TBAF (5 mL) in THF was added dropwise to a solution of **14b** (1.61 g, 4.89 mmol) in THF (100 mL) cooled to 0°C. The reaction mixture was warmed to room temperature and stirred in the dark for 3 h. The volume of THF was reduced *in vacuo* and EtOAc was added, washed with water (3 x 50 mL), brine (25 mL), and dried over Na₂SO₄. The desired crude product was obtained as a red oil in 95% yield (1.20 g).

¹H NMR (400 MHz, CDCl₃) δ 7.64 (s, 1H), 6.86 (s, 1H), 3.11 (s, 6H)

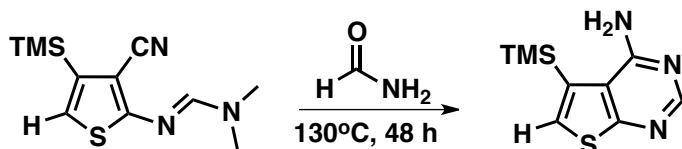
¹³C NMR (300 MHz, CDCl₃) δ 167.0, 154.3, 128.3, 115.2, 99.4, 96.5, 40.8, 35.2

MS (ESI+) m/z : 258.06 $[M + H]^+$

General protocol for the cyclization of C-4 or C-5 substituted fragments **14** to thieno[2,3-*d*]pyrimidin-4-amines **15**:

3-Cyano-4-(trimethylsilyl)thiophen-2-yl)-*N,N*-dimethylformimidamide (**14a,b**, ~0.3 mmol) was stirred with formamide (anhydrous, excess, ~2.5 mL) in a dry 15 mL pressure vessel. The vessel was flushed with argon and the mixture was heated to 130°C for 45 hours. The dark red solution was diluted with ethyl acetate, washed with water (25 mL), brine (10 mL), and dried over Na₂SO₄. The crude mixture was purified by flash column chromatography (5 - 30% EtOAc/hexanes, dry loading) to afford the desired thieno[2,3-*d*]pyrimidin-4-amine products.

5-(Trimethylsilyl)thieno[2,3-*d*]pyrimidin-4-amine (**15a**):



Isolated as a pink solid in 80% yield (59 mg).

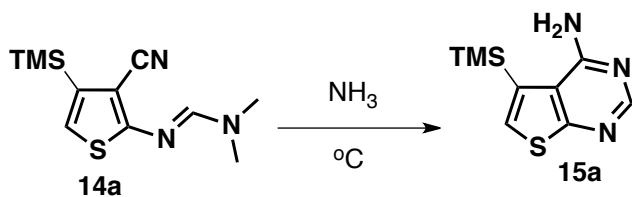
¹H NMR (400 MHz, CDCl₃) δ 8.46 (s, 1H), 7.43 (s, 1H), 5.36 (bs, 2H), 0.46 (s, 9H)

¹³C NMR (125 MHz, CDCl₃) δ 170.7, 158.7, 153.4, 133.0, 131.1, 119.7, 0.3

²⁹Si NMR (99 MHz, CDCl₃) δ -7.399

HRMS (ESI+) calculated for C₈H₁₃N₂SSi m/z $[M + H]^+$: 224.06722, found m/z 224.06705

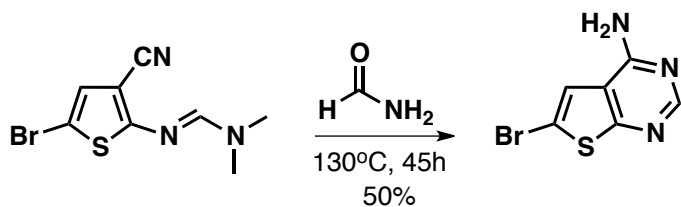
Attempted Experimental Protocols Towards the Synthesis of 15a from 14a (Table 1.2):



Entry 1: 3-Cyano-4-(trimethylsilyl)thiophen-2-yl)-*N,N*-dimethylformimidamide (**14a**, 50.0 mg, 0.2 mmol) was added to a dry 50 mL three-neck flask. To this was condensed liquid ammonia (10 mL, 400 mmol) via cold finger and stirred under argon at -78°C . Dry THF (1 mL) was added to the mixture to ensure the dissolution of **14a** and the mixture continued to stir at -78°C for 3 hours. TLC (25% EtOAc/Hex) indicated the presence of starting material without any conversion. Dry THF (2 mL) was added to the reaction mixture and stirred under argon at -42°C for 2 hours. The mixture was then warmed to room temperature to allow the excess ammonia to evaporate. Upon drying under high vacuum for 1 hour, 48 mg of **14a** was recovered (as indicated by ^1H NMR).

Entry 2: 3-Cyano-4-(trimethylsilyl)thiophen-2-yl)-*N,N*-dimethylformimidamide (**14a**, 50.0 mg, 0.2 mmol) was added to a dry 15 mL pressure vessel. To this was added 10 mL of 1M ammonia in EtOH. The reaction mixture was stirred and heated to 50°C under argon for 15 hours. TLC (25% EtOAc/Hex) indicated the presence of starting material without any conversion. The reaction mixture was stirred for another 27 hours at 100°C under argon. Upon drying under reduced pressure for 1 hour, 45 mg of **14a** was recovered (as indicated by ^1H NMR).

6-Bromo-thienof[2,3-d]pyrimidin-4-amine (15b):



Isolated as a brown solid in 50% yield (45 mg).

¹H NMR (300 MHz, D₆-DMSO) δ 8.22 (s, 1H), 7.72 (s, 1H), 7.57 (bs, 2H)

¹³C NMR (75 MHz, D₆-DMSO) δ 167.5, 157.7, 154.9, 123.3, 116.7, 109.7

MS (ESI+) *m/z* 232.0 [M+H]⁺

Experimental Protocols of Attempted Syntheses of 19g via fragment 14b:

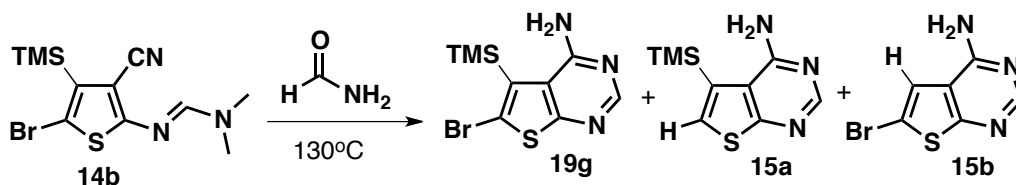


Table 1.3 Entry 1: Fragment **14b** (76 mg, 0.23 mmol) and dry formamide (5 mL, 46 mmol) were added to a dry 15 mL pressure vessel. The mixture was stirred and heated under argon to 130°C for 72 hours. The solution was diluted with ethyl acetate, washed with water (25 mL), brine (10 mL), and dried over MgSO₄. The crude mixture was purified by flash column chromatography (5 - 30% EtOAc/hexanes, dry loading) to give 12 mg (23%) of **15a** as a pale pink solid (according to ¹H NMR).

Table 1.3 Entry 2: Fragment **14b** (40 mg, 0.12 mmol) and dry formamide (1 mL, 24 mmol) were added to a dry 15 mL pressure vessel. In the absence of light, the

mixture was stirred and heated under argon to 130°C for 30 hours. The solution was diluted with ethyl acetate, washed with water (25 mL), brine (10 mL), and dried over MgSO₄. The crude mixture was purified by flash column chromatography (5 - 30% EtOAc/hexanes, dry loading) to give 7 mg (18%) of **15a** as a pale pink solid and 8 mg (21%) of **15b** as a tan solid (according to ¹H NMR).

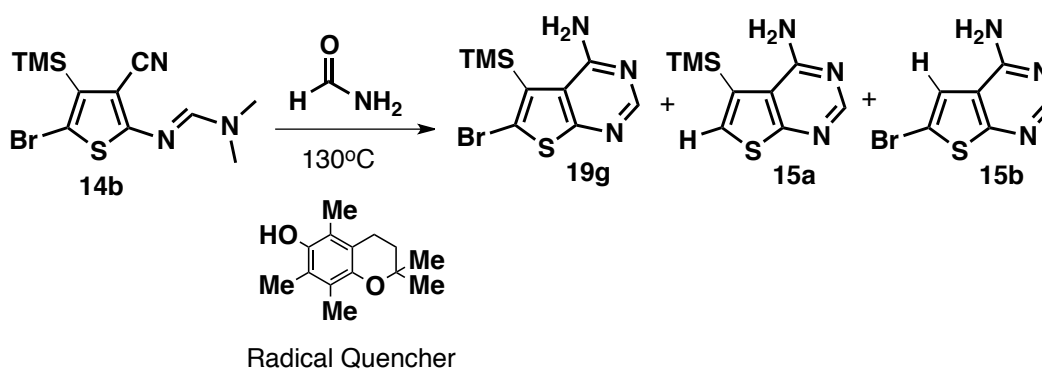


Table 1.4 Entry 1: Fragment **14b** (16 mg, 0.05 mmol), 2,2,5,7,8-Pentamethyl-6-chromanol (11 mg, 0.05 mmol), and dry formamide (1 mL, 9 mmol) were added to a dry 15 mL pressure vessel. The mixture stirred under argon, in the absence of light, for 19 hours at 130°C. Characterization by LCMS suggested a 1:1 ratio of **15a**:**15b** without any product (**19g**) formation.

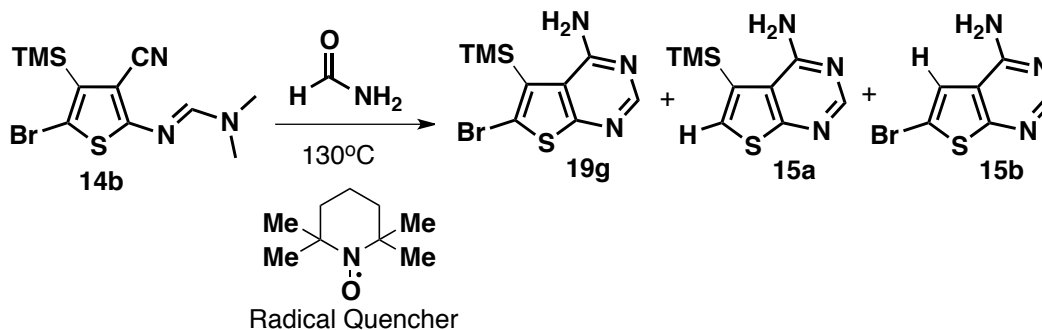


Table 1.4 Entry 2: Fragment **14b** (15 mg, 0.04 mmol), TEMPO (7 mg, 0.04 mmol), and dry formamide (1 mL, 9 mmol) were added to a dry 15 mL pressure vessel. The mixture stirred under argon, in the absence of light, for 19 hours at 130°C. Characterization by LCMS suggested a 1:1 ratio of **15a:15b** without any product (**19g**) formation.

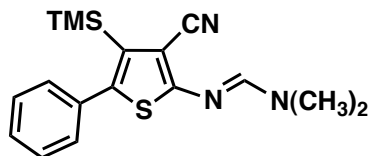
Library parallel synthesis of thieno[2,3-*d*]pyrimidin-4-amine compounds (19)

General protocol for the Suzuki coupling reactions using fragment 14b:



The boronic acid or boronate ester (1.5 eq.), Pd(PPh₃)₄ (0.1 eq.) and fragment **14b** were dissolved in toluene/ethanol (3:1) (approximate concentration with respect to **14b** of 0.1 M). The mixture was degassed and flushed with argon. Aqueous 2M Na₂CO₃ (2.5 eq.) was added and the mixture was again degassed and flushed with argon. The reaction mixture was stirred at 85°C overnight. The crude was filtered through a plug of celite, rinsed with 10 mL of solvent and concentrated under vacuum. The residue was purified on silica gel using a CombiFlash instrument to give the desired products (the common solvent gradient was from 2% EtOAc in hexanes to 100% EtOAc, unless otherwise indicated).

N'-(3-cyano-5-phenyl-4-(trimethylsilyl)thiophen-2-yl)-*N,N*-dimethylformimidamide (**16a**, R₅= a):



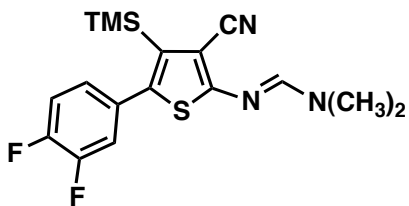
Isolated as a beige solid in 90% yield (179 mg).

^1H NMR (400 MHz, CDCl_3) δ 7.71 (s, 1H), 7.36-7.33 (m, 5H), 3.12 & 3.08 (2s, 6H), 0.12 (s, 9H)

^{13}C NMR (75 MHz, CDCl_3) δ 167.8, 154.6, 139.1, 136.3, 135.9, 130.6, 128.5, 128.1, 118.0, 102.7, 40.7, 35.2, 0.4.

HRMS (ESI+) calculated for $\text{C}_{17}\text{H}_{22}\text{N}_3\text{SSi}$ m/z $[\text{M} + \text{H}]^+$: 328.12982, found m/z 328.12920

N'-(3-cyano-5-(3,4-difluorophenyl)-4-(trimethylsilyl)thiophen-2-yl)-*N,N*-dimethylformimidamide (16b, $\text{R}_5 = \text{c}$):



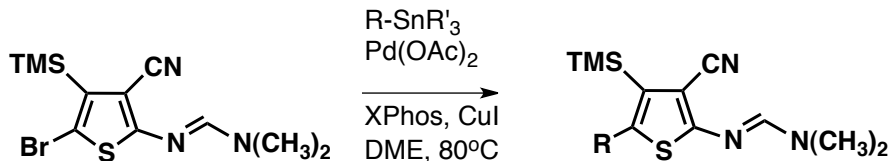
Isolated as an orange solid in 90% yield (231 mg).

^1H NMR (400 MHz, CDCl_3) δ 7.70 (s, 1H), 7.18 – 7.10 (m, 2H), 7.08 – 7.04 (m, 1H), 3.12 (s, 3H), 3.10 (s, 3H), 0.15 (s, 9H)

^{13}C NMR (75 MHz, CDCl_3) δ 168.1, 151.8 (dd, $J_{\text{CF}} = 74, 15$ Hz), 148.5 (dd, $J_{\text{CF}} = 74, 15$ Hz), 137.5, 136.1, 132.8, 127.0, 119.6 (d, $J_{\text{CF}} = 15$ Hz), 117.7, 117.0 (d, $J_{\text{CF}} = 15$ Hz), 102.8, 40.8, 35.2, 0.4

MS (ESI+) m/z 364.21 $[\text{M} + \text{H}]^+$

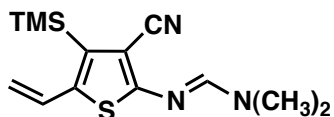
General protocol for Stille cross-coupling reactions using fragment **14b**:



Palladium acetate (1 eq.) and XPhos (2 eq.) in DME (2 mL) were heated under argon to 85°C in a 2-dram vial for 10 min. To this mixture cesium carbonate (2 eq.), copper (I) iodide (1.6 eq.) and fragment **14b** (0.3 mmol) were added and tributyl(vinyl)tin (0.2 mL, 0.53 mmol, 1.8 eq.). The vial was flushed with argon and the reaction mixture was stirred at 80°C for 15 h. The reaction mixture was diluted with EtOAc (10 mL), washed with water (3 x 10 mL) and brine (10 mL), dried over Na₂SO₄, and concentrated under vacuum. The crude residue was purified by column chromatography on silica gel using a CombiFlash instrument and a solvent gradient from 10% EtOAc in hexanes to 100% EtOAc.

N'-(3-cyano-4-(trimethylsilyl)-5-vinylthiophen-2-yl)-*N,N*-dimethylformimidamide

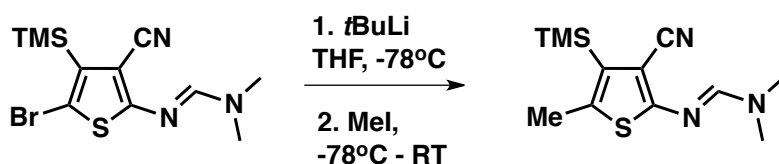
(**16c**, R₅ = i):



Isolated as beige solid in 75% yield (63 mg) and 95% purity (as determined by LCMS). The impurity was determined to be the dehalogenated thiophene. However, this compound (**16c**) was eliminated from the library for the subsequent steps.

^1H NMR (400 MHz, CDCl_3) δ 7.72 (s, 1H), 6.86 (dd, $J = 16.9, 10.8$ Hz, 1H), 5.36 (d, $J = 17.0$ Hz, 1H), 5.10 (d, $J = 10.8$ Hz, 1H), 3.12&3.10 (2bs, 6H), 0.41 (s, 9H)
 ^{13}C NMR (75 MHz, CDCl_3) δ 166.3, 154.8, 138.1, 137.5, 130.7, 117.5, 113.6, 103.0, 40.7, 35.1, 0.8
HRMS (ESI+) calculated for $\text{C}_{13}\text{H}_{20}\text{N}_3\text{SSi}$ m/z $[\text{M} + \text{H}]^+$: 278.11417, found m/z 278.11400

N'-(3-cyano-5-methyl-4-(trimethylsilyl)thiophen-2-yl)-*N,N*-dimethylformimidamide (16d, $R_5 \equiv \text{j}$):



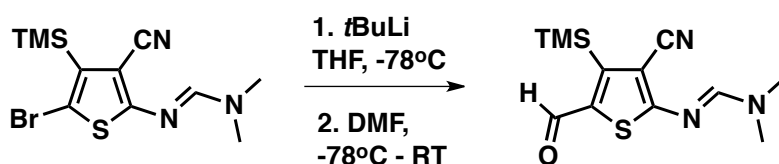
A solution of **14b** (75.2 mg, 0.23 mmol) in THF (4 mL) was cooled to -78°C under argon. To this *t*BuLi (0.3 mL of 1.7 M solution in pentane) was added dropwise and stirred for 5 minutes. Iodomethane (0.1 mL, 1.91 mmol) was added and stirred for 30 minutes at -78°C . The reaction was quenched with NH_4Cl at room temperature. THF was removed *in vacuo* and the red oil was taken up in EtOAc (20 mL) and washed with saturated ammonium chloride solution (10 mL), water (3 x 10 mL), brine (10 mL), and dried over Na_2SO_4 . The crude mixture was purified by flash column chromatography (3 - 80% EtOAc/hex, solid loading) to afford the desired product as an orange solid in 36% yield (22 mg).

^1H NMR (400 MHz, CDCl_3) δ 7.65 (s, 1H), 3.08 (s, 6H), 2.38 (s, 3H), 0.38 (s, 9H)

^{13}C NMR (126 MHz, CDCl_3) δ 165.6, 154.3, 134.6, 134.2, 117.8, 102.0, 40.5, 34.9, 16.9, 0.5

HRMS (ESI+) calculated for $\text{C}_{12}\text{H}_{20}\text{N}_3\text{SSi}$ $[\text{M} + \text{H}]^+$ 266.11417, found 266.11371

N'-(3-cyano-5-formyl-4-(trimethylsilyl)thiophen-2-yl)-*N,N*-dimethylformimidamide (16e, $\text{R}_5 = \text{k}$):



A solution of **14b** (62.8 mg, 0.19 mmol) in THF (5 mL) was cooled to -78°C under argon. To this *t*BuLi (0.2 mL of 1.7 M solution in pentane) was added dropwise and stirred for 5 minutes. Dry DMF (0.1 mL, 0.84 mmol) was added and stirred for 1 h at -78°C and 15 h at RT. The reaction was quenched with NH_4Cl at RT. THF was removed *in vacuo* and the red oil was taken up in EtOAc (20 mL) and washed with saturated ammonium chloride solution (10 mL), water (3 x 10 mL), brine (10 mL), and dried over Na_2SO_4 . The crude mixture was purified by flash column chromatography (3 - 80% EtOAc/hexanes, solid loading) to afford the desired product as an orange solid in 31% yield (16.4 mg).

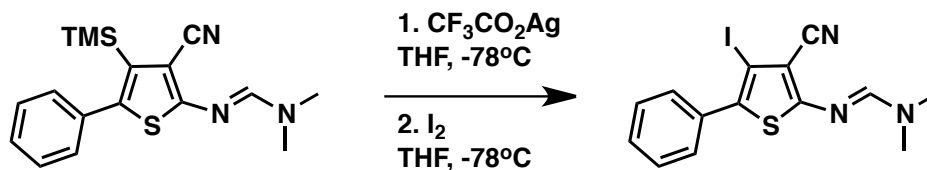
^1H NMR (400 MHz, CDCl_3) δ 9.83 (s, 1H), 7.83 (s, 1H), 3.19 (s, 3H), 3.18 (s, 3H), 0.51 (s, 9H)

^{13}C NMR (75 MHz, CDCl_3) δ 185.6, 182.7, 174.5, 156.2, 154.4, 137.8, 116.5, 41.3, 35.8, 1.1

MS (ESI+) m/z 280.22 $[\text{M} + \text{H}]^+$

N'-(3-cyano-4-iodo-5-phenylthiophen-2-yl)-*N,N*-dimethylformimidamide (17a, R₅

≡ a):



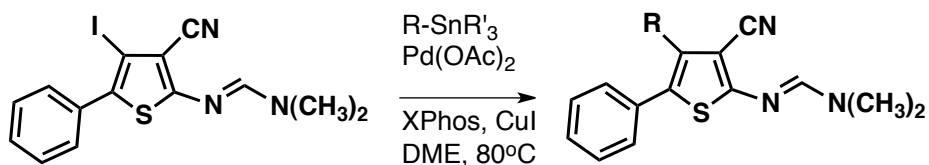
Silver trifluoroacetate (93.2 mg, 0.42 mmol) was added to a solution of *N'*-(3-cyano-5-phenyl-4-(trimethylsilyl)thiophen-2-yl)-*N,N*-dimethylformimidamide (**16a**, 69 mg, 0.21 mmol) in THF (20 mL) cooled to -78°C and stirred under argon for 15 minutes. Iodine (214.2 mg, 0.84 mmol) dissolved in THF (10 mL) was added dropwise to the cold mixture and stirred in the dark at -78°C for 4 h. EtOAc was added and the mixture was filtered through Celite. The filtrate was washed with 2 M sodium thiosulfate, brine, and was dried over Na_2SO_4 . The crude mixture was purified by flash column chromatography (5-30% EtOAc/hex, solid loading) to afford the desired product as an orange solid in 99% yield (80 mg).

^1H NMR (400 MHz, CDCl_3) δ 7.77 (s, 1H), 7.58 – 7.51 (m, 2H), 7.40 (dtd, $J = 6.9, 5.5, 1.5$ Hz, 3H), 3.13 (s, 6H)

^{13}C NMR (75 MHz, CDCl_3) δ 167.2, 154.7, 134.1, 130.7, 129.5, 128.7, 128.6, 116.8, 105.7, 78.1, 40.9, 35.3

HRMS (ESI+) calculated for $\text{C}_{14}\text{H}_{13}\text{N}_3\text{IS}$ m/z $[\text{M} + \text{H}]^+$: 381.98694, found m/z 381.98667

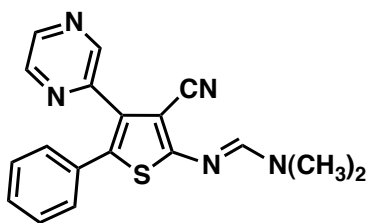
General protocol for Stille cross-coupling reactions using fragment 17a:



Palladium acetate (1 eq.) and XPhos (2 eq.) in DME (2 mL) were heated under argon to 85°C in a 2-dram vial for 10 min. To this mixture was added cesium carbonate (2 eq.), fragment **17a** (1 eq. 0.3 mmol) and stannane (1.77 eq.). The vial was flushed with argon and the reaction mixture was stirred at 80°C for 15 h. The reaction mixture was diluted with EtOAc (10 mL), washed with water (3 x 10 mL) and brine (10 mL), dried over Na₂SO₄, and concentrated under vacuum. The crude residue was purified by column chromatography on silica gel using a CombiFlash instrument and a solvent gradient from % EtOAc in hexanes to 100% EtOAc, unless otherwise indicated.

N'-(3-cyano-5-phenyl-4-(pyrazin-2-yl)thiophen-2-yl)-*N,N*-dimethylformimidamide

(**18a**, R₄ = b, R₅ = a):



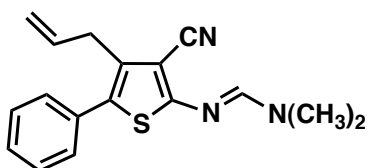
Isolated as beige solid in 41% yield (8.0 mg) and 95% purity (as determined by LCMS).

¹H NMR (400 MHz, CDCl₃) δ 8.67 (dd, *J* = 2.6, 1.6 Hz, 1H), 8.46 (d, *J* = 2.6 Hz, 1H), 8.36 (d, *J* = 1.5 Hz, 1H), 7.85 (s, 1H), 7.28 - 7.25 (m, 3H), 7.17 - 7.14 (m, 2H), 3.15 (2bs, 3H)

^{13}C NMR (126 MHz, CDCl_3) δ 166.9, 154.6, 149.3, 145.8, 144.5, 143.1, 132.7, 132.2, 131.1, 129.4, 129.1, 128.5, 115.9, 99.2, 40.9, 35.3

HRMS (ESI+) calculated for $\text{C}_{18}\text{H}_{16}\text{N}_5\text{S}$ m/z $[\text{M} + \text{H}]^+$: 334.11209, found m/z 334.11144

N'-(4-allyl-3-cyano-5-phenylthiophen-2-yl)-*N,N*-dimethylformimidamide (**18b**, $\text{R}_4 = \text{H}$, $\text{R}_5 = \text{a}$):



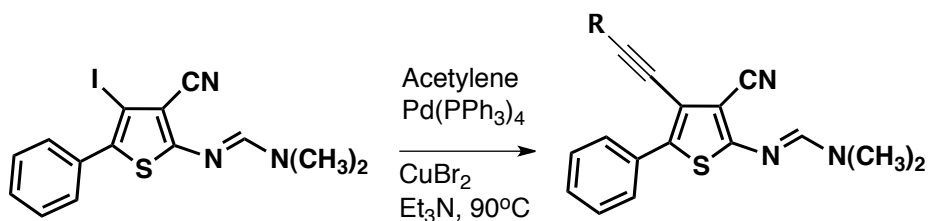
Isolated as a mixture of the desired product and the dehalogenated thiophene (20% by ^1H NMR) in 115% yield (10 mg). This compound (**18b**) was eliminated from the library for the subsequent steps.

^1H NMR (500 MHz, CDCl_3) δ 7.78 (s, 1H), 7.44 – 7.35 (m, 4H), 6.02 (ddd, $J = 22.7, 10.3, 5.6$ Hz, 1H), 5.16 (dd, $J = 10.2, 1.5$ Hz, 1H), 5.09 (dd, $J = 17.1, 1.6$ Hz, 1H), 3.40 (dd, $J = 3.9, 1.7$ Hz, 2H), 3.12 (s, 3H), 3.11 (s, 3H)

^{13}C NMR (126 MHz, CDCl_3) δ 165.5, 154.3, 135.5, 133.4, 128.9, 128.8, 127.8, 127.5, 116.7, 116.3, 100.3, 40.8, 35.3, 35.2, 32.3

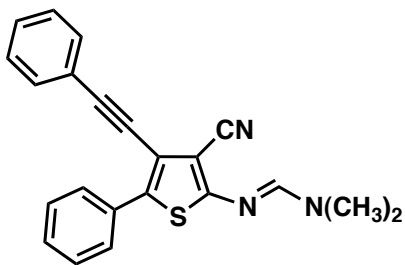
MS (ESI+) m/z 296.2 $[\text{M} + \text{H}]^+$

Protocol A for Sonogashira cross-coupling reactions using fragment 17a:



Triethylamine (0.5 mL) was added to a vial of the iodide **17a** (0.1 mmol), acetylene (0.02 mL, 0.16 mmol), copper (II) bromide (2.7 mg, 0.012 mmol), and Pd(PPh₃)₄ (9.4 mg, 0.008 mmol). The vial was purged with argon, capped, and heated to 90°C for 13 h. Extracted with EtOAc (3x10 mL) and washed with saturated sodium bicarbonate (5 mL), water (3 x 5 mL), brine (5 mL), and dried over Na₂SO₄. The crude mixture was purified by flash column chromatography on silica gel (solid loading) using a solvent gradient from 2% EtOAc in hexanes to 100% EtOAc (unless otherwise indicated) to afford the desired product.

N'-(3-cyano-5-phenyl-4-(phenylethynyl)thiophen-2-yl)-*N,N*-dimethylformimidamide (**18c**, R₄ = d, R₅ = a):



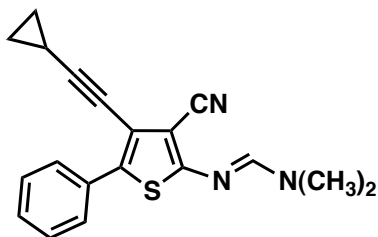
Isolated as a red-orange solid in 95% yield (28 mg).

¹H NMR (400 MHz, CDCl₃) δ 7.86 (d, *J* = 7.4 Hz, 2H), 7.83 (s, 1H), 7.57 – 7.51 (m, 2H), 7.42 (t, *J* = 7.5 Hz, 2H), 7.37 – 7.30 (m, 4H), 3.15 (2bs, 6H)

¹³C NMR (126 MHz, CDCl₃) δ 164.2, 154.6, 134.0, 133.3, 131.9, 128.8, 128.7, 128.5, 128.2, 127.5, 122.9, 116.6, 115.5, 100.9, 94.7, 83.3, 40.9, 35.3

HRMS (ESI+) calculated for C₂₂H₁₈N₃S m/z [M + H]⁺: 356.12159, found m/z 356.12098

N'-(3-cyano-4-(cyclopropylethynyl)-5-phenylthiophen-2-yl)-*N,N*-dimethylformimidamide (18d, R₄ = e, R₅ = a):



Isolated beige solid in 90% yield (15 mg, based on the recovery of starting material).

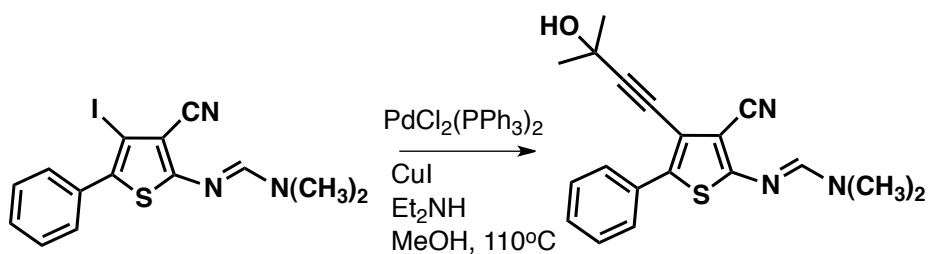
¹H NMR (500 MHz, CDCl₃) δ 7.78 – 7.75 (m, 3H), 7.37 (dd, J = 10.7, 4.9 Hz, 2H), 7.30 – 7.26 (m, 1H), 3.10 (s, 6H), 1.49 (tt, J = 8.0, 5.2 Hz, 1H), 0.91 – 0.87 (m, 2H), 0.87 – 0.83 (m, 2H)

¹³C NMR (126 MHz, CDCl₃) δ 163.8, 154.5, 133.30, 132.9, 128.6, 127.9, 127.1, 117.2, 115.6, 101.4, 99.6, 69.4, 40.9, 35.2, 9.15, 0.7

HRMS (ESI+) calculated for C₁₉H₁₈N₃S m/z [M + H]⁺: 320.12159, found m/z 320.12139

Protocol B for Sonogashira cross-coupling reactions using fragment 17a:

N'-(3-cyano-4-(3-hydroxy-3-methylbut-1-yn-1-yl)-5-phenylthiophen-2-yl)-*N,N*-dimethylformimidamide (18e, R₄ = f, R₅ = a)



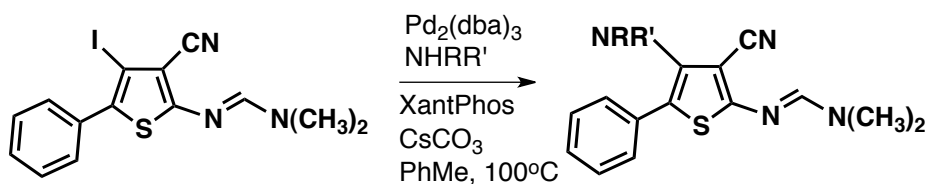
To a 2 mL microwave vial of **17a** (35.9 mg, 0.09 mmol), PdCl₂(PPh₃)₂ (3.3 mg, 0.005 mmol), 2-methyl-3-butyn-2-ol (0.01 mL, 0.11 mmol), and copper (I) iodide (0.9 mg, 0.005 mmol) was added MeOH (0.4 mL) and diethylamine (0.2 mL). The mixture was stirred and heated in a Biotage reactor to 110°C for 20 min. Extracted with EtOAc, washed with water (3 x 5 mL), brine (5 mL), and dried over Na₂SO₄. The crude mixture was purified by flash column chromatography (2 - 100% EtOAc/hexanes, solid loading) to afford the desired product as a yellow solid in 66% yield (21 mg).

¹H NMR (400 MHz, CDCl₃) δ 7.79 (s, 1H), 7.76 (m, 2H), 7.41 – 7.36 (m, 2H), 7.33 – 7.29 (m, 1H), 3.13 (s, 6H), 2.04 (s, 1H), 1.63 (s, 6H)

¹³C NMR (126 MHz, CDCl₃) δ 163.9, 154.4, 134.1, 133.0, 128.6, 128.1, 127.2, 115.8, 115.2, 100.8, 98.9, 75.9, 65.8, 40.8, 35.2, 31.2

MS (ESI+) *m/z* 338.2 [M+H]⁺

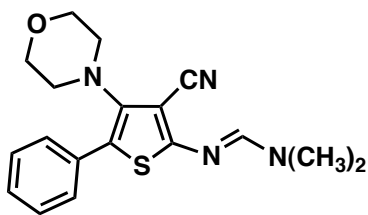
General protocol for Buchwald-Hartwig amination reactions using fragment **17a**:



The amine (5 eq.) was added to a degassed solution of fragment **17a** (~ 0.03 mmol scale), Pd₂(dba)₃ (5 mole%), XantPhos (11 mole%), and cesium carbonate (1.7 eq.) in toluene (1 mL). The vial was purged with argon and the reaction mixture stirred at 100°C for 18 h. A second portion of Pd₂(dba)₃ (5 mole%) and XantPhos (11 mole%) were added and the reaction mixture was stirred at 100°C for an additional 18 h. The reaction mixture was diluted with EtOAc (10 mL), washed with water (3 x 10 mL) and brine (10 mL), dried over Na₂SO₄, and concentrated under vacuum. The crude residue was purified by column chromatography on silica gel using a CombiFlash instrument and a solvent gradient from 2% EtOAc in hexanes to 100% EtOAc (unless otherwise indicated) to afford the desired product.

N'-(3-cyano-4-morpholino-5-phenylthiophen-2-yl)-*N,N*-dimethylformimidamide

(**18f**, R₄ = g, R₅ = a):



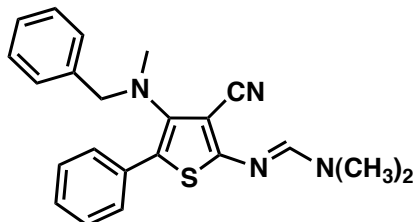
Isolated as a beige solid in 90% yield (10 mg).

¹H NMR (500 MHz, CDCl₃) δ 7.74 (s, 1H), 7.50 (d, *J* = 7.3 Hz, 2H), 7.35 (t, *J* = 7.5 Hz, 2H), 7.29 (d, *J* = 7.3 Hz, 1H), 3.75 – 3.71 (m, 4H), 3.12 (s, 3H), 3.10 (s, 3H), 3.10 – 3.07 (m, 4H)

¹³C NMR (126 MHz, CDCl₃) δ 164.4, 153.9, 143.8, 133.6, 129.3, 128.4, 127.6, 118.4, 116.3, 96.6, 67.5, 51.7, 40.9, 35.2

HRMS (ESI+) calculated for C₁₈H₂₁ON₄S m/z [M + H]⁺: 341.14306, found m/z 341.14218

N'-(4-(benzyl(methyl)amino)-3-cyano-5-phenylthiophen-2-yl)-*N,N*-dimethylformimidamide (18g, R₄ = h, R₅ = a):



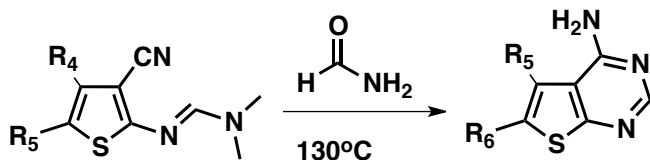
The crude residue was purified by column chromatography on a CombiFlash instrument using a solvent gradient from 3% EtOAc/Hexanes to 100% EtOAc with 0.1% triethylamine. The desired product was obtained in 45% yield (19 mg), 70% purity (as determined by ¹H NMR). The impurity was determined to be the dehalogenated thiophene, which was eliminated in the following step.

¹H NMR (400 MHz, CDCl₃) δ 7.76 (s, 1H), 7.50 – 7.44 (m, 1H), 7.38 – 7.27 (m, 5H), 7.25 – 7.21 (m, 4H), 4.16 (s, 2H), 3.14 – 3.07 (m, 6H), 2.74 (s, 3H)

¹³C NMR (75 MHz, CDCl₃) δ 164.2, 153.9, 144.6, 138.4, 133.7, 129.1, 128.9, 128.3, 128.2, 127.6, 127.3, 127.1, 125.3, 121.9, 120.1, 116.6, 96.9, 60.1, 41.1, 35.2

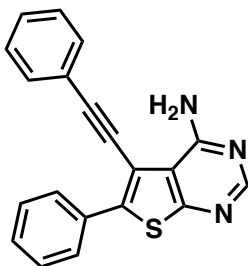
HRMS (ESI+) calculated for C₂₂H₂₃N₄S m/z [M + H]⁺: 375.16379, found m/z 375.16296

General protocol for the cyclization of C-4 and C-5 substituted fragments 18 to thieno[2,3-d]pyrimidin-4-amines 19:



The di-substituted fragments **18** (typically, 0.04 mmol) and dry formamide (excess, >200 eq.) were added to a dry 15 mL pressure vessel. The vessel was flushed with argon and the mixture stirred at 130°C for 48 h. The dark red solution was diluted with EtOAc, washed with water (25 mL), brine (10 mL), and dried over Na₂SO₄. The crude mixture was purified by flash column chromatography (5 - 100% EtOAc/hex, solid loading) to afford the desired product.

6-phenyl-5-(phenylethynyl)thieno[2,3-d]pyrimidin-4-amine (**19a**):



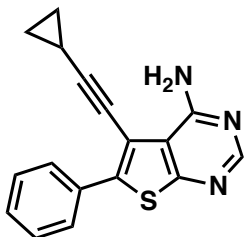
Isolated as a brown solid in 85% yield (12 mg).

¹H NMR (500 MHz, CDCl₃) δ 8.45 (s, 1H), 7.96- 7.94 (m, 1H), 7.94- 7.93 (m, 1H), 7.51- 7.47 (m, 4H), 7.45 - 7.37 (m, 4H), ~6.30 (br, 2H)

¹³C NMR (126 MHz, CDCl₃) δ 165.3, 158.4, 154.6, 143.9, 133.0, 131.4, 129.4, 129.3, 129.0, 128.9, 128.6, 122.0, 116.5, 108.8, 94.8, 85.2

HRMS (ESI⁺) calculated for C₂₀H₁₄N₃S *m/z* [M + H]⁺: 328.09029, found *m/z* 328.09015

5-(cyclopropylethynyl)-6-phenylthieno[2,3-d]pyrimidin-4-amine (19b):



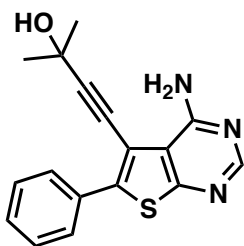
Isolated as a beige solid in 85% yield (11 mg).

^1H NMR (500 MHz, CDCl_3) δ 8.39 (s, 1H), 7.88-7.81 (m, 2H), 7.49-7.35 (m, 3H), 1.52 (tt, $J = 8.2, 5.0$ Hz, 1H), 0.98 - 0.92 (m, 2H), 0.84 (m, 2H)

^{13}C NMR (126 MHz, CDCl_3) δ 164.9, 158.4, 154.4, 143.0, 133.1, 129.1, 128.8, 128.4, 116.7, 109.3, 99.5, 71.6, 8.8, 0.6

HRMS (ESI+) calculated for $\text{C}_{17}\text{H}_{14}\text{N}_3\text{S}$ m/z $[\text{M} + \text{H}]^+$: 292.09029, found m/z 292.09030

4-(4-amino-6-phenylthieno[2,3-d]pyrimidin-5-yl)-2-methylbut-3-yn-2-ol (19c):

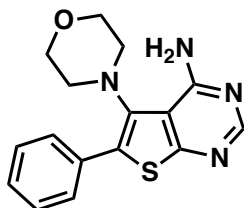


Isolated the desired product in >100% yield (10 mg, product not stable and releases acetone). This compound (**19c**) was eliminated from the library for the subsequent steps.

^1H NMR (500 MHz, CD_3OD) δ 8.29 (s, 1H), 7.90 (d, $J = 7.3$ Hz, 2H), 7.47 (dt, $J = 24.9, 7.2$ Hz, 3H), 5.49 (s, 6H)

^{13}C NMR (126 MHz, CD_3OD) δ 165.2, 160.2, 155.2, 144.2, 133.8, 130.5, 129.9, 129.4, 109.9, 101.8, 77.9, 66.1, 54.8, 31.3
MS (ESI+) m/z 310.2 $[\text{M} + \text{H}]^+$

5-morpholino-6-phenylthieno[2,3-d]pyrimidin-4-amine (19d):



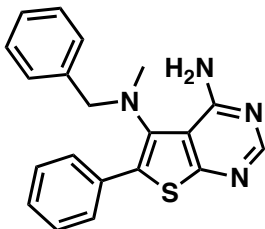
The crude mixture was purified by flash column chromatography (5 - 100% EtOAc/hexanes with 0.1% Et_3N , solid loading) to afford the desired product as a beige solid in 50% yield (21 mg).

^1H NMR (500 MHz, CDCl_3) δ 8.42 (s, 1H), 7.49 - 7.41 (m, 5H), 3.84 (d, $J = 10.6$ Hz, 2H), 3.60 (td, $J = 11.5, 2.3$ Hz, 2H), 3.03 (td, $J = 11.6, 2.8$ Hz, 2H), 2.95 (d, $J = 11.8$ Hz, 2H), 1.60 (s, 1H)

^{13}C NMR (126 MHz, CDCl_3) δ 164.5, 158.8, 154.3, 138.3, 133.4, 131.2, 131.0, 129.2, 128.6, 113.9, 67.8, 53.2

HRMS (ESI+) calculated for $\text{C}_{16}\text{H}_{17}\text{ON}_4\text{S}$ m/z $[\text{M} + \text{H}]^+$: 313.11176, found m/z 313.11125

*N*⁵-benzyl-*N*⁵-methyl-6-phenylthieno[2,3-*d*]pyrimidine-4,5-diamine (19e):



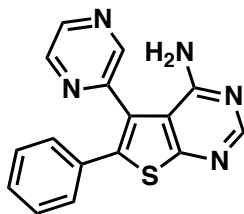
The crude mixture was purified by flash column chromatography (5 - 100% EtOAc/hexanes with 0.1% Et₃N, solid loading) to afford the desired product as a pale orange solid in 53% yield (9 mg).

¹H NMR (500 MHz, CDCl₃) δ 8.41 (s, 1H), 7.47 - 7.36 (m, 5H), 7.29 - 7.21 (m, 3H), 7.12 - 7.06 (m, 2H), 3.99 (d, *J* = 13.3 Hz, 1H), 3.66 (d, *J* = 13.3 Hz, 1H), 2.77 (s, 3H)

¹³C NMR (126 MHz, CDCl₃) δ 164.4, 158.6, 154.3, 139.3, 138.1, 133.7, 130.8, 130.6, 128.9, 128.9, 128.7, 128.5, 127.7, 114.2, 60.7, 43.5

HRMS (ESI+) calculated for C₂₀H₁₉N₄S *m/z* [M + H]⁺: 347.13249, found *m/z* 347.13188

6-phenyl-5-(pyrazin-2-yl)thieno[2,3-*d*]pyrimidin-4-amine (19f):



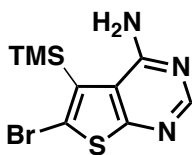
Isolated as a beige solid in 95% yield (7 mg).

^1H NMR (500 MHz, CDCl_3) δ 8.68 (dd, $J = 2.6, 1.5$ Hz, 1H), 8.50 (d, $J = 2.6$ Hz, 1H), 8.48 (s, 1H), 8.29 (d, $J = 1.4$ Hz, 1H), 7.36 - 7.30 (m, 3H), 7.22 - 7.19 (m, 2H)

^{13}C NMR (126 MHz, CDCl_3) δ 167.3, 159.1, 154.1, 150.8, 149.0, 143.1, 143.0, 141.9, 132.9, 130.2, ~129.4 (3 x C), 126.1, 115.9

HRMS (ESI+) calculated for $\text{C}_{16}\text{H}_{12}\text{N}_5\text{S}$ m/z $[\text{M} + \text{H}]^+$: 306.08079, found m/z 306.08165

6-bromo-5-(trimethylsilyl)thieno[2,3-d]pyrimidin-4-amine (19g):



Was not isolated, too impure for characterization. Evidence of formation was suggested by LCMS analysis (Table 1.6).

1.5 Acknowledgements

A majority of the work in this chapter is from a manuscript in preparation with authors: Chun-Yuen Leung, Dr. John Mancuso, and Prof. Youla S. Tsantrizos. Thank you to J.M. for pioneering this project as well as the synthesis of **12** and **13** (Scheme 1.9). Chun-Yeun Leung's work focused on the mono-substitution of **15a** (Scheme 1.9) at the C5 (β to the sulfur atom) position of the thienopyrimidine for publication.

1.6 References

1. Satyanarayanajois, S. D.; Hill, R. A. Medicinal chemistry for 2020. *Future Med. Chem.* **2011**, *3*, 1765–1786.
2. Rawlins, M. D. M. Cutting the cost of drug development? *Nature Rev. Drug Discov.* **2004**, *3*, 360–364.
3. (a) Collier, R. Rapidly rising clinical trial costs worry researchers. *CMAJ.* **2009**, *180*, 277–278. (b) Collier, R. Drug development cost estimates hard to swallow. *CMAJ*, **2009**, *180*, 279–280.
4. Arnott, J. A.; Planey, S. L. The influence of lipophilicity in drug discovery and design. *Expert Opin. Drug Discov.* **2012**, *7*, 863–875.
5. Palucki, M. Higgins, J. D.; Kwong, E.; Templeton, A. C. Strategies at the Interface of Drug Discovery and Development: Early Optimization of the Solid State Phase and Preclinical Toxicology Formulation for Potential Drug Candidates. *J. Med. Chem.* **2010**, *53*, 5897–5905.
6. Di, L.; Kerns, E. H.; Carter, G. T. Drug-like Property Concepts in Pharmaceutical design. *Curr. Pharma. Des.* **2009**, *15*, 2184-2194.
7. Viswanadhan, V. N.; Balan, C.; Hulme, C.; Cheetham, J. C.; Sun, Y. Knowledge-based Approaches in the design and selection of compound libraries for drug discovery. *Curr. Opin. Drug Discov. Develop.* **2002**, *5*, 400-406.
8. Meanwell, N. A. Improving Drug Candidates by Design: A Focus on Physicochemical Properties As a Means of Improving Compound Disposition and Safety. *Chem. Res. Toxicol.* **2011**, *24*, 1420–1456.

-
9. Lipinski, C. A.; Lombardo, F.; Dominy, B. W.; Feeney, P. J. Experimental and computational approaches to estimate solubility and permeability in drug discovery and development settings. *Adv. Drug Delivery Rev.* **1997**, *23*, 3–25.
10. Gleeson, M. P.; Hersey, A.; Montanari, D.; Overington, J. Probing the links between in vitro potency, ADMET and physicochemical parameters. *Nature Rev. Drug Discov.* **2011**, *10*, 197–208.
11. (a) Veber D. F.; Johnson S. R.; Cheng H. Y.; Smith B. R.; Ward, K. W.; Kopple, K. D. Molecular properties that influence the oral bioavailability of drug candidates. *J. Med. Chem.* **2002**, *45*, 2615-23. (b) Leeson, P.; Springthorpe, B. The influence of drug-like concepts on decision-making in medicinal chemistry. *Nature Rev. Drug Discov.* **2007**, *6*, 881–890. (c) Gleeson M. P. Generation of a set of simple, interpretable ADMET rules of thumb. *J. Med. Chem.* **2008**, *51*, 817-34. (d) Johnson, T. J.; Dress, K. R.; Edwards, M. Using the Golden Triangle to optimize clearance and oral absorption. *Bioorg. Med. Chem. Lett.* **2009**, *19*, 5560–5564. (e) Tyrchana, C.; Blomberg, N.; Engkvista, O.; Kogej, T.; Muresan, S. Physicochemical property profiles of marketed drugs, clinical candidates and bioactive compounds. *Bioorg. Med. Chem. Lett.* **2009**, *19*, 6943–6947. (f) Ritchie, T. J.; Macdonald, S. J. F. The impact of aromatic ring count on compound developability - are too many aromatic rings a liability in drug design? *Drug Discov. Today*, **2009**, *14*, 1011-1020. (g) Lovering, F.; Bikker, J.; Humblet, C. Escape from flatland: increasing saturation as an approach to improving clinical success. *J. Med. Chem.* **2009**, *52*, 6752-6756. (h) Tian S.; Li Y.; Wang J.; Zhang, J.; Hou, T. ADME evaluation in drug discovery. 9. Prediction of oral

bioavailability in humans based on molecular properties and structural fingerprints. *Mol. Pharm.* **2011**, *8*, 841-51. (i) Leeson P. D.; St-Galley S. A. The influence of the 'organizational factor' on compound quality in drug discovery. *Nature Rev. Drug Discov.* **2011**, *10*, 749-65.

12. Lipinski, C.; Hopkins, A. Navigating chemical space for biology and medicine. *Nature* **2004**, *432*, 855-861.

13. Martin, E. J.; Critchlow, R. E. Beyond Mere Diversity: Tailoring Combinatorial Libraries for Drug Discovery. *J. Comb. Chem.* **1999**, *1*, 32-45.

14. Lajiness, M. S. M.; Vieth, M. M.; Erickson, J. J. Molecular properties that influence oral drug-like behavior. *Curr. Opin. Drug Discov. Dev.* **2004**, *7*, 470-477.

15. (a) Bemis, G. W.; Murcko, M. A. The properties of known drugs. 1. Molecular frameworks. *J. Med. Chem.* **1996**, *39*, 2887-2893. (b) Bemis, G. W.; Murcko, M. A. Properties of Known Drugs. 2. Side Chains. *J. Med. Chem.* **1999**, *42*, 5095-5099. (c) Ghose, A. K.; Viswanadhan, V. N.; Wendoloski, J. J. A Knowledge-Based Approach in Designing Combinatorial or Medicinal Chemistry Libraries for Drug Discovery. 1. A Qualitative and Quantitative Characterization of Known Drug Databases. *J. Com. Chem.* **1999**, *1*, 55-68.

16. (a) Marugan, J. J.; Zheng, W.; Southall, N.; Huang, W.; McCoy, J. G.; Titus, S.; Patnaik, S. WO **2012**/044993. (b) Brewster, W. K.; Demeter, D. A.; Erickson, W. R.; Klittich, C. J. R.; Lowe, C.T.; Rieder, B. J.; Nugent, J. S.; Yerkes, C. N.; Zhu, Y. WO **2007**/046809. (c) Brewster, W. K.; Klittich, C. J. R.; Balko, T. W.;

Breax, N. T.; Erickson, W. R.; Hunter, J. E.; Lowe, C. T.; Ricks, M. J.; Siddall, T. L.; Yerkes, C. N.; Zhu, Y. US Patent Application **2006/0089370**.

17. Tani, N.; Rahnasto-Rilla, M.; Wittekindt, C.; Salminen, K.A.; Ritvanen, A.; Ollakka, R.; Koskiranta, J.; Raunio, H.; Juvonen, R. O. Antifungal activities of novel non-azole molecules against *S. cerevisiae* and *C. albicans*. *Eur. J. Med. Chem.* **2012**, *47*, 270-277.

18. Babu, Y.; Chand, P.; Wu, M.; Kotian, P. L.; Kumar, V. S.; Lin, T.-H.; El-Kattan, Y.; Ghosh, A. K. WO **2006/050161**.

19. (a) Jorda, R. R.; Paruch, K. K.; Krystof, V. V. Cyclin-dependent kinase Inhibitors Inspired by Roscovitine: Purine Bioisosteres. *Curr. Pharm. Des.* **2012**, *18*, 2974–2980. (b) Garcia, I.; Feist, H.; Cao, R.; Michalik, M.; Peseke, K. Synthesis of (2,3,4,6-Tetra-O-Acetyl- α -D-Glycopyranosyl) Thiophene Derivatives as new C-Nucleoside Analogues. *J. Carbohydr. Chem.* **2001**, *20*, 681–687. (c) Herrera, L.; Feist, H.; Quincoces, J.; Michalik, M.; Peseke, K. Synthesis of (Methyl 3-O-Benzyl-4,6-O-benzylidene-2-deoxy- α -d-altropyranosid-2-yl)thiophene Derivatives as Precursors of New Iso-C-nucleoside Analogues. *J. Carbohydr. Chem.* **2003**, *22*, 171–178. (d) Waechter, H.; Fuentes, D. P.; Suarez, J. A. Q.; Michalik, D.; Villinger, A.; Kragl, U.; Vogelb, C. A versatile approach to novel homo-C-nucleosides based on aldehydes and acetylenic ketones derived from ribo- and 2-deoxy-ribofuranose C-glycosides. *ARKIVOC*, **2012**, *3*, 110–133.

20. (a) Edgar, K. A.; Wallin, J. J.; Berry, M.; Lee, L. B.; Prior, W. W.; Sampath, D.; Friedman, L. S.; Belvin, M. Isoform-Specific Phosphoinositide 3-Kinase

Inhibitors Exert Distinct Effects in Solid Tumors. *Cancer Res.* **2010**, *70*, 1164-1172. (b) Heffron, T. P.; Wei, B. Q.; Olivero, A.; Staben, S. T.; Tsui, V.; Do, S.; Dotson, J.; Folkes, A. J.; Goldsmith, P.; Goldsmith R.; Gunzner, J.; Lesnick, J.; Lewis, C.; Mathieu, S.; Nonomiya, J.; Shuttleworth, S.; Sutherlin, D. P.; Wan, N. C.; Wang, S.; Wiesmann, C.; Zhu, B.-Y. Rational design of phosphoinositide 3-kinase α inhibitors that exhibit selectivity over the phosphoinositide 3-kinase β isoform. *J. Med. Chem.* **2011**, *54*, 7815-7833.

21. McClellan, W. J.; Dai, Y.; Abad-Zapatero, C.; Albert, D. H.; Bouska, J. J.; Glaser, K. B.; Magoc, T. J.; Marcotte, P. A.; Osterling, D. J.; Stewart, K. D.; Davidsen, S. K.; Michaelides, M. R. Discovery of potent and selective thienopyrimidine inhibitors of Aurora kinases. *Bioorg. Med. Chem. Lett.* **2011**, *21*, 5620-5624.

22. Rheault, T. R.; Ceferro, T. R.; Dickerson, S. H.; Donaldson, K. H.; Gaul, M. D.; Goetz, A. S.; Mullin, R. J.; McDonald, O. B.; Petrov, K. G.; Rusnak, D. W.; Shewchuk, L. M.; Spehar, G. M.; Truesdale, A. T.; Vanderwall, D. E.; Wood, E. R.; Uehling, D. E. Thienopyrimidine-based dual EGFR/ErbB-2 inhibitors. *Bioorg. Med. Chem. Lett.* **2009**, *19*, 817-820.

23. (a) Dai, Y.; Guo, Y.; Frey, R. R.; Ji, Z.; Curtin, M. L.; Ahmed, A. A.; Albert, D. H.; Arnold, L.; Arries, S. S.; Barlozzari, T.; Bauch, J. L.; Bouska, J. J.; Bousquet, P. F.; Cunha, G. A.; Glaser, K. B.; Guo, J.; Li, J.; Marcotte, P. A.; Marsh, K. C.; Moskey, M. D.; Pease, L. J.; Stewart, K. D.; Stoll, V. S.; Tapang, P.; Wishart, N.; Davidsen, S. K.; Michaelides, M. R. Thienopyrimidine Ureas as Novel and Potent Multi-targeted Receptor Tyrosine Kinase Inhibitors. *J. Med.*

Chem. **2005**, *48*, 6066-6083. (b) Luke, R. W.; Ballard, P.; Buttar, D.; Campbell, L.; Curwen, J.; Emery, S. C.; Griffen, A. M.; Hassall, L.; Hayter, B. R.; Jones, C. D.; McCoull, W.; Mellor, M.; Swain, M. L.; Tucker, J. A. Novel thienopyrimidine and thiazolopyrimidine kinase inhibitors with activity against Tie-2 *in vitro* and *in vivo*. *Bioorg. Med. Chem. Lett.* **2009**, *19*, 6670-6674.

24. (a) Axten, J. M.; Medina, J. R.; Feng, Y.; Shu, A.; Romeril, S. P.; Grant, S. W.; Li, W. H. H.; Heerding, D. A.; Minthorn, E.; Mencken, T.; *et al.* Discovery of 7-Methyl-5-(1-{{3-(trifluoromethyl)phenyl}acetyl}-2,3-dihydro-1 H-indol-5-yl)-7 H-pyrrolo[2,3- *d*]pyrimidin-4-amine (GSK2606414), a Potent and Selective First-in-Class Inhibitor of Protein Kinase R (PKR)-like Endoplasmic Reticulum Kinase (PERK). *J. Med. Chem.* **2012**, *55*, 7193–7207. (b) Axten, J. M.; Grant, S. W.; Heerding, D. A.; Medina, J. R.; Romeril, S. P.; Tang, J. WO **2011**/119663.

25. Horiuchi, T.; Chiba, J.; Uoto, K.; Soga, T. Discovery of novel thieno[2,3-*d*]pyrimidin-4-yl hydrazone-based inhibitors of Cyclin D1-CDK4: Synthesis, biological evaluation, and structure–activity relationships. *Bioorg. Med. Chem. Lett.* **2009**, *19*, 305-308.

26. Sleebs, B. E.; Nikolakopoulos, G.; Street, I. P.; Falk, H.; Baell, J. B. Identification of 5,6-substituted 4-aminothieno[2,3-*d*]pyrimidines as LIMK1 inhibitors. *Bioorg. Med. Chem. Lett.* **2011**, *21*, 5992–5994.

27. (a) Norman, R. A.; Toader, D.; Ferguson, A. D. Structural approaches to obtain kinase selectivity. *Trends Pharmacol. Sci.* **2012**, *33*, 273–278. (b) Endicott, J. A.; Noble, M. E. M.; Johnson, L. N. The Structural Basis for Control of Eukaryotic Protein Kinases. *Annu. Rev. Biochem.* **2012**, *81*, 587–613. (c)

Cargnello, M.; Roux, P. P. Activation and Function of the MAPKs and Their Substrates, the MAPK-Activated Protein Kinases. *Microbiol. Mol. Biol. Rev.* **2011**, *75*, 50–83. (d) Noble, M. E. M.; Endicott, J. A.; Johnson, L. N. Protein kinase inhibitors: insights into drug design from structure. *Science*, **2004**, *303*, 1800–1805. (e) Gschwind, A.; Zwick, E.; Prenzel, N.; Leserer, M.; Ullrich, A. Cell communication networks: epidermal growth factor receptor transactivation as the paradigm for interreceptor signal transmission. *Oncogene*, **2001**, *20*, 1594–1600.

28. Osaki, M. M.; Oshimura, M. M.; Ito, H. H. PI3K-Akt pathway: its functions and alterations in human cancer. *Apoptosis*, **2004**, *9*, 667–676. Edgar, K. A.; Wallin, J. J.; Berry, M.; Lee, L. B.; Prior, W. W.; Sampath, D.; Friedman, L. S.; Belvin, M. Isoform-Specific Phosphoinositide 3-Kinase Inhibitors Exert Distinct Effects in Solid Tumors. *Cancer Res.* **2010**, *70*, 1164–1172.

29. Cavener, D. R.; Gupta, S.; McGrath, B. C. PERK in beta cell biology and insulin biogenesis. *Trends Endocrin. Met.* **2010**, *21*, 714–721.

30. (a) Lee, J. C.; Laydon, J. T.; McDonnell, P. C.; Gallagher, T. F.; Kumar, S.; Green, D.; McNulty, D.; Blumenthal, M. J.; Keys, J. R.; Land vatter, S. W.; Strickler, J. E.; McLaughlin, M. M.; *et al.* A protein kinase involved in the regulation of inflammatory cytokine biosynthesis. *Nature*. **1994**, *372*, 739–746. (b) Mourey, R. J.; Burnette, B. L.; Brustkern, S. J.; Daniels, J. S.; Hirsch, J. L.; Hood, W. F.; Meyers, M. J.; Mnich, S. J.; Pierce, B. S.; Saabye, M. J.; *et al.* A benzothioephene inhibitor of mitogen-activated protein kinase-activated protein kinase 2 inhibits tumor necrosis factor alpha production and has oral anti-

inflammatory efficacy in acute and chronic models of inflammation. *J. Pharmacol. Exp. Ther.* **2010**, *333*, 797–807. (c) Ronkina, N.; Menon, M. B.; Schwermann, J.; Tiedje, C.; Hitti, E.; Kotlyarov, A.; Gaestel, M. MAPKAP kinases MK2 and MK3 in inflammation: Complex regulation of TNF biosynthesis via expression and phosphorylation of tristetraprolin. *Biochem. Pharmacol.* **2010**, *80*, 1915–1920.

31. (a) Hegen, M.; Gaestel, M.; Nickerson-Nutter, C. L.; Lin, L. L.; Telliez, J. B. MAPKAP kinase 2- deficient mice are resistant to collagen-induced arthritis. *J. Immunol.* **2006**, *177*, 1913–1917. (b) Cuadrado, A.; Nebreda, A. R. Mechanisms and functions of p38 MAPK signalling. *Biochem. J.* **2010**, *429*, 403–417.

32. (a) Chong, Z. Z.; Shang, Y. C.; Wang, S.; Maiese, K. A Critical Kinase Cascade in Neurological Disorders: PI 3-K, Akt, and mTOR. *Future Neurol.* **2012**, *7*, 733–748. (b) Nicolia, V.; Fuso, A.; Cavallaro, R. A.; Di Luzio, A.; Scarpa, S. B vitamin deficiency promotes tau phosphorylation through regulation of GSK3 β and PP2A. *J. Alzheimers Dis.* **2010**, *19*, 895–907. (c) Schaffer, B. A. J.; Bertram, L.; Miller, B. L.; Mullin, K.; Weintraub, S.; Johnson, N.; Bigio, E. H.; *et al.* Association of GSK3 β with Alzheimer disease and frontotemporal dementia. *Arch. Neurol-Chicago.* **2008**, *65*, 1368–1374. (d) Vohra, B. P. S.; Fu, M.; Heuckeroth, R. O. Protein Kinase C and Glycogen Synthase Kinase-3 Control Neuronal Polarity in Developing Rodent Enteric Neurons, whereas SMAD Specific E3 Ubiquitin Protein Ligase 1 Promotes Neurite Growth But Does Not Influence Polarity. *J. Neurosci.* **2007**, *27*, 9458–9468. (e) Goold, R. G.; Gordon-Weeks, P. R. The MAP kinase pathway is upstream of the activation of GSK3 β

that enables it to phosphorylate MAP1B and contributes to the stimulation of axon growth. *Mol. Cell. Neurosci.* **2005**, *28*, 524–534. (f) Jope, R. S.; Johnson, G. V. W. The glamour and gloom of glycogen synthase kinase-3. *Trends Biochem. Sci.* **2004**, *29*, 95–102. (g) Geschwind, D. H. Tau phosphorylation, tangles, and neurodegeneration: the chicken or the egg? *Neuron* **2003**, *40*, 457–460.

33. (a) Raven, J. F.; Koromilas, A. E. PERK and PKR: old kinases learn new tricks. *Cell Cycle*, **2008**, *7*, 1146–1150. (b) McNamara, C. R.; Degtarev, A. Small-molecule inhibitors of the PI3K signaling network. *Future Med. Chem.* **2011**, *3*, 549–565. (c) Roskoski, R., Jr. ERK1/2 MAP kinases: Structure, function, and regulation. *Pharmacol. Res.* **2012**, *66*, 105–143.

34. Fischer, C.; Shah, S.; Hughes, B. L.; Nikov, G. N.; Crispino, J. L.; Middleton, R. E.; Szewczak, A. A.; Munoz, B.; Shearman, M. S. Quinazolinones as γ -secretase modulators. *Bioorg. Med. Chem. Lett.* **2011**, *21*, 773-776.

35. (a) Barbay, J. K.; Leonard, K.; Chakravarty, D.; Shook, B. C.; Wang, A. WO **2010/045009**. (b) Chakravarty, D.; Shook, B.C. WO **2010/045017**. (c) Barbay, J. K.; Chakravarty, D.; Shook, B. C.; Wang, A. WO **2010/045006**.

36. Alzheimer A. Uber eine eigenartige erkrankung der hirnrinde. *Allg Zeitschrift Psych.* **1907**, *64*, 146–148.

37. (a) Hardy, J.; Selkoe, D. J. The amyloid hypothesis of Alzheimer's disease: Progress and problems on the road to therapeutics. *Science* **2002**, *297*, 353–356. (b) Clinton, L. K.; Blurton-Jones, M.; Myczek, K.; Trojanowski, J. Q.; LaFerla, F. M. Synergistic Interactions between A β , Tau, and α -Synuclein: Acceleration of Neuropathology and Cognitive Decline. *J. Neurosci.* **2010**, *30*, 7281–7289. (c)

Small, S. A.; Duff, K. Linking A β and Tau in Late-Onset Alzheimer's Disease: A Dual Pathway Hypothesis. *Neuron* **2008**, *60*, 534–542. (d) Meraz-Ríos, M. A.; Lira-De León, K. I.; Campos-Peña, V.; De Anda-Hernández, M. A.; Mena-López, R. Tau oligomers and aggregation in Alzheimer's disease. *J. Neurochem.* **2010**, *112*, 1353–1367.

38. (a) Citron, M. Alzheimer's disease: strategies for disease modification. *Nature Rev. Drug Discov.* **2010**, *9*, 387–398. (b) Jakob-Roetne, R.; Jacobsen, H. Alzheimer's Disease: From Pathology to Therapeutic Approaches. *Angew. Chem. Int. Ed.* **2009**, *48*, 3030–3059. (c) Ehrnhoefer, D. E.; Wong, B. K. Y.; Hayden, M. R. Convergent pathogenic pathways in Alzheimer's and Huntington's diseases: shared targets for drug development. *Nature Rev. Drug Discov.* **2011**, *10*, 853–867.

39. Panza, F.; Solfrizzi, V.; Frisardi, V.; Capurso, C. Disease-Modifying Approach to the Treatment of Alzheimer's Disease: From α -Secretase Activators to γ -Secretase Inhibitors and Modulators. *Drugs Aging* **2009**, *26*, 537-555. (b) Imbimbo, B. P. Alzheimer's disease: γ -secretase inhibitors. *Drug Discov. Today Ther. Strat.* **2008**, *5*, 169–175. (c) Panza, F.; Frisardi, V.; Imbimbo, B. P.; Capurso, C.; Loggoscino, G.; Sancarlo, D.; Seripa, D.; *et al.* REVIEW: γ -Secretase Inhibitors for the Treatment of Alzheimer's Disease: The Current State. *CNS Neurosci. Ther.* **2010**, *16*, 272–284.

40. Hopkins, C. R. ACS Chemical Neuroscience Molecule Spotlight on Semagacestat (LY450139). *ACS Chem. Neurosci.* **2010**, *1*, 533–534.

-
41. Hopkins, C. R. ACS Chemical Neuroscience Molecule Spotlight on Begacestat (GSI-953). *ACS Chem. Neurosci.* **2012**, *3*, 3–4.
42. Sperling, R.; Jack, C., Jr. Testing the Right Target and Right Drug at the Right Stage. *Sci. Transl. Med.* **2011**, *3*, 111cm33.
43. Fernandez, D. Physicochemical Features of the hERG Channel Drug Binding Site. *J. Biol. Chem.* **2003**, *279*, 10120–10127.
44. Dauer, W.; Przedborski, S. Parkinson's Disease - Mechanisms and Models. *Neuron*, **2003**, *39*, 21–21.
45. Calabresi, P.; Di Filippo, M.; Ghiglieri, V.; Tambasco, N.; Picconi, B. Levodopa-induced dyskinesias in patients with Parkinson's disease: filling the bench-to-bedside gap. *Lancet neurol.* **2010**, *9*, 1106–1117.
46. Dorsey, E. R.; Constantinescu, R.; Thompson, J. P.; Biglan, K. M.; Holloway, R. G.; Kieburtz, K.; *et al.* Projected number of people with Parkinson disease in the most populous nations, 2005 through 2030. *Neurology* **2007**, *68*, 384–386.
47. (a) Ikeda, K.; Kurokawa, M.; Aoyama, S.; Kuwana, Y. Neuroprotection by adenosine A2A receptor blockade in experimental models of Parkinson's disease. *J. Neurochem.* **2007**, *80*, 262–270. (b) Kurokawa, M.; Kirk, I. P.; Kirkpatrick, K. A., Kase, H.; Richardson, P. J. Inhibition by KF17837 of adenosine A2A receptor-mediated modulation of striatal GABA and ACh release. *Brit. J. Pharmacol.* **2012**, *113*, 43–48.
48. Stiles, G. L. Adenosine receptors. *J. Biol. Chem.* **1992**, *267*, 6451–6454.

-
49. Chen, W.; Wang, H.; Wei, H.; Gu, S.; Wei, H. Istradefylline, an adenosine A2A receptor antagonist, for patients with Parkinson's Disease: A meta-analysis. *J. Neurol. Sci.* **2012**, <http://dx.doi.org/10.1016/j.jns.2012.08.030>
50. Hickey, P.; Stacy, M. Adenosine A2A Antagonists in Parkinson's Disease: What's Next? *Curr. Neurol. Neurosci. Rep.* **2012**, *12*, 376–385.
51. Moro, S.; Gao, Z.-G.; Jacobson, K. A.; Spalluto, G. Progress in the pursuit of therapeutic adenosine receptor antagonists. *Med. Res. Rev.* **2006**, *26*, 131–159.
52. (a) Sabnis, R. W.; Rangnekar, D. W.; Sonawane, N. D. 2-aminothiophenes by the Gewald reaction. *J. Heterocyclic Chem.* **1999**, *36*, 333-345. (b) Gewald, K.; Schinke, E.; Boettcher, H. Heterocyclen aus CH-aciden Nitrilen, VIII. 2-Amino-thiophene aus methylenaktiven Nitrilen, Carbonylverbindungen und Schwefel. *Chem. Ber.* **1966**, *99*, 94-100.
53. Huang, X.-G.; Liu, J.; Ren, J.; Wang, T.; Chen, W.; Zeng, B.-B. A facile and practical one-pot synthesis of multisubstituted 2-aminothiophenes via imidazole-catalyzed Gewald reaction. *Tetrahedron* **2011**, *67*, 6202-6205.
54. Barnes, D. M.; Haight, A. R.; Hameury, T.; McLaughlin, M. A.; Mei, J.; Tedrow, J. S.; Toma, J. D. R. New conditions for the synthesis of thiophenes via the Knoevenagel/Gewald reaction sequence. Application to the synthesis of a multitargeted kinase inhibitor. *Tetrahedron* **2006**, *62*, 11311-11319.
55. Huang, Y.; Dömling, A. The Gewald multicomponent reaction. *Mol. Divers.* **2010**, *15*, 3–33.
56. (a) Hesse, S.; Perspicace, E.; Kirsch, G. Microwave-assisted synthesis of 2-aminothiophene-3-carboxylic acid derivatives, 3H-thieno[2,3-*d*]pyrimidin-4-one

and 4-chlorothieno[2,3-*d*]pyrimidine. *Tetrahedron Lett.* **2007**, *48*, 5261-5264. (b) Tranberg, C. E.; Zickgraf, A.; Giunta, B. N.; Luetjens, H.; Figler, H.; Murphree, L. J.; Falke, R.; Fleischer, H.; Linden, J.; Scammells, P. J.; Olsson, R. A. 2-Amino-3-aryl-4,5-alkylthiophenes: Agonist Allosteric Enhancers at Human A₁ Adenosine Receptors. *J. Med. Chem.* **2002**, *45*, 382-389.

57. Foloppe, N.; Fisher, L. M.; Howes, R.; Kierstan, P.; Potter, A.; Robertson, A. G. S.; Surgenor, A. E. Structure-Based Design of Novel Chk1 Inhibitors: Insights into Hydrogen Bonding and Protein–Ligand Affinity. *J. Med. Chem.* **2005**, *48*, 4332–4345.

58. Han, Y.; Ebinger, K.; Vandevier, L. E.; Maloney, J. W.; Nirschl, D. S.; Weller, H. N. Efficient and library-friendly synthesis of furo- and thieno[2,3-*d*]pyrimidin-4-amine derivatives by microwave irradiation. *Tetrahedron Lett.* **2010**, *51*, 629–632.

59. Yoon, D. S.; Han, Y.; Stark, T. M.; Haber, J. C.; Gregg, B. T.; Stankovich, S. B. Efficient Synthesis of 4-Aminoquinazoline and Thieno[3,2-*d*]pyrimidin-4-ylamine Derivatives by Microwave Irradiation. *Org. Lett.* **2004**, *6*, 4775–4778.

60. (a) Engel, J. D. Mechanism of the Dimroth rearrangement in adenosine. *Biochem. Biophys. Res. Co.* **1975**, *64*, 581–586. (b) Ravi Kanth, S.; Venkat Reddy, G.; Hara Kishore, K.; Shanthan Rao, P.; Narsaiah, B.; Surya Narayana Murthy, U. Convenient synthesis of novel 4-substitutedamino-5-trifluoromethyl-2,7-disubstituted pyrido[2,3-*d*]pyrimidines and their antibacterial activity. *Eur. J. Med. Chem.* **2006**, *41*, 1011–1016.

-
61. Grembecka, J.; He, S.; Shi, A.; Purohit, T.; Muntean, A. G.; Sorenson, R. J.; Showalter, H. D.; Murai, M. J.; Belcher, A. M.; *et al.* Menin-MLL inhibitors reverse oncogenic activity of MLL fusion proteins in leukemia. *Nature Chem. Biol.* **2012**, *8*, 277–284.
62. (a) Sham, H. L.; Konradi, A.W.; Hom, R. K.; Probst, G. D.; Bowers, S.; Truong, A.; Neitz, R. J.; Sealy, J.; Toth, G. WO **2010/091310**. (b) Bowers, S.; Truong, A. P.; Neitz, R. J.; Hom, R. K.; Sealy, J. M.; Probst, G. D.; *et al.* *Bioorg. Med. Chem. Lett.* **2011**, *21*, 5521-5527.
63. (a) Miller, R. E.; Rantanen, T.; Ogilvie, K. A.; Groth, U.; Snieckus, V. Combined Directed *ortho* Metalation–Halogen Dance (HD) Synthetic Strategies. HD–Anionic *ortho* Fries Rearrangement and Double HD Sequences. *Org. Lett.* **2010**, *12*, 2198-2201. (b) Getmanenko, Y.; Tongwa, P.; Timofeeva, T. V.; Marder, S. R. Base-Catalyzed Halogen Dance Reaction and Oxidative Coupling Sequence as a Convenient Method for the Preparation of Dihalo-bisheteroarenes. *Org. Lett.* **2010**, *12*, 2136-2139. (c) Schürch, M.; Spina, M.; Khan, A. F.; Mihovilovic, M. D.; Stanetty, P. Halogen dance reactions - A review. *Chem. Soc. Rev.* **2007**, *36*, 1046-1057. (d) Schlosser, M. The 2x3 Toolbox of Organometallic Methods for Regiochemically Exhaustive Functionalization. *Angew. Chem. Int. Ed.* **2005**, *44*, 376-393. (e) Lukevics, E.; Arsenyan, P.; Belyakov, S.; Popelis, J.; Pudova, O. Regiospecific silylation of 2,5-dibromothiophene: a reinvestigation. *Tetrahedron Lett.* **2001**, *42*, 2039-2041.
64. (a) Lin, Y.-S.; Park, J.; De Schutter, J. W.; Huang, X. F.; Berghuis, A. M.; Sebag, M.; Tsantrizos, Y. S. Design and Synthesis of Active Site Inhibitors of the

Human Farnesyl Pyrophosphate Synthase: Apoptosis and Inhibition of ERK Phosphorylation in Multiple Myeloma Cells. *J. Med. Chem.* **2012**, *55*, 3201-3215.

(b) De Schutter, J. W.; Zaretsky, S.; Welbourn, S.; Pause, A.; Tsantrizos, Y. S. Novel bisphosphonate inhibitors of the human farnesyl pyrophosphate synthase. *Bioorg. Med. Chem. Lett.* **2010**, *20*, 5781-5786.

65. (a) Feng, X. J.; Wu, P. L.; Tam, H. L.; Li, K. F.; Wong, M. S.; Cheah, K. W. Fluorene-Based π -Conjugated Oligomers for Efficient Three-Photon Excited Photoluminescence and Lasing. *Chem. Eur. J.* **2009**, *15*, 11681-11691. (b) Ye, X.-S.; Wong, H. N. C. Synthetic Applications of 3, 4-Bis (trimethylsilyl) thiophene: Unsymmetrically 3, 4-Disubstituted Thiophenes and 3, 4-Didehydrothiophene. *J. Org. Chem.* **1997**, *62*, 1940-1954.

66. (a) Mehta, S.; Larock, R. C. Iodine/Palladium Approaches to the Synthesis of Polyheterocyclic Compounds. *J. Org. Chem.* **2010**, *75*, 1652–1658. (b) Durka, K.; Górká, J.; Kurach, P.; Luliński, S.; Serwatowski, J. Electrophilic *ipso*-iodination of silylated arylboronic acids. *J. Organomet. Chem.* **2010**, *695*, 2635–2643.

67. Wittig, G.; Pockels, U.; Dröge, H. Über die Austauschbarkeit von aromatisch gebundenem Wasserstoff gegen Lithium mittels Phenyl-lithiums. *Ber. Dtsch. Chem. Ges.* **1938**, *71*, 1903 – 1912.

68. Gilman, H.; Langham, W.; Jacoby, A. L. Metalation as a Side Reaction in the Preparation of Organolithium Compounds *J. Am. Chem. Soc.* **1939**, *61*, 106 – 109.

69. (a) Peyron, C.; Navarre, J.-M.; Van Craynest, N.; Benhida, R. First example of base-promoted tandem alkylation–bromination of 2-bromothiophene via halogen dance process: a remarkable temperature effect. *Tetrahedron Lett.* **2005**, *46*,

3315–3318. (b) Gannon II, M. K.; Detty, M. R. Generation of 3- and 5-Lithiothiophene-2-carboxylates via Metal–Halogen Exchange and Their Addition Reactions to Chalcogenoxanthenes *J. Org. Chem.* **2007**, *72*, 2647-2650. (c) Sonoda, M.; Kinoshita, S.; Luu, T.; Fukuda, H.; Miki, K.; Umeda, R.; Tobe, Y. Selective Metallation of 3-Halothiophenes: Practical Methods for the Synthesis of 2-Bromo-3-formylthiophene. *Synthetic Commun.* **2009**, *39*, 3315–3323.

70. (a) Schlosser, M.; Cottet, F. Silyl-Mediated Halogen/Halogen Displacement in Pyridines and Other Heterocycles. *Eur. J. Org. Chem.* **2002**, 4181-4184. (b) Heiss, C.; Marzi, E.; Mongin, F.; Schlosser, M. Remote Trimethylsilyl Groups Interfering with the ortho Deprotonation of Fluoroarenes and Chloroarenes. *Eur. J. Org. Chem.* **2007**, 669–675. (c) Heiss, C.; Rausis, T.; Schlosser, M. Promoting or Preventing Haloarylithium Isomerizations: Differential Basicities and Solvent Effects as the Crucial Variables. *Synthesis*, **2005**, *4*, 0617 – 0621. (d) Gorecka, J.; Heiss, C.; Scopelliti, R.; Schlosser, M. Buttressing Effects on Haloarene Deprotonation: A Merely Kinetic or Also Thermodynamic Phenomenon? *Org. Lett.* **2004**, *6*, 4591 - 4593.

71. (a) Taylor, E. C.; Hendess, R. W. Synthesis of Pyrrolo[2, 3-*d*]pyrimidines. The Aglycone of Toyocamycin1, 2. *J. Am. Chem. Soc.* **1965**, *87*, 1995–2003. (b) Schnyder, A.; Beller, M.; Mehlretter, G.; Nsenda, T.; Studer, M.; Indolese, A. F. Synthesis of Primary Aromatic Amides by Aminocarbonylation of Aryl Halides Using Formamide as an Ammonia Synthon. *J. Org. Chem.* **2001**, *66*, 4311-4315. (c) Noura, I.; Kostakis, I. K.; Dubouilh, C.; Chosson, E.; Iannelli, M.; Besson, T. Decomposition of formamide assisted by microwaves, a tool for synthesis of

-
- nitrogen-containing heterocycles. *Tetrahedron Lett.* **2008**, *49*, 7033-7036. (d)
- Cataldo, F.; Patane, G.; Compagnini, G. Synthesis of HCN Polymer from Thermal Decomposition of Formamide. *J. Macromol. Sci. Pure*, **2009**, *46*, 1039-1048. (e)
- Harada, K. *Nature*, **1967**, *214*, 479-480. (e) Bredereck, H.; Gompper, R.; Morlcok, G. Neue Pyrimidin-Synthese aus β -Dicarbonyl-Verbindungen und Formamid. *Angew. Chem.* **1956**, *68*, 151.
72. Seyferth, D.; White, D. L. Acid-catalyzed isomerization of 1, 2-bis(trimethylsilyl) benzene and related compounds. *J. Am. Chem. Soc.* **1972**, *94*, 3132 – 3138.
73. Bennetau, B.; Dunogues, J. Unusual electrophilic substitution in the aromatic series via organosilicon intermediates. *Synlett*, **1993**, *3*, 171 - 176.
74. Garcia, Y.; Schoenebeck, F.; Legault, C. Y.; Merlic, C. A.; Houk, K. N. Theoretical Bond Dissociation Energies of Halo-Heterocycles: Trends and Relationships to Regioselectivity in Palladium-Catalyzed Cross-Coupling Reactions. *J. Am. Chem. Soc.* **2009**, *131*, 6632 – 6639.
75. Litvinov, V. The Chemistry of Thienopyrimidines. *Adv. Heterocycl Chem.* **2006**, *92*, 83 – 143.
76. Gronowitz, S.; Holm, B. On the halogenation of halothiophenes with N-chloro- and N-bromosuccinimide. *Acta Chem. Scand. B.* **1976**, *30*, 423 - 429.
77. (a) Zhao, J.; Qiu, D.; Shi, J.; Wang, H. Synthesis of Dithieno[2,3-*b*:4',3'-*d*]siloles and Their Selective Bromination. *J. Org. Chem.* **2012**, *77*, 2929 - 2934.
- (b) Kauch, M.; Hoppe, D. Synthesis of Halogenated Phenols by Directed ortho-Lithiation and ipso-Iododesilylation Reactions of O-Aryl N-Isopropylcarbamates.

Synthesis, **2006**, *10*, 1578-1589. (c) Keay, B. A. Synthesis of multi-substituted furan rings: the role of silicon. *Chem. Soc. Rev.* **1999**, *28*, 209-215.

78. (a) Walling, C.; El-Taliawi, G. M.; Zhao, C. Radical chain carriers in N-bromosuccinimide brominations. *J. Am. Chem. Soc.* **1983**, *105*, 5119-5124. (b) Pearson, R. E.; Martin, J. C. The Identity of the Chain-Carrying Species in Brominations with N-Bromosuccinimide: Selectivity of Substituted N-Bromosuccinimides toward Substituted Toluenes. *J. Am. Chem. Soc.* **1963**, *85*, 3142–3146. (c) Djerassi, C. Brominations with N-Bromosuccinimide and Related Compounds. The Wohl-Ziegler Reaction. *Chem. Rev.* **1948**, *43*, 271–317. (d) Horner, L.; Winkelmann, E. H. Neuere Methoden der präparativen organischen Chemie II 14. N-Bromsuccinimid, Eigenschaften und Reaktionsweisen Studien zum Ablauf der Substitution XV. *Angew. Chem.* **1959**, *71*, 349-365. (e) Líška, J.; Borsig, E.; Tkáč, I. A route to preparation of bromomethylated poly (2,6-dimethyl-1,4-phenylene oxide). *Angew. Makromol. Chem.* **1993**, *211*, 121–129.

79. Terazima, M.; Nogami, Y.; Tominaga, T. Diffusion of a radical from an initiator of a free radical polymerization: a radical from AIBN. *Chem. Phys. Lett.* **2000**, *332*, 503–507.

2. Nitrogen-Containing Bisphosphonates and the Mevalonate Pathway

2.1 Introduction

2.1.1 History of Bisphosphonates

Bisphosphonates (BPs) are chemically stable analogs of pyrophosphate compounds, whereby the core structure is made up of P-C-P bonds (Figure 2.1).¹ Attached to the central carbon atom of BPs are two substituents, termed R₁ and R₂, which are not present in pyrophosphate. Commonly, the R₁ substituent is a hydroxyl group, now known as the “bone hook”.^{2,3} All compounds are broadly classified into two categories, non-nitrogen-containing and nitrogen-containing bisphosphonates (*N*-BPs), depending on the absence or presence of nitrogen atoms in the R₂ substituent, respectively. The first generation of bisphosphonates was non-nitrogen-containing, such as Etidronate and Clodronate (Figure 2.1). Second and third generations were nitrogen-containing bisphosphonates, such as Pamidronate and Risedronate (RIS).⁴

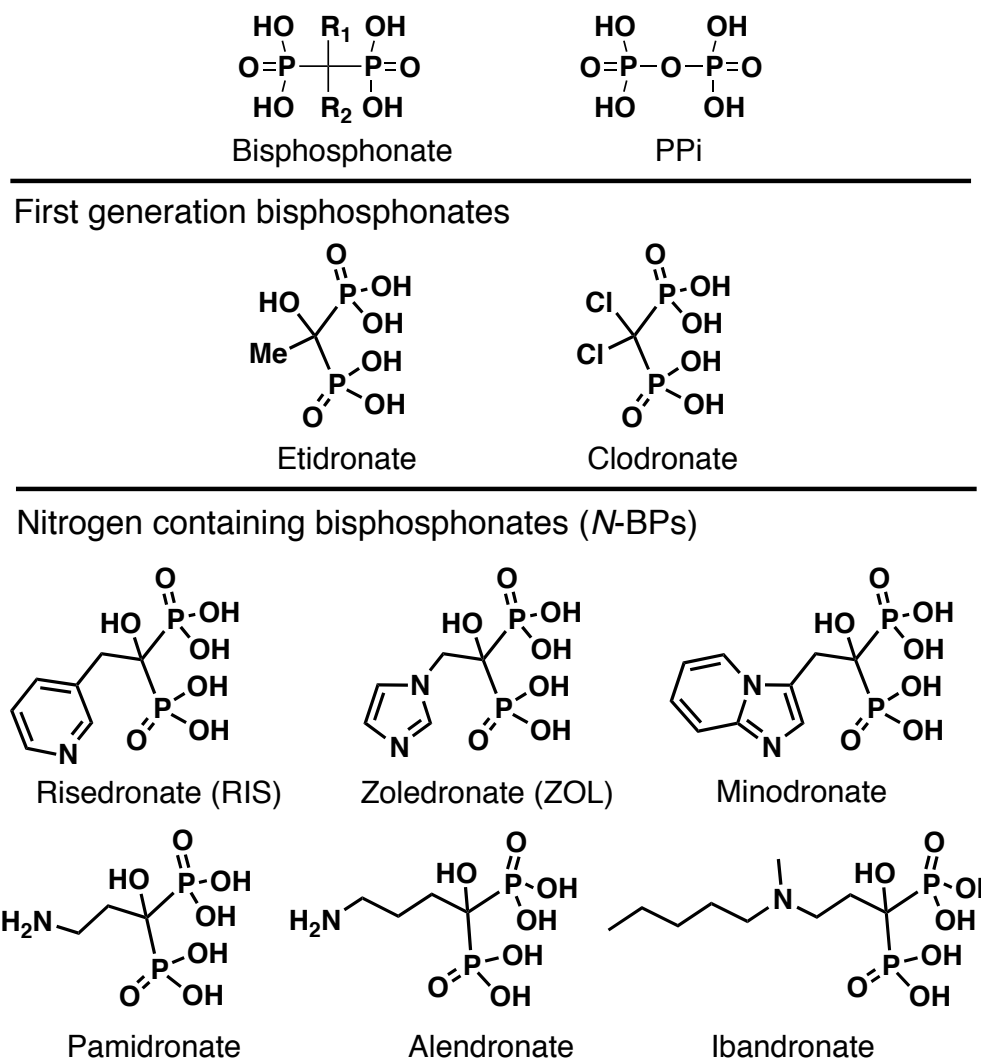


Figure 2.1 Structures of bisphosphonates and inorganic pyrophosphate.

Although the first BPs were originally synthesized in the late 1800s, their biological properties were not discovered until much later.⁵ Bisphosphonates were first used as corrosion inhibitors and then in industrial processes as, for example, complexing agents in oil, textile, and fertilizer industries. They have also been used as water softeners due to their ability to sequester and prevent the precipitation of calcium, which is useful for domestic and industrial water systems.⁶

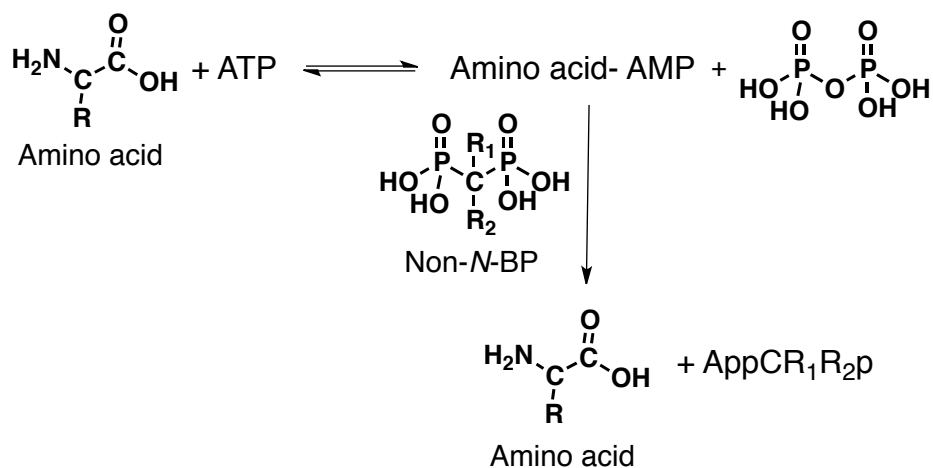
Interest in the potential clinical applications of bisphosphonates began with studies demonstrating the ability of BPs to prevent the experimentally induced calcification of soft tissues, such as skin, kidneys, and blood vessels *in vivo*. It appeared that BPs were disrupting crystal formation after adsorption to mineral surfaces via physicochemical mechanisms.⁷ These studies lead to the important discovery that BPs were able to inhibit hydroxyapatite (HAP) crystal dissolution, which lead to studies to determine whether BPs could prevent bone resorption clinically.⁸

The first human use of BPs was in 1969, when a child with fibrodysplasia ossificans progressiva (a disorder characterized by the ossification of soft tissue) was given etidronate.⁹ Since that time, BPs have become a first line of treatment for bone-related disorders such as osteoporosis, Paget's disease, and cancer. Interestingly, the newer generations of *N*-BPs have almost completely replaced the first generation etidronate and clodronate (Figure 2.1), especially for the treatment of osteoporosis. Clodronate, however, has remained in use for the treatment of cancers of the bone.^{10,11,12}

2.1.2 Bisphosphonate Mechanism of Action: ATP Analogs and the Mevalonate Pathway

Although BPs have been used clinically in humans for the past 40 years, the mechanism of action was only deciphered within the last decade. Interestingly, the two classes of BPs (Figure 2.1) exert biological activity according to very different mechanisms.¹³ The non-*N*-BPs (*e.g.* etidronate and clodronate) are metabolized by osteoclasts, the cells responsible for bone resorption, into toxic

and non-hydrolysable ATP analogs, such as AppCCl₂p (Scheme 2.1). A class of aminoacyl-tRNA synthetases catalyzes the condensation of amino acids with ATP to generate amino acid-AMP derivatives (Figure 2.2), which can then condense with non-*N*-BPs. The amino acid is regenerated and AppCR₁R₂p is formed (Scheme 2.1). Accumulation of these metabolites inhibits intracellular metabolic enzymes in organelles like mitochondria, inhibiting bone resorption and causing osteoclast apoptosis.¹⁴



Scheme 2.1 Metabolism of non-nitrogen-containing BPs.

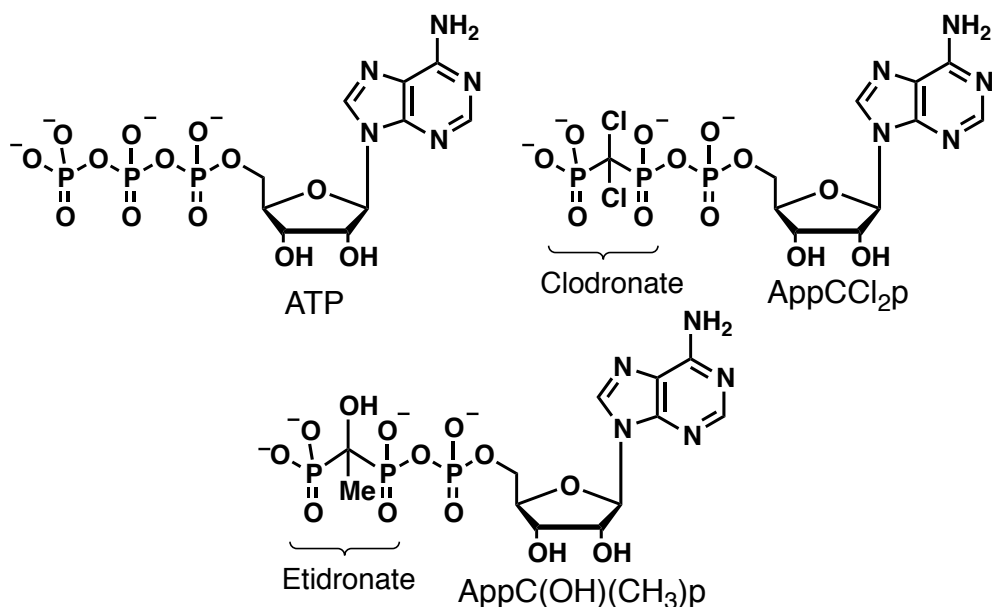


Figure 2.2 Structures of ATP and AppCR₁R₂p metabolites.

The more potent *N*-BPs (*e.g.* RIS and ZOL; Figure 2.1) prevent bone resorption and osteoclast maturation via inhibition of a key enzyme and recruitment to the bone surface.^{15,16} The major target of *N*-BPs is farnesyl pyrophosphate synthase (FPPS), a critical enzyme in the mevalonate pathway (Figure 2.3).¹⁷ *N*-BPs bind to the active site and inhibit FPPS, thereby downregulating the production of isoprenoids (*i.e.* farnesyl pyrophosphate, FPP and geranylgeranyl pyrophosphate, GGPP; Scheme 2.2), steroids, and cholesterol. Isoprenoids FPP and GGPP are synthesized by the sequential condensation of five-carbon dimethylallyl pyrophosphate (DMAPP) with multiple isopentenyl pyrophosphate (IPP) units (Scheme 2.2). Limiting isoprenoid synthesis also limits the post-translational modification (isoprenylation) of key regulatory enzymes, small guanosine tri-phosphate-binding proteins (GTPases), which is required for proper cellular localization and function. GTPases (*e.g.* Ras, Rho, and Rac)

control many cellular functions of osteoclasts such as stress fiber assembly, membrane ruffling, and survival.^{4,18}

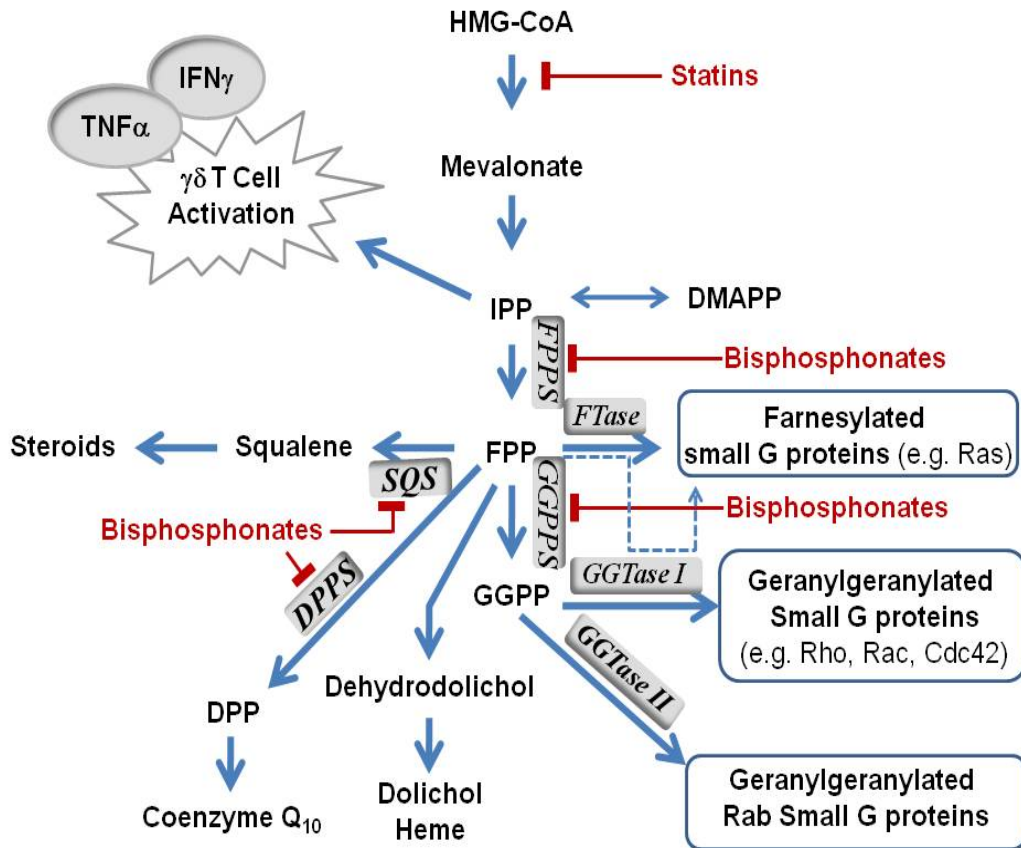
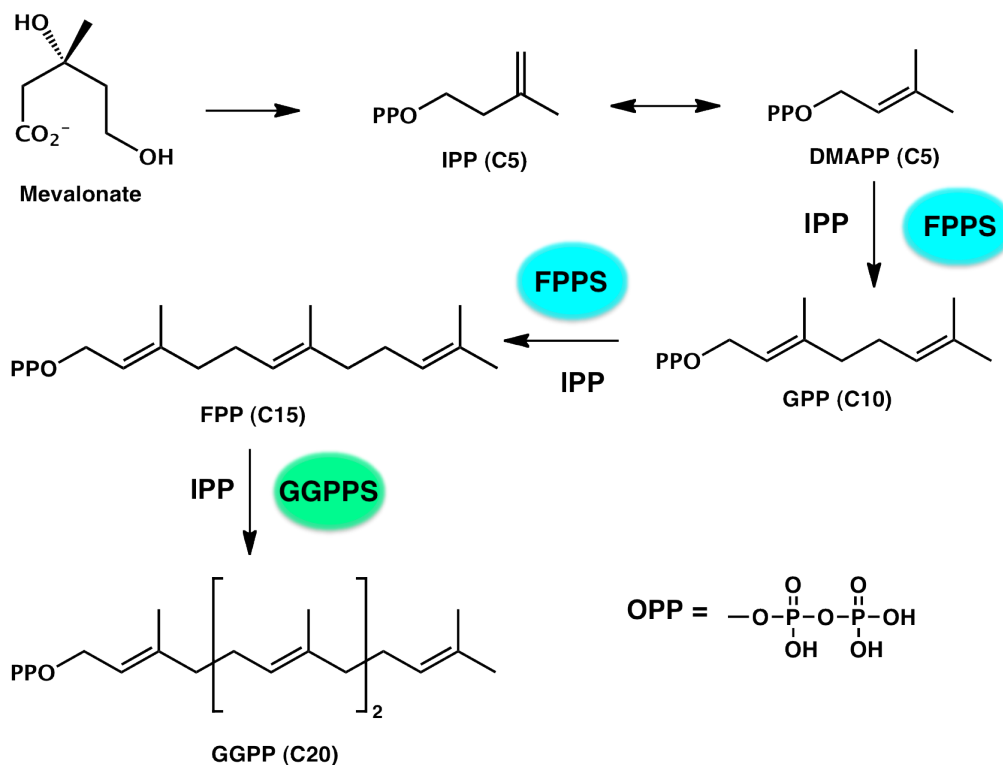


Figure 2.3 The mevalonate pathway.



1

Scheme 2.2 Isoprenoid biosynthesis.

Inhibition of FPPS by *N*-BPs causes accumulation of IPP, an FPPS substrate (Figure 2.3; Scheme 2.2). This accumulation of IPP triggers an acute response of fever and “flu-like” symptoms in patients after the first *N*-BP administration by intravenous infusion.¹³ Monocytes in the blood take up the *N*-BP, leading to FPPS inhibition and accumulation of IPP, which is also an antigen recognized by a subset of $\gamma\delta$ T cells ($V\gamma 2V\delta 2$ T cells) that are key players in the human immune system. Activation of $\gamma\delta$ T cells leads to the release of $\text{TNF}\alpha$, causing a pro-inflammatory acute phase response in humans.^{19,20}

Accumulation of IPP and DMAPP (Scheme 2.2) in cells such as osteoclasts, cultured tumor cells, and macrophages that have taken up *N*-BPs also lead to the production of ATP analogs, ApppI (or IPP-AMP) and ApppD (or

DMAPP-AMP), respectively (Figure 2.4). Although the exact mechanism of metabolite formation has not been confirmed, evidence indicates that the same class of aminoacyl-tRNA synthetases that catalyzes AppCR₁R₂p synthesis (Scheme 2.1) may also conjugate IPP and DMAPP with AMP. These ApppI/D metabolites, like the AppCR₁R₂p analogs (Figure 2.2), cause cell death by inhibition of mitochondrial enzymes.²¹ Therefore, *N*-BPs cause an immune response as well as cell apoptosis by two different mechanisms, isoprenylation inhibition and ApppI/D accumulation.

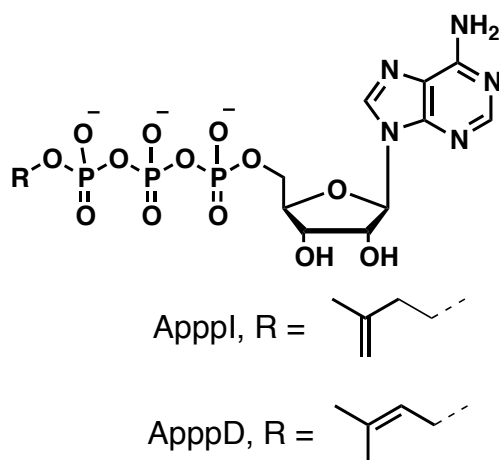


Figure 2.4 Structures of ApppI and ApppD metabolites.

2.1.3 *N*-BPs and Isoprenylation in Non-Bone Related Therapeutics

Over the last decade, the mechanisms by which *N*-BPs exert their biological activity have been elucidated, providing the opportunity to explore other potential applications of this class of drugs. Indeed, *N*-BPs have demonstrated interesting activities unrelated to bone including anti-viral²², anti-parasitic²³, and anti-cancer^{24,25} effects.

N-BPs exert indirect and direct anti-tumor activity (Figure 2.5). Decreased osteoclast activity and bone resorption deprive tumor cells of the nutrients and growth factors that they require for metastasis and proliferation, indirectly exerting anti-cancer effects.²⁶ Furthermore, *N*-BPs have inhibited the formation of capillary-like blood vessels in animals and reduced endothelial cell adhesion and proliferation (surrounding tumors), indicating the potential to suppress tumor-associated angiogenesis.^{27,25a,b,h} Moreover, inhibition of human FPPS (hFPPS) in the body leads to intracellular accumulation of IPP, which triggers the release of IFN γ and TNF α leading to an immune response.^{19,20} Therefore, *N*-BPs may help kill cancer cells by boosting the activity of the body's own $\gamma\delta$ T cells, which are capable of recognizing cancer cells with cancer antigens or stress-induced molecules. Studies have shown that $\gamma\delta$ T cells recognize many different tumor types such as lymphoma, renal carcinoma, multiple myeloma, and melanomas.^{28,29}

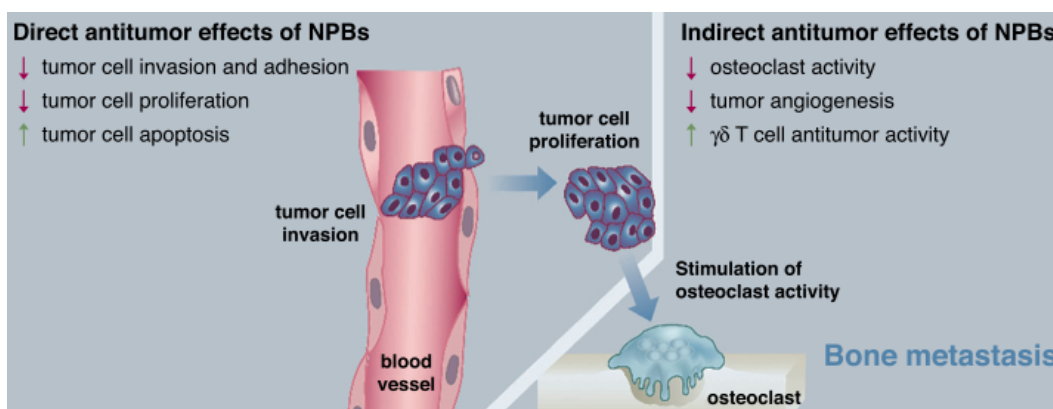


Figure 2.5 Direct and indirect antitumor effects of *N*-BPs.²⁶

Inhibiting hFPPS and to a lesser extent, hGGPPS, *N*-BPs deplete cells of isoprenoids, FPP and GGPP (Scheme 2.2). Other structurally similar human

enzymes, such as decaprenyl synthase (hDPPS) and squalene synthase (hSQS) are also targeted in a non-selective manner by some of the currently known *N*-BPs. Therefore, *N*-BPs downregulate the production of important cellular components as well as the availability of isoprenoids for post-translational modifications (Figure 2.3).³⁰

A number of human cancers have oncogenic mutations of the RAS family of GTPases. As mentioned, isoprenoids, particularly FPP and GGPP, are crucial for the proper localization and function of GTPases. These GTPases regulate the ability of a tumor cell to proliferate, grow, migrate, and survive. Therefore, there has been a great interest in developing isoprenylation inhibitors as anti-cancer therapeutics. Initially, this interest began with a search for inhibitors for prenyltransferases (PTs), the enzymes responsible for transferring isoprenoids onto GTPases, specifically, farnesyltransferase (FTase) and geranylgeranyltransferase 1 (GGT1).³¹ Unfortunately, despite encouraging preclinical results, farnesyltransferase inhibitors (FTIs; Table 2.1) were not as successful as expected in their clinical efficacy due to (an unknown) redundancy mechanism. Surprisingly, K-Ras was geranylgeranylated by GGT1 instead of farnesylated upon FTase inhibition.³²

Table 2.1 Farnesyltransferase and geranylgeranyltransferase I inhibitors in clinical trials.³⁹

| Compound | IC ₅₀ (nM) ^a | Phase | # of Trials ^b | Diseases |
|-------------|---------------------------------------|-------|--------------------------|----------|
| FTIs | | | | |

| | | | | |
|---|-----|------------|----|--|
| Tipifarnib | 0.9 | I, II, III | 80 | Cancer |
| Lonafarnib | 1.9 | I, II, III | 33 | Cancer, Progeria Syndrome, Hepatitis D |
| BMS-214662 | 1.4 | I | 6 | Cancer |
| L-778,123 | 2 | I | 2 | Cancer |
| GGTI | | | | |
| GGTI-2418 | 9.5 | I | 1 | Cancer |
| ^a Berndt, N. <i>et al.</i> Ref. 31 ^b Number of clinical trials from www.ClinicalTrials.gov | | | | |

A number of GTPases are geranylgeranylated, either as part of a redundancy mechanism during FTase treatment or exclusively. K-Ras and N-Ras, for example, are normally farnesylated but can be geranylgeranylated when FTase is inhibited.³³ Other GTPases, such as Rho, Rac, Ral, and cell division cycle 42 (CDC42) are exclusively geranylgeranylated. Although all of these geranylgeranylated proteins play key roles in cell survival, only one GGT1 inhibitor (GGTI-2418; Table 2.1)³⁴ has entered Phase I clinical trials.³¹

Currently, there is evidence that GGPP mediated pathways also play a significant role in modulating disease pathologies.³¹ Geranylgeranylated GTPases regulate important cell functions such as actin organization, endocytosis, exocytosis, gene expression, and cell cycle progression.³⁵ Rho GTPases, for example, are implicated in metastasis³⁶ and may actually drive oncogenesis in some Ras-dependant cancers. Therefore, inhibition of protein geranylgeranylation may be an effective target for the treatment of a variety of diseases.³¹

The development of potent *N*-BPs with favorable bioavailability will be extremely useful to study the effects of selectively limiting the quantity of FPP and/or GGPP available for isoprenylation *in vivo*. As described above, selective modulation of isoprenoid levels and activities of FPPS and GGPPS will be extremely useful to further study and help elucidate disease mechanisms. In combination with recent developments, such as mapping protein prenylation^{31,37} and new conditional knockout mouse models,³⁸ selective *N*-BPs will allow for new opportunities to improve the treatment of disease.³⁹

2.1.4 Synthesis and Structure Activity Relationships (SAR) of *N*-BPs

Although *N*-BPs have demonstrated a variety of non-bone-related biological effects, related to inhibition of FPPS and GGPPS,²⁵ effectiveness is ultimately limited by their low bioavailability, very poor cell membrane permeability, and the high bone affinity of their polar bisphosphonate group.¹³ Calcium ions of hydroxyapatite (HAP) are chelated by bisphosphonates in a bidentate coordination through the oxygen atoms. If the R₁ side chain (Figure 2.1) is a hydroxyl group (as in the case of RIS and ZOL; Figure 2.1), the affinity for bone is much greater due to the tridentate coordination with metal ions. Hence, the R₁ hydroxyl group has been referred to as the “bone hook” of *N*-BPs (Figure 2.3).^{2,3,4} It is likely that *N*-BPs exert biological effects in the body primarily on osteoclasts because they accumulate in the bone.⁴⁰ Osteoclasts are then able to take up the *N*-BPs, most likely through fluid-phase endocytosis.⁴¹ Therefore, the largest hurdle to explore the full therapeutic potential of *N*-BPs is to increase bioavailability and non-

skeletal tissue distribution (Figure 2.6) by reduction of their polarity and bone affinity.¹³

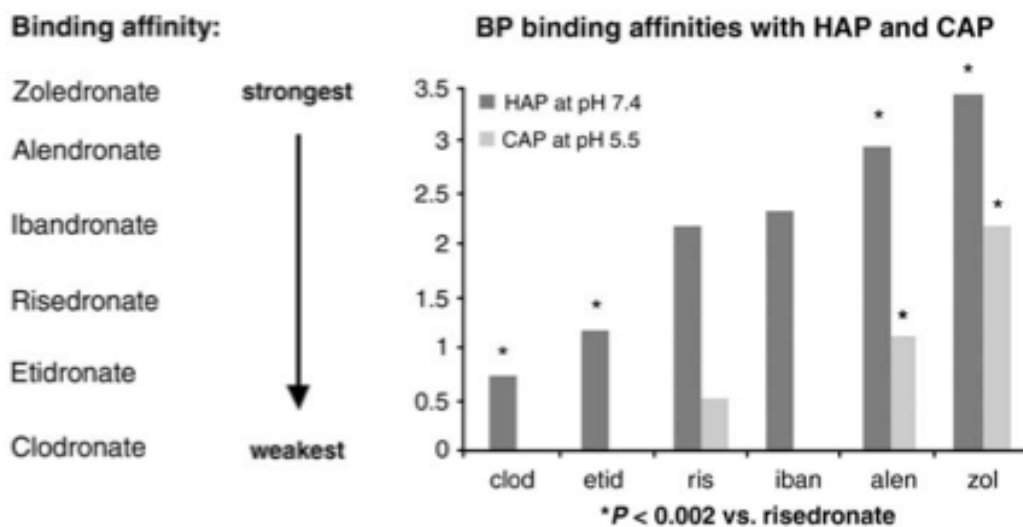
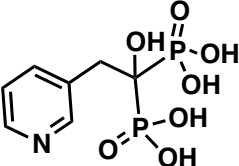
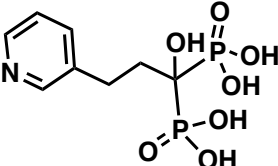
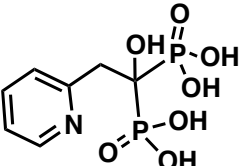
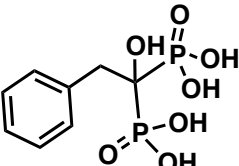


Figure 2.6 Binding affinities of BPs with hydroxyapatite (HAP) and carbonated hydroxyapatite (CAP).³

Interestingly, even minor modifications to the structure of *N*-BPs have had a large impact on their *in vitro* and *in vivo* activities. The addition of a primary, secondary, or tertiary nitrogen atom in the R₂ side chain leads to more potent *N*-BPs.⁴² However, altering the position or relative orientation of the nitrogen in the pyridine ring side chain of RIS or removing it completely has a negative impact on the inhibition potency of these analogs towards FPPS (Table 2.2). Moving the nitrogen (*e.g.* NE-58051 and NE-58018) disrupts the favorable hydrogen bond geometry between the inhibitor and FPPS in the active site, leading to a loss in potency (Table 2.2). Likewise, removal of the nitrogen (*e.g.* analog NE-58022) leads to a significant loss in potency. Kinetic studies have shown that nitrogen

plays a role in the initial competitive phase of binding and in stabilization of the final isomerized state of FPPS.⁴³

Table 2.2 Effect of modifying nitrogen orientation in RIS on FPPS inhibition.

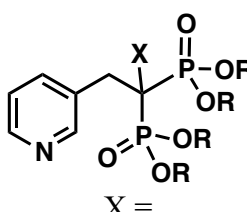
| Compound | Structure | Final K_i (nM) ^a |
|----------|---|-------------------------------|
| RIS |  | 0.36 ± 0.06 |
| NE-58051 |  | 78.0 ± 8.2 |
| NE-58018 |  | 0.74 ± 0.12 |
| NE-58022 |  | 302.6 ± 17.6 |

^aFrom Dunford, J. E., *et. al.* Ref 43

Attempts have been made to reduce the affinity of *N*-BPs to hydroxyapatite by removing the “bone hook” C α hydroxyl moiety. Analogs of RIS (Figure 2.1) were synthesized where the R₁ hydroxyl group was replaced with hydrogen and halides.⁴⁴ The acidity of methylene bisphosphonic acid is roughly the same first pK_a value as inorganic pyrophosphate (PPi; Figure 2.1), generating a potentially useful mimic.⁴⁵

Bone affinity, as well as hFPPS inhibition, was determined for α -halo-RIS (**20a-c**) and the α -H (**20d**) analogs (Table 2.3). As predicted, replacement of the α -OH group with hydrogen or a halide lead to a significant decrease in hydroxapatite (HAP) affinity. Interestingly, all α -analogs (**20a-d**) showed similar affinities, indicating that the α -OH group of RIS has a major impact on affinity through a direct coordination with bone minerals. All analogs inhibited hFPPS in the nanomolar range, with potencies decreasing in the order F > H > Cl > Br (IC₅₀ values 16.4, 34.2, 94.6, and 340.4, respectively). The comparable first pKa values of α -F analog, as well the small size of F may account for the lowest IC₅₀ value of the group. Whereas, the large size of the α -Cl may explain why it was the least potent inhibitor.⁴⁴

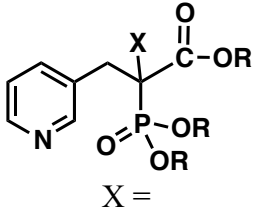
Table 2.3 Relative bone affinity and hFPPS inhibition of RIS analogs **20a-d**.

| Inhibitor |  X = | HAP Affinity (retention time, min) | hFPPS Inhibition IC ₅₀ (nM) |
|------------------------|--|--|---|
| RIS | OH | 9.97 ± 0.09 | 5.7 ± 0.57 ^b |
| 20a | F | 5.93 ± 0.07 | 16.4 ± 0.5 |
| 20b | Br | 6.03 ± 0.03 | 94.6 ± 16.1 |
| 20c | Cl | 5.73 ± 0.15 | 340.4 ± 37 |
| 20d^a | H | 5.83 ± 0.17 | 34.2 ± 2 |

^a By Procter & Gamble Pharmaceuticals
^b From Kavanagh, J. L.; *et. al.* Ref 46

Phosphonocarboxylate analogs of RIS were also synthesized to determine the effect of replacing a phosphonate on FPPS potency, affinity to bone, and geranylgeranyl transferase II (GGTII) inhibition. All compounds (**21a-e**) lost all potency against hFPPS (Table 2.4). The bone affinity of **21e** (Table 2.4)⁴⁷ was also less than RIS and **20a-d** (Table 2.3). Interestingly, despite a loss of hFPPS inhibition (Table 2.4), these compounds demonstrate anti-resorptive properties and inhibit tumor cell invasion *in vitro* and *in vivo*, similar to *N*-BPs. These compounds were found to exert their biological activity on GGTII. The halo-analogs preferentially inhibited GGTII activity (with IC₅₀ values 16.3, 16.4, and 17.7 for **21b**, **21c**, and **21d**, respectively) where **21b** with the small, electronegative α -F had slightly better potency.⁴⁴

Table 2.4 Relative bone affinity, hFPPS and GGTII inhibition of phosphonocarboxylate RIS analogs (**21a-e**).

| Inhibitor |  X = | HAP Affinity (retention time, min) | hFPPS Inhibition IC ₅₀ (μM) | GGTII Inhibition IC ₅₀ (μM) |
|-------------------------|--|--|--|--|
| 21a ^a | OH | 4.6 ± 0.06 | 254 ± 21 | 21 ± 5.7 |
| 21b | F | N/A | > 600 | 16.3 ± 0.3 |
| 21c | Br | N/A | > 600 | 16.4 ± 0.3 |
| 21d | Cl | N/A | > 600 | 17.7 ± 0.6 |
| 21e | H | N/A | N/A | 35.3 ± 8.7 |

^a From Ref. 47

All *N*-BPs in clinical use (Figure 2.1) have extremely poor bioavailability when administered both orally and intravenously. The amount of absorption of *N*-BPs ranges from 0.7% to 2.5%, where the most potent *N*-BPs are the most poorly absorbed ($F = \sim 1\%$).⁴⁸ Due to their highly hydrophilic nature, *N*-BPs are poorly absorbed in the gastrointestinal tract upon oral administration and instead require paracellular transport. Furthermore, only 50% of the absorbed drug remains in the body, accumulating almost exclusively in bone tissue, the rest is excreted in the urine without being metabolized.¹⁸ Consequently, efforts have been made to increase the lipophilicity of *N*-BPs to potentially increase exposure of these drugs to soft tissue and the peripheral blood, leading to improved cell or tissue penetration and biological activity.^{49,50}

Previous work has demonstrated that the current small, polar *N*-BP drugs are potent inhibitors of human FPPS (hFPPS; Table 2.5) and lack significant activity against related enzymes such as the human GGPPS (hGGPPS).⁵¹ Interestingly, by increasing the lipophilicity of *N*-BPs the potency against hGGPPS has also increased in some cases. It has been predicted that selectivity for GGPPS could be achieved by increasing the size of the inhibitor such that it would be too large to fit into the smaller hFPPS active site.⁵²

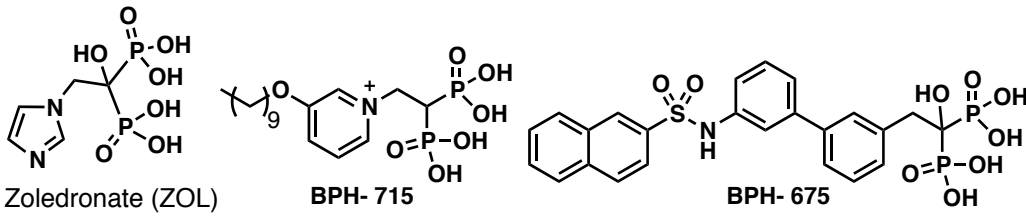
Table 2.5 Comparison of *N*-BP inhibition activities (IC_{50}) against hFPPS and hGGPPS.

| Compound | Experimental Inhibition, IC_{50} (μ M) | |
|----------|---|--------|
| | hFPPS | hGGPPS |
| | | |

| | | |
|---|---------------------|-----------------------|
| Ibandronate | 0.02 ^a | 83 ± 13 ^c |
| Pamidronate | 0.20 ^a | 180 ± 20 ^c |
| Risedronate | 0.01 ^a | 350 ± 50 ^c |
| Zoledronate | 0.0041 ^b | 100 ^d |
| ^a From Dunford, J., <i>et al.</i> Ref 42 ^b From Kavanagh, K. L., <i>et al.</i> Ref 46 ^c From Szabo, C. M., <i>et al.</i> Ref 51 ^d From Hudock, M. P., <i>et al.</i> Ref 53 | | |

Oldfield and co-workers explored these observations and predictions about lipophilicity and inhibitor size with the synthesis of a library of novel *N*-BPs.^{30b,50,54} A variety of lipophilic *N*-BPs, such as **BPH-715** and **BPH-675** (Table 2.6), were synthesized and tested for activity against hFPPS, hGGPPS and hDPPS (decaprenyl diphosphate synthase). Pyridinium *N*-BPs (*e.g.* **BPH-715**) were found to be dual hFPPS/hGGPPS inhibitors with low affinity to bone, capable of reducing Ras prenylation and increasing tumor cell apoptosis. In particular, **BPH-715** was 100-fold more potent than ZOL in tumor cell growth inhibition. This jump in potency may be attributed to the increased lipophilicity and therefore, improved bioavailability of the new *N*-BPs.¹¹ Moreover, dual inhibitors may act synergistically by preventing cross-prenylation of GTPases, as is the case upon treatment with FTIs.⁵⁰

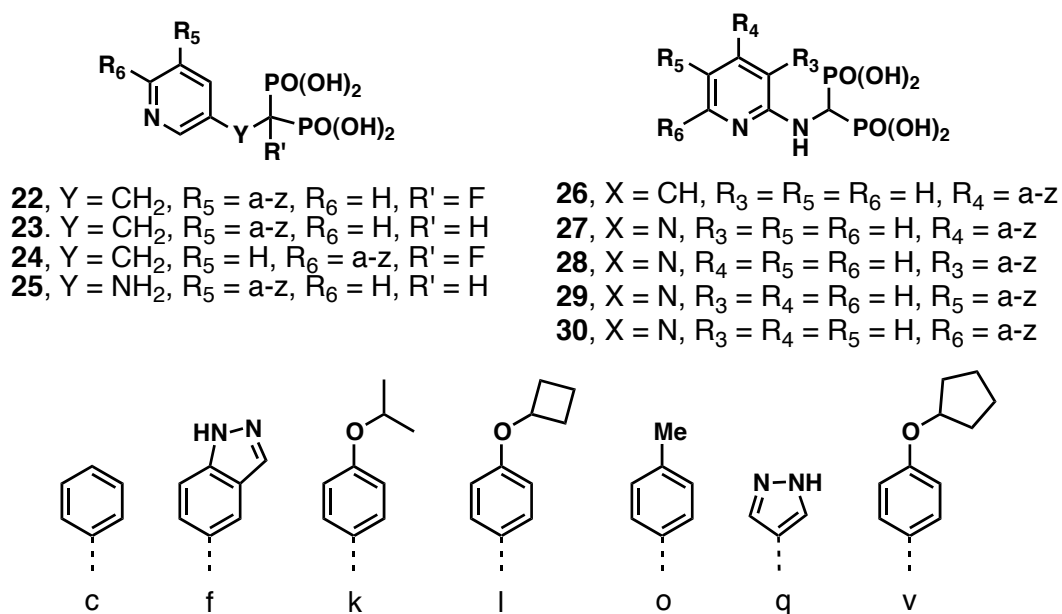
Table 2.6 Comparison of key lipophilic *N*-BP properties and activities to ZOL.

|  | | | | | | |
|--|----------------------|-----------------------------------|---|--|--|--|
| Inhibitor | SlogP ^(a) | hFPPS IC ₅₀ (μM) | hGGPPS IC ₅₀ (μM) ^{a,c} | hDPPS IC ₅₀ (μM) ^c | γδ T cell Activation ED ₅₀ (μM) ^c | NCI-H460 Tumor Cell Growth Inhibition EC ₅₀ (μM) ^d |
| ZOL | -5.52 | 0.0041 ^b | 100 | 5.5 | 1 | 15 |
| BPH-715 | -1.23 | 0.1 ^c | 0.28 | 0.585 | 0.8 | ~0.15 |
| BPH-675 | -2.93 | 126 ^c | 2.7 | 45 | 0 | 5 |

^a From Hudock, M. P., *et al.* Ref 53
^b From From Kavanagh, K. L., *et al.* Ref 46
^c From Zhang, Y., *et al.* Ref 30b
^d From Zhang, Y., *et al.* Ref 54c

Although there may be favorable qualities to structurally flexible dual inhibitors, targeting enzymes in biological pathways with selective and structurally rigid compounds tends to decrease the level of off-target toxicities. Selective inhibitors are also useful tools to study how disease pathologies may be related to a specific target pathway. It was this approach to medicinal chemistry that lead to the discovery of the isoprenylation redundancy mechanism of prenyltransferases, where GGT1 compensated for FTase *in vivo* upon FTase inhibition.^{24,31}

Recently, our group synthesized a library of selective hFPPS inhibitors with improved lipophilicity and bioavailability (Scheme 2.3).²⁴ The library was generated according to a divergent, parallel synthesis approach allowing for ample structural diversity for SAR analysis. Inhibitors such as RIS and ZOL (Figure 2.1) are competitive with allylic pyrophosphates (*i.e.* DMAPP and GPP; Scheme 2.2) by binding in the same sub-pocket, leaving room for IPP to simultaneously occupy the active site (Figure 2.7). The compound library was designed with the goal to fully occupy the hFPPS active site, particularly the IPP sub-pocket, and thereby take advantage of hydrophobic interactions between the inhibitor and protein.



Scheme 2.3 Key compounds from the library.²⁴

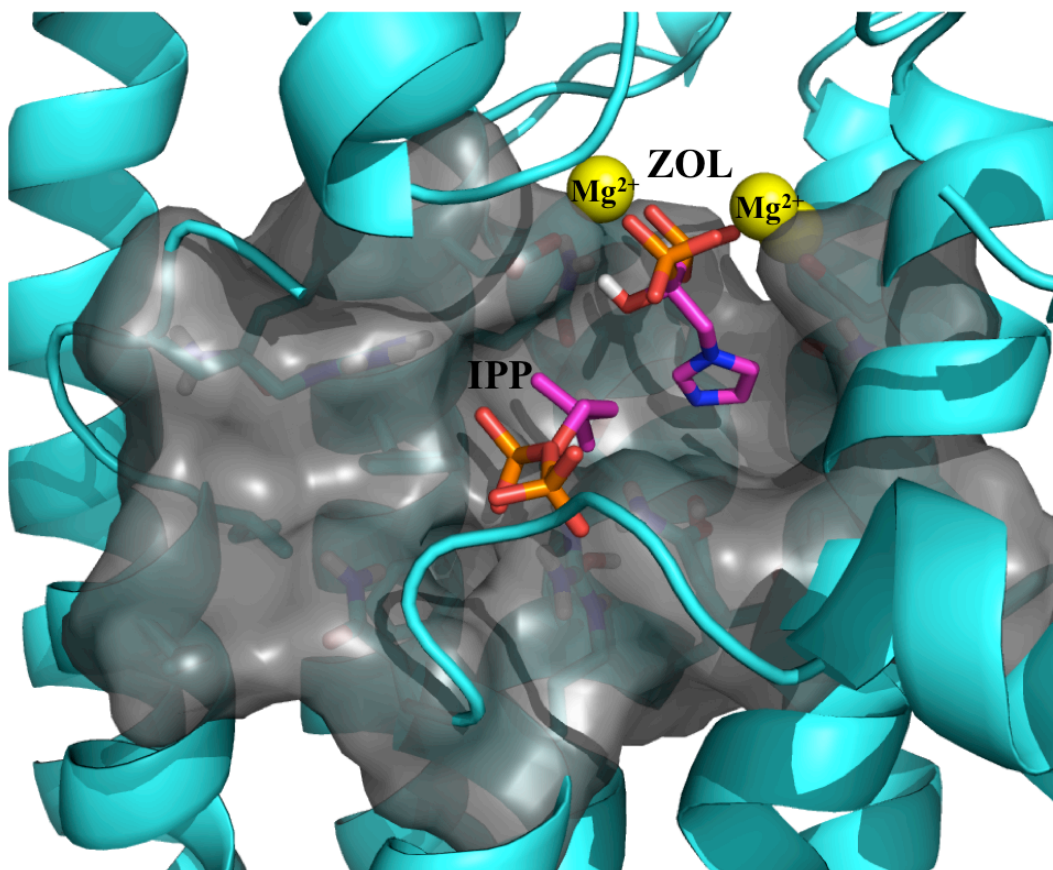


Figure 2.7 hFPPS (PDB 2F8Z) crystallized with IPP and ZOL in active site.²⁴

During hit-to-lead optimization, compounds **26-30** with 2-aminopyridine scaffolds were the most potent inhibitors in the library (Scheme 2.3). Of this group, scaffold **28** analogs with lipophilic R₄ substituents (*i.e.* **28k**, **28l**, **28o**, and **28v**) were the most potent against hFPPS (Table 2.7). For example, **28k** (IC₅₀ = 28 nM) was only ~2-fold less active than RIS. Furthermore, these potent inhibitors were completely inactive against hGGPPS, unlike other lipophilic *N*-BPs (Table 2.6). In addition to being an extremely selective hFPPS inhibitor, **28v** demonstrated better potency than RIS and ZOL against multiple myeloma tumor cell lines (Table 2.7), indicating that this enhanced cell-based potency may be due

in part to increased lipophilicity. These results highlight the significant therapeutic potential of optimized *N*-BP leads, such as **28**, for improved bioavailability.²⁴

Table 2.7 Biological activities of key 2-aminopyridine *N*-BPs.²⁴

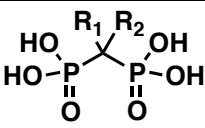
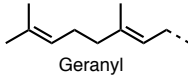
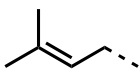
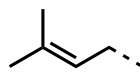
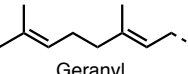
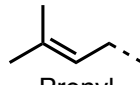
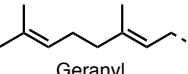
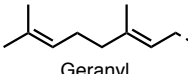
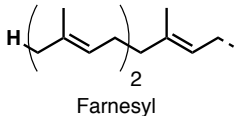
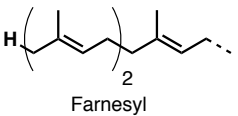
| Inhibitor | | hFPPS IC ₅₀ (nM) | hGGPPS IC ₅₀ (nM) | MM cells EC ₅₀ (μM) | | |
|------------|---|-----------------------------------|------------------------------------|--------------------------------|-----------|----------|
| | | | | JJN3 | RPMI-8226 | KMS 28PE |
| ZOL | - | 4.1 ^a | IN | 9.4 | 10.5 | 6.4 |
| RIS | - | 11 | IN | 10.0 | - | 10.6 |
| 28k | | 28 | IN | - | - | - |
| 28l | | 35 | IN | - | - | - |
| 28v | | 32 | IN | 8.6 | 3.6 | 3.2 |

^a From Kavanagh, K. L., *et. al.* Ref 46
IN = Inactive

A small library of mono- and di-isoprenoid bisphosphonates was recently reported by Wiemer and co-workers to be hGGPPS inhibitors (Table 2.8).⁵⁵ The most potent hGGPPS inhibitor, digeranyl bisphosphonate (DGBP, **34**), was found

to reduce the levels of GGPP without FPP depletion because it is inactive against hFPPS *in vitro*. This selectivity may be due to the bulky V-shape conformation of the inhibitor, where it is too large to fit into the active site of hFPPS. The *ex vivo* geranylgeranylation of Rap1 GTPases was also inhibited by DGBP (**34**).^{55a}

Table 2.8 Biological activity of mono- and di-substituted isoprenoid BPs.

| Inhibitor |  | | hGGPPS IC ₅₀ (μM) ^a | Rap1 (μM) ^a |
|-----------|---|---|---|---------------------------|
| | R ₁ | R ₂ | | |
| 31 |  Geranyl | H | 10 | 25 |
| 32 |  Prenyl |  Prenyl | > 100 | > 100 |
| 33 |  Geranyl |  Prenyl | 3 | 25 |
| 34 |  Geranyl |  Geranyl | 0.2 | 25 |
| 35 |  Farnesyl |  Farnesyl | INSOL | INSOL |
| ZOL | - | - | >100 | 100 |

^a From Weimer, A. J., *et al.* Ref 55a
INSOL = Insoluble in assay conditions

The mechanism of apoptosis of human chronic myelogenous leukemia (K562) cells induced by hGGPPS inhibition was studied with DGBP (**34**). The results of these studies suggest that apoptosis upon DGBP treatment occurs through two simultaneous mechanisms, whereby the caspase cascade is induced and increased levels of FPP lead to decreased gene expression of HMG-CoA reductase (the target of statins in the mevalonate pathway; Figure 2.3), FPPS, and SQS. Interestingly, DGBP acted synergistically with Lovastatin and ZOL to inhibit tumor cell growth. These results underscore the importance of (a) selective inhibition as a means of studying biological pathways, and (b) the important role that hGGPPS plays in cell survival and growth, and subsequently the validity of targeting hGGPPS in drug discovery.⁵⁶

Although great advancements have been made to understand the mechanisms of action of *N*-BPs since their discovery 40 years ago, there is much room for improvement. As the synthesis and subsequent biological evaluation of structurally diverse *N*-BPs has demonstrated that even minor modifications can have a major impact on the potency and selectivity of these inhibitors, further SAR studies are required to overcome the limitations of poor bioavailability and selectivity.

2.2 Results and Discussion

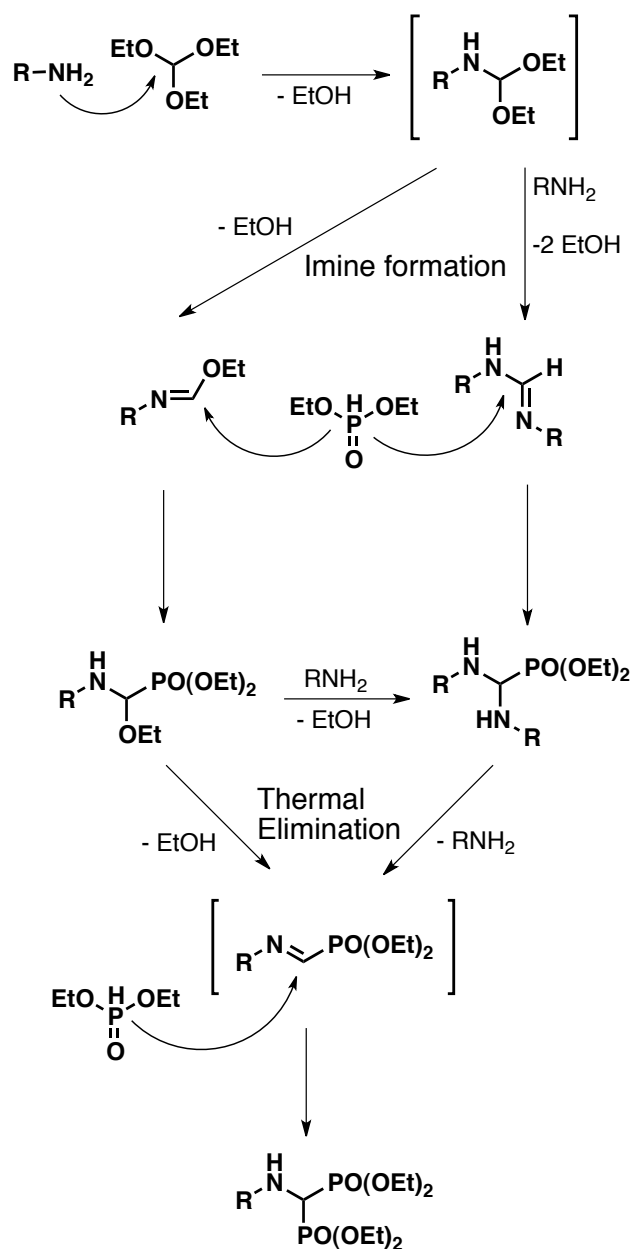
A small library of compounds was designed and synthesized with the main objective to identify hits selective for inhibiting hGGPPS versus hFPPS for further optimization. Taking into consideration the advantages and disadvantages of previously reported *N*-BPs, we decided to start the search with two lipophilic

scaffolds that were highly amenable to parallel synthesis to generate the structural diversity that may be required for SAR analysis. Our library of thieno[2,3-*d*]pyrimidin-4-ylamine compounds fit these requirements (Scheme 1.9 and 1.10) as did commercially available 2-aminobenzothiazoles.

2.2.1 Synthetic Studies

The small library of α -Amino bisphosphonate analogs were synthesized according to slightly modified published protocols.²⁴ In general, the heterocyclic amine, triethyl orthoformate, and diethylphosphite were heated in toluene to 130°C for 1-3 days to give the tetraethoxy-protected bisphosphonic esters in moderate to good yields. The bisphosphonic acids were isolated in good yields following deprotection with trimethylsilylbromide (TMS-Br) and MeOH.²⁴

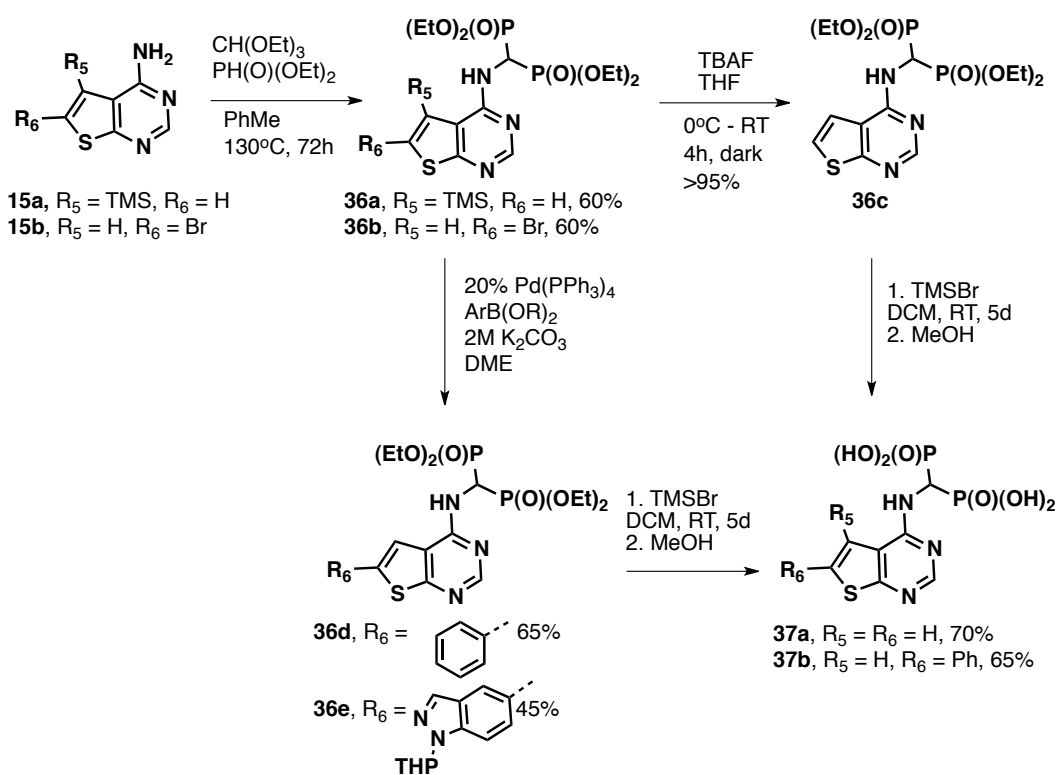
Conversion of the amine starting material to the protected BP can take up to three days to go to completion. This is likely due to the many different possible pathways of the reaction mechanism (Scheme 2.4). The first step involves the addition of the amine to triethyl orthoformate, followed by elimination of EtOH and/or addition of another amine to give an imine. Diethylphosphite attacks the imine to give a monophosphonate. Thermal elimination of EtOH or amine generates a monophosphonate imine, which is attacked by a second diethylphosphite to synthesize the final bisphosphonate ester product.⁵⁷



Scheme 2.4 General mechanism of α -amino *N*-BP synthesis.

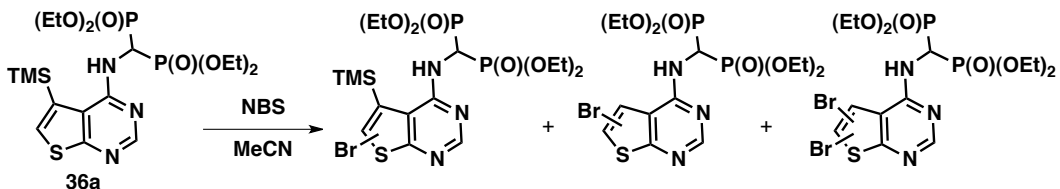
Mono-substituted thienopyrimidine *N*-BPs **36a** and **36b** were synthesized from thieno[2,3-*d*]pyrimidin-4-ylamines **15a** and **15b** (Scheme 1.9) in good yields (Scheme 2.5). The TMS group was removed from **36a** with TBAF in THF to give **36c** in excellent yield. The bromine substituted *N*-BP (**36b**) was investigated as a

branching point to synthesize structurally diverse mono-substituted thieno[2,3-*d*]pyrimidin-4-ylamine *N*-BPs via Suzuki cross-coupling reactions with aromatic boronates. Two analogs were isolated in good yield (**36d** and **36e**). Compounds **36c** and **36d** were successfully deprotected with TMSBr in DCM to give **37a** and **37b**, respectively. Simultaneous hydrolysis of the tetraethyl bisphosphonate esters and the THP protected indazole in refluxing 6N HCl overnight⁴⁴ was unsuccessfully attempted with analog (**36e**). Degradation occurred under these reaction conditions.



Scheme 2.5 Mono-substituted thieno[2,3-*d*]pyrimidin-4-ylamine *N*-BPs.

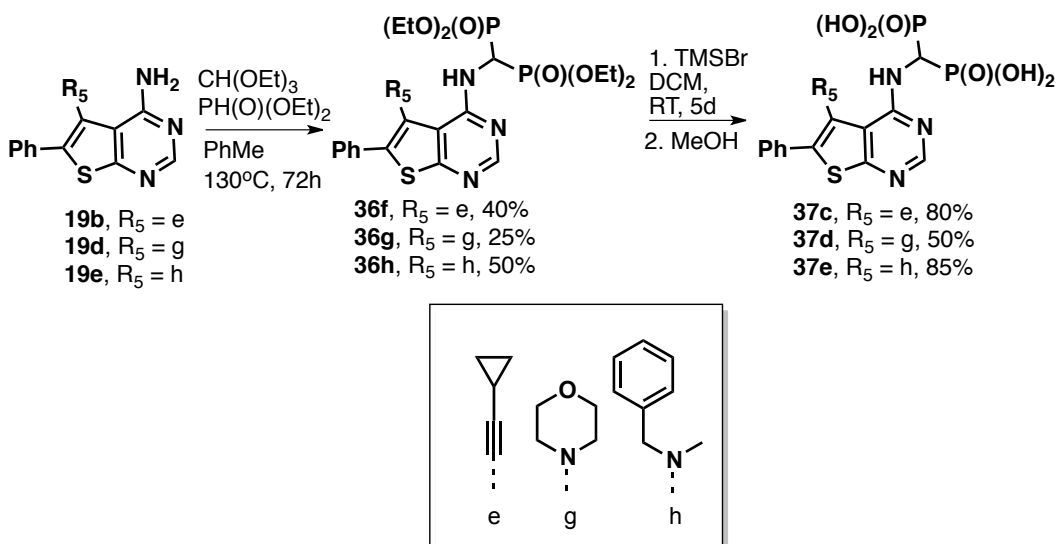
Issues with intermediate stability in the synthesis of **15b** (Table 1.9) hampered *N*-BP parallel synthesis (Scheme 2.5). To circumvent this instability of this intermediate, we attempted to brominate **15a** under a variety of conditions (Table 1. 6). This line of thought was also extended to *N*-BP **36a**. The non-radical electrophilic bromination of **36a** with NBS at RT in ACN after 18 hours gave unusual results (Scheme 2.6). By MS, three thienopyrimidine products were formed, 1) with a TMS group and one bromine atom; 2) with one bromine but without the TMS group; and 3) with two bromine atoms but without the TMS group. The substitution patterns were not elucidated of these three compounds and this synthetic route was not pursued.



Scheme 2.6 Attempted bromination of *N*-BP **36a**.

Di-substituted thieno[2,3-*d*]pyrimidin-4-ylamine *N*-BPs were also synthesized from di-substituted analogs (**19**; Scheme 1.10) in a similar manner (Scheme 2.7). The yields of **42e-g** were variable due to the difference in sterics and electronics of the R_5 groups. The thienopyrimidine (**19d**) with the bulkiest R_5 group gave the bisphosphonate (**36f**) in the poorest yield. The very bulky morpholino-group may have hindered imine formation from the amine or attack by diethylphosphite (Scheme 2.4). The cyclopropylethynyl group of **19b** was not

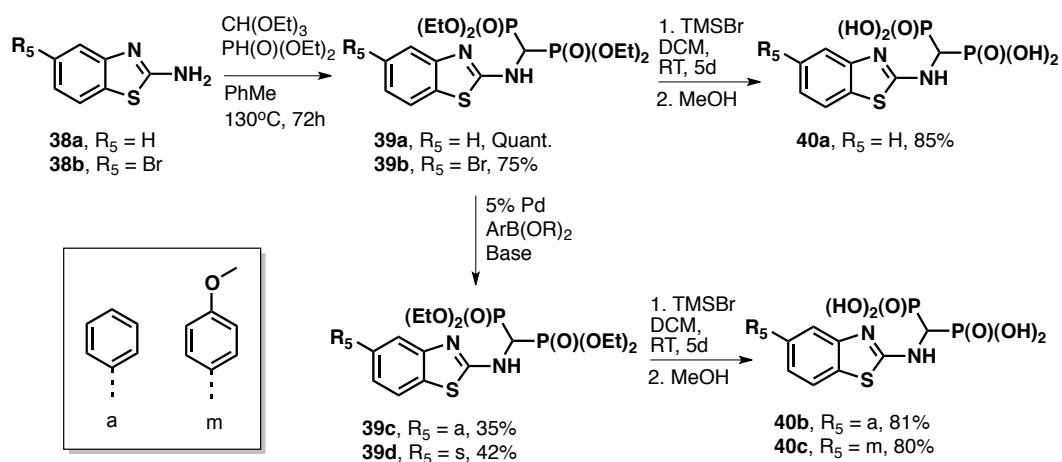
bulky but was conjugated to the thienopyrimidine ring and may have decreased the nucleophilicity of the amine, thereby decreasing imine formation (Scheme 2.4). The best yield was obtained for **36h**, with a non-conjugated, bulky yet flexible R_5 group. The amine (**19e**) did not likely suffer from decreased nucleophilicity or steric hindrance by the R_5 group (**h**).



Scheme 2.7 Synthesis of di-substituted thieno[2,3-*d*]pyrimidin-4-ylamine *N*-BPs.

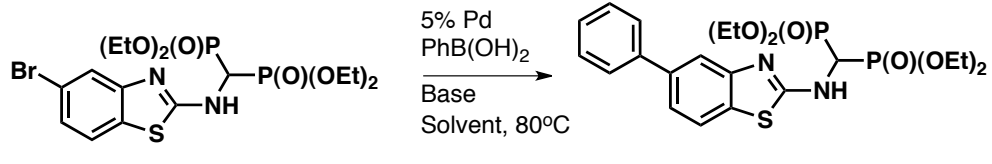
The 2-aminobenzothiazole *N*-BPs were synthesized from commercially available starting material (Scheme 2.8). The tetraethyl bisphosphonate esters **39a** ($R_5 = \text{H}$) and **39b** ($R_5 = \text{Br}$) were synthesized in good yield according to the standard protocol. The bromine-substituted **39b** was subjected to a few different protocols to determine optimal Suzuki cross-coupling conditions for efficient library synthesis. The initial Suzuki reaction conditions (Table 2.9, entry 1) were only moderately successful with phenylboronic acid. However, the yields suggested by LCMS were very poor with a great amount of starting material

decomposition when the base was changed to cesium carbonate in dioxane (entry 2, Table 2.9) and DMF (entry 3, Table 2.9). A very different protocol was attempted with a successful 60% yield as estimated by LCMS (entry 4, Table 2.9). Although the yield was not significantly better than entry 1, the amount of by-product formation appeared to be drastically reduced with these different reaction conditions. Therefore, this protocol was employed to synthesize **39c** and **39d** in moderate yield (Scheme 2.8). The use of the bulky bidentate phosphine ligand, dppf, may have increased the rate of reductive elimination in the Suzuki cross-coupling reaction mechanism by forcing the required *cis*-conformation of the two aryl groups around the Pd-metal center, leading to improved yields. The deprotected bisphosphonic acids **40a-c** were also isolated in good yields (Scheme 2.8).



Scheme 2.8 Synthesis of 2-aminobenzothiazole *N*-BPs.

Table 2.9 Trial Suzuki cross-coupling reaction conditions with 2-amino-5-bromobenzothiazole *N*-BPs.

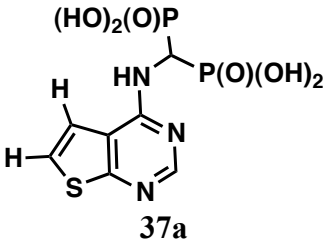
|  | | | | | |
|--|------------------------------------|-----------------------------------|-----------------------------|----------|---|
| Entry | Pd Source | Base | Solvent | Time (h) | Yield |
| 1 | Pd(PPh ₃) ₄ | 2M K ₂ CO ₃ | DME | 19 | 39c (40%) + decomposition (60%) ^a |
| 2 | Pd(PPh ₃) ₄ | Cs ₂ CO ₃ | Dioxane | 40 | decomposition (100%) ^b |
| 3 | Pd(PPh ₃) ₄ | Cs ₂ CO ₃ | DMF | 40 | 39c (15%) + decomposition (80%) ^b |
| 4 | Pd(dppf)Cl ₂ -DCM | K ₃ PO ₄ | DMF:H ₂ O (10:1) | 19 | 39c (60%) + decomposition (40%) ^b |
| ^a Isolated yield ^b Yield suggested by LCMS | | | | | |

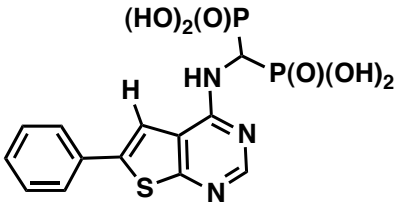
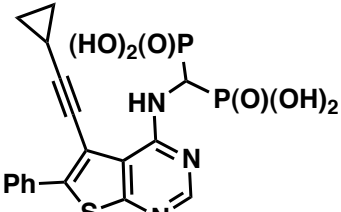
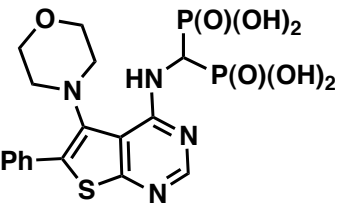
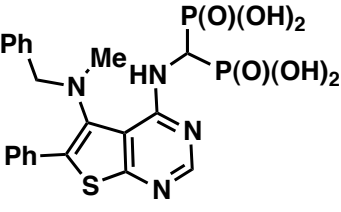
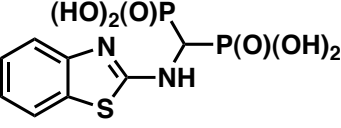
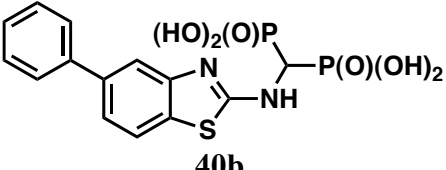
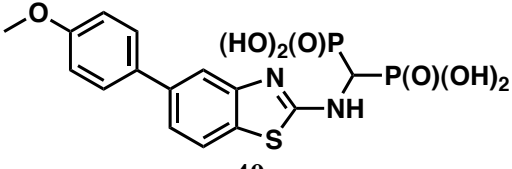
2.2.2 Biological Activity

As the goal was to find a hit with selectivity for hGGPPS over hFPPS, all members of the library were screened at fixed concentrations in our optimized assays (refer to experimental section).²⁴ Full dose-response inhibition curves (IC₅₀) were not determined for this initial screening. The hFPPS *in vitro* inhibition results are shown in Table 2.10. The C-6 mono-substituted thienopyrimidines (**37a**, **37b**) demonstrated 79% and 72% (entries 1 and 2) inhibitory activity against hFPPS at 10 μM, respectively. Although this inhibition may indicate that these *N*-

BPs remain small enough to fit in the active site pocket, an x-ray crystal structure with the inhibitors bound is required to determine binding mode. As predicted, the di-substituted *N*-BPs (**37c**, **37d**, and **37e**) did not show any significant inhibitory activity at any tested concentration (Table 2.10 entries, 3, 4, and 5). These poor inhibition results may support previously reported data, which suggest that the active site of hFPPS cannot accommodate these large *N*-BPs, allowing for the possibility of selective hGGPPS inhibitors with this bulky scaffold.^{55a} Interestingly, the *N*-BP inhibitors with a benzothiazole core (**40a**, **46b**, and **40c**) did not display significant hFPPS inhibition (Table 2.10, entries 6, 7, and 8), despite being comparable in size to the thienopyrimidine scaffold. Perhaps these negative results are a symptom of a lack of hetero-atoms required to form key binding interactions in the hFPPS active site.^{44,58,59} Therefore, scaffolds with additional hetero-atoms incorporated into the ring systems, such as thiazolopyridines, could provide interesting inhibition results upon investigation.

Table 2.10 Inhibition data for hFPPS.

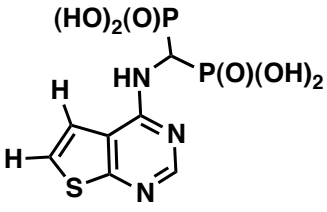
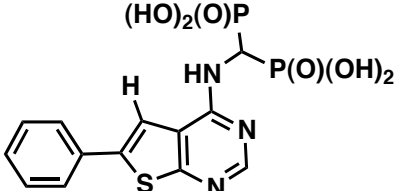
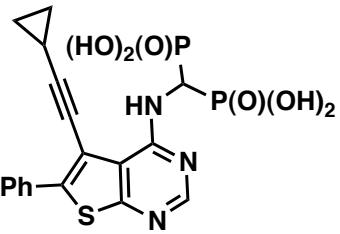
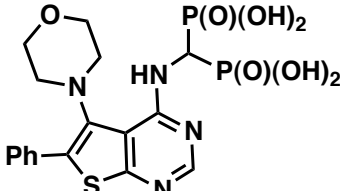
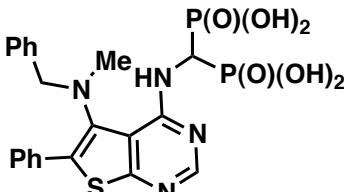
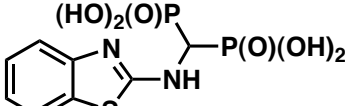
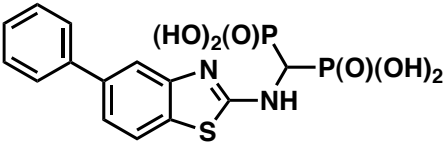
| Entry | Inhibitor | % hFPPS Inhibition ^{a,b} | | | |
|-------|---|-----------------------------------|------------------|-----------------|-------------------|
| | | 100 (μ M) | 10 (μ M) | 1 (μ M) | 0.1 (μ M) |
| 1 |  <p style="text-align: center;">37a</p> | ND | 79 | 36 | ND |

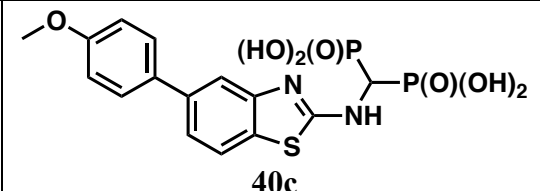
| | | | | | |
|---|--|-----|-----|-----|----|
| 2 |  <p>37b</p> | ND | 72 | 19 | ND |
| 3 |  <p>37c</p> | ND | <5 | <5 | <5 |
| 4 |  <p>37d</p> | ND | 9 | <5 | <5 |
| 5 |  <p>37e</p> | ND | <5 | <5 | <5 |
| 6 |  <p>40a</p> | 27 | <10 | <10 | ND |
| 7 |  <p>40b</p> | 13 | <5 | <5 | ND |
| 8 |  <p>40c</p> | <15 | <15 | <15 | ND |
| <p>^a Average values of three determinations with standard deviation < 6</p> <p>^b Range of variability of assay values is two-fold</p> <p>ND = Not determined</p> | | | | | |

Hits for hGGPPS inhibition were identified for further SAR (Table 2.11). Interestingly, C-6 mono-substituted thienopyrimidine **37b** demonstrated the most potent activity against hGGPPS (Table 2.11, entry 2). At 10 μM , **37b** was equipotent (where the range of variability of the optimized assay is two-fold) to the unsubstituted thienopyrimidine **37a** (Table 2.11, entry 1). The addition of the phenyl ring may allow for favourable binding interactions (such as π – cation) between hGGPPS and **37b** in the active site, which are unavailable to **37a**. Unfortunately, only one (**37d**) of the three di-substituted thienopyrimidine *N*-BPs exhibited inhibition activity (Table 2.11, entries 3, 4, and 5). Although these large scaffolds may be able to selectively occupy the active site of hGGPPS over hFPPS, more SAR will be required to investigate the active site binding interactions required for potent inhibition. Unexpectedly, none of the benzothiazole *N*-BPs displayed any significant hGGPPS inhibition (Table 2.11, entries 6, 7, and 8). Perhaps the incorporation of additional hetero-atoms as well as adjusting the substituent substitution pattern may enable better interactions with the enzyme and, therefore, produce better inhibition results.

Table 2.11 Inhibition data for hGGPPS.

| Entry | Inhibitor | % hGGPPS Inhibition ^{a,b} | | | |
|-------|-----------|------------------------------------|-------------------------|------------------------|--------------------------|
| | | 20 (μM) | 10 (μM) | 1 (μM) | 0.1 (μM) |
| | | | | | |

| | | | | | |
|---|--|----|------|----|----|
| 1 |  <p>37a</p> | ND | 37 | 23 | 18 |
| 2 |  <p>37b</p> | 57 | 45 | 36 | <5 |
| 3 |  <p>37c</p> | ND | < 20 | ND | ND |
| 4 |  <p>37d</p> | 43 | < 20 | ND | ND |
| 5 |  <p>37e</p> | ND | < 20 | ND | ND |
| 6 |  <p>40a</p> | ND | < 20 | ND | ND |
| 7 |  <p>40b</p> | ND | < 20 | ND | ND |

| | | | | | |
|--|---|----|------|----|----|
| 8 |  <p style="text-align: center;">40c</p> | ND | < 20 | ND | ND |
| ^a Average values of three determinations with standard deviations < 6 ^b Range of variability of assay values is two-fold ND = Not determined | | | | | |

2.3 Conclusions

Synthesis of the first thieno[2,3-*d*]pyrimidin-4-ylamine (**37**) and benzothiazole (**40**) scaffold *N*-BP inhibitors are reported in good yield. A small library of inhibitors with favorable SPR was tested for potency and selectivity for hGGPPS over hFPPS. Two hits with a thienopyrimidine scaffold (**37b** and **37d**) were identified as a starting point for further SAR studies with the goal to improve hGGPPS binding and potency.

2.4 Experimental

2.4.1 General Information

All intermediate compounds were purified by normal phase flash column chromatography on silica gel using an automated CombiFlash flash column chromatography instrument and the solvent gradient indicated. The purified tetraester *N*-BP compounds were analyzed for homogeneity by HPLC; homogeneity was confirmed by C18 reversed phase HPLC, using a Waters ALLIANCE® instrument (e2695 with 2489 UV detector and 3100 mass spectrometer), equipped with a Waters Atlantis T3 C18 5 μm column using the following conditions: Solvent A: H₂O, 0.1% formic acid; Solvent B: CH₃CN,

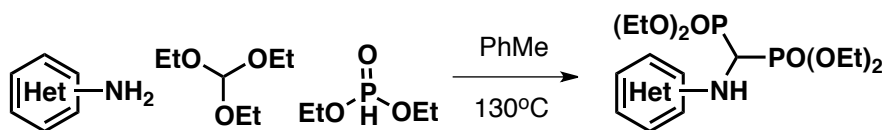
0.1% formic acid; Mobile phase: linear gradient from 95% A and 5% B to 5% A and 95% B in 13 min, then 2 min at 100% B; Flow rate: 1 mL/min.

In general, the tetraester *N*-BP intermediates were purified to >90% homogeneity before proceeding to the final deprotection step and the isolation of the bisphosphonic acids (*i.e.* final inhibitors). After ester hydrolysis, the final bisphosphonic acid products were precipitated and washed with HPLC grade DCM, MeOH, and small amounts of de-ionized H₂O to obtain the inhibitors as white solids; quantitative conversion of each tetraester to the corresponding bisphosphonic acid was confirmed by ³¹P NMR.

Key intermediates and all final products were characterized by ¹H and ¹³C NMR and MS; final compounds were further characterized by high-resolution mass spectrometry (HRMS). Chemical shifts (δ) are reported in ppm relative to the internal deuterated solvent or external H₃PO₄ (δ 0.00 ³¹P), unless indicated otherwise. HRMS spectra were recorded at the McGill University, MS facilities using electrospray ionization (ESI+/-) and Fourier transform ion cyclotron resonance mass analyzer (FTMS).

2.4.2 Synthesis of Key Compounds

General protocol for tetraethyl bisphosphonic ester synthesis:

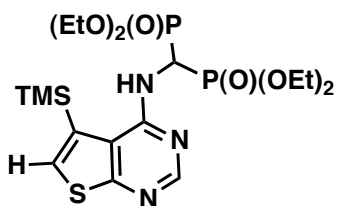


Triethyl orthoformate (2 eq.) and diethylphosphite (7 eq.) were added to a 15 mL pressure vessel containing a solution of heterocyclic amine in PhMe. The vessel was flushed with argon and the mixture stirred at 130°C for 72 hours. The

reaction mixture was concentrated and then purified by flash column chromatography (5-100% EtOAc/hexanes, 100% - 80% EtOAc/MeOH, solid loading) to afford the desired product.

Tetraethyl ((5-(trimethylsilyl)thieno[2,3-d]pyrimidin-4-yl)amino)methylene

bisphosphonate (36a, R₅ = TMS):



Isolated in 60% yield (37 mg).

¹H NMR (400 MHz, CD₃OD) δ 8.50 (s, 1H), 7.45 (s, 1H), 5.98 (td, J= 22.0, 9.9 Hz, 1H), 5.78 (d, J = 10.3 Hz, 1H), 4.28-4.12 (m, 8H), 1.26 (td, J = 7.1, 1.7 Hz, 12H), 0.52 (s, 9H)

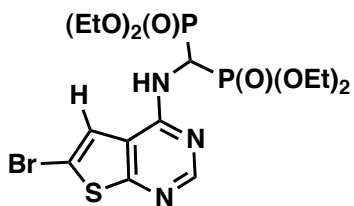
¹³C NMR (126 MHz, CD₃OD) δ 170.1, 156.2, 152.7, 133.0, 131.3, 120.3, 63.4 (d, J_{CP} = 122.5 Hz), 44.2 (t, J_{CP} = 583 Hz), 16.3, 0.1

³¹P NMR (81 MHz, CD₃OD) δ 14.81

MS (ESI+) *m/z* 532.15 [M + Na]⁺

Tetraethyl ((6-bromothieno[2,3-d]pyrimidin-4-yl)amino)methylene

bisphosphonate (36b, R₆ = Br):



Isolated in 60% yield (19 mg).

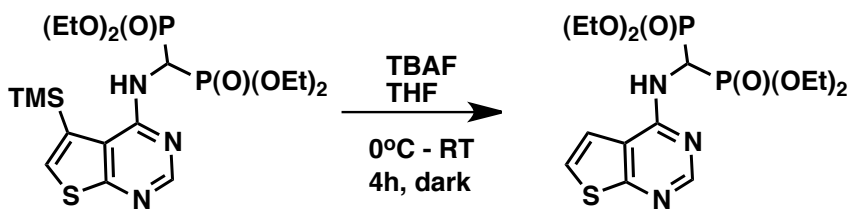
^1H NMR (400 MHz, CD_3OD) δ 8.44 (s, 1H), 7.84 (s, 1H), 5.94 (t, $J = 23.6$ Hz, 1H), 4.29 – 4.00 (m, 8H), 1.27 (dt, $J = 11.3, 7.1$ Hz, 12H)

^{13}C NMR (126 MHz, CD_3OD) δ 167.3, 154.8, 153.1, 121.7, 118.0, 112.0, 63.7, 44.2 (t, $J_{\text{CP}} = 580$ Hz), 15.2

^{31}P NMR (81 MHz, CD_3OD) δ 18.32

MS (ESI+) m/z 538.03 $[\text{M} + \text{Na}]^+$

Tetraethyl ((thieno[2,3-d]pyrimidin-4-ylamino)methylene) bisphosphonate (36c):



A solution of **36a** (47.4 mg, 0.093 mmol) in THF (2mL) was cooled to 0°C. To this was added 0.1 mL (23.6 mg, 0.1 mmol) of a 1M solution of TBAF in THF. Upon stirring for 20 minutes at 0°C, the mixture was warmed to ambient temperature and stirred for 4h in the dark. THF was removed *in vacuo* and the crude mixture was dissolved in 10 mL of EtOAc, washed with water (1 x 5 mL) and brine (1 x 5 mL), and dried over sodium sulfate. The desilylated product was obtained quantitatively as a pale yellow solid (41 mg).

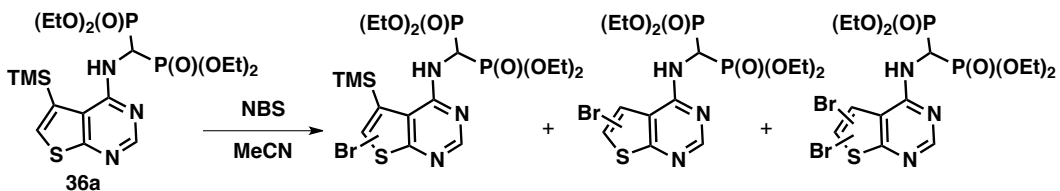
^1H NMR (500 MHz, CD_3OD) δ 8.47 (s, 1H), 7.72 (d, $J = 6.0$ Hz, 1H), 7.57 (d, $J = 6.0$ Hz, 1H), 6.00 (t, $J = 23.7$ Hz, 1H), 4.20 (m, 8H), 1.26 (m, 12H)

^{13}C NMR (126 MHz, CD_3OD) δ 167.6, 157.6, 154.1, 125.1, 119.8, 118.5, 65.2, 45.6 (t, $J_{\text{CP}} = 150.1$ Hz), 16.6

^{31}P NMR (81 MHz, CD_3OD) δ 18.52

MS (ESI+) m/z calculated for $\text{C}_{15}\text{H}_{25}\text{N}_3\text{NaO}_6\text{P}_2\text{S}$ $[\text{M} + \text{Na}]^+$ 460.08370, found 461.08320

Experimental Protocol for the Attempted Bromination of **36a** in Scheme 2.6:



Dry MeCN (7 mL) was added to **36a** (60 mg, 0.12 mmol) resulting in a pale yellow solution. NBS (22 mg, 0.12 mmol) was then added in one portion. The reaction mixture stirred under argon, in the absence of light, for 16 h at room temperature. TLC (10% MeOH/EtOAc) indicated the presence of remaining starting material. Another 15 mg of NBS was added and the mixture continued to stir for 20 h. The crude mixture was diluted with EtOAc (10 mL), washed with water (3 x 5 mL) and brine (5 mL), and dried over Na_2SO_4 . Purification by flash column chromatography (5-100% EtOAc/hexanes, 100% - 80% EtOAc/MeOH, solid loading) lead to the isolation of an inseparable mixture of three products with different substitution patterns (as determined by MS and ^{31}P NMR).

General protocol for Suzuki cross-coupling reactions with thienopyrimidine N-BP

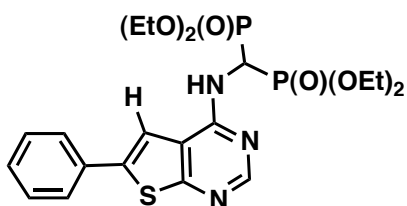
36b:

To a vial charged with **36b** (1 eq.), boronic acid (1.2 eq.), and $\text{Pd}(\text{PPh}_3)_4$ (20mol%) was added DME (~2 mL) followed by 2M K_2CO_3 (2.5 eq.). The

reaction mixture was degassed, purged with argon, and stirred at 80°C for 18 h. The mixture was filtered through Celite, washed with saturated sodium bicarbonate, and dried over Na₂SO₄. The crude material was purified by flash column chromatography (5-100% EtOAc/hexanes, 100% - 80% EtOAc/MeOH, solid loading) to afford the desired product.

Tetraethyl ((6-phenylthieno[2,3-d]pyrimidin-4-yl)amino)methylene

bisphosphonate (36d):



Isolated in 65% yield (38 mg).

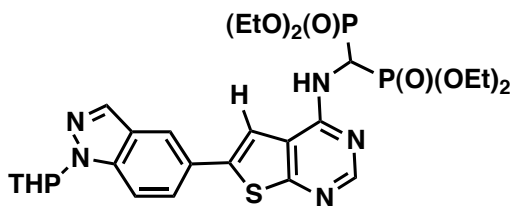
¹H NMR (500 MHz, CD₃OD) δ 8.45 (s, 1H), 8.04 (s, 1H), 7.75 (d, *J* = 7.3 Hz, 2H), 7.48 (t, *J* = 7.6 Hz, 2H), 7.41 (d, *J* = 7.3 Hz, 1H), 6.00 (t, *J* = 23.6 Hz, 1H), 4.22 (dd, *J* = 7.7, 3.2 Hz, 8H), 1.45 – 1.09 (m, 12H)

¹³C NMR (126 MHz, CD₃OD) δ 167.0, 157.2, 154.1, 142.7, 134.6, 130.4, 130.1, 127.2, 119.8, 115.2, 65.2, 45.6, 16.7

³¹P NMR (81 MHz, CD₃OD) δ 17.00

MS (ESI+) *m/z* 536.15 [M + Na]⁺

Tetraethyl ((6-(1-(tetrahydro-2H-pyran-2-yl)-1H-indazol-5-yl)thieno[2,3-d]pyrimidin-4-yl)amino)methylene bisphosphonate (36e):



Isolated in 70% yield (31 mg).

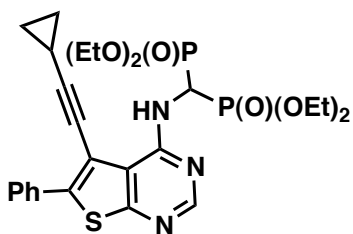
^1H NMR (400 MHz, CD_3OD) δ 8.46 (d, $J = 5.1$ Hz, 1H), 8.13 (d, $J = 3.3$ Hz, 1H), 8.03 (s, 1H), 7.83 (q, $J = 8.7$ Hz, 1H), 7.71 (d, $J = 6.1$ Hz, 1H), 7.57 (d, $J = 6.1$ Hz, 1H), 6.00 (dt, $J = 25.3, 21.9$ Hz, 1H), 5.86 (d, $J = 7.4$ Hz, 1H), 4.31 – 4.11 (m, 8H), 4.02 (d, $J = 10.7$ Hz, 1H), 3.90 – 3.76 (m, 1H), 3.88 – 3.75 (m, 1H), 2.51 (dd, $J = 20.7, 12.4$ Hz, 1H), 2.10 (dd, $J = 29.1, 12.5$ Hz, 2H), 1.92 – 1.61 (m, 3H), 1.40 – 1.15 (m, 12H)

^{13}C NMR (126 MHz, CD_3OD) δ 165.8 (d, $J_{\text{CP}} = 95.2$ Hz), 155.8 (d, $J_{\text{CP}} = 70.3$ Hz), 152.5, 141.7, 139.5, 134.2, 126.9, 125.0, 123.7, 118.5, 113.3, 110.9, 85.2 (d, $J_{\text{CP}} = 6.8$ Hz), 67.2, 63.7, 44.2 (t, $J_{\text{CP}} = 150.7$ Hz), 29.2, 24.9, 22.2, 15.2

^{31}P NMR (81 MHz, CD_3OD) δ 18.50

MS (ESI+) m/z 660.20 $[\text{M} + \text{Na}]^+$

Tetraethyl (((5-(cyclopropylethynyl)-6-phenylthieno[2,3-d]pyrimidin-4-yl)amino)methylene)bisphosphonate (36f, $\text{R}_5 = \text{e}$, $\text{R}_6 = \text{a}$):



Isolated in 40% yield (46 mg).

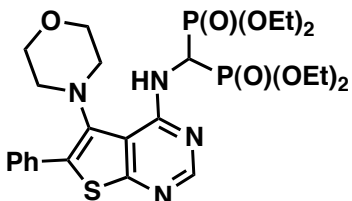
^1H NMR (400 MHz, CD_3OD) δ 8.48 (s, 1H), 7.89 – 7.85 (m, 2H), 7.53 – 7.44 (m, 3H), 5.94 (dt, $J = 22.3, 10.1$ Hz, 1H), 4.30 – 4.20 (m, 8H), 1.72 – 1.65 (m, 1H), 1.32 (t, $J = 7.1$ Hz, 12H), 1.03 – 0.99 (m, 2H), 0.98 – 0.94 (m, 2H)

^{13}C NMR (126 MHz, CD_3OD) δ 165.0, 157.5, 154.8, 144.6, 133.8, 130.6, 129.9, 129.3, 118.2, 109.8, 102.8, 71.5, 65.3, 45.4 (t, $J_{\text{CP}} = 149$ Hz), 16.8, 9.4, 1.1

^{31}P NMR (81 MHz, CD_3OD) δ 16.45

HRMS (ESI+) m/z calculated for $\text{C}_{26}\text{H}_{34}\text{SN}_3\text{O}_6\text{P}_2$ $[\text{M} + \text{H}]^+$ 578.16348, found 578.16381

Tetraethyl (((5-morpholino-6-phenylthieno[2,3-d]pyrimidin-4-yl)amino)methylene)bisphosphonate (36g, R₅ = g, R₆ = a):



Isolated in 25% yield (34 mg).

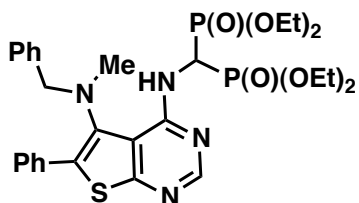
^1H NMR (500 MHz, CD_3OD) δ 8.74 (d, $J = 10.0$ Hz, 1H), 8.45 (s, 1H), 7.62 – 7.50 (m, 5H), 5.83 (td, $J = 22.1, 10.1$ Hz, 1H), 4.31 – 4.16 (m, 8H), 3.98 – 3.84 (m, 2H), 3.81 – 3.71 (m, 2H), 3.11 – 2.91 (m, 4H), 1.37 – 1.21 (m, 12H)

^{13}C NMR (126 MHz, CD_3OD) δ 164.0, 154.7, 139.5, 134.4, 134.1, 132.1, 130.6, 129.6, 115.4, 106.4, 68.2, 65.3, 54.3, 16.7

^{31}P NMR (81 MHz, CD_3OD) δ 16.90

HRMS (ESI+) m/z calculated for $\text{C}_{25}\text{H}_{37}\text{SN}_4\text{O}_7\text{P}_2$ $[\text{M} + \text{H}]^+$ 599.18450, found 599.18527

Tetraethyl (((5-(benzyl(methyl)amino)-6-phenylthieno[2,3-d]pyrimidin-4-yl)amino)methylene)bisphosphonate (36h, R₅ = h, R₆ = a):



Isolated in 45% yield (61 mg).

¹H NMR (300 MHz, CD₃OD) δ 8.43 (s, 1H), 7.58 – 7.46 (m, 3H), 7.41 – 7.34 (m, 2H), 7.25 – 7.15 (m, 3H), 7.07 – 6.96 (m, 2H), 5.88 (t, *J* = 22.4 Hz, 1H), 4.32 – 4.11 (m, 8H), 3.99 (d, *J* = 13.5 Hz, 1H), 3.90 (d, *J* = 13.5 Hz, 1H), 2.99 (s, 3H), 1.35 – 1.18 (m, 12H)

¹³C NMR (75 MHz, CD₃OD) δ 164.1, 154.5, 138.8, 138.5, 134.3, 133.0, 132.0, 130.4, 129.9, 129.5, 129.4, 128.4, 65.1, 60.1, 45.7, 30.7, 16.7

³¹P NMR (81 MHz, CD₃OD) δ 16.68

HRMS (ESI+) *m/z* calculated for C₂₉H₃₉SN₄O₆P₂ [M + H]⁺ 633.20502, found 633.20601

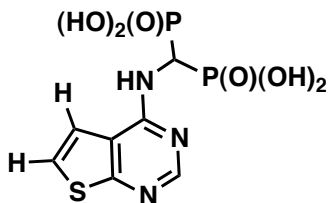
General protocol for hydrolysis of bisphosphonic esters:



TMSBr (15 eq) was added dropwise to a cooled solution of tetraethyl bisphosphonic ester (1 eq) in DCM (3 mL). The reaction mixture slowly warmed

to room temperature and stirred for 5 days. MeOH was added and stirred for 2 h. DCM, MeOH, and excess TMSBr were removed *in vacuo*. The desired product was purified by trituration.

(Thieno[2,3-d]pyrimidin-4-ylamino)methylene bisphosphonic acid (37a):



Isolated in 70% yield (21 mg).

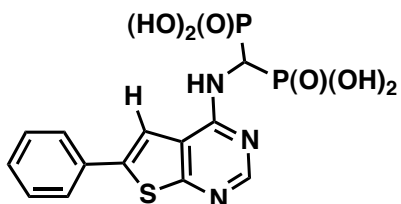
¹H NMR (500 MHz, D₂O, ND₄OD, DMSO internal standard) δ 8.28 (s, 1H), 7.55 (d, *J* = 5.9 Hz, 1 H), 7.43 (d, *J* = 6.1 Hz, 1H), 4.59 (t, *J* = 19.1 Hz, 1H)

¹³C NMR (126 MHz, D₂O, ND₄OD, DMSO internal standard) δ 164.3, 157.3, 154.2, 123.4, 119.8, 117.9, 51.7 (t, *J*_{CP} = 125.6 Hz)

³¹P NMR (81 MHz, D₂O, ND₄OD) δ 13.31

HRMS (ESI-) *m/z* calculated for C₇H₈SN₃O₆P₂ [M – H]⁻ 323.96873, found 323.96125

(6-phenylthieno[2,3-d]pyrimidin-4-ylamino)methylene bisphosphonic acid (37b):



Isolated in 63% yield (19 mg).

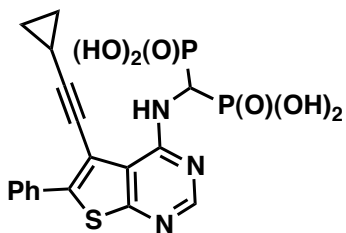
^1H NMR (400 MHz, D_2O , ND_4OD) δ 8.18 (s, 1H), 7.80 (s, 1H), 7.71 (d, $J = 7.4$ Hz, 2H), 7.42 (t, $J = 7.6$ Hz, 2H), 7.33 (t, $J = 7.4$ Hz, 1H)

^{13}C NMR (126 MHz, D_2O , ND_4OD) δ 163.1, 156.2, 153.6, 139.2, 133.2, 129.3, 128.6, 125.9, 118.6, 114.8

^{31}P NMR (81 MHz, D_2O , ND_4OD) δ 13.29

HRMS (ESI-) m/z calculated for $\text{C}_{13}\text{H}_{12}\text{SN}_3\text{O}_6\text{P}_2$ $[\text{M} - \text{H}]^-$ 399.99166, found 399.99268

((5-(Cyclopropylethynyl)-6-phenylthienof[2,3-d]pyrimidin-4-yl)amino)methylene bisphosphonic acid (37c):



Isolated in 80% yield (28 mg).

^1H NMR (400 MHz, D_2O , ND_4OD) δ 8.39 (s, 1H), 8.05 – 7.99 (m, 2H), 7.72 – 7.66 (m, 2H), 7.66 – 7.59 (m, 1H), 1.89 – 1.81 (m, 1H), 1.12 – 1.06 (m, 2H), 1.06 – 0.99 (m, 2H)

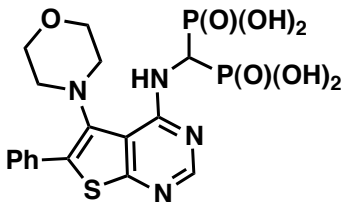
^{13}C NMR (75 MHz, D_2O , ND_4OD) δ 161.7, 153.9, 140.9, 132.6, 129.2, 128.9, 128.5, 122.6, 116.6, 109.8, 102.1, 70.3, 8.3, 0.2

^{31}P NMR (81 MHz, D_2O , ND_4OD) δ 13.60

HRMS (ESI-) m/z calculated for $\text{C}_{18}\text{H}_{16}\text{N}_3\text{O}_6\text{P}_2\text{S}$ $[\text{M} - \text{H}]^-$ 464.02403, found 464.02405

((5-morpholino-6-phenylthieno[2,3-d]pyrimidin-4-yl)amino)methylene

bisphosphonic acid (37d):



Isolated in 50% yield (12 mg).

^1H NMR (400 MHz, D_2O , ND_4OD) δ 8.40 – 8.38 (m, 1H), 7.83 – 7.78 (m, 2H), 7.73 – 7.69 (m, 3H), 4.35 – 4.29 (m, 2H), 3.89 – 3.83 (m, 2H), 3.35 – 3.28 (m, 2H), 3.14 – 3.05 (m, 2H)

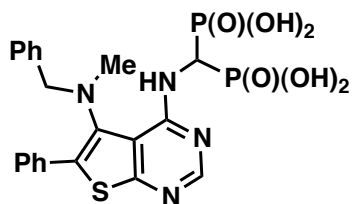
^{13}C NMR (126 MHz, D_2O , ND_4OD) δ 160.4, 157.4, 153.8, 139.5, 133.4, 131.2, 129.6, 129.1, 128.4, 113.8, 67.1, 52.3

^{31}P NMR (81 MHz, D_2O , ND_4OD) δ 14.16

HRMS (ESI-) m/z calculated for $\text{C}_{17}\text{H}_{19}\text{N}_4\text{O}_7\text{P}_2\text{S}$ $[\text{M} - \text{H}]^-$ 485.04528, found 485.04552

((5-(benzyl(methyl)amino)-6-phenylthieno[2,3-d]pyrimidin-4-yl)amino)methylene

bisphosphonic acid (37e):



Isolated in 85% yield (42 mg).

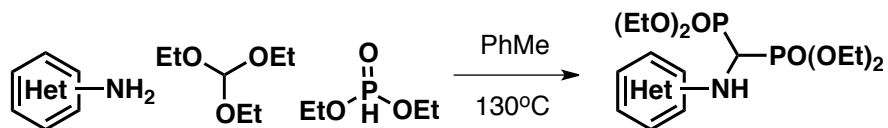
^1H NMR (500 MHz, D_2O , ND_4OD) δ 8.32 (s, 1H), 7.58 – 7.44 (m, 3H), 7.38 (s, 3H), 7.14 (s, 2H), 7.09 – 7.03 (m, 2H), 4.43 (d, $J = 13.5$ Hz, 1H), 4.11 (d, $J = 13.4$ Hz, 1H), 3.01 (s, 3H)

^{13}C NMR (126 MHz, D_2O , ND_4OD) δ 160.8, 157.3, 153.7, 137.6, 136.8, 133.3, 130.8, 129.8, 128.6, 128.3, 127.9, 127.2, 126.9, 114.5, 58.5, 43.3

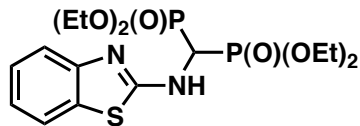
^{31}P NMR (81 MHz, D_2O , ND_4OD) δ 12.76

HRMS (ESI-) m/z calculated for $\text{C}_{21}\text{H}_{21}\text{N}_4\text{O}_6\text{P}_2\text{S}$ $[\text{M} - \text{H}]^-$ 519.06673, found 519.06625

Benzothiazole *N*-BP synthesis using the general protocol for tetraethyl bisphosphonic ester synthesis:



Tetraethyl ((benzo[d]thiazol-2-ylamino)methylene)bisphosphonate (39a):



Isolated in quantitative yield (446 mg).

^1H NMR (500 MHz, D_6 -DMSO) δ 8.77 (d, $J = 9.9$ Hz, 1H), 7.68 (d, $J = 7.8$ Hz, 1H), 7.42 (d, $J = 7.9$ Hz, 1H), 7.25 – 7.19 (m, 1H), 7.04 (dd, $J = 11.0, 4.2$ Hz, 1H), 5.22 – 5.11 (m, 1H), 4.15 – 3.97 (m, 8H), 1.15 (dt, $J = 17.8, 7.0$ Hz, 12H)

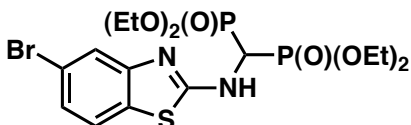
^{13}C NMR (126 MHz, D_6 -DMSO) δ 165.9, 151.5, 131.4, 126.1, 121.9, 121.6, 118.9, 63.4 (d, $J_{\text{CP}} = 27.5$ Hz), 48.8 (t, $J_{\text{CP}} = 146.3$ Hz), 40.2, 39.4, 16.6

^{31}P NMR (81 MHz, $\text{D}_6\text{-DMSO}$) δ 18.59

MS (ESI+) m/z 437.30 $[\text{M}+\text{H}]^+$

Tetraethyl (((5-bromobenzo[d]thiazol-2-yl)amino)methylene)bisphosphonate

(39b, $\text{R}_5 = \text{Br}$):



Isolated in 75% yield (759 mg).

^1H NMR (500 MHz, CD_3OD) δ 7.62 (d, $J = 1.8$ Hz, 1H), 7.53 (d, $J = 8.4$ Hz, 1H), 7.23 (dd, $J = 8.4, 1.9$ Hz, 1H), 5.36 (t, $J = 22.8$ Hz, 1H), 4.25 – 4.16 (m, 8H), 1.28 (dd, $J = 12.9, 7.0$ Hz, 12H)

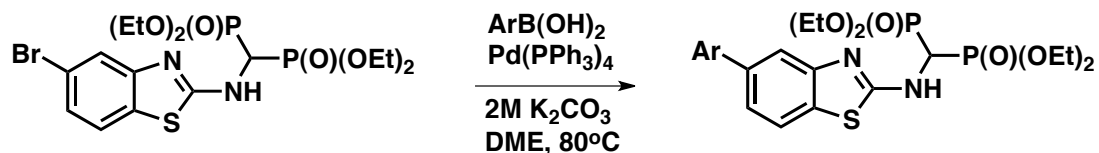
^{13}C NMR (126 MHz, CD_3OD) δ 167.2, 152.5, 130.1, 124.6, 121.9, 121.2, 118.9, 63.7, 15.2

^{31}P NMR (81 MHz, CD_3OD) δ 17.56

MS (ESI+) m/z 538.8 $[\text{M}+\text{Na}]^+$

General protocol (A) for Suzuki cross-coupling reactions with 2-

aminobenzothiazole N-BP 39b:

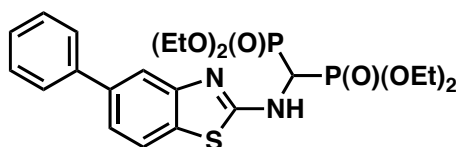


DME (2 mL) was added to a vial of **39b** (1 eq., ~0.2 mmol), boronic acid (1.5 eq.), and $\text{Pd}(\text{PPh}_3)_4$ (5mmol%). The vial was purged and flushed with argon. A 2M aqueous K_2CO_3 solution (2.5 eq.) was added to the reaction mixture. Upon

flushing with argon again, the mixture stirred at 80°C overnight. The mixture was filtered through Celite and washed with (1:1) EtOAc/MeOH. The crude mixture was purified by flash column chromatography (5-100% EtOAc/hexanes – 80% EtOAc/MeOH, solid loading) to afford the desired product.

Tetraethyl (((5-phenylbenzo[d]thiazol-2-yl)amino)methylene)bisphosphonate

(39c, R₅ = a):



Isolated in 35% yield (41 mg).

¹H NMR (500 MHz, CD₃OD) δ 7.72 (d, *J* = 1.5 Hz, 1H), 7.68 (d, *J* = 8.2 Hz, 1H), 7.65 – 7.61 (m, 2H), 7.43 (t, *J* = 7.7 Hz, 2H), 7.38 (dd, *J* = 8.2, 1.7 Hz, 1H), 7.33 (t, *J* = 7.4 Hz, 1H), 5.41 (t, *J* = 22.9 Hz, 1H), 4.23 (m, 8H), 1.29 (m, 12H)

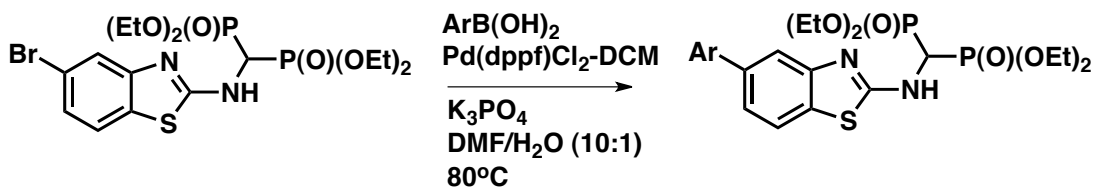
¹³C NMR (126 MHz, CD₃OD) δ 166.5, 151.6, 140.9, 139.5, 129.9, 128.5, 126.9, 126.6, 121.1, 120.8, 116.7, 63.9, 63.7, 47.4, 15.2

³¹P NMR (81 MHz, CD₃OD) δ 17.68

MS (ESI+) *m/z* 513.2 [M+Na]⁺

General protocol (B) for Suzuki cross-coupling reactions with 2-

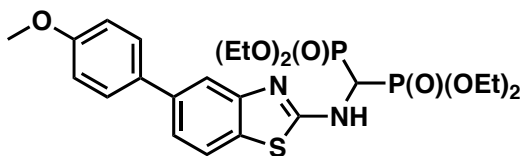
aminobenzothiazole BP 39b:



DMF:H₂O (10/1, 3 mL) was added to a vial of **39b** (1 eq., ~0.2 mmol), boronic acid (1.2 eq.), K₃PO₄ (1.2 eq.) and Pd(dppf)Cl₂-DCM (5mmol%). The vial was purged and flushed with argon. Upon flushing with argon again, the mixture stirred at 80°C overnight. The mixture was filtered through Celite and washed with (1:1) EtOAc/MeOH. The crude mixture was purified by flash column chromatography (5-100% EtOAc/hexanes – 80% EtOAc/MeOH, solid loading) to afford the desired product.

Tetraethyl (((5-(4-methoxyphenyl)benzo[d]thiazol-2-yl)amino)methylene)

bisphosphonate (39d, R₅ = m):



Isolated in 42% yield (58 mg).

¹H NMR (400 MHz, CD₃OD) δ 7.66 (dd, *J* = 12.5, 4.9 Hz, 2H), 7.57 (d, *J* = 8.8 Hz, 2H), 7.35 (dd, *J* = 8.2, 1.8 Hz, 1H), 7.00 (d, *J* = 8.8 Hz, 2H), 5.40 (t, *J* = 22.9 Hz, 1H), 4.30 – 4.16 (m, 8H), 3.83 (s, 3H), 1.30 (td, *J* = 7.1, 3.6 Hz, 12H)

¹³C NMR (126 MHz, CD₃OD) δ 160.7, 140.6, 134.8, 129.1, 122.2, 122.1, 117.6, 115.3, 106.4, 65.2, 55.8, 16.7

³¹P NMR (81 MHz, CD₃OD) δ 17.68

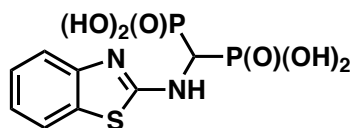
MS (ESI+) *m/z* 543.2 [M+Na]⁺

Benzothiazole bisphosphonic acid synthesis according to general protocol for

hydrolysis of bisphosphonic esters:



(Benzof[d]thiazol-2-ylamino)methylene bisphosphonic acid (40a):



Isolated in 85% yield (125 mg).

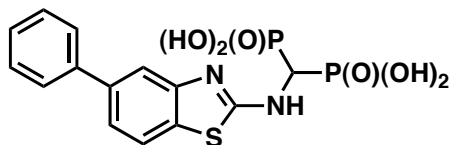
^1H NMR (500 MHz, D_2O , ND_4OD) δ 7.80 (d, $J = 7.8$ Hz, 1H), 7.30 (d, $J = 8.0$ Hz, 1H), 7.22 (t, $J = 7.7$ Hz, 1H), 7.01 (t, $J = 7.6$ Hz, 1H)

^{13}C NMR (126 MHz, D_2O , ND_4OD) δ 151.4, 129.6, 126.1, 121.4, 121.3, 116.9

^{31}P NMR (81 MHz, D_2O , ND_4OD) δ 12.52

HRMS (ESI-) m/z calculated for $\text{C}_8\text{H}_9\text{SN}_2\text{O}_6\text{P}_2$ $[\text{M} - \text{H}]^-$ 322.96620, found 322.96642

((5-Phenylbenzo[d]thiazol-2-yl)amino)methylene bisphosphonic acid (40b):



Isolated in 81% yield (26 mg).

^1H NMR (500 MHz, D_2O , ND_4OD) δ 7.63 (d, $J = 7.4$ Hz, 3H), 7.55 (s, 1H), 7.41 (t, $J = 7.7$ Hz, 2H), 7.30 (dd, $J = 14.5, 7.4$ Hz, 2H)

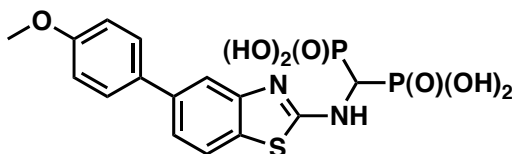
^{13}C NMR (126 MHz, D_2O , ND_4OD) δ 213.8, 152.2, 140.6, 138.8, 129.1, 127.6, 127.0, 121.7, 120.0, 114.9

^{31}P NMR (81 MHz, D_2O , ND_4OD) δ 12.77

HRMS (ESI-) m/z calculated for $\text{C}_{14}\text{H}_{13}\text{SN}_2\text{O}_6\text{P}_2$ $[\text{M} - \text{H}]^-$ 398.99750, found 398.99806

((5-(4-methoxyphenyl)benzo[d]thiazol-2-yl)amino)methylene bisphosphonic acid

(40c):



Isolated in 80% yield (37 mg).

^1H NMR (500 MHz, D_2O , ND_4OD) δ 7.68 (m, 3H), 7.59 (s, 1H), 7.33 (d, $J = 8.2$ Hz, 1H), 7.11 – 7.06 (m, 2H), 3.85 (s, 3H)

^{13}C NMR (126 MHz, D_2O , ND_4OD) δ 156.5, 152.2, 151.4, 138.3, 133.9, 128.4, 126.1, 121.7, 119.7, 119.1, 117.0, 116.8, 114.5, 71.8, 21.1

^{31}P NMR (81 MHz, D_2O , ND_4OD) δ 12.93

HRMS (ESI-) m/z calculated for $\text{C}_{15}\text{H}_{15}\text{SN}_2\text{O}_7\text{P}_2$ $[\text{M} - \text{H}]^-$ 429.00807, found 429.00818

2.4.3 Biological Assays

Reagents for Enzymatic Assay: Liquid scintillation cocktail was purchased from MP Biomedicals: Ecolite (#882475), ligroin was purchased from Sigma Aldrich, ^3H -IPP was purchased from American Radiolabeled Chemicals (ART 0377A: 1 mCi/mL, 60 Ci/ mmol in 0.1 M Tris pH 7.5), and unlabeled IPP and GPP were

purchased from Isoprenoids, Lc. as ammonium salts.

hFPPS Solution: The hFPPS enzyme was stored at -80 °C as a 2 µg/µL solution in the eluent buffer (50 mM HEPES at pH 7.5, 500 mM NaCl, 250 mM imidazole, 5% glycerol, and 0.5 mM TCEP).

IPP Solution: ³H-IPP was diluted with IPP to a specific activity of 33 mCi/mmol and 100 µM concentration in 1 M Tris at pH 7.7. It was stored at -10 °C, warmed to 0 °C, and kept on ice during assay setup.

GPP Solution: GPP was dissolved and diluted to a concentration of 100 µM in 1 M Tris at pH 7.7. It was stored at -10 °C, warmed to 0 °C, and kept on ice during assay setup.

Expression and Purification of Recombinant hFPPS: A plasmid encoding *N*-terminally His₆-tagged human FPPS (vector p11; SGC Oxford) was transformed into *E. coli* BL21(DE3) cells. The cells were induced overnight for hFPPS expression in the presence of 1 mM IPTG at 18°C and lysed in a buffer containing 50 mM HEPES (pH 7.5), 500 mM NaCl, 10 mM β-mercaptoethanol, 5 mM imidazole, and 5% (v/v) glycerol. Once the lysate was cleared by centrifugation, it was passed through a Ni-NTA agarose column. Elution was accomplished with an increasing imidazole gradient. Fractions containing hFPPS were pooled and applied to a Superdex 200 column, whereby the protein was eluted in high purity in a buffer containing 10 mM HEPES (pH 7.5), 10 mM β-mercaptoethanol, 500 mM NaCl, and 5% glycerol. The protein sample was concentrated to 12.5 mg/mL with a spin column concentrator.

In Vitro hFPPS Inhibition Assay: The assay was based on a literature procedure with minor modifications.¹⁷ All assays were run in triplicate using 40 ng of the

human recombinant FPPS and 10 μ M of both substrates, GPP and IPP (3 H-IPP, 3.33 mCi/mmol), in a final volume of 100 μ L buffer containing 50 mM Tris at pH 7.7, 0.5 mM TCEP, 2 mM MgCl₂, and 20 μ g/mL BSA. Assays were run with a 10 min preincubation period; the enzyme and inhibitor were incubated in the assay buffer in a volume of 80 μ L at 37 °C for 10 min. After 10 min, the GPP and IPP substrates were added to start the reaction and bring the inhibitor and substrate to the desired final concentrations. After the addition of all substrates, assays were incubated at 37 °C for 20 min. Upon termination of the assays by the addition of 200 μ L of HCl/methanol (1:4), followed by incubation for 10 min at 37 °C, the assay mixture was extracted with 700 μ L of ligroin (in order to separate reaction products from the unused substrate). Once the aqueous and organic layers separated, 300 μ L of the ligroin upper phase was combined with 8 mL of scintillation cocktail. The radioactivity was counted using a Beckman Coulter LS6500 liquid scintillation counter.

Expression, Purification, and *In Vitro* Inhibition Assay of Recombinant hGGPPS:

A plasmid encoding *N*-terminally His6-tagged human GGPPS (vector pNIC28-Bsa4, SGC Oxford) was transformed into *E. coli* BL21(DE3) cells as previously reported.⁶⁰ The protocols for both the purification and *in vitro* assay of hGGPPS were used as described by Kavanagh and co-workers.⁶⁰

2.5 Acknowledgments

Both hFPPS and hGGPPS assays were optimized by Y.-S. Lin. Thank you to Y.-S. Lin and J. W. De Schutter for taking the time to teach me the assay

techniques and methods. I am very grateful to J. W. De Schutter for testing inhibitors in Table 2.11 for hGGPPS inhibition.

2.6 References

1. Papapoulos, S. E. Bisphosphonates: how do they work? *Best Pract. Res. Cl. En.* **2008**, *22*, 831–847.
2. Papapoulos, S. E. Bisphosphonate actions: Physical chemistry revisited. *Bone*, **2006**, *38*, 613–616.
3. Russell, R. Determinants of structure–function relationships among bisphosphonates. *Bone*, **2007**, *40*, S21–S25.F
4. Green, J. R. Zoledronic acid: pharmacologic profile of a potent bisphosphonate *J. Organomet. Chem.* **2005**, *690*, 2439–2448.
5. (a) Menshutkin, N. Saure. *Ann. Chem. Pharmacol.* **1865**, *133*, 317–320.
(b) Von Baeyer, H.; Hofmann, K. A. Saure. *Berichte Dtsch. Chem. Ges.* **1897**, *20*, 1973–1978.
6. Russell, R. G. G. Inhibition of bone resorption by alendronate and risedronate does not require osteoclast apoptosis. *Bone* **2001**, *49*, 2–19.
7. (a) Schibler, D.; Russell, R. G. G.; Fleisch, H. *Clin. Sci.* **1968**, *35*, 363–372. (b) Fleisch, H. A.; Russell, R. G. G.; Bisaz, S.; Muehlbauer, R. C.; Williams, D. A. *Eur. J. Clin. Invest.* **1970**, *1*, 12–18.
8. (a) Russell, R. G. G.; Muehlbauer, R. C.; Bisaz, S.; Williams, D. A.; Fleisch, H. *Calcif. Tissue Res.* **1970**, *6*, 83–196. (b) Fleisch, H.; Russell, R. G. G.; Bisaz, S.; Casey, P. A.; Muehlbauer, R. C. *Calcif. Tissue Res.* **1968**, *2*, 10-10A.

-
9. Russell, R. G. G.; Smith, R.; Bishop, M. C.; Price, D. A.; Squire, C. M. *Lancet* **1973**, *299*, 10-12.
10. Clézardin, P.; Benzaïd, I.; Croucher, P. I. Bisphosphonates in preclinical bone oncology. *Bone* **2011**, *49*, 66–70.
11. Ebetino, F. H., Hogan, A.-M. L., Sun, S., Tsoumpra, M. K., Duan, X., Triffitt, J. T., Kwaasi, A. A.; Dunford, J. E.; Barnett, B. L.; Oppermann, U.; Lundy, M. W.; Boyde, A.; Kashemirov, B. A.; McKenna, C. E.; Russell, R. G. G. The relationship between the chemistry and biological activity of the bisphosphonates. *Bone*, **2011**, *49*, 20–33.
12. (a) Powles, T.; Paterson, A.; McCloskey, E.; Schein, P.; Scheffler, B.; Tidy, A.; Ashley, S.; Smith, I.; Ottestad, L.; Kanis, *J. Breast Cancer Res.* **2006**, *8*, R13.
(b) Correction in: *Breast Cancer Res.* **2006**, *8*, 406.
13. Rogers, M. J.; Crockett, J. C.; Coxon, F. P.; Mönkkönen, J. Biochemical and molecular mechanisms of action of bisphosphonates. *Bone* **2011**, *49*, 34–41.
14. (a) Frith, J. C.; Mönkkönen, J.; Auriola, S.; Mönkkönen, H.; Rogers, M. J. *Arth. Rheum.* **2001**, *44*, 2201–2210. (b) Lehenkari, P. P.; Kellinsalmi, M.; Napankangas, J. P.; Ylitalo, K. V.; Mönkkönen, J.; Rogers, M. J.; Azhayev, A.; Väänänen, H. K.; Hassinen, I. E. *Mol. Pharmacol.* **2002**, *61*, 1255–1262.
15. Fleisch, H. Bisphosphonates: Mechanisms of Action. *Endocr. Rev.* **1998**, *19*, 80–100.
16. (a) Evans, C. E.; Braidman, I. P. *Bone Miner.* **1994**, *26*, 95-107. (b) Lowik, C. W.; van der Pluijm, G.; van der Wee-Pals, L. J.; van Treslong-de Groot, H. B.; Bijvoet, O. L. *J. Bone Miner. Res.* **1988**, *3*, 185-192.

-
17. Dunford, J. E.; Kwaasi, A. A.; Rogers, M. J.; Barnett, B. L.; Ebetino, F. H.; Russell, R. G. G.; Oppermann, U.; Kavanagh, K. L. Structure–Activity Relationships Among the Nitrogen Containing Bisphosphonates in Clinical Use and Other Analogues: Time-Dependent Inhibition of Human Farnesyl Pyrophosphate Synthase. *J. Med. Chem.* **2008**, *51*, 2187–2195.
18. Drake, M. T.; Clarke, B. L.; Khosla, S. Bisphosphonates: mechanism of action and role in clinical practice. *Mayo Clin. Proc.* **2008**, *83*, 1032–1045.
19. (a) Roelofs, A. J.; Jauhiainen, M.; Mönkkönen, H.; Rogers, M. J.; Mönkkönen, J.; Thompson, K. *Br. J. Haematol.* **2009**, *144*, 245–250. (b) Thompson, K.; Rogers, M. J. *J. Bone Miner. Res.* **2004**, *19*, 278–288. (c) Gober, H. J.; Kistowska, M.; Angman, L.; Jenö, P.; Mori, L.; De Libero, G. *J. Exp. Med.* **2003**, *197*, 163–168. (d) Thompson, K.; Roelofs, A. J.; Jauhiainen, M.; Mönkkönen, H.; Mönkkönen, J.; Rogers, M. *J. Adv. Exp. Med. Biol.* **2010**, *658*, 11–20.
20. Bukowski, J. F.; Dascher, C. C.; Das, H. *Biochemical Biophys. Res. Co.* **2005**, *328*, 746–750.
21. (a) Mönkkönen, H.; Auriola, S.; Lehenkari, P.; Kellinsalmi, M.; Hassinen, I. E.; Vepsäläinen, J.; Mönkkönen, J. *Br. J. Pharmacol.* **2006**, *147*, 437–445. (b) Jauhiainen, M.; Mönkkönen, H.; Räikkönen, J.; Mönkkönen, J.; Auriola, S. *J. Chromatogr. B Analyt. Technol. Biomed. Life Sci.* **2009**, *877*, 2967–2975. (c) Mitrofan, L. M.; Pelkonen, J.; Mönkkönen, J. *Bone* **2009**, *45*, 1153–1160.
22. (a) Poccia, F.; Gioia, C.; Martini, F.; Sacchi, A.; Piacentini, P.; Tempestilli, M.; Agrati, C.; Amendola, A.; Abdeddaim, A.; Vlassi, C.; Malkovsky, M.;

D'Offizi, G. Zoledronic acid and interleukin-2 treatment improves immunocompetence in HIV-infected persons by activating V γ 9V δ 2 T cells. *AIDS*, **2009**, *23*, 555–565. (b) Song, Y.; Chan, J. M. W.; Tovian, Z.; Secrest, A.; Nagy, E.; Krysiak, K.; Bergan, K.; Parniak, M. A.; Oldfield, E. Bisphosphonate inhibitors of ATP-mediated HIV-1 reverse transcriptase catalyzed excision of chain-terminating 3'-azido, 3'-deoxythymidine: A QSAR investigation. *Bioorg. Med. Chem.* **2008**, *16*, 8959–8967. (c) Parniak, M. A.; Mellors, J. A.; Oldfield, E.; Tovian, Z.; Chan, J. M. W. WO **2005/023270A2** (d) Agrati, C.; Alonzi, T.; De Santis, R.; Castilletti, C.; Abbate, I.; Capobianchi, M. R.; D'Offizi, G.; Siepi, F.; Fimia, G. M.; Tripodi, M.; Poccia, F. Activation of V γ 2V δ 2 T cells by non-peptidic antigens induces the inhibition of subgenomic HCV replication. *Int. Immunol.* **2005**, *18*, 11–18.

23. (a) Martin, M. B.; Grimley, J. S.; Lewis, J. C.; Heat, H. T.; Bailey, B. N.; Kendrick, H.; Yardley, V.; Caldera, A.; Lira, R.; Urbina, J. A.; Moreno, S. N. J.; Docampo, R.; Croft, S. L.; Oldfield, E. Bisphosphonates inhibit the growth of *Trypanosoma brucei*, *Trypanosoma cruzi*, *Leishmania donovani*, *Toxoplasma gondii*, and *Plasmodium falciparum*: a potential route to chemotherapy. *J. Med. Chem.* **2001**, *44*, 909–916. (b) Subhash, G.; Chan, J. M. W.; Lea, C. R.; Meints, G. A.; Lewis, J. C.; Tovian, Z. S.; Flessner, R. M.; Loftus, T. C.; Bruchhaus, I.; Kendrick, H.; Croft, S. L.; Kemp, R. G.; Kobayashi, S.; Nozaki, T.; Oldfield, E. Effects of bisphosphonates on the growth of *Entamoeba histolytica* and *Plasmodium* species *in vitro* and *in vivo*. *J. Med. Chem.* **2004**, *47*, 175–187. (c) Hudock, M. P.; Sanz-Rodriguez, C. E.; Song, Y.; Chan, J. M. W.; Zhang, Y.;

Odeh, S.; Kosztowski, T.; Leon-Rossell, A.; Concepcio`n, J. L.; Yardley, V.; Croft, S. L.; Urbina, J. A.; Oldfield, E. Inhibition of *Trypanosoma cruzi* hexokinase by bisphosphonates. *J. Med. Chem.* **2006**, *49*, 215–223.

24. Lin, Y.-S.; Park, J.; De Schutter, J. W.; Huang, X. F.; Berghuis, A. M.; Sebag, M.; Tsantrizos, Y. S. Design and Synthesis of Active Site Inhibitors of the Human Farnesyl Pyrophosphate Synthase: Apoptosis and Inhibition of ERK Phosphorylation in Multiple Myeloma Cells. *J. Med. Chem.* **2012**, *55*, 3201–3215.

25. (a) Clézardin, P.; Fournier, P.; Boissier, S.; Peyruchaud, O. *In vitro* and *in vivo* antitumor effects of bisphosphonates. *Curr. Med. Chem.* **2003**, *10*, 173–180. (b)

Green, J. R. Antitumor effects of bisphosphonates, *Cancer* **2003**, *97*, 840–847. (c)

Verdijk, R.; Franke, H. R.; Wolbers, F.; Vermes, I. Differential effects of bisphosphonates on breast cancer cell lines, *Cancer Lett.* **2007**, *246*, 308–312. (d)

Sato, K.; Yuasa, T.; Nogawa, M.; Kimura, S.; Segawa, H.; Yokota, A.; Maekawa, T. A third-generation bisphosphonate (YM529) successfully prevented the growth of bladder cancer *in vitro* and *in vivo*. *Br. J. Cancer* **2006**, *95*, 1354–1361. (e)

Wada, A.; Fukui, K.; Sawai, Y.; Imanaka, K.; Kiso, S.; Tamura, S.; Shimomura, I.; Hayashi, N. Pamidronate induced anti-proliferative, apoptotic, and anti-migratory effects in hepatocellular carcinoma. *J. Hepatol.* **2006**, *44*, 142–150. (f)

Chuah, C.; Barnes, D. J.; Kwok, M.; Corbin, A.; Deininger, M. W.; Druker, B. J.; Melo, J. V. Zoledronate inhibits proliferation and induces apoptosis of imatinib-resistant chronic myeloid leukaemia cells. *Leukemia* **2005**, *19*, 1896–1904. (g)

Inoue, R.; Matsuki, N. A.; Jing, G.; Kanematsu, T.; Abe, K.; Hirata, M. The inhibitory effect of alendronate, a nitrogen-containing bisphosphonate on the

PI3K–Akt–NfκB pathway in osteosarcoma cells. *Br. J. Pharmacol.* **2005**, *146*, 633–641. (h) Yamagishi, S.; Abe, R.; Inagaki, Y.; Nakamura, K.; Sugawara, H.; Inokuma, D.; Nakamura, H.; Shimizu, T.; Takeuchi, M.; Yoshimura, A.; Bucala, R.; Shimizu, H.; Imaizumi, T. Minodronate, a newly developed nitrogen-containing bisphosphonate, suppresses melanoma growth and improves survival in nude mice by blocking vascular endothelial growth factor signaling. *Am. J. Pathol.* **2004**, *165*, 1865–1874.

26. Clezardin, P.; Ebetino, F. H.; Fournier, P. G. J. Bisphosphonates and Cancer-Induced Bone Disease: Beyond Their Antiresorptive Activity. *Cancer Res.* **2005**, *65*, 4971–4974.

27. (a) Bezzi, M.; Hasmim, M.; Bieler, G.; Dormond, O.; Rüegg, C. Zoledronate sensitizes endothelial cells to tumor necrosis factor-induced programmed cell death. *J. Biol. Chem.* **2003**, *278*, 43603–43614. (b) Giraud, E.; Inoue, M.; Hanahan, D. An amino- bisphosphonate targets MMP-9-expressing macrophages and angiogenesis to impair cervical carcinogenesis. *J. Clin. Invest.* **2004**, *114*, 623–633.

28. (a) Smyth, M. J.; Godfrey, D. I.; Trapani, J. A. A fresh look at tumor immunosurveillance and immunotherapy. *Nat. Immunol.* **2001**, *2*, 293–299. (b) Anderson, K. C.; Kyle, R. A.; Dalton, W. S.; Landowski, T.; Shain, K.; Jone, R.; Hazlehurst, L.; Berenson, J. Multiple myeloma: new insights and therapeutic approaches. *Hematology* **2000**, 166–179. (c) Schultze, J. L.; Nadler, L. M. T cell mediated immunotherapy for B cell lymphoma. *J. Mol. Med.* **1999**, *77*, 322–331.

(d) Groh, V.; Steinle, A.; Bauer, S.; Spies, T. Recognition of stress-induced MHC molecules by intestinal epithelial $\gamma\delta$ T cells. *Science* **1998**, *279*, 1737–1740.

29. Stresing, V.; Daubin , F.; Benza id, I.; M nkk nen, H.; Cl zardin, P. Bisphosphonates in cancer therapy. *Cancer Lett.* **2007**, *257*, 16–35.

30. (a) Lolli, M. L.; Rolando, B.; Tosco, P.; Chaurasia, S.; Di Stilo, A.; Lazzarato, L.; Gorassini, E.; Ferracini, R.; Oliaro-Bosso, S.; Fruttero, R.; Gasco, A. Synthesis and preliminary pharmacological characterisation of a new class of nitrogen-containing bisphosphonates (N-BPs). *Bioorg. Med. Chem.* **2010**, *18*, 2428. (b) Zhang, Y.; Cao, R.; Yin, F.; Lin, F.-Y.; Wang, H.; Krysiak, K.; No, J.-H.; Mukkamala, D.; Houlihan, K.; Li, J.; Morita, C. T.; Oldfield, E. Lipophilic Pyridinium Bisphosphonates: Potent $\gamma\delta$ T Cell Stimulators. *Angew. Chem., Int. Ed.* **2010**, *49*, 1136.

31. Berndt, N.; Hamilton, A. D.; Sebt, S. M. Targeting protein prenylation for cancer therapy. *Nature Rev. Cancer* **2011**, *11*, 775–791.

32. (a) Van Cutsem, E. van de Velde, H.; Karasek, P.; Oettle, H.; Vervenne, W. L.; Szawlowski, A.; Schoffski, P.; Post, S.; Verslype, C.; Neumann, H.; Safran, H.; Humblet, Y.; Perez Ruixo, J.; Ma, Y.; Von Hoff, D. Phase III trial of gemcitabine plus tipifarnib compared with gemcitabine plus placebo in advanced pancreatic cancer. *J. Clin. Oncol.* **2004**, *22*, 1430–1438. (b) Rao, S.; Cunningham, D.; de Gramont, A.; Scheithauer, W.; Smakal, M.; Humblet, Y.; Kourteva, G.; Iveson, T.; Andre, T.; Dostalova, J.; Illes, A.; Belly, R.; Perez-Ruixo, J. J.; Park, Y. C.; Palmeret, P. A. Phase III double-blind placebo-controlled study of farnesyl transferase inhibitor R115777 in patients with refractory advanced colorectal

cancer. *J. Clin. Oncol.* **2004**, *22*, 3950–3957. (c) Blumenschein, G.; Ludwig, C.; Thomas, G.; Tan, E.; Fanucchi, M.; Santoro, A.; Crawford, J.; Breton, J.; O'Brien, M.; Khuri, F. A randomized phase III trial comparing lonafarnib/carboplatin/paclitaxel versus carboplatin/paclitaxel (CP) in chemotherapy-naïve patients with advanced or metastatic non-small cell lung cancer. *Lung Cancer* **2005**, *49*, S30. (d) Harousseau, J. L.; Martinelli, G.; Jedrzejczak, W. W.; Brandwein, J. M.; Bordessoule, D.; Masszi, T.; Ossenkoppele, G. J.; Alexeeva, J. A.; Beutel, G.; Maertens, J.; Vidriales, M.-B.; Dombret, H.; Thomas, X.; Burnett, A. K.; Robak, T.; Khuageva, N. K.; Golenkov, A. K.; Tothova, E.; Mollgard, L.; Park, Y. C.; Bessems, A.; De Porre, P.; Howeset, A. J. A randomized phase 3 study of tipifarnib compared with best supportive care, including hydroxyurea, in the treatment of newly diagnosed acute myeloid leukemia in patients 70 years or older. *Blood* **2009**, *114*, 1166–1173.

33. (a) Rowell, C. A.; Kowalczyk, J. J.; Lewis, M. D.; Garcia, A. M. Direct demonstration of geranylgeranylation and farnesylation of Ki-Ras *in vivo*. *J. Biol. Chem.* **1997**, *272*, 14093–14097. (b) Whyte, D. B.; Kirschmeier, P.; Hockenberry, T. N.; Nunez-Oliva, I.; James, L.; Catino, J. J.; Bishop, W. R.; Pai, J.-K. K- and N-Ras are geranylgeranylated in cells treated with farnesyl protein transferase inhibitors. *J. Biol. Chem.* **1997**, *272*, 14459–14464. (c) Lerner, E. C.; Zhang, T. T.; Knowles, D. B.; Qian, Y.; Hamilton, A. D.; Sebt, S. M. Inhibition of the prenylation of K-Ras, but not H- or N-Ras, is highly resistant to CAAX peptidomimetics and requires both a farnesyltransferase and a geranylgeranyltransferase I inhibitor in human tumor cell lines. *Oncogene* **1997**,

-
- 15, 1283–1288. (d) Sun, J.; Qian, Y.; Hamilton, A. D.; Sebti, S. M. Both farnesyltransferase and geranylgeranyltransferase I inhibitors are required for inhibition of oncogenic K-Ras prenylation but each alone is sufficient to suppress human tumor growth in nude mouse xenografts. *Oncogene* **1998**, *16*, 1467–1473.
34. O'Dwyer, P. J.; Gallagher, M.; Nguyen, B.; Waddell, M. J.; Chiorean, E. G. Phase I accelerated dose-escalating safety and pharmacokinetic (PK) study of GGTI-2418, a novel geranylgeranyltransferase I inhibitor in patients with refractory solid tumors. *Ann. Oncol.* **2010**, *21*, ii42.
35. (a) Wennerberg, K. The Ras superfamily at a glance. *J. Cell Sci.*, **2005**, *118*, 843–846. (b) Hoffman, G. R.; Nassar, N.; Cerione, R. A. Structure of the Rho family GTP-binding protein Cdc42 in complex with the multifunctional regulator RhoGDI. *Cell* **2000**, *100*, 345–356.
36. (a) Clark, E. A.; Golub, T. R.; Lander, E. S.; Hynes, R. O. Genomic analysis of metastasis reveals an essential role for RhoC. *Nature* **2000**, *406*, 532–535. (b) Hakem, A.; Sanchez-Sweetman, O.; You-Ten, A.; Duncan, G.; Wakeham, A.; Khokha, R.; Mak, T. W. RhoC is dispensable for embryogenesis and tumor initiation but essential for metastasis. *Genes Dev.* **2005**, *19*, 1974–1979.
37. (a) Nguyen, U. T.; Guo, Z.; Delon, C.; Wu, Y.; Deraeve, C.; Franzel, B.; Bon, R. S.; Blankenfeldt, W.; Goody, R. S.; Waldmann, H.; Wolters, D.; Alexandrov, K.; Analysis of the eukaryotic prenylome by isoprenoid affinity tagging. *Nature Chem. Biol.* **2009**, *5*, 227–235. (b) Maurer-Stroh, S.; Koranda, M.; Benetka, W.; Schneider, G.; Sirota, F. L.; Eisenhaber, F. Towards complete sets of farnesylated and geranylgeranylated proteins. *PLoS Comput. Biol.* **2007**, *3*, e66. (c) Perez-Sala

D. Protein isoprenylation in biology and disease: general overview and perspectives from studies with genetically engineered animals. *Front. Biosci.* **2007**, *12*, 4456–4472.

38. Liu, M.; Sjogren, A. K.; Karlsson, C.; Ibrahim, M. X.; Andersson, K. M.; Olofsson, F. J.; Wahlstrom, A. M.; Dalin, M.; Yu, H.; Chen, Z.; Yang, S. H.; Young, S. G.; Bergo, M. O. Targeting the protein prenyltransferases efficiently reduces tumor development in mice with K-RAS-induced lung cancer. *Proc. Natl. Acad. Sci. USA* **2010**, *107*, 6471–6476.

39. Li, L.; Zhang, W.; Cheng, S.; Cao, D.; Parent, M. Isoprenoids and Related Pharmacological Interventions: Potential Application in Alzheimer's Disease. *Mol. Neurobiol.* **2012**, *46*, 64–77.

40. Russell, R. G. G.; Xia, Z.; Dunford, J. E.; Oppermann, U.; Kwaasi, A.; Hulley, P. A.; Kavanagh, K. L.; Triffitt, J. T.; Lundy, M. W.; Phipps, R. J.; Barnett, B. L.; Coxon, F. P.; Rogers, M. J.; Watts, N. B.; Ebetino, F. H. Bisphosphonates: An Update on Mechanisms of Action and How These Relate to Clinical Efficacy. *Ann. NY Acad. Sci.* **2007**, *1117*, 209–257.

41. Thompson, K.; Rogers, M. J.; Coxon, F. P.; Crockett, J. C. Cytosolic entry of bisphosphonate drugs requires acidification of vesicles after fluid-phase endocytosis. *Mol. Pharmacol.* **2006**, *69*, 1624–1632.

42. Dunford, J. E.; Thompson, K.; Coxon, F. P.; Luckman, S. P.; Hahn, F. M.; Poulter, C. D.; Ebetino, F. H.; Rogers, M. J. Structure-activity relationships for inhibition of farnesyl diphosphate synthase *in vitro* and inhibition of bone

resorption *in vivo* by nitrogen-containing bisphosphonates. *J. Pharmacol. Exp. Ther.* **2001**, *296*, 235–242.

43. Dunford, J. E.; Kwaasi, A. A.; Rogers, M. J.; Barnett, B. L.; Ebetino, F. H.; Russell, R. G. G.; Oppermann, U.; Kavanagh, K. L. Structure–Activity Relationships Among the Nitrogen Containing Bisphosphonates in Clinical Use and Other Analogues: Time-Dependent Inhibition of Human Farnesyl Pyrophosphate Synthase. *J. Med. Chem.* **2008**, *51*, 2187–2195.

44. Marma, M. S.; Xia, Z.; Stewart, C.; Coxon, F.; Dunford, J. E.; Baron, R.; Kashemirov, B. A.; Ebetino, F. H.; Triffitt, J. T.; Russell, R. G. G.; McKenna, C. E. Synthesis and Biological Evaluation of α -Halogenated Bisphosphonate and Phosphonocarboxylate Analogues of Risedronate. *J. Med. Chem.* **2007**, *50*, 5967–5975.

45. (a) Berkowitz, D. B.; Bose, M. (R-Monofluoroalkyl)phosphonates: a class of isoacidic and “tunable” mimics of biological phosphates. *J. Fluorine Chem.* **2001**, *112*, 13-33. (b) McKenna, C. E.; Shen, P.-D. Fluorination of methanediphosphonate esters by perchloryl fluoride synthesis of fluoromethanediphosphonic acid and difluoromethanediphosphonic acid. *J. Org. Chem.* **1981**, *46*, 4573-4576. (c) Blackburn, G. M.; England, D. A.; Kolkman, F. Monofluoro- and difluoromethylenebisphosphonic acids: isopolar analogs of pyrophosphoric acid. *Chem. Commun.* **1981**, 930-932.

46. Kavanagh, K. L.; Guo, K.; Dunford, J. E.; Wu, X.; Knapp, S.; Ebetino, F. H.; Rogers, M. J.; Russell, R. G. G.; Oppermann, U. The molecular mechanism of

nitrogen-containing bisphosphonates as antiosteoporosis drugs. *Proc. Natl. Acad. Sci. USA* **2006**, *103*, 7829–7834.

47. (a) Coxon, F. P.; Ebetino, F. H.; Mules, E. H.; Seabra, M. C.; McKenna, C. E.; Rogers, M. J. Phosphonocarboxylate inhibitors of Rab geranylgeranyl transferase disrupt the prenylation and membrane localization of Rab proteins in osteoclasts *in vitro* and *in vivo*. *Bone* **2005**, *37*, 349-358. (b) Coxon, F. P.; Helfrich, M. H.; Larijani, B.; Muzylak, M.; Dunford, J. E.; Marshall, D.; McKinnon, A. D.; Nesbitt, S. A.; Horton, M. A.; Seabra, M. C.; Ebetino, F. H.; Rogers, M. J. Identification of a novel phosphonocarboxylate inhibitor of Rab geranylgeranyl transferase that specifically prevents Rab prenylation in osteoclasts and macrophages. *J. Biol. Chem.* **2001**, *276*, 48213-48222.

48. Cremers, S.; Papapoulos, S. Pharmacology of bisphosphonates. *Bone*, **2011**, *49*, 42–49.

49. Simoni, D.; Gebbia, N.; Invidiata, F. P.; Eleopra, M.; Marchetti, P.; Rondanin, R.; Baruchello, R.; Provera, S.; Marchioro, C.; Tolomeo, M.; Marinelli, L.; Limongelli, V.; Novellino, E.; Kwaasi, A.; Dunford, J.; Buccheri, S.; Caccamo, N.; Dieli, F. Design, synthesis, and biological evaluation of novel aminobisphosphonates possessing an *in vivo* antitumor activity through a $\gamma\delta$ -T lymphocytes-mediated activation mechanism. *J. Med. Chem.* **2008**, *51*, 6800–6807.

50. Oldfield, E. Targeting Isoprenoid Biosynthesis for Drug Discovery: Bench to Bedside. *Acc. Chem. Res.* **2010**, *43*, 1216–1226.

-
51. Szabo, C. M.; Matsumura, Y.; Fukura, S.; Martin, M. B.; Sanders, J. M.; Sengupta, S.; Cieslak, J. A.; Loftus, T. C.; Lea, C. R.; Lee, H.-J.; Koohang, A.; Coates, R. M.; Sagami, H.; Oldfield, E. Inhibition of Geranylgeranyl Diphosphate Synthase by Bisphosphonates and Diphosphates: A Potential Route to New Bone Antiresorption and Antiparasitic Agents. *J. Med. Chem.* **2002**, *45*, 2185–2196.
52. Cao, R.; Chen, C. K. M.; Guo, R.-T.; Wang, A. H. J.; Oldfield, E. Structures of a potent phenylalkyl bisphosphonate inhibitor bound to farnesyl and geranylgeranyl diphosphate synthases. *Proteins* **2008**, *73*, 431–439.
53. Hudock, M. P.; Zhang, Y.; Guo, R.-T.; Cao, R.; No, J. H.; Liang, P.-H.; Ko, T.-P.; Chang, T.-H.; Chang, S.-C.; Song, Y.; Axelson, J.; Kumar, A.; Wang, A. H. J.; Oldfield, E. Inhibition of Geranylgeranyl Diphosphate Synthase by Bisphosphonates: A Crystallographic and Computational Investigation. *J. Med. Chem.* **2008**, *51*, 5594–5607.
54. (a) No, J. H. J.; de Macedo Dossin, F. F.; Zhang, Y. Y.; Liu, Y.-L. Y.; Zhu, W. W.; Feng, X. X.; Yoo, J. A. J.; Lee, E.; Wang, K.; Hui, R.; Freitas-Junior, L. H.; Oldfield, E. Lipophilic analogs of zoledronate and risedronate inhibit Plasmodium geranylgeranyl diphosphate synthase (GGPPS) and exhibit potent antimalarial activity. *Proc. Natl. Acad. Sci. USA* **2012**, *109*, 4058–4063. (b) Wang, H.; Sarikonda, G.; Puan, K. J.; Tanaka, Y.; Feng, J.; Giner, J. L.; Cao, R.; Mönkkönen, J.; Oldfield, E.; Morita, C. T. Indirect Stimulation of Human V2V2 T Cells through Alterations in Isoprenoid Metabolism. *J. Immunol.* **2011**, *187*, 5099–5113. (c) Zhang, Y. Cao, R.; Yin, F.; Hudock, M. P.; Guo, R.-T.; Krysiak, K.; Mukherjee, S.; Gao, Y.-G.; Robinson, H.; Song, Y.; No, J. H.; Bergan, K.;

Leon, A.; Cass, L.; Goddard, A.; Chang, T.-K.; Lin, F.-Y.; Van Beek, E.; Papapoulos, S.; Wang, A. H. J.; Kubo, T.; Ochi, M.; Mukkamala, D.; Oldfield, E. Lipophilic Bisphosphonates as Dual Farnesyl/Geranylgeranyl Diphosphate Synthase Inhibitors: An X-ray and NMR Investigation. *J. Am. Chem. Soc.* **2009**, *131*, 5153–5162.

55. (a) Wiemer, A. J.; Yu, J. S.; Lamb, K. M.; Hohl, R. J.; Wiemer, D. F. Mono- and dialkyl isoprenoid bisphosphonates as geranylgeranyl diphosphate synthase inhibitors. *Bioorg. Med. Chem.* **2008**, *16*, 390–399. (b) Wiemer, A. J.; Tong, H.; Swanson, K. M.; Hohl, R. J. Digeranyl bisphosphonate inhibits geranylgeranyl pyrophosphate synthase. *Biochem. Biophys. Res. Comm.* **2007**, *353*, 921–925. (c) Shull, L. W.; Wiemer, A. J.; Hohl, R. J.; Wiemer, D. F. Synthesis and biological activity of isoprenoid bisphosphonates. *Bioorg. Med. Chem.* **2006**, *14*, 4130–4136.

56. Dudakovic, A.; Wiemer, A. J.; Lamb, K. M.; Vonnahme, L. A.; Dietz, S. E.; Hohl, R. J. Inhibition of Geranylgeranyl Diphosphate Synthase Induces Apoptosis through Multiple Mechanisms and Displays Synergy with Inhibition of Other Isoprenoid Biosynthetic Enzymes. *J. Pharmacol. Exp. Ther.* **2007**, *324*, 1028–1036.

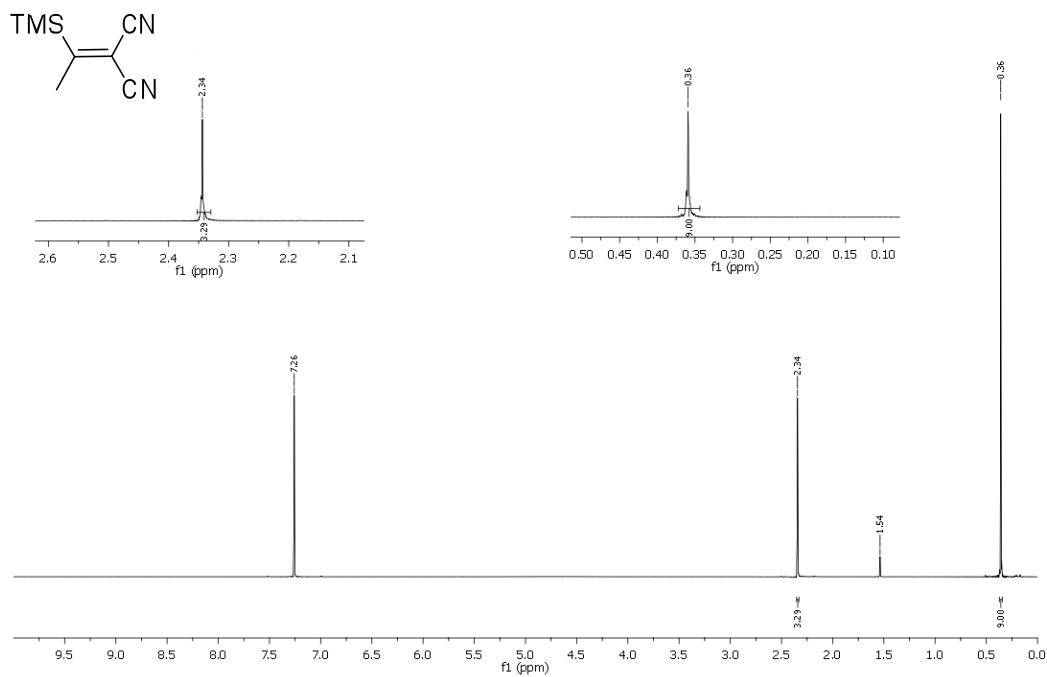
57. Dąbrowska, E.; Burzyńska, A.; Mucha, A.; Matczak-Jon, E.; Sawka-Dobrowolska, W.; Berlicki, Ł.; Kafarski, P. Insight into the mechanism of three component condensation leading to aminomethylenebisphosphonates. *J. Organomet. Chem.* **2009**, *694*, 3806–3813.

-
58. Rondeau, J.-M.; Bitsch, F.; Bourgier, E.; Geiser, M.; Hemmig, R.; Kroemer, M.; Lehmann, S.; Ramage, P.; Rieffel, S.; Strauss, A.; Green, J. R.; Jahnke, W. Structural Basis for the Exceptional *in vivo* Efficacy of Bisphosphonate Drugs. *ChemMedChem*, **2006**, *1*, 267–273.
59. Martin, M. B.; Arnold, W.; Heath, H. T. III; Urbina, J. A.; Oldfield, E. Nitrogen-containing bisphosphonates as carbocation transition state analogs for isoprenoid biosynthesis. *Biochem. Biophys. Res. Commun.* **1999**, *263*, 754–758.
60. Kavanagh, K.; Dunford, J.; Bunkoczi, G.; Russell, R. G. G.; Oppermann, O. The crystal structure of human geranylgeranyl pyrophosphate synthase reveals a novel hexameric arrangement and inhibitory product binding. *J. Biol. Chem.* **2006**, *281*, 22004–22012.

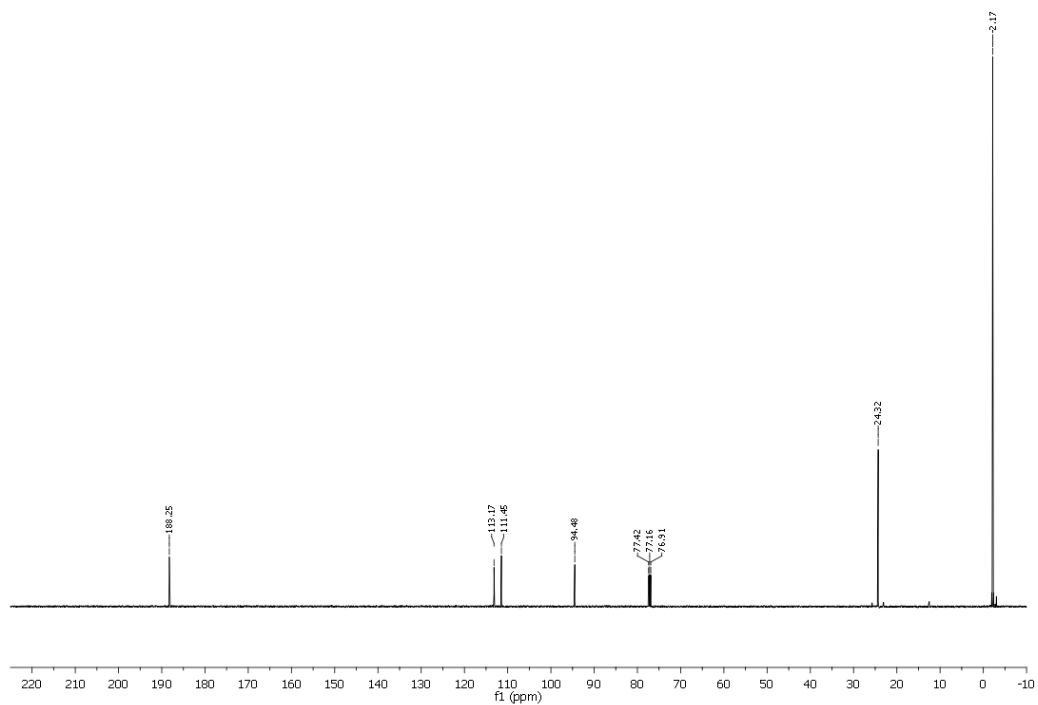
Appendix – Spectral Data

NMR Spectra of compound **12**

^1H NMR (400 MHz, CDCl_3)

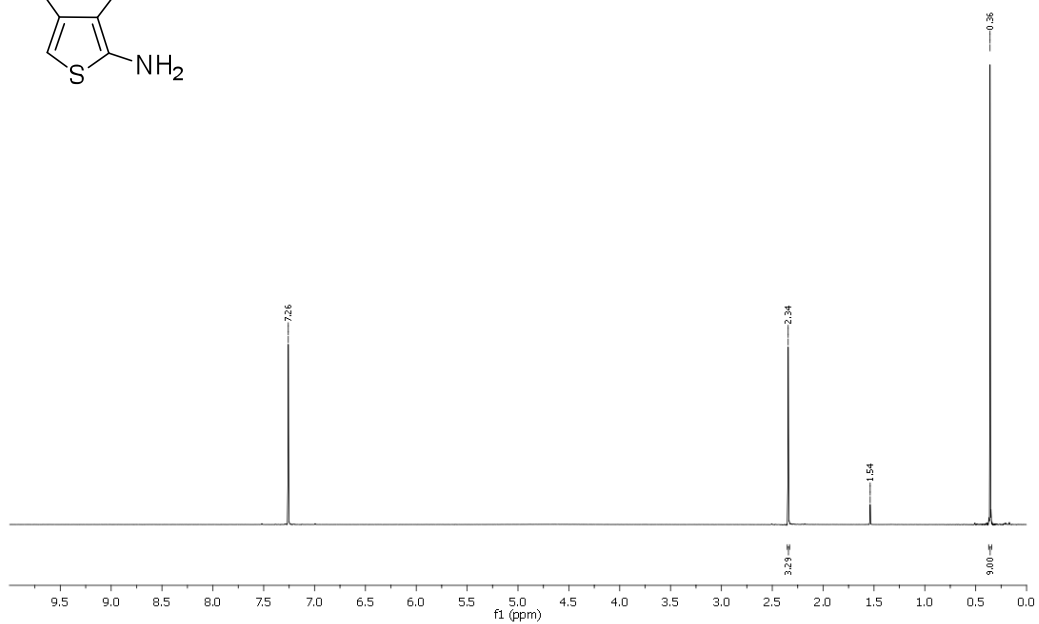
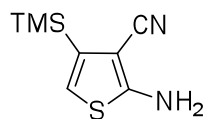


^{13}C NMR (126 MHz, CDCl_3)

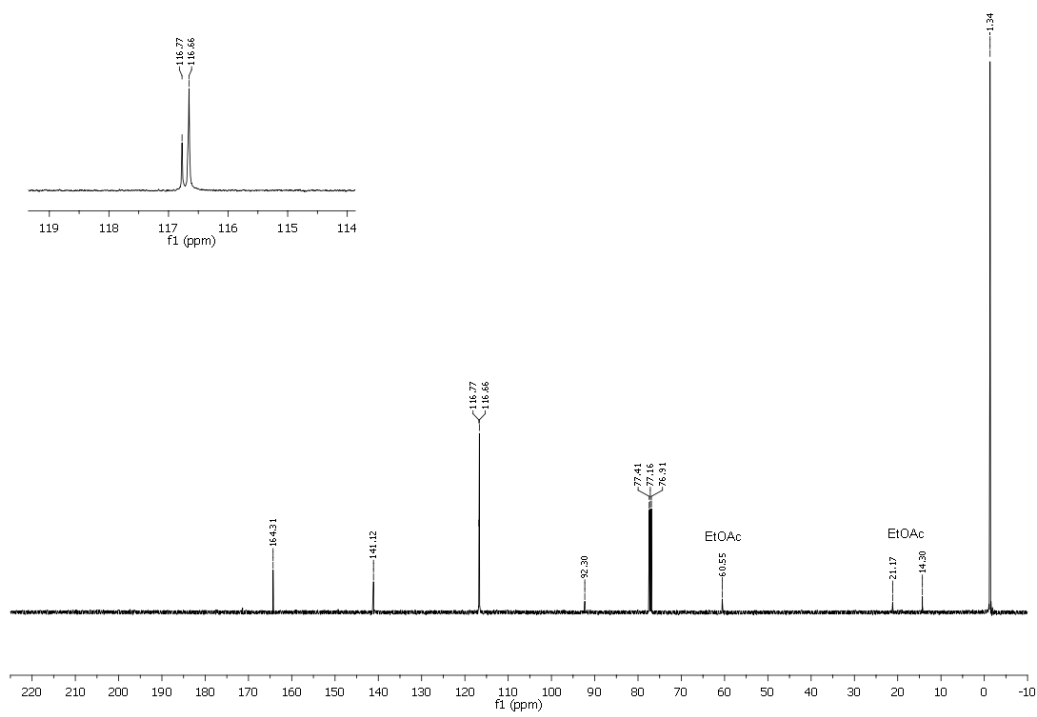


NMR Spectra of compound **13**

^1H NMR (400 MHz, CDCl_3)

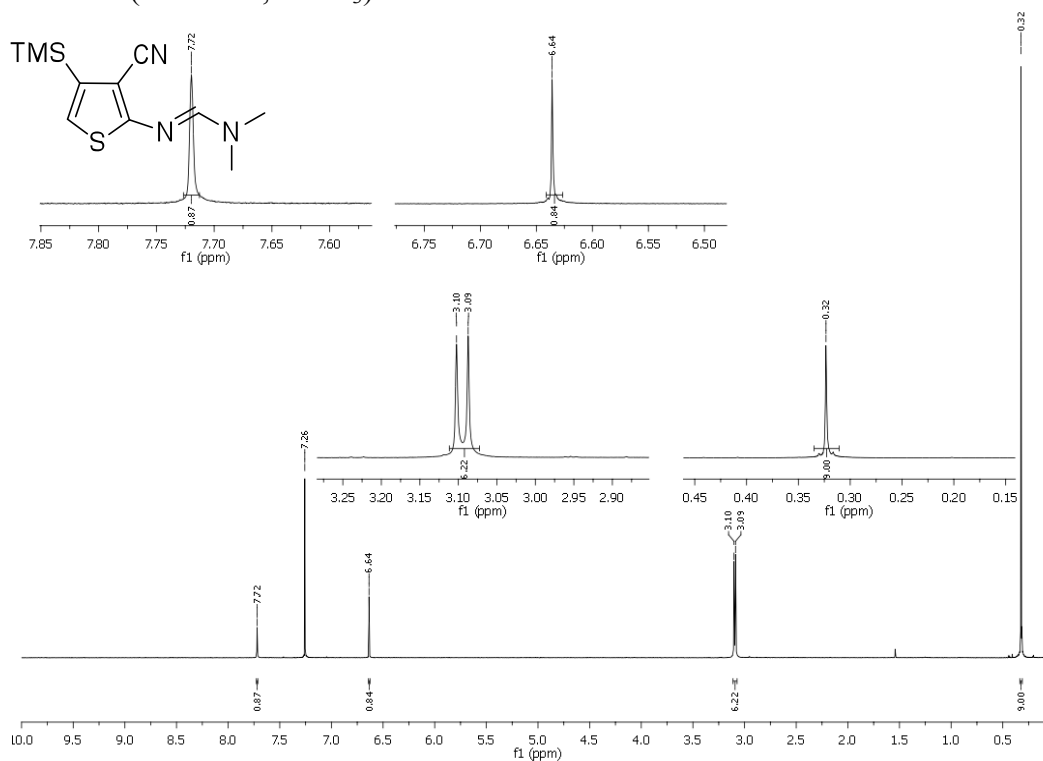


^{13}C NMR (126 MHz, CDCl_3)

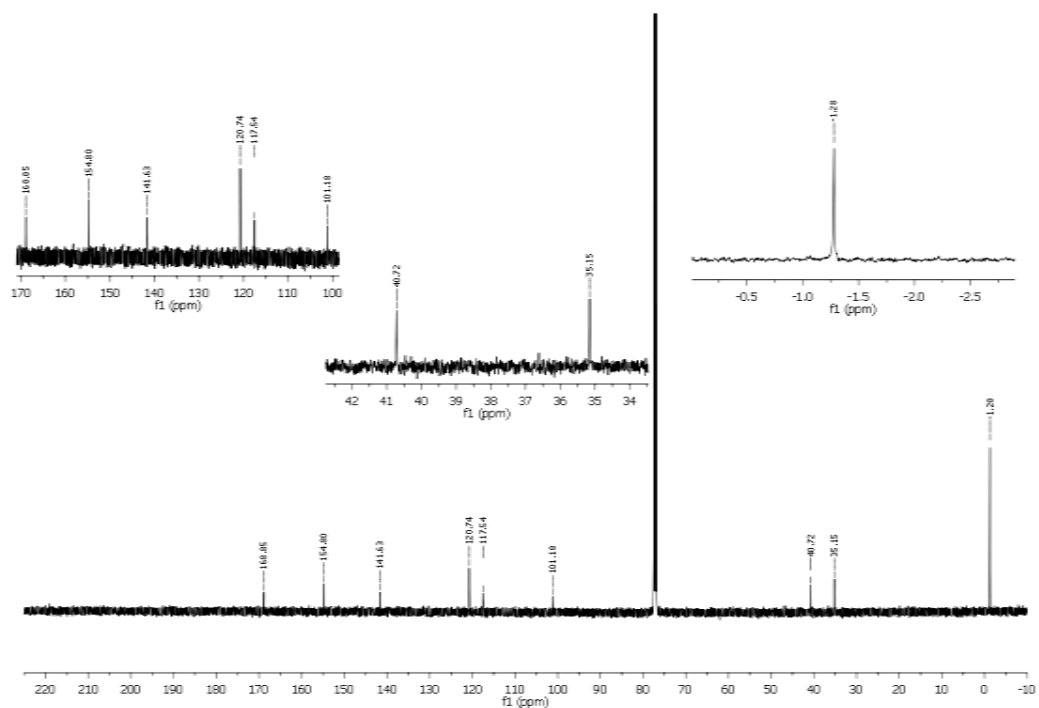


NMR Spectra of compound **14a**

^1H NMR (500 MHz, CDCl_3)

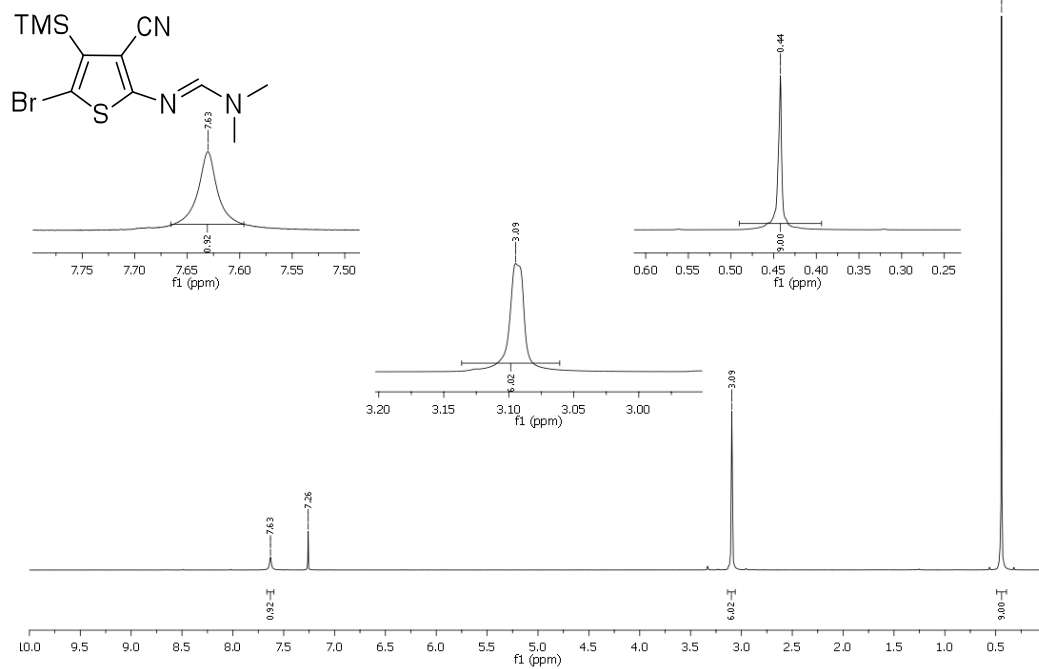


^{13}C NMR (126 MHz, CDCl_3)

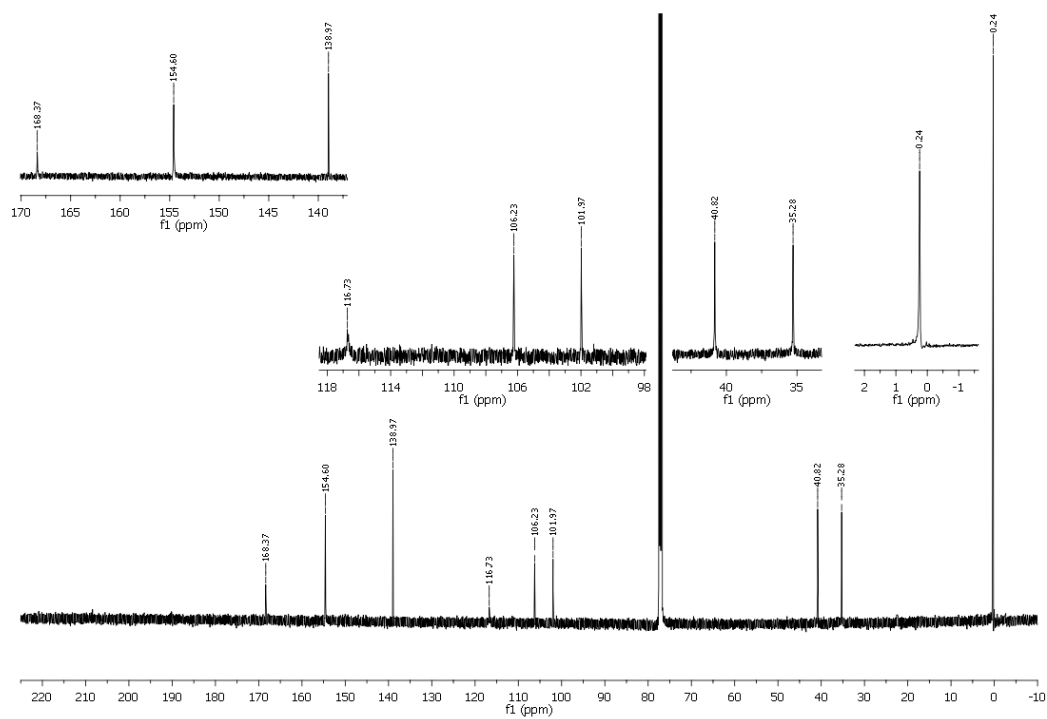


NMR Spectra of compound **14b**

^1H NMR (500 MHz, CDCl_3)

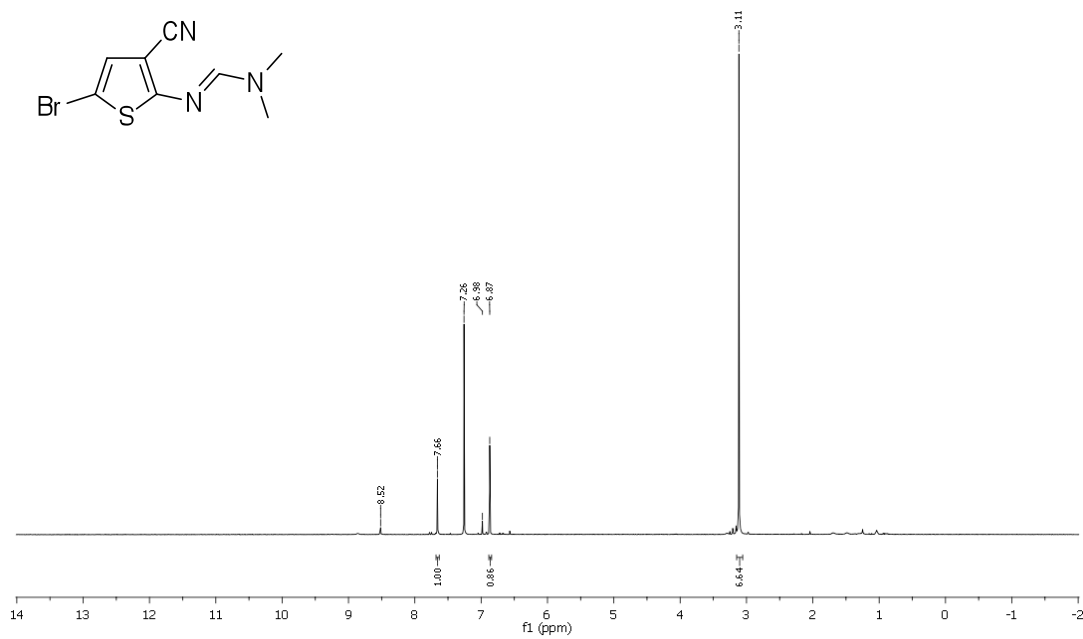
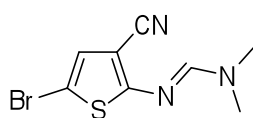


^{13}C NMR (126 MHz, CDCl_3)

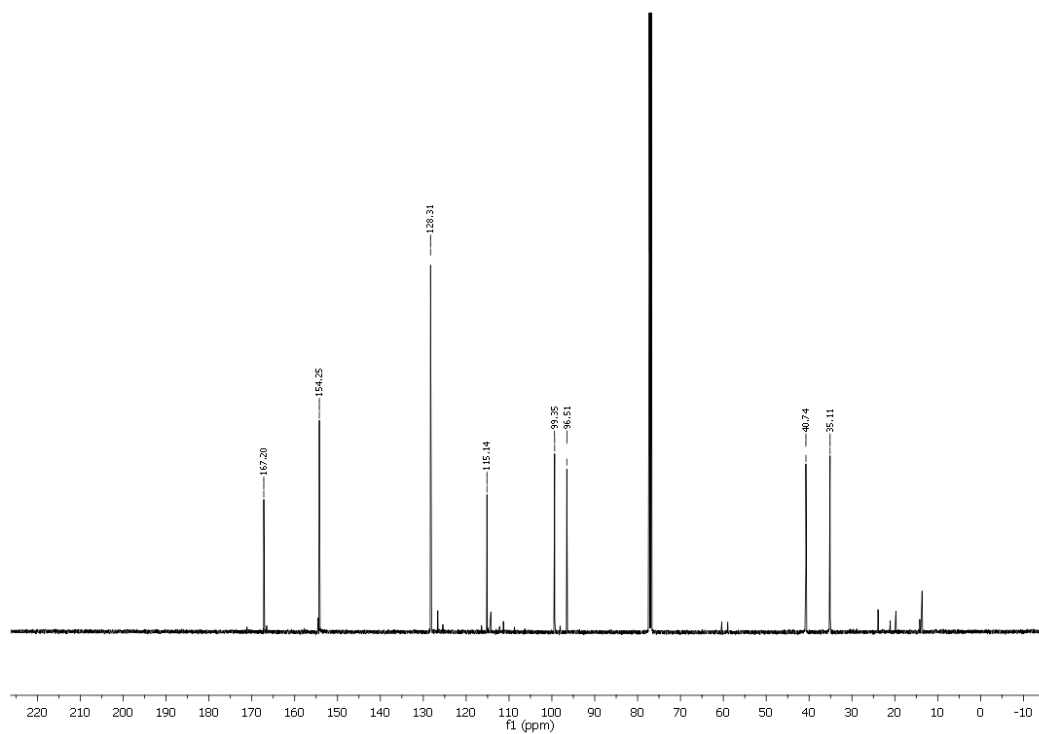


NMR Spectra of compound **14c**

^1H NMR (400 MHz, CDCl_3)

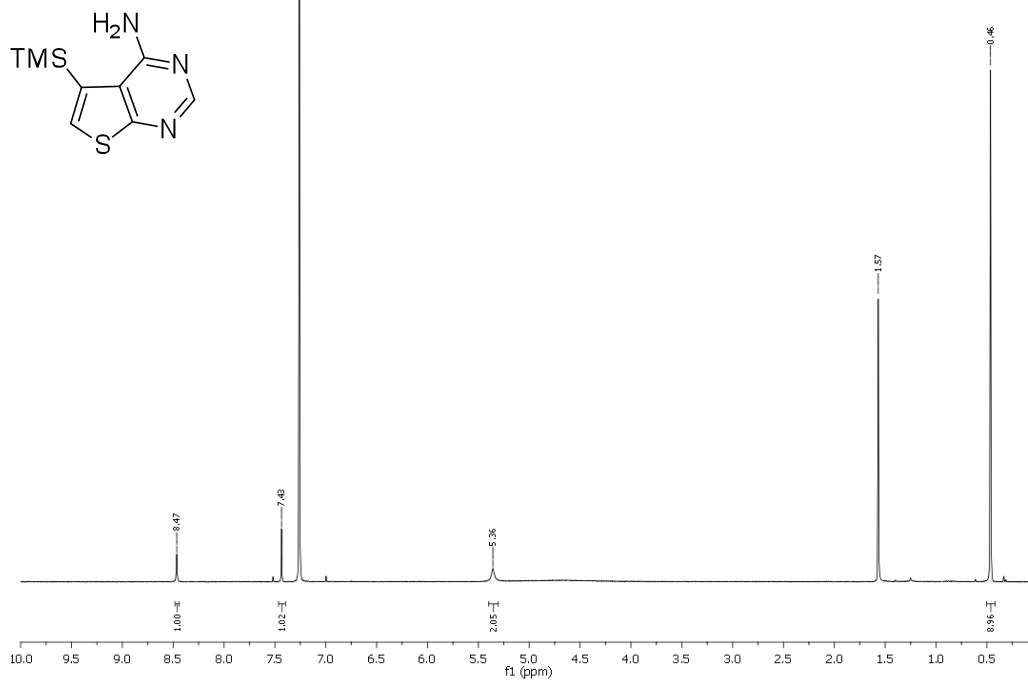


^{13}C NMR (126 MHz, CDCl_3)

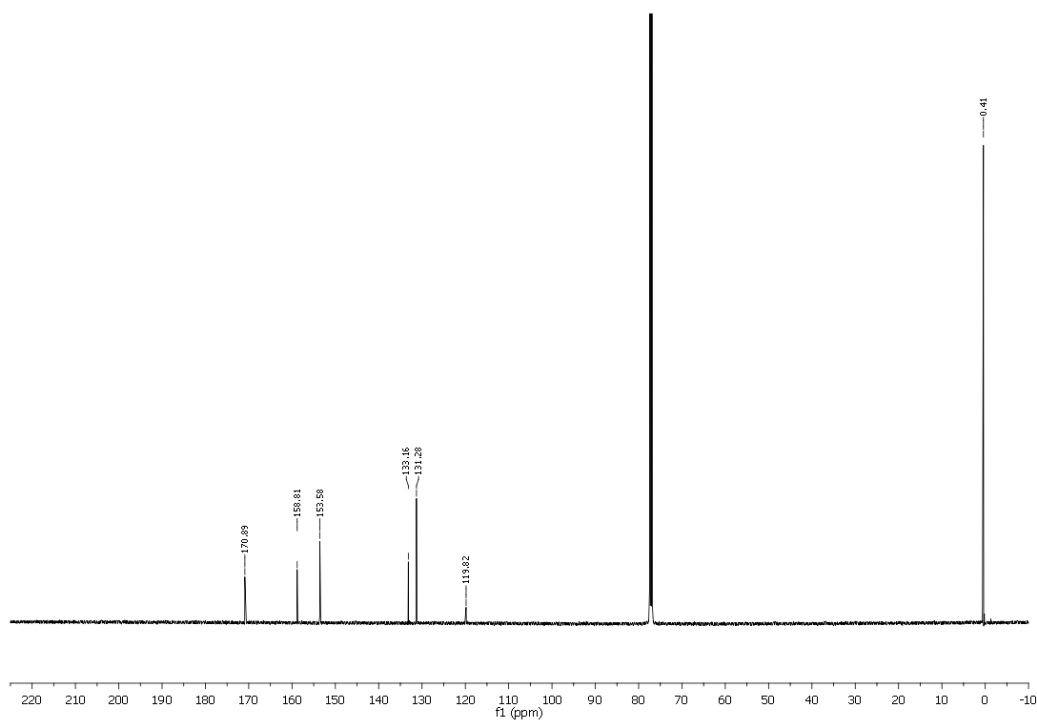


NMR Spectra of compound **15a**

^1H NMR (400 MHz, CDCl_3)

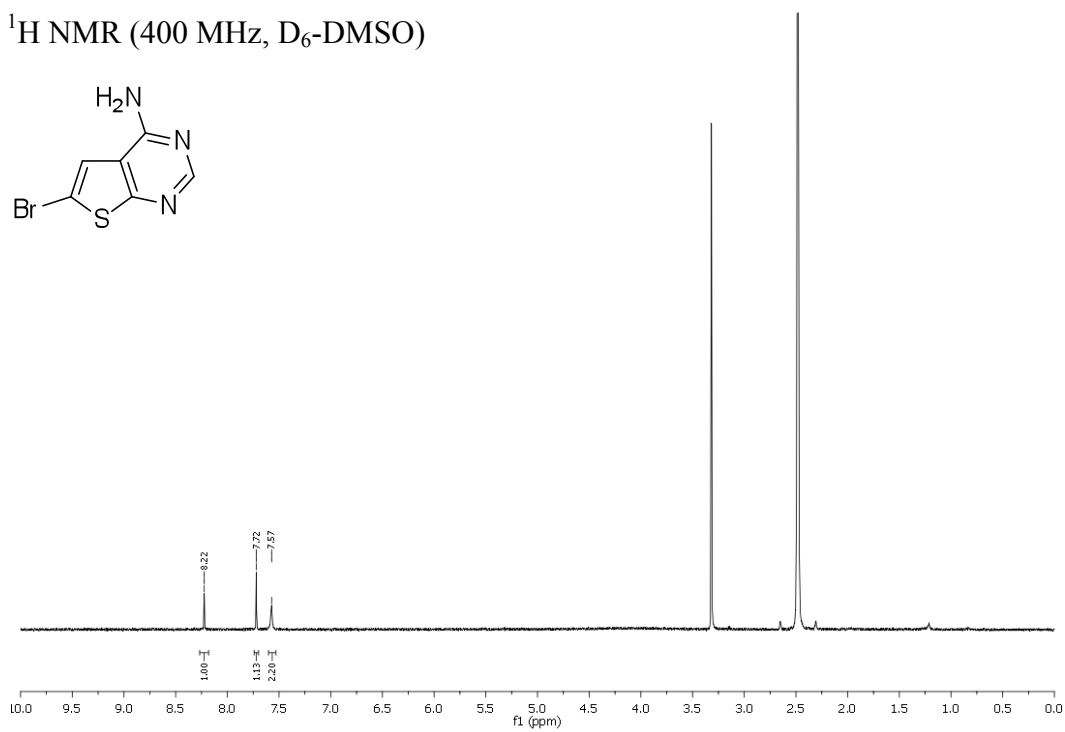
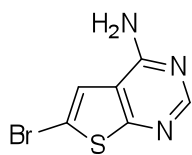


^{13}C NMR (126 MHz, CDCl_3)

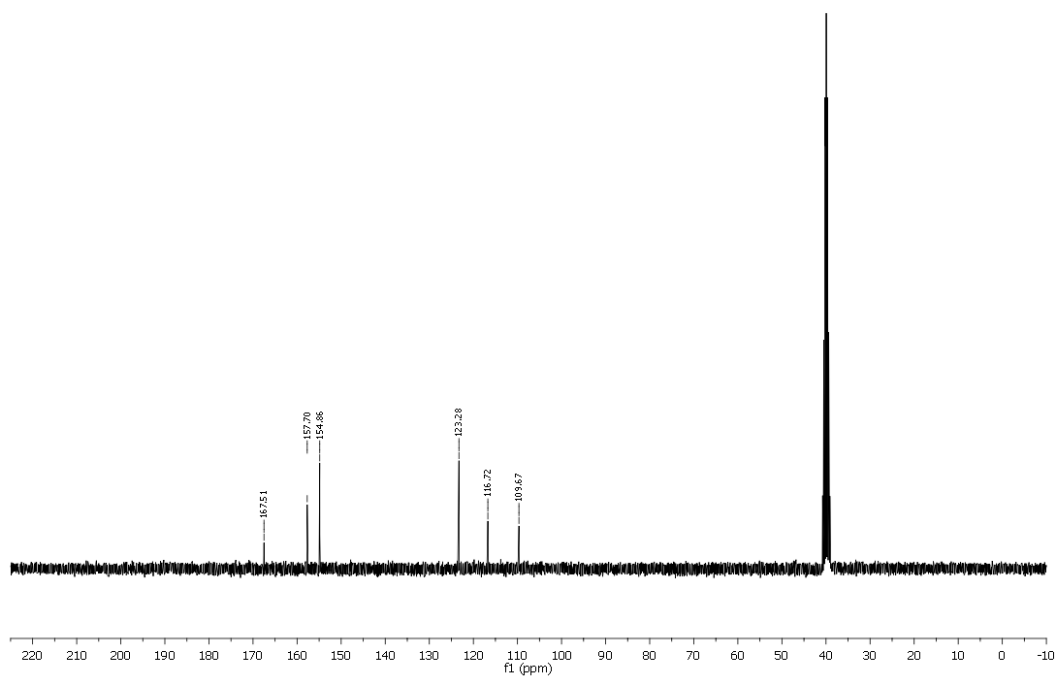


NMR Spectra of compound **15b**

^1H NMR (400 MHz, $\text{D}_6\text{-DMSO}$)

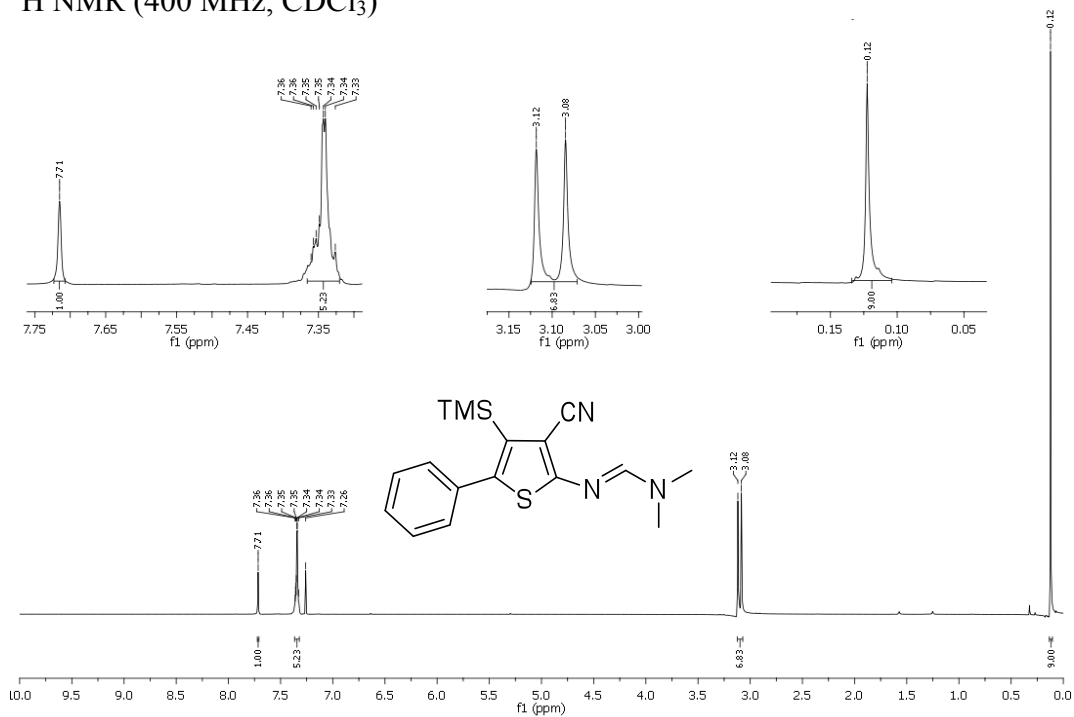


^{13}C NMR (75 MHz, $\text{D}_6\text{-DMSO}$)

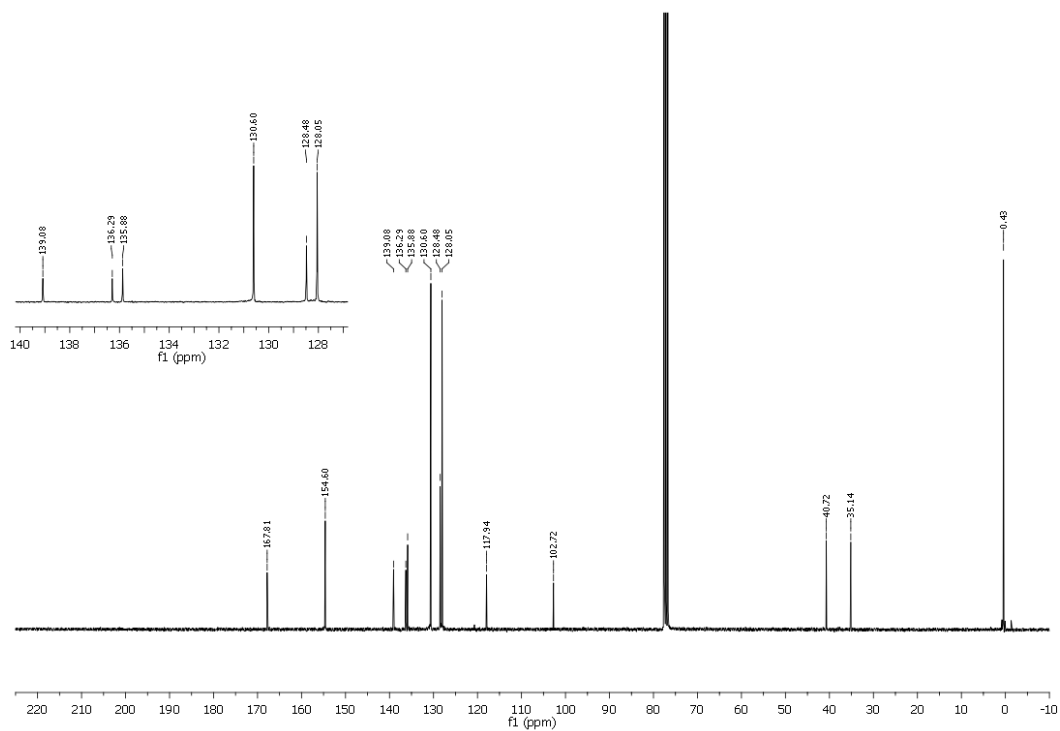


NMR Spectra of compound **16a**

^1H NMR (400 MHz, CDCl_3)

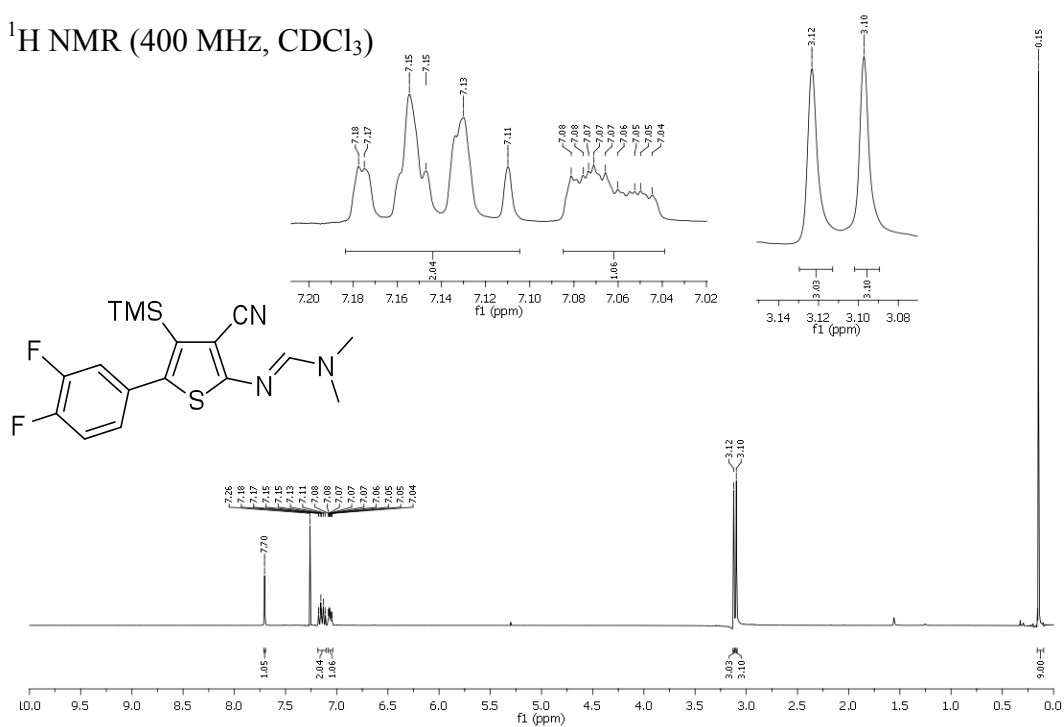


^{13}C NMR (125 MHz, CDCl_3)

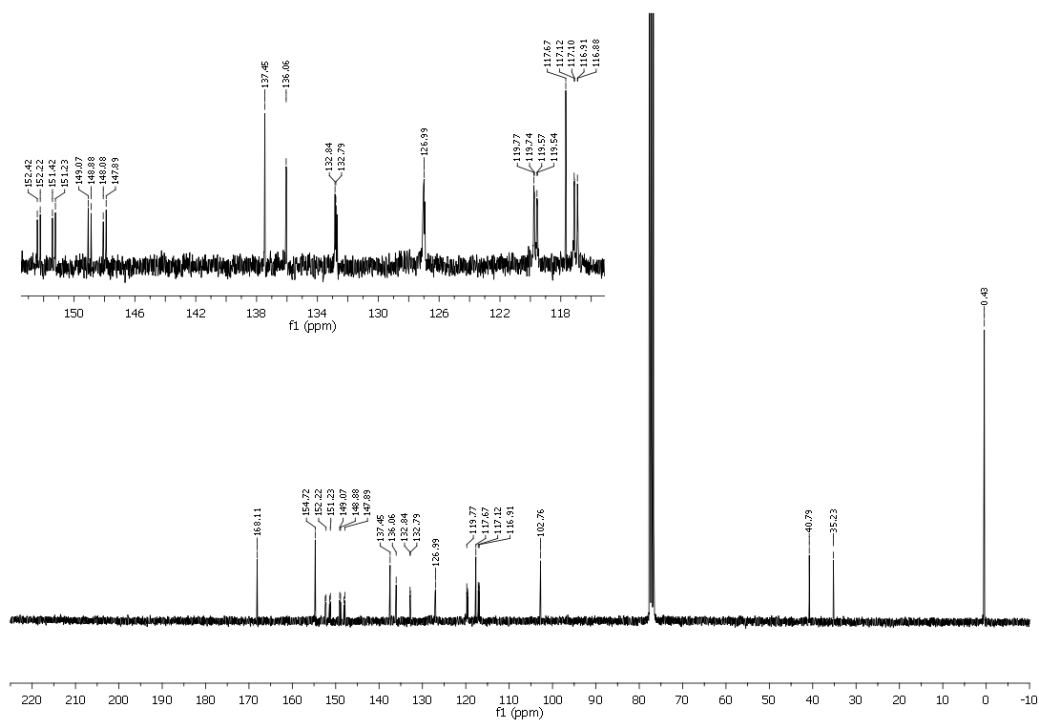


NMR Spectra of compound **16b**

^1H NMR (400 MHz, CDCl_3)

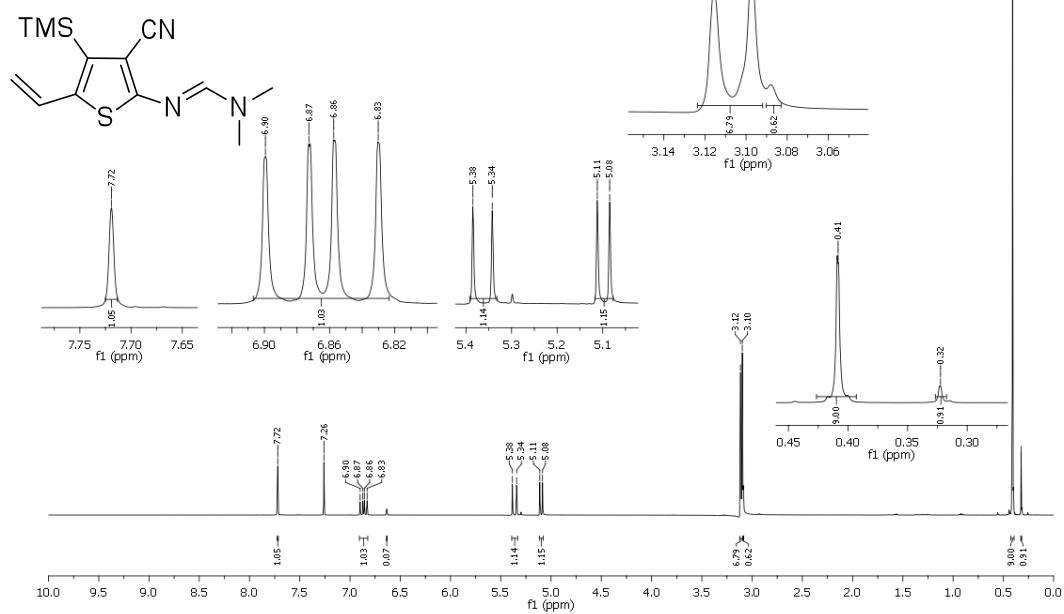


^{13}C NMR (75 MHz, CDCl_3)

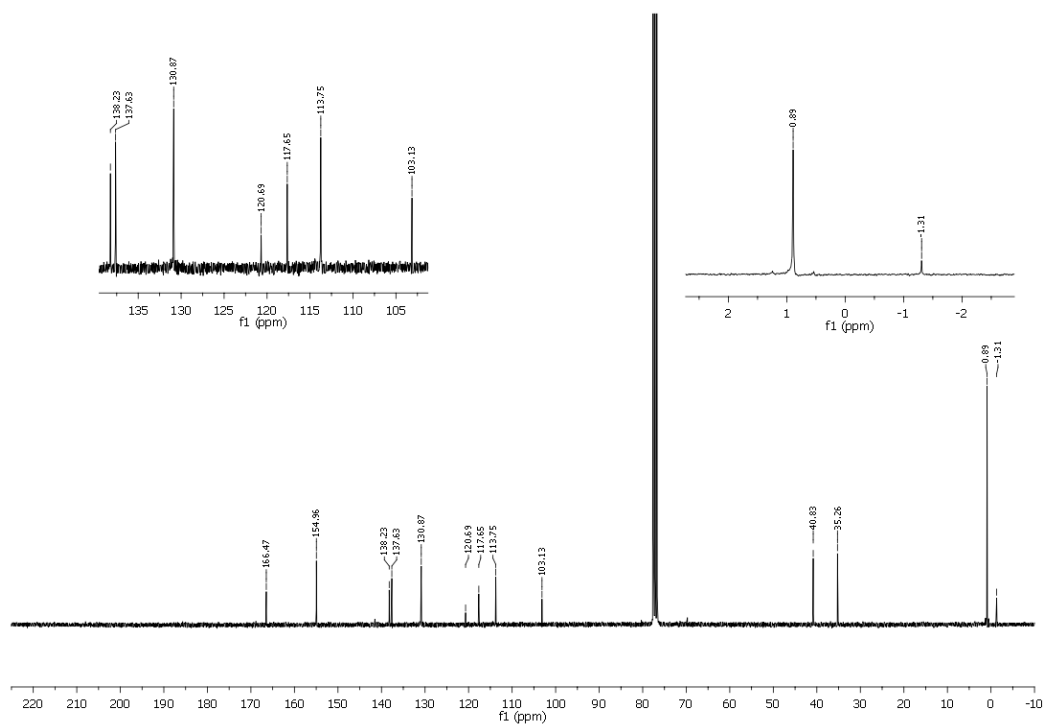


NMR Spectra of compound **16c**

¹H NMR (400 MHz, CDCl₃)

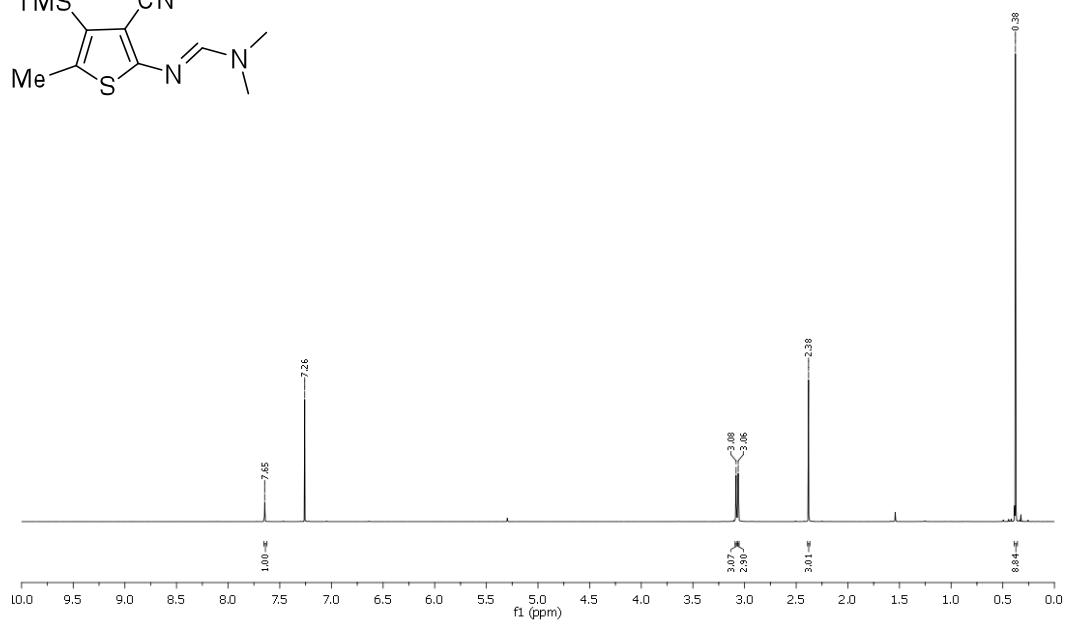
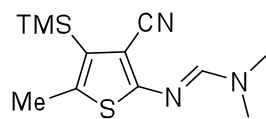


¹³C NMR (75 MHz, CDCl₃)

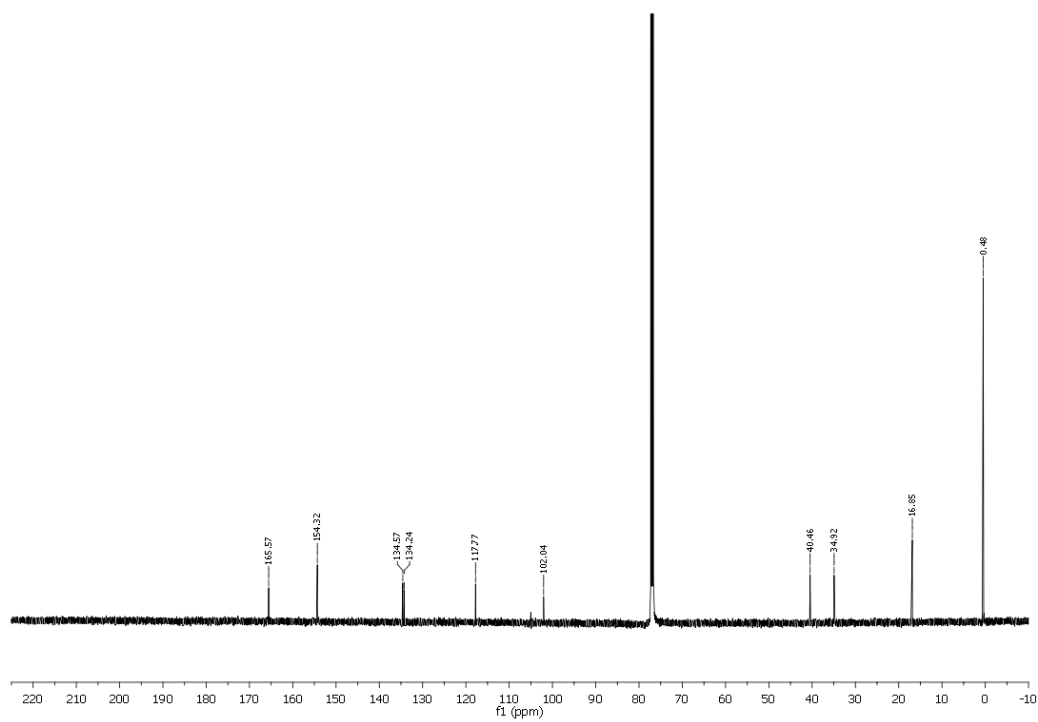


NMR Spectra of compound **16d**

^1H NMR (400 MHz, CDCl_3)

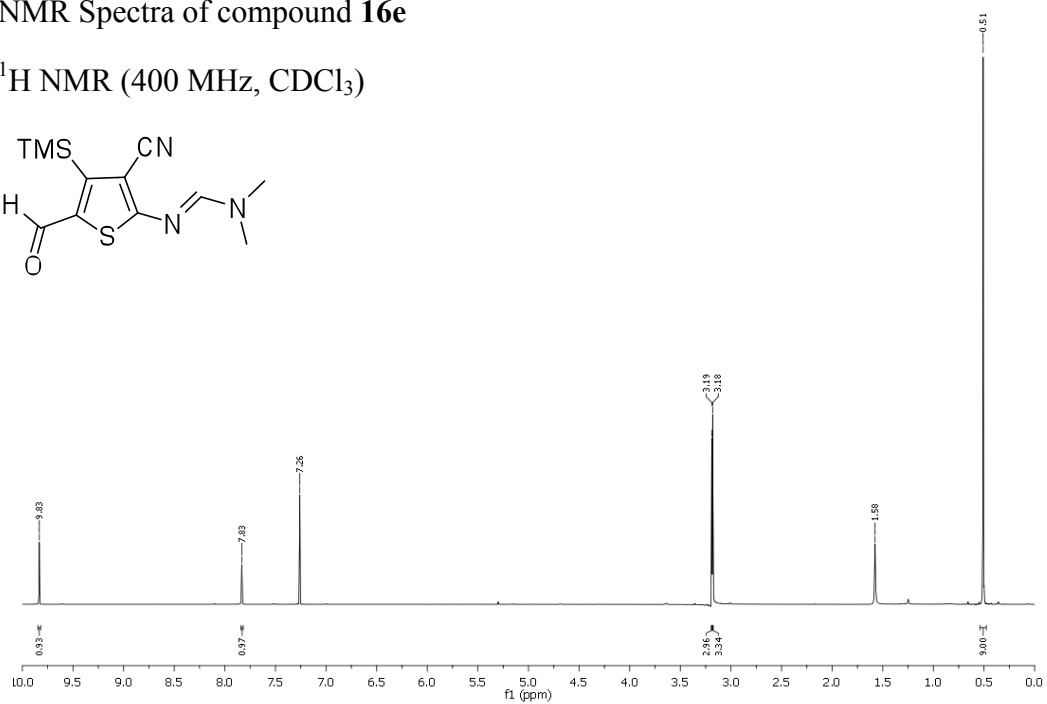
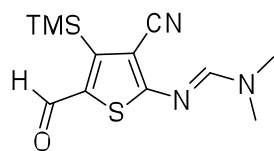


^{13}C NMR (125 MHz, CDCl_3)

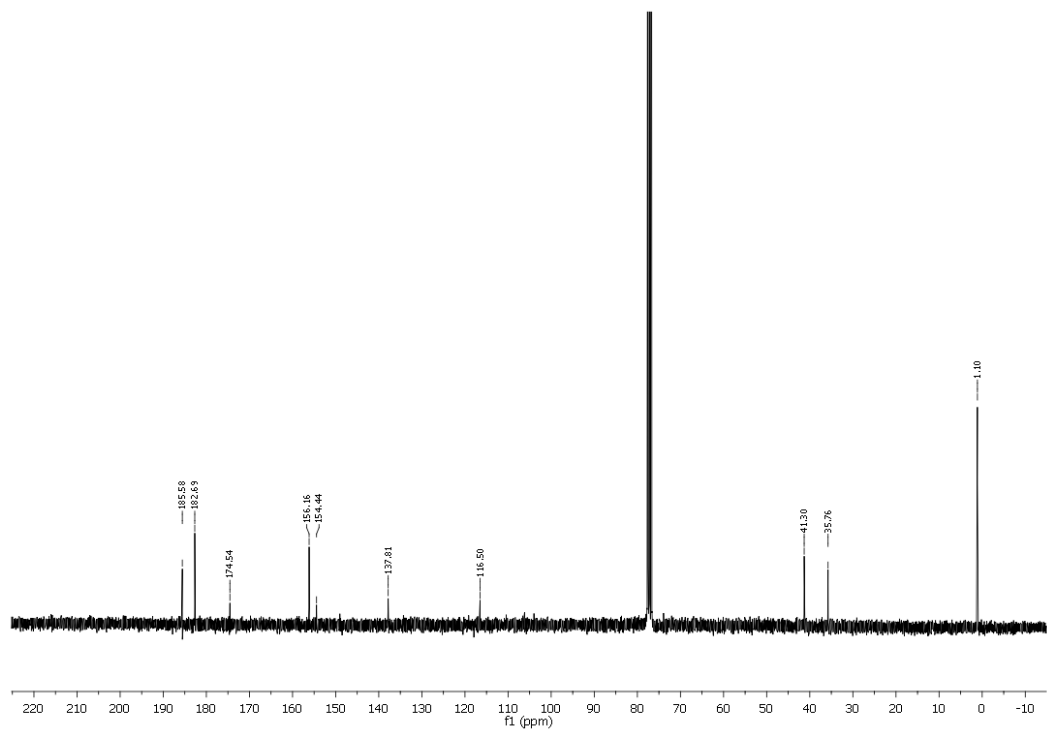


NMR Spectra of compound **16e**

^1H NMR (400 MHz, CDCl_3)

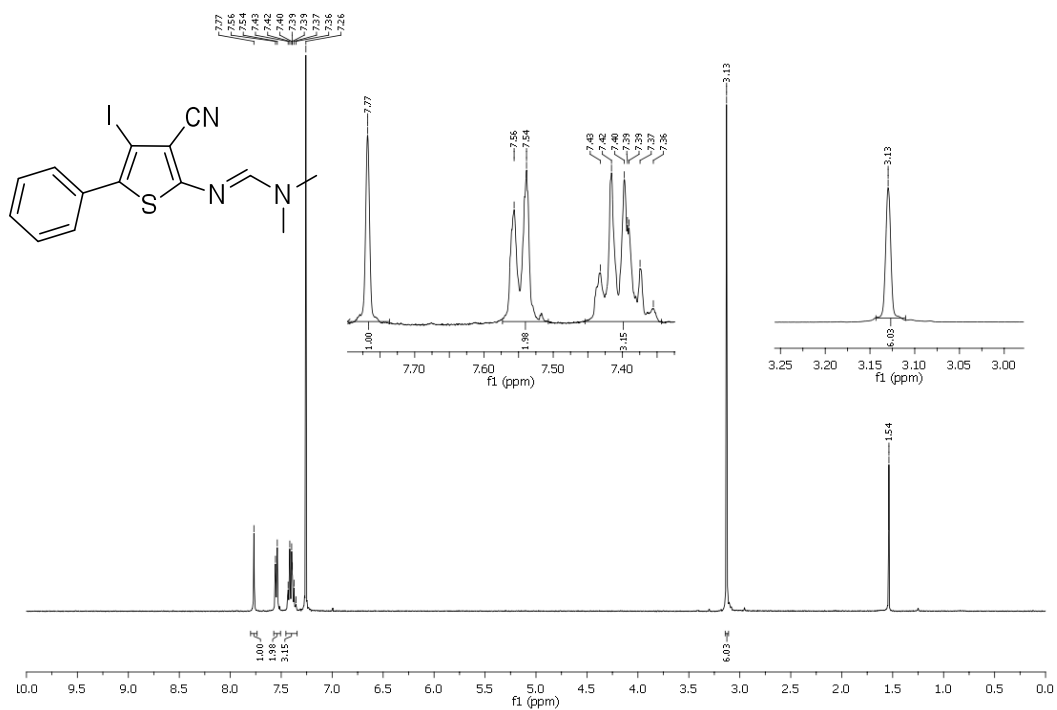


^{13}C NMR (75 MHz, CDCl_3)

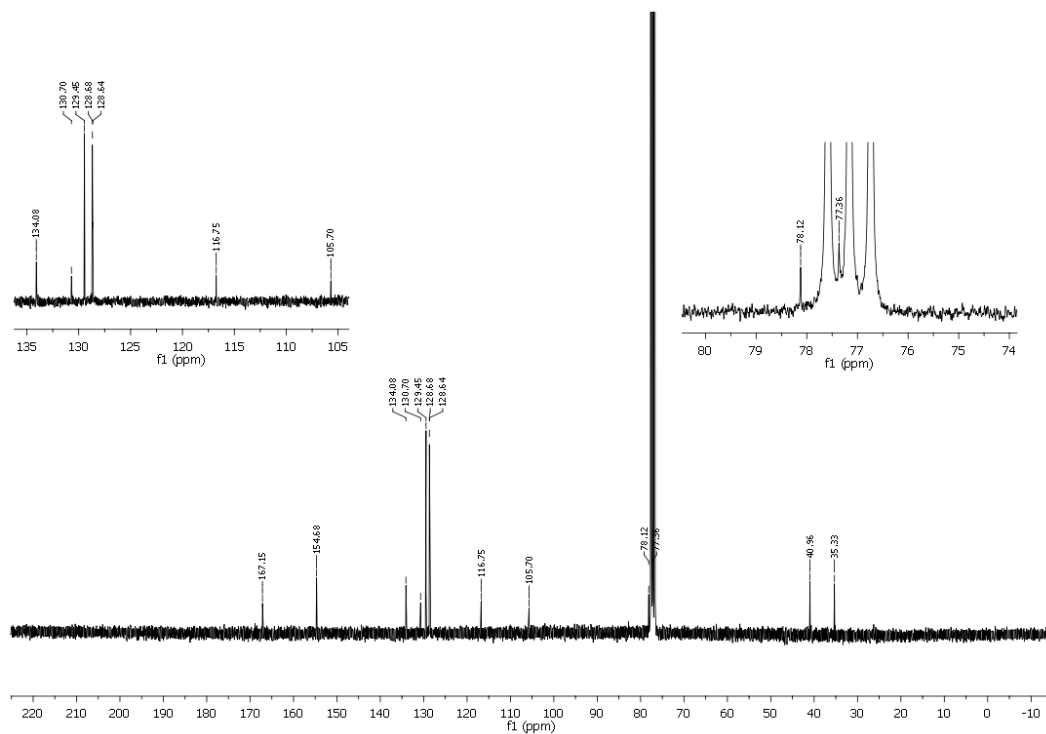


NMR Spectra of compound **17a**

^1H NMR (400 MHz, CDCl_3)

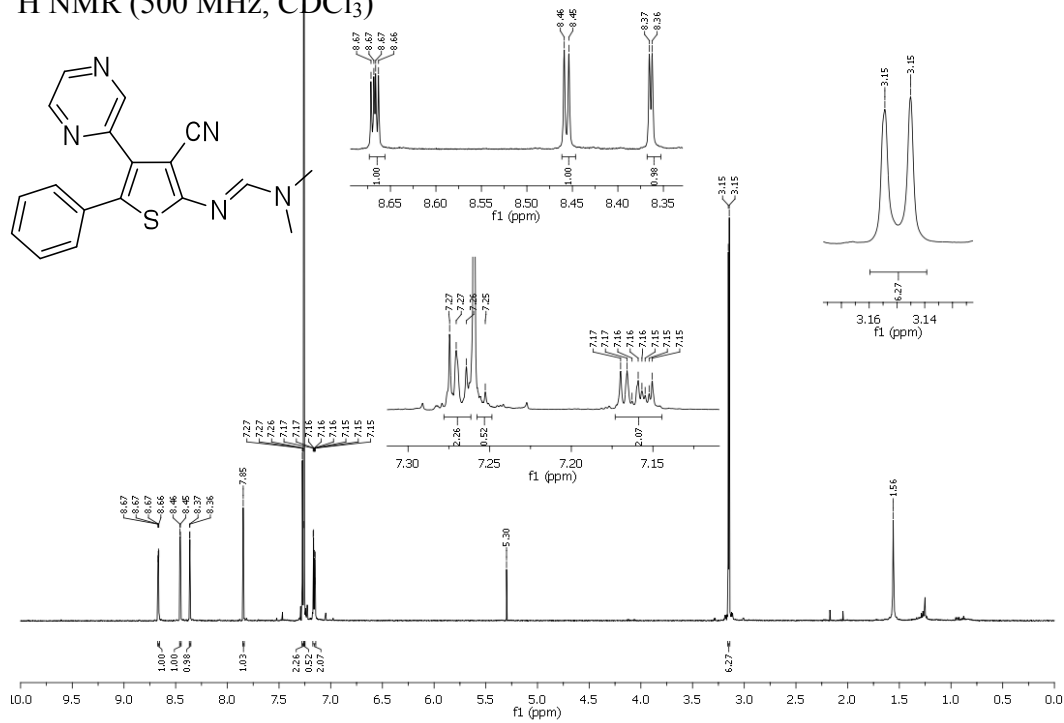


^{13}C NMR (75 MHz, CDCl_3)

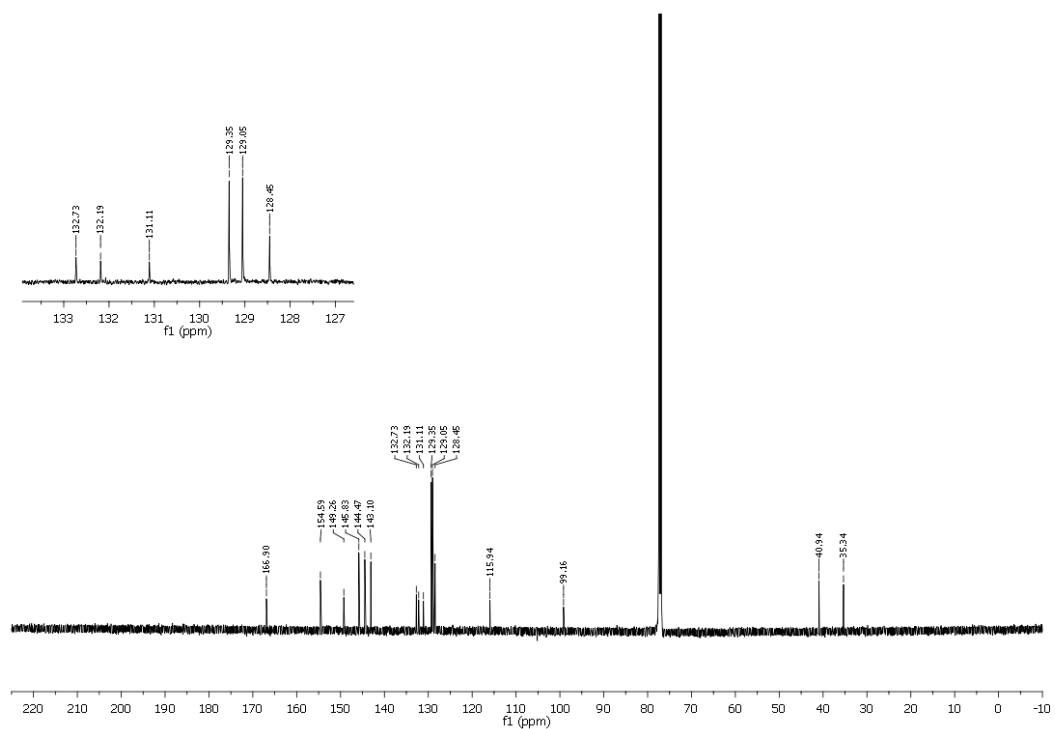


NMR Spectra of compound **18a**

^1H NMR (500 MHz, CDCl_3)

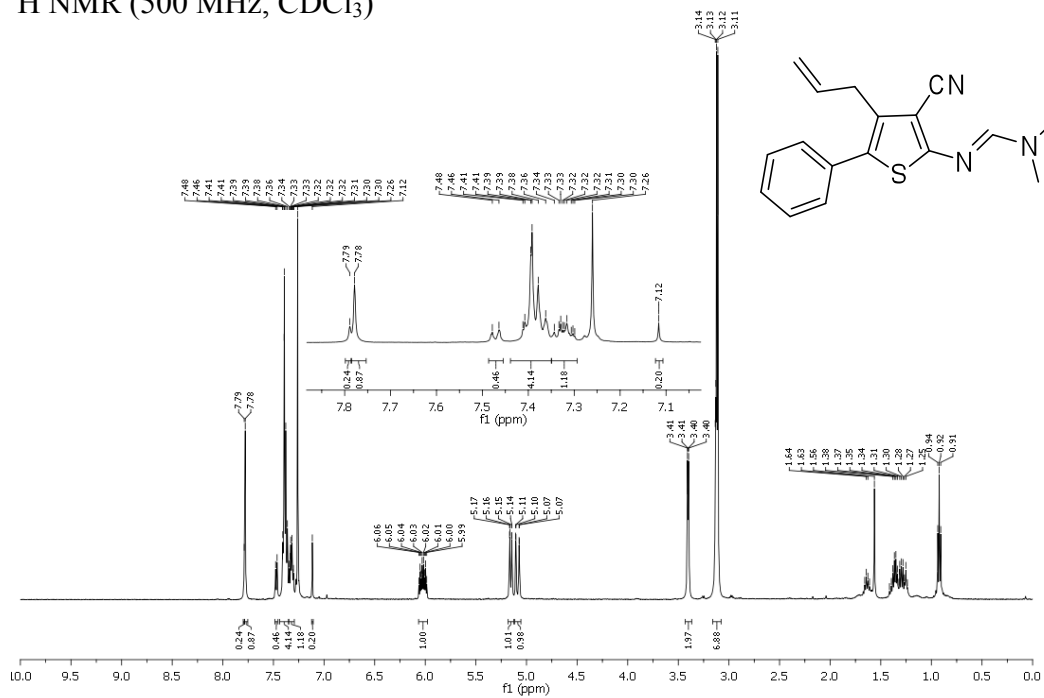


^{13}C NMR (125 MHz, CDCl_3)

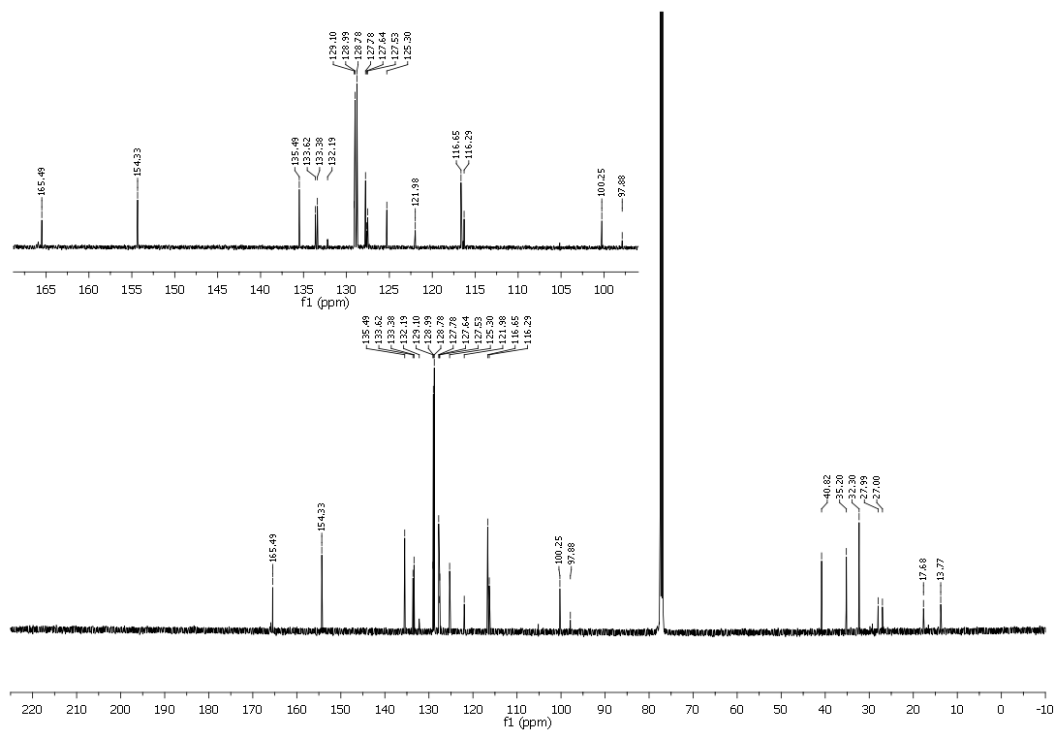


NMR Spectra of compound **18b**

¹H NMR (500 MHz, CDCl₃)

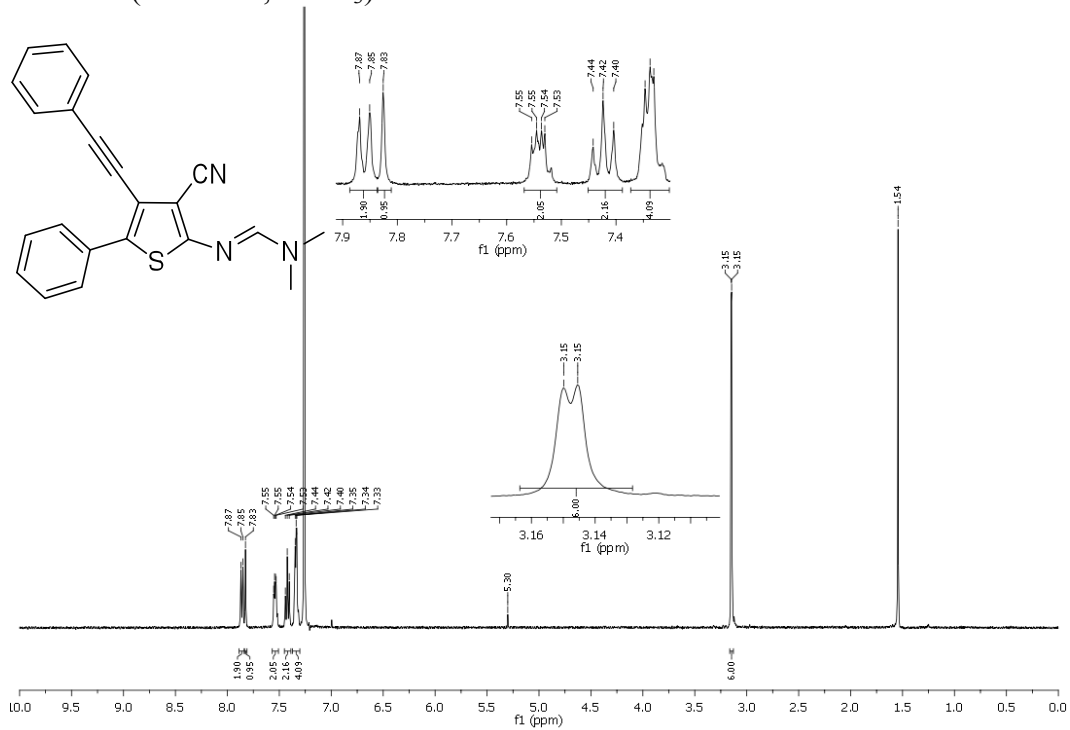


¹³C NMR (126 MHz, CDCl₃)

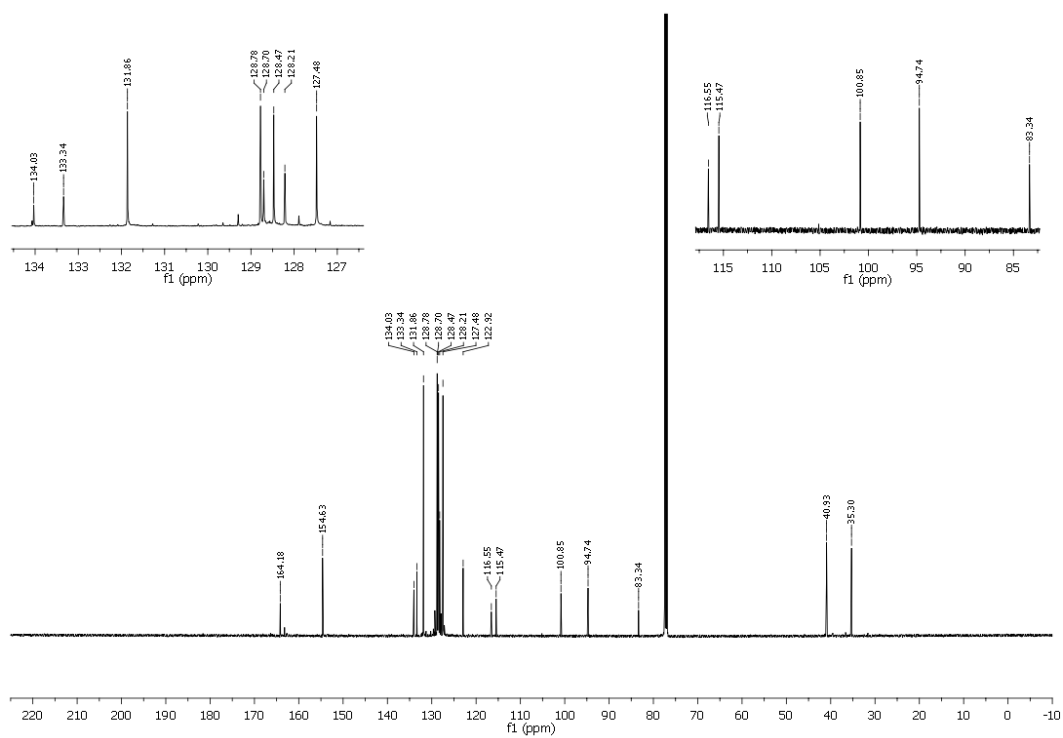


NMR Spectra of compound **18c**

^1H NMR (400 MHz, CDCl_3)

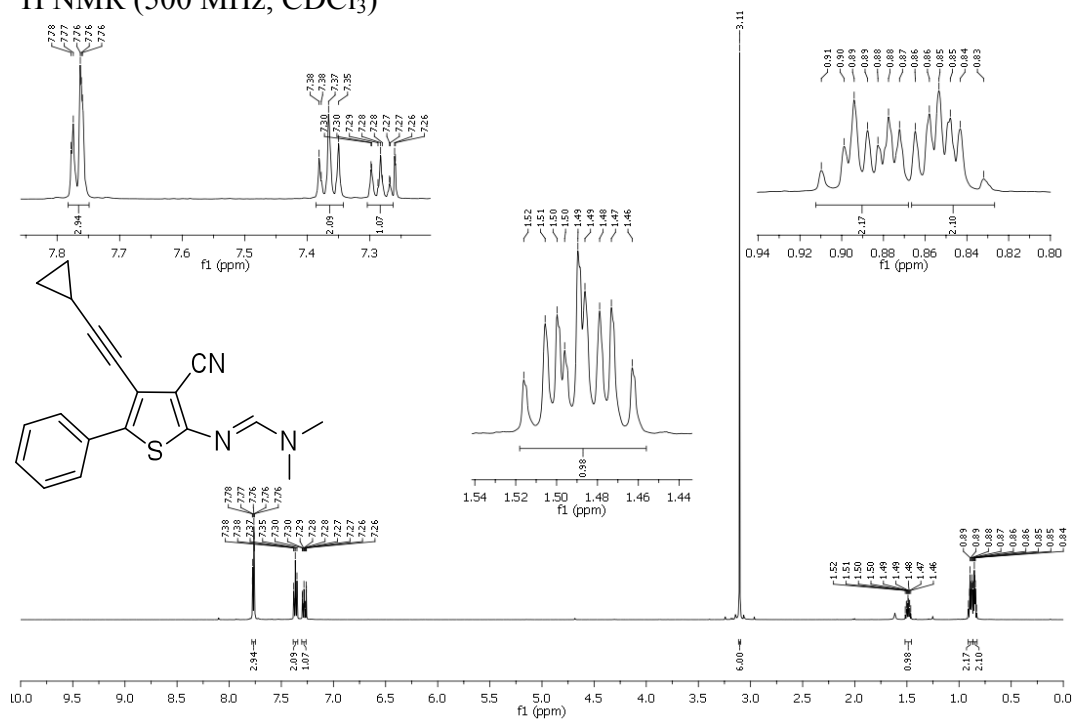


^{13}C NMR (125 MHz, CDCl_3)

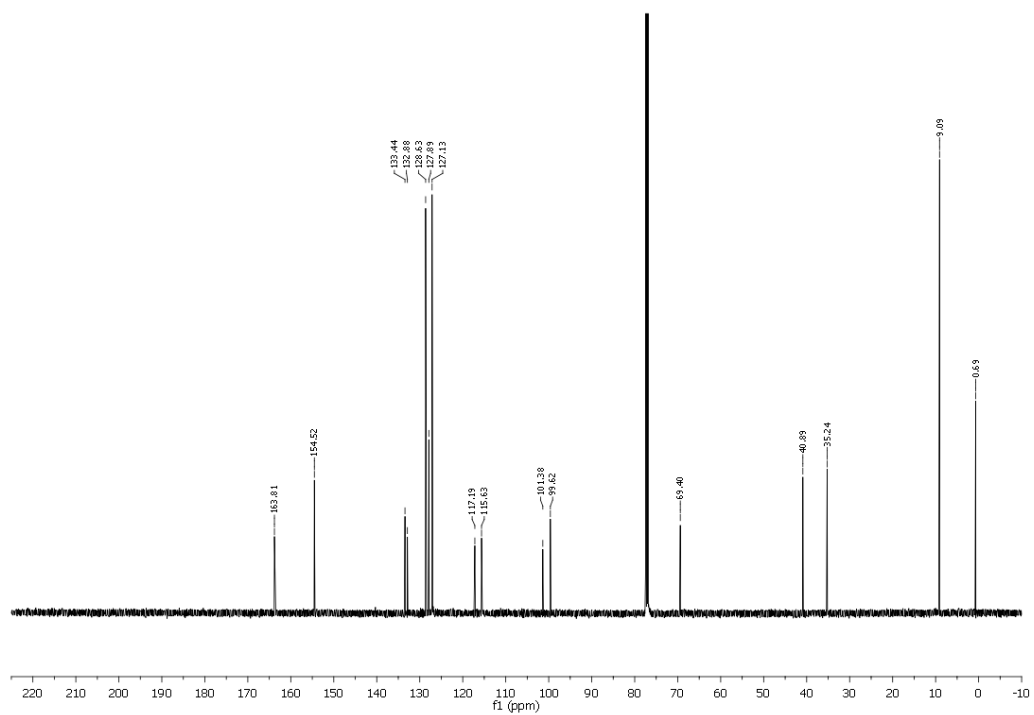


NMR Spectra of compound **18d**

^1H NMR (500 MHz, CDCl_3)

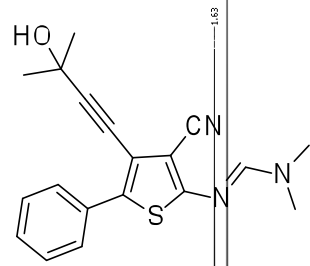
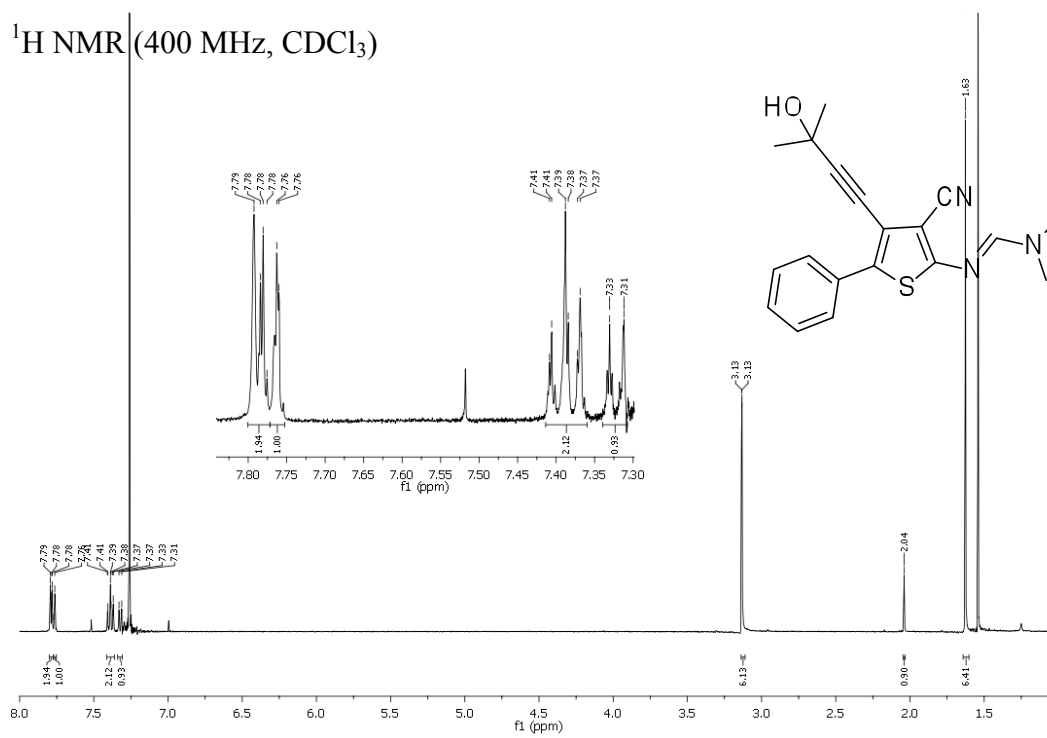


^{13}C NMR (125 MHz, CDCl_3)

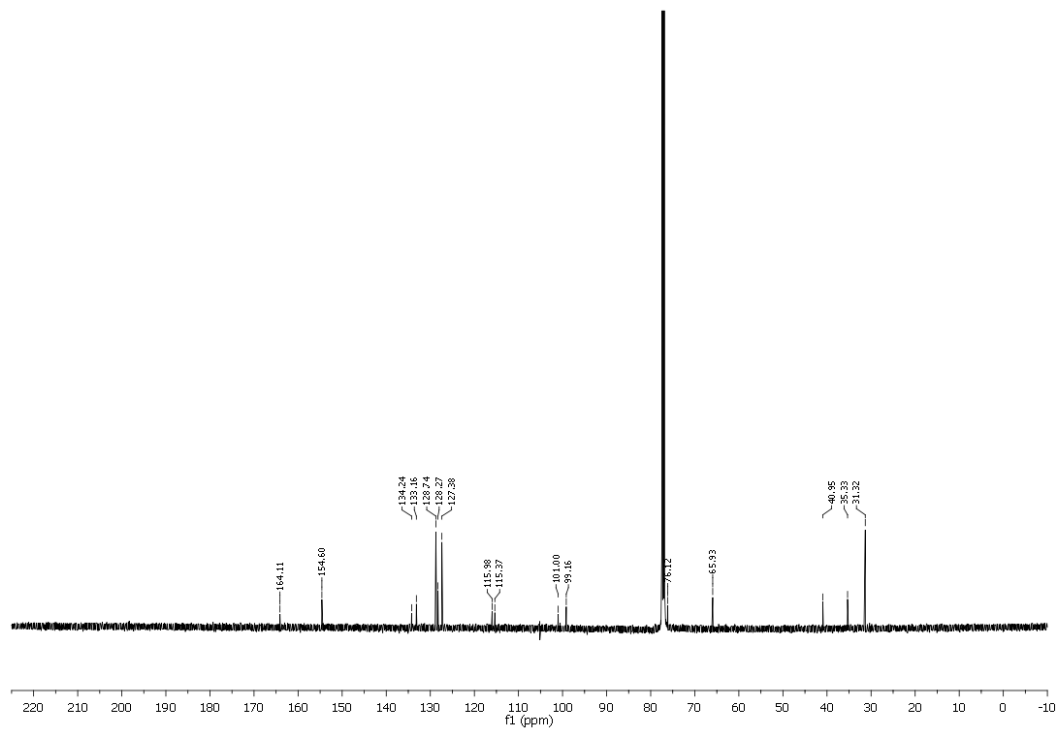


NMR Spectra of compound **18e**

^1H NMR (400 MHz, CDCl_3)

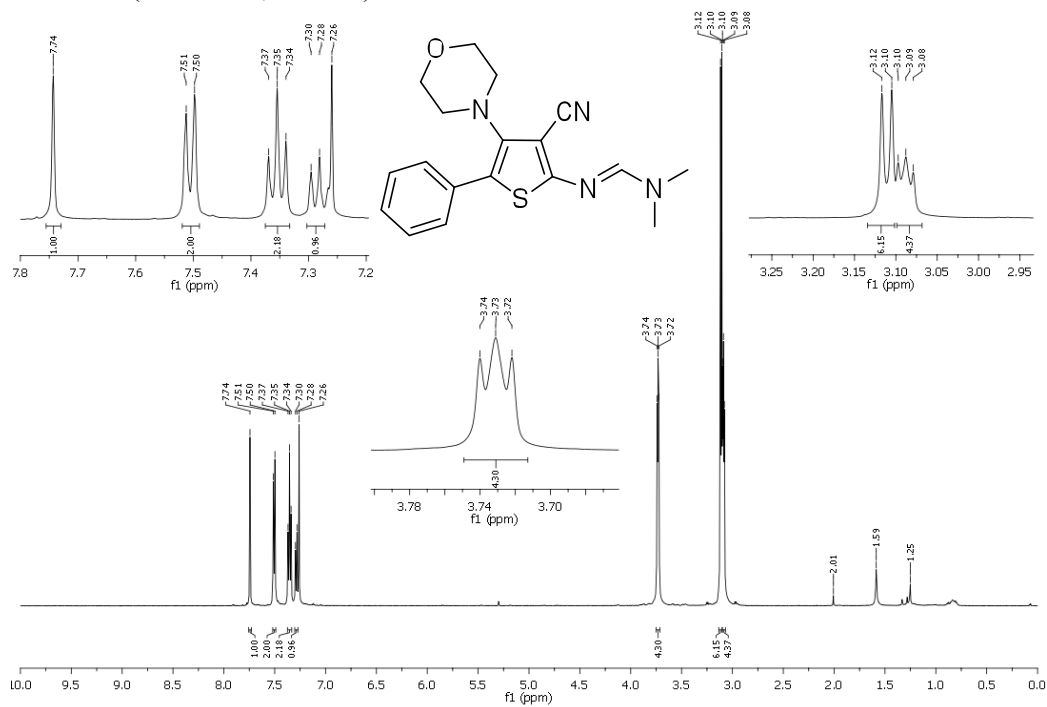


^{13}C NMR (126 MHz, CDCl_3)

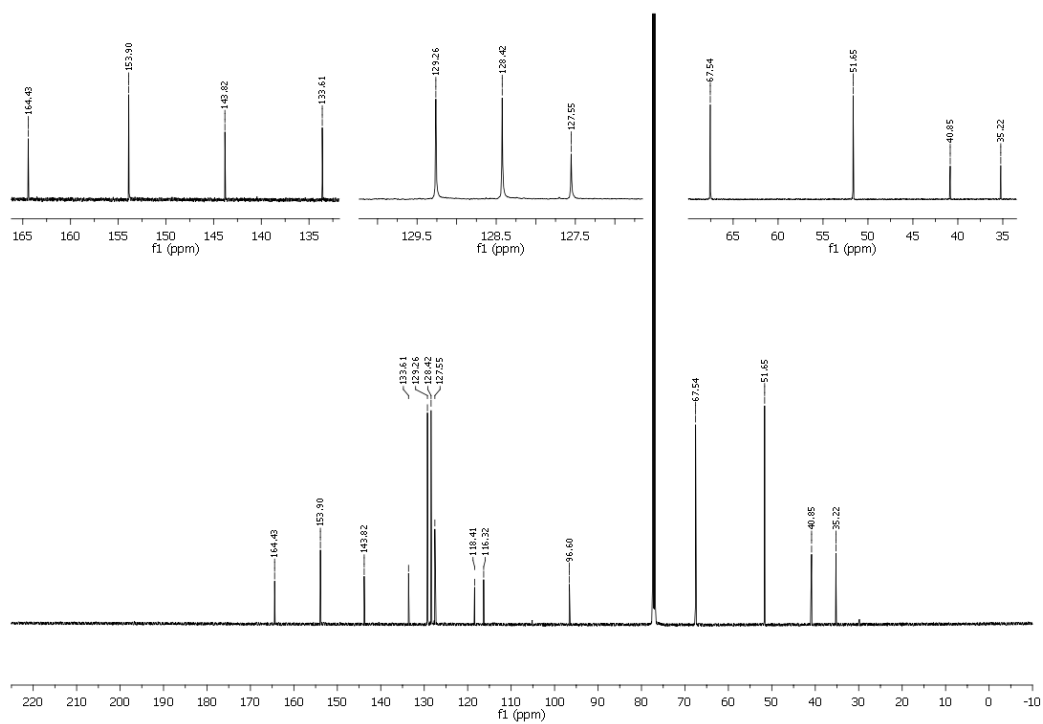


NMR Spectra of compound **18f**

^1H NMR (400 MHz, CDCl_3)

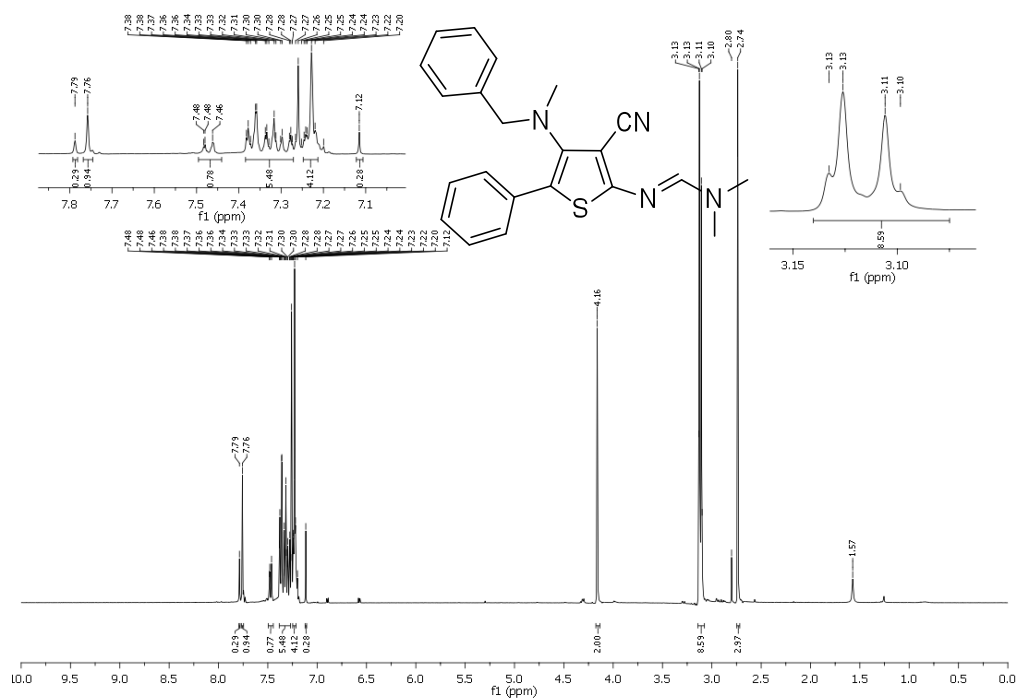


^{13}C NMR (125 MHz, CDCl_3)

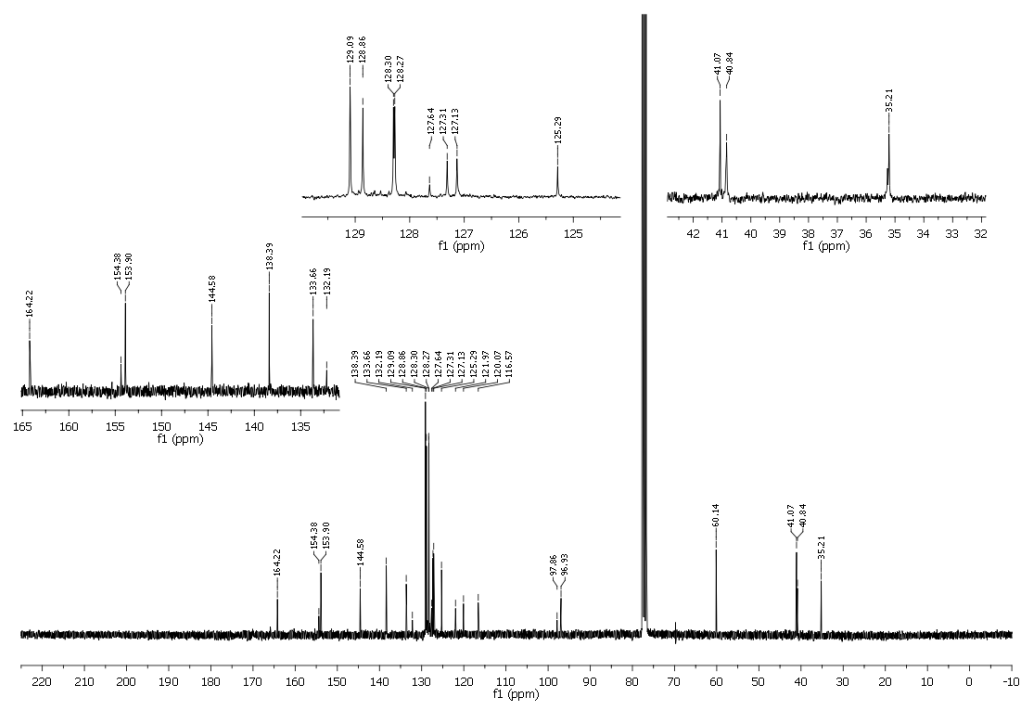


NMR Spectra of compound **18g**

^1H NMR (400 MHz, CDCl_3)

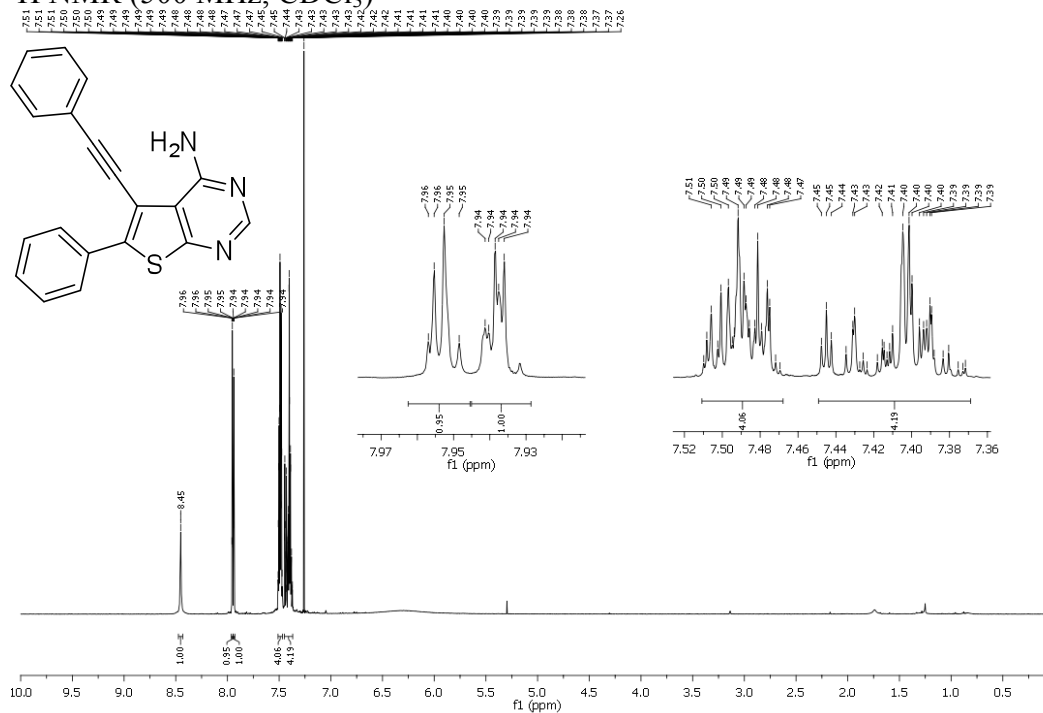


^{13}C NMR (75 MHz, CDCl_3)

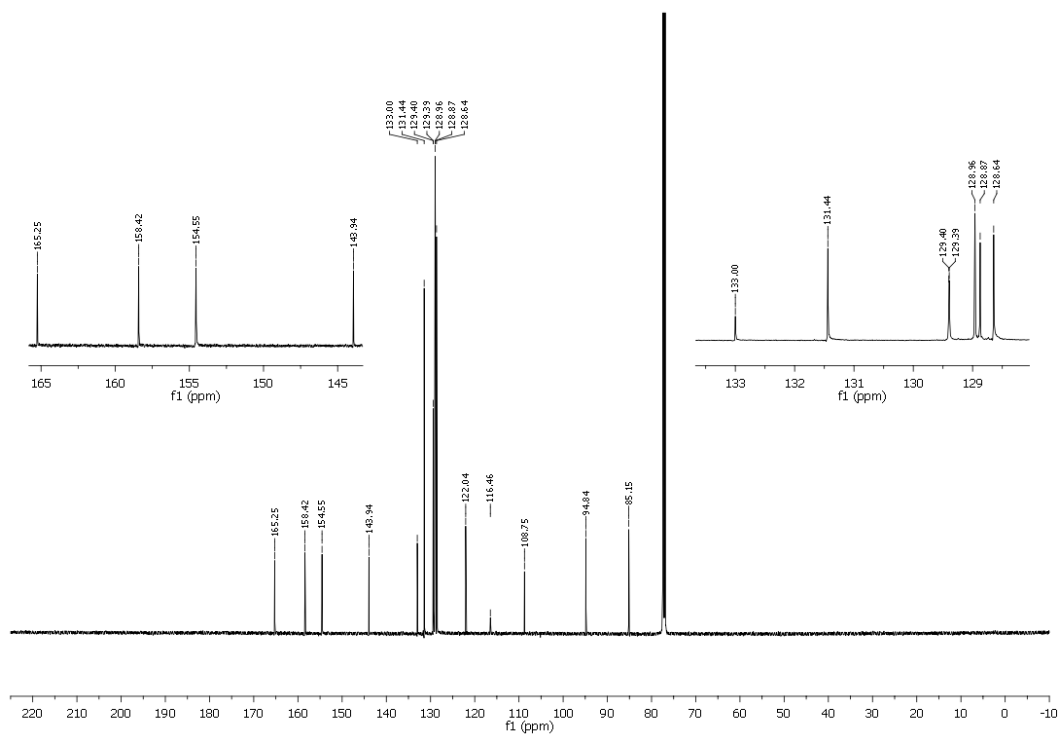


NMR Spectra of compound **19a**

¹H NMR (500 MHz, CDCl₃)

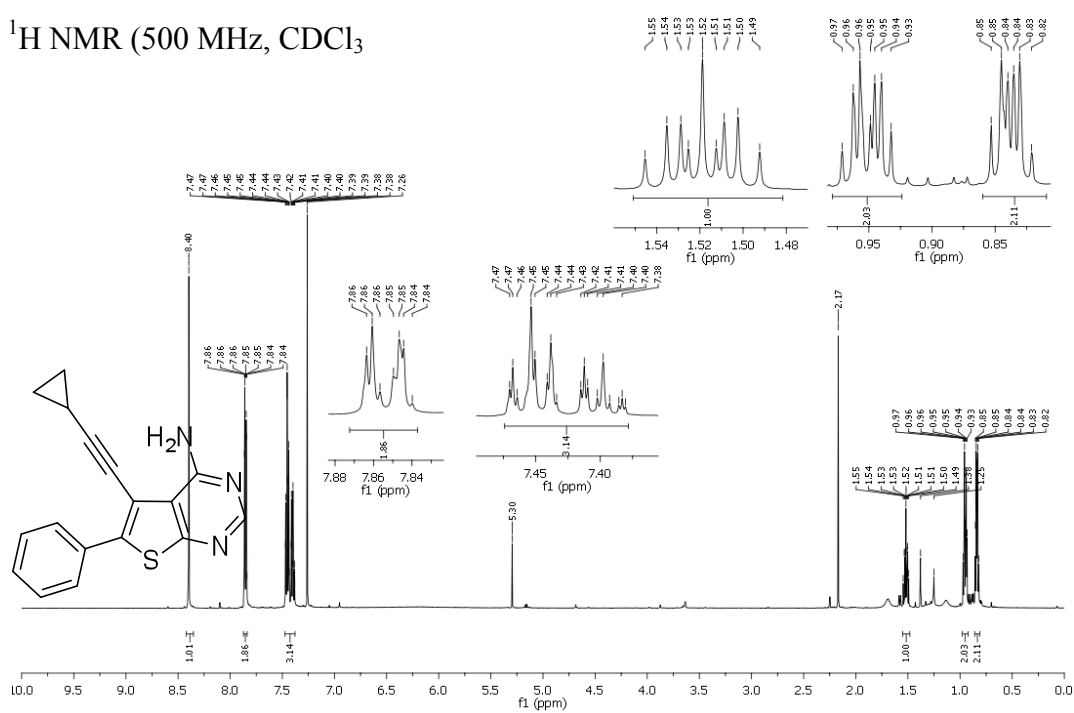


¹³C NMR (125 MHz, CDCl₃)



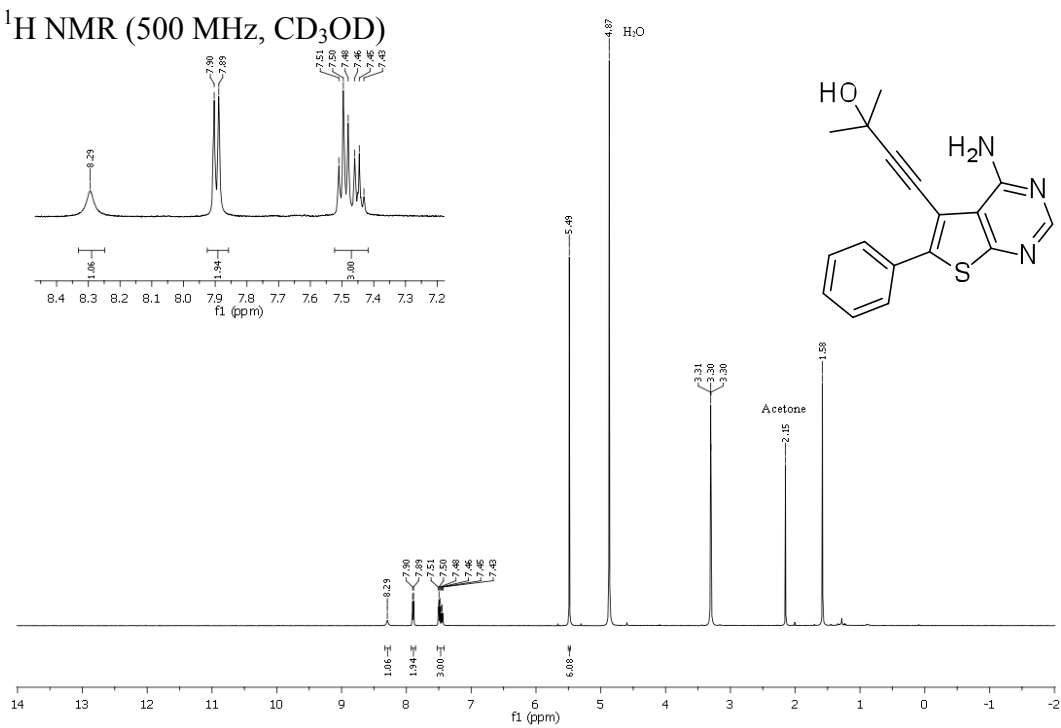
NMR Spectra of compound **19b**

¹H NMR (500 MHz, CDCl₃)

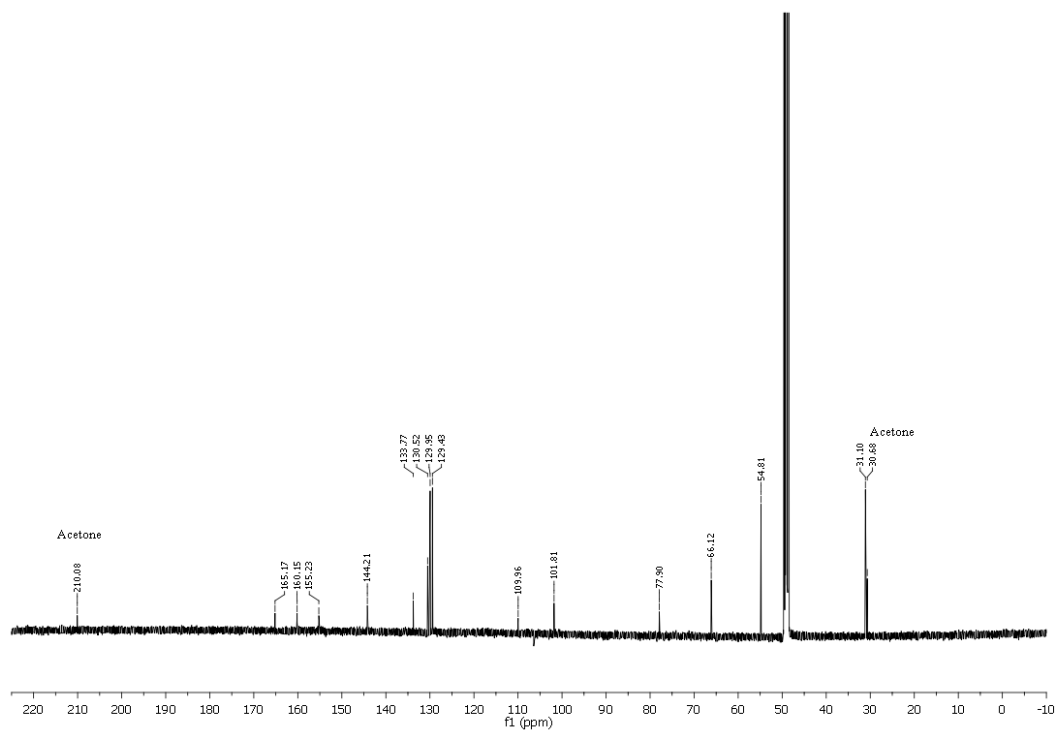


NMR Spectra of compound **19c**

^1H NMR (500 MHz, CD_3OD)

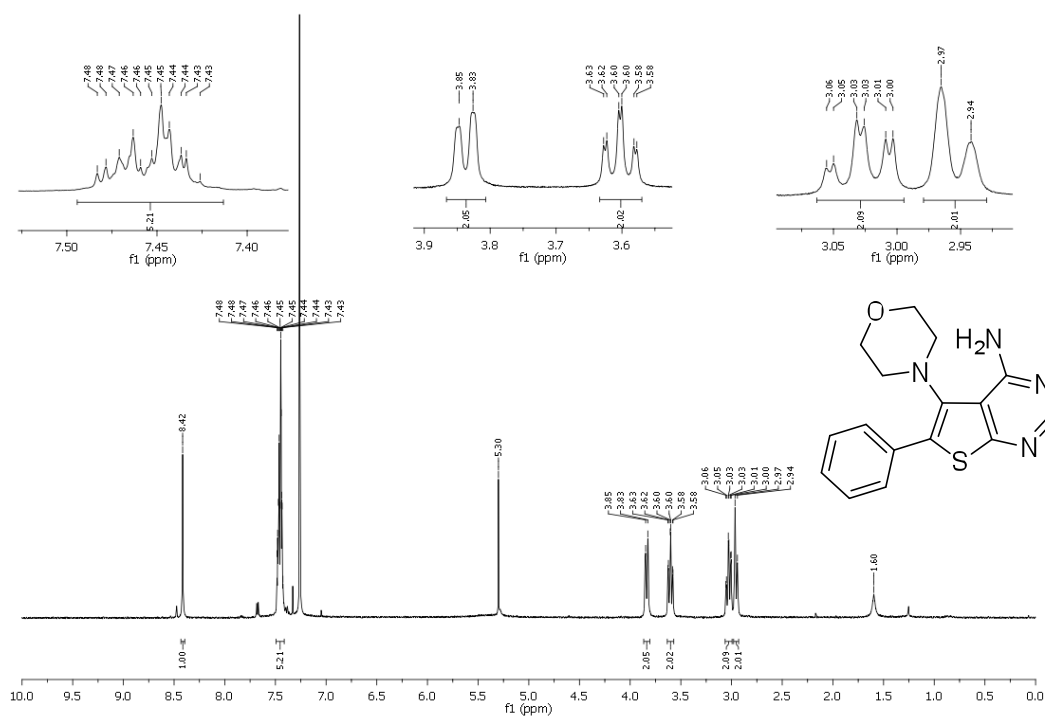


^{13}C NMR (125 MHz, CDCl_3)

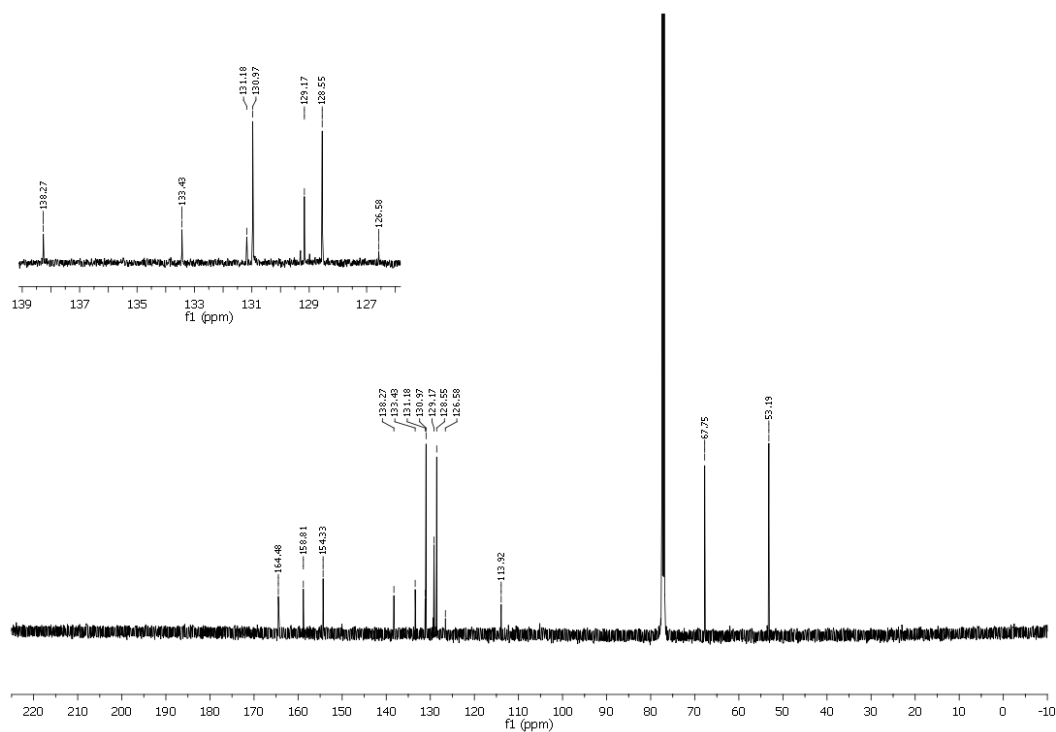


NMR Spectra of compound **19d**

^1H NMR (400 MHz, CDCl_3)

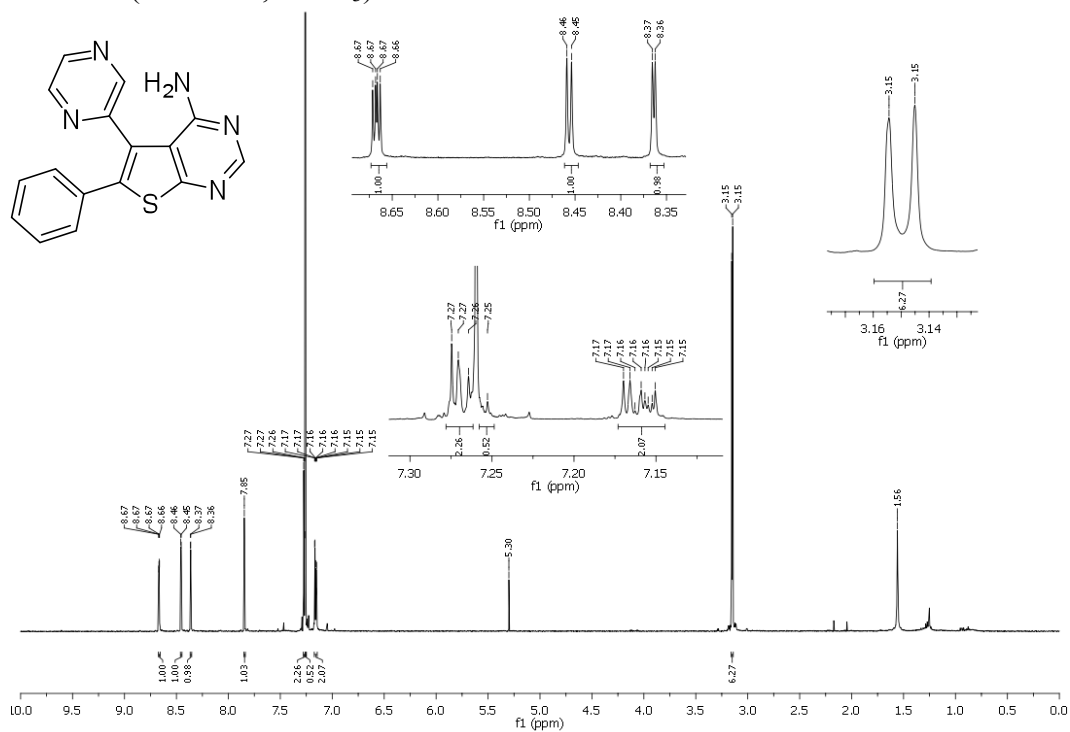


^{13}C NMR (125 MHz, CDCl_3)

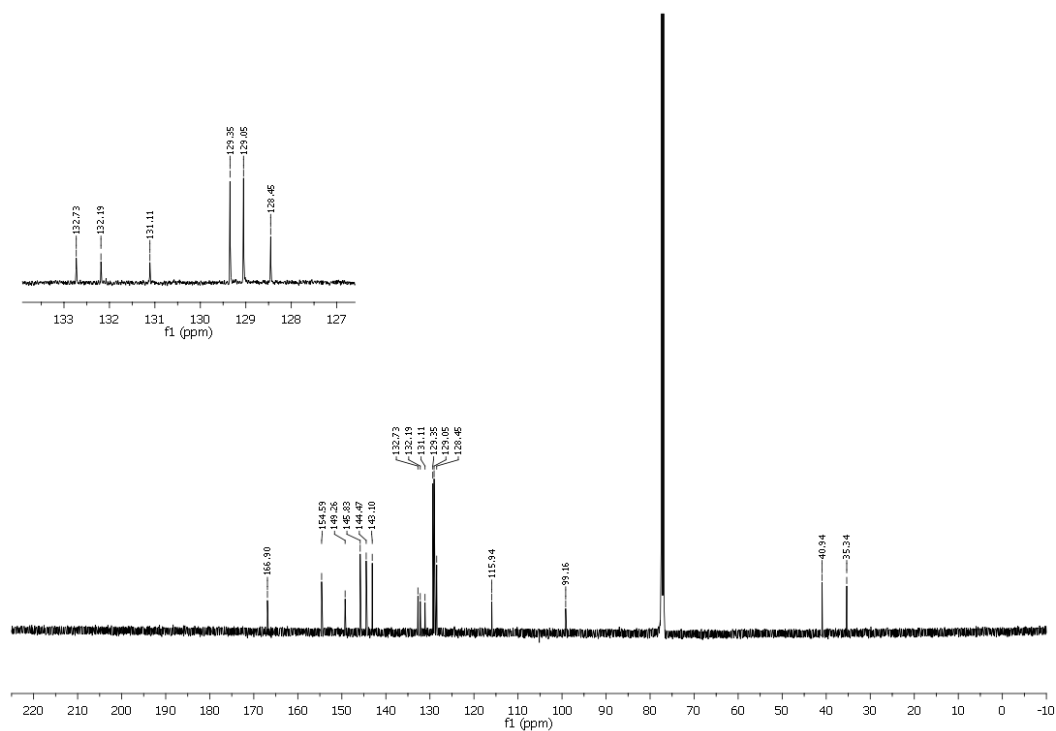


NMR Spectra of compound **19f**

^1H NMR (500 MHz, CDCl_3)

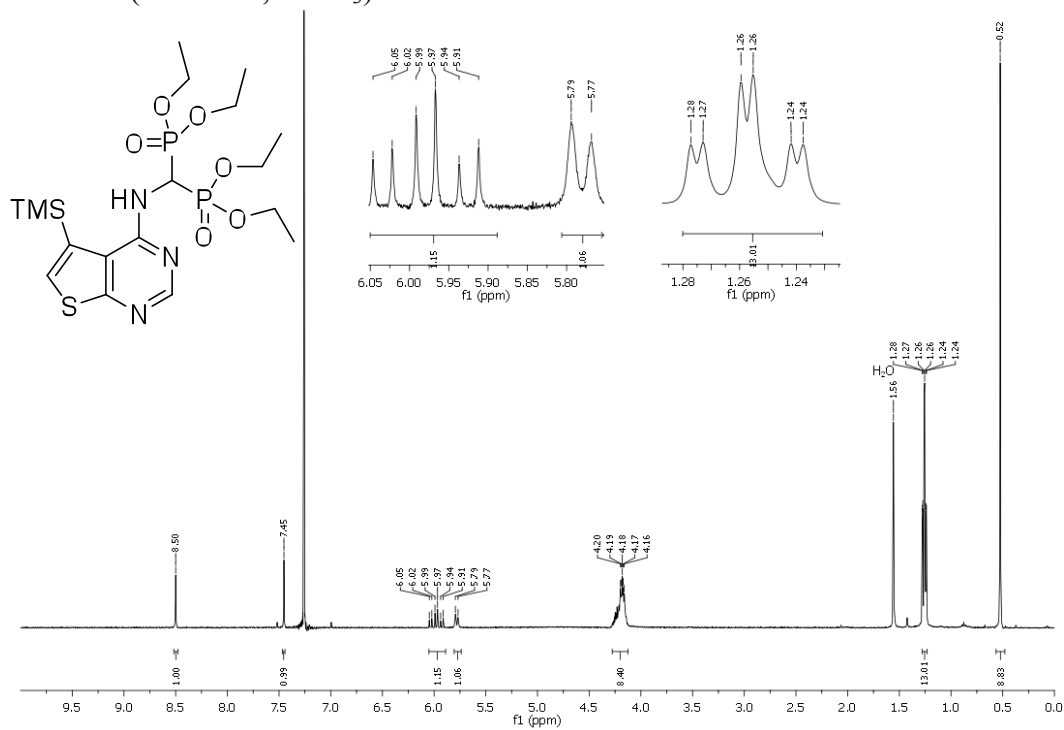


^{13}C NMR (125 MHz, CDCl_3)

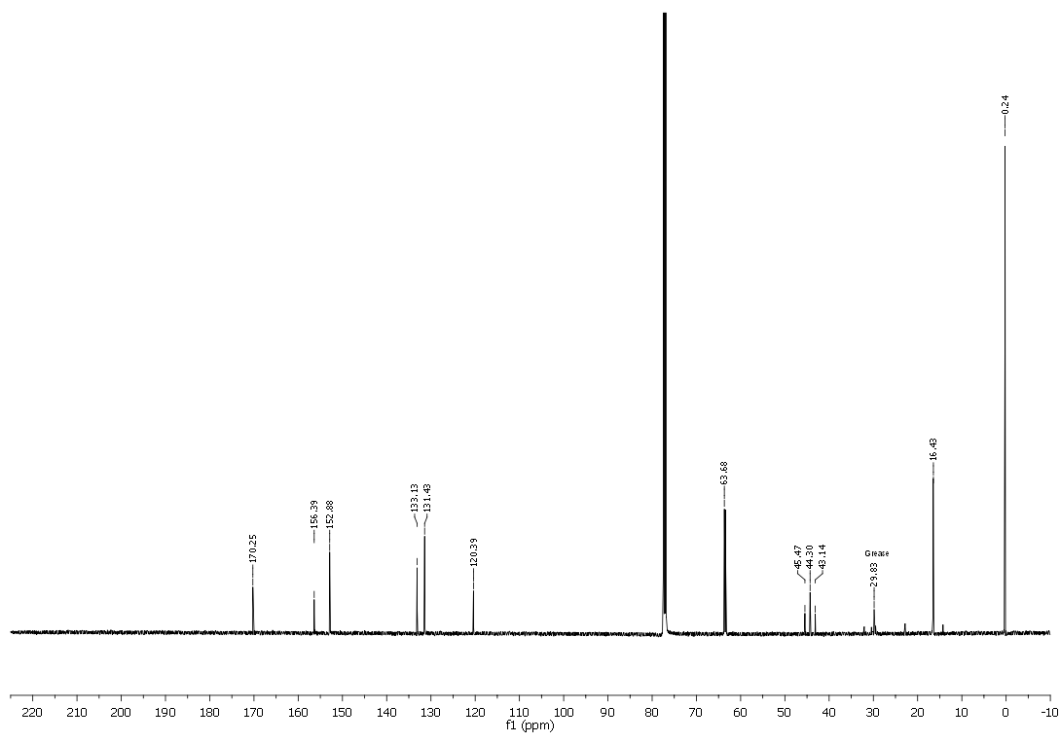


NMR Spectra of compound **36a**

^1H NMR (400 MHz, CDCl_3)

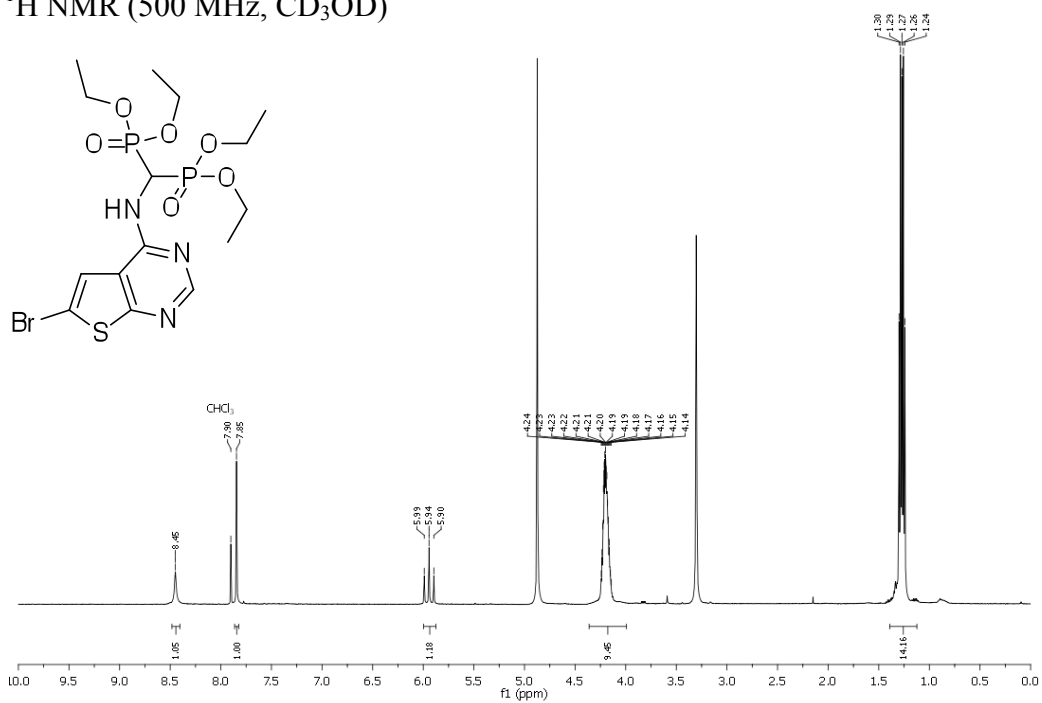


^{13}C NMR (125 MHz, CDCl_3)

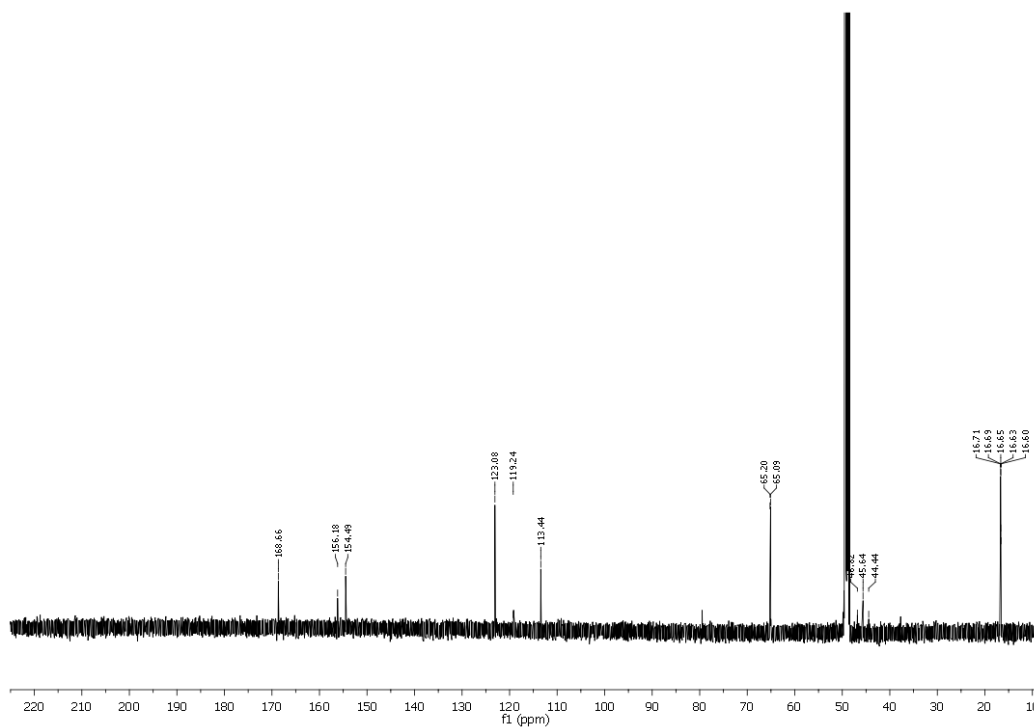


NMR Spectra of compound **36b**

^1H NMR (500 MHz, CD_3OD)

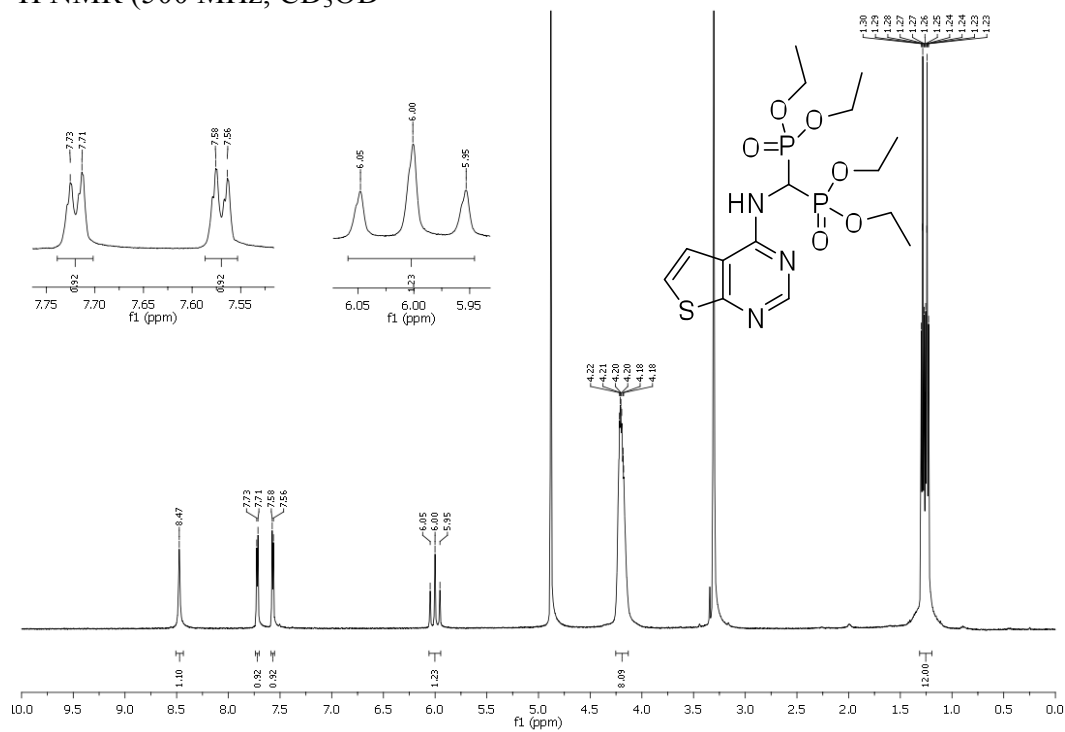


^{13}C NMR (125 MHz, CD_3OD)

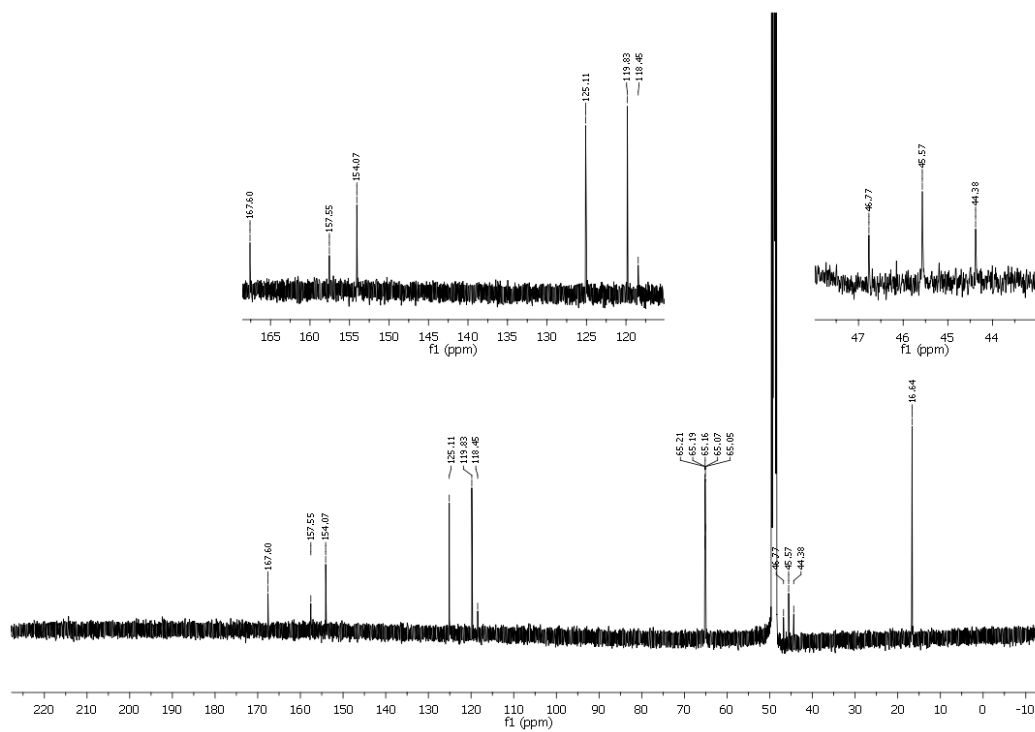


NMR Spectra of compound **36c**

^1H NMR (500 MHz, CD_3OD)

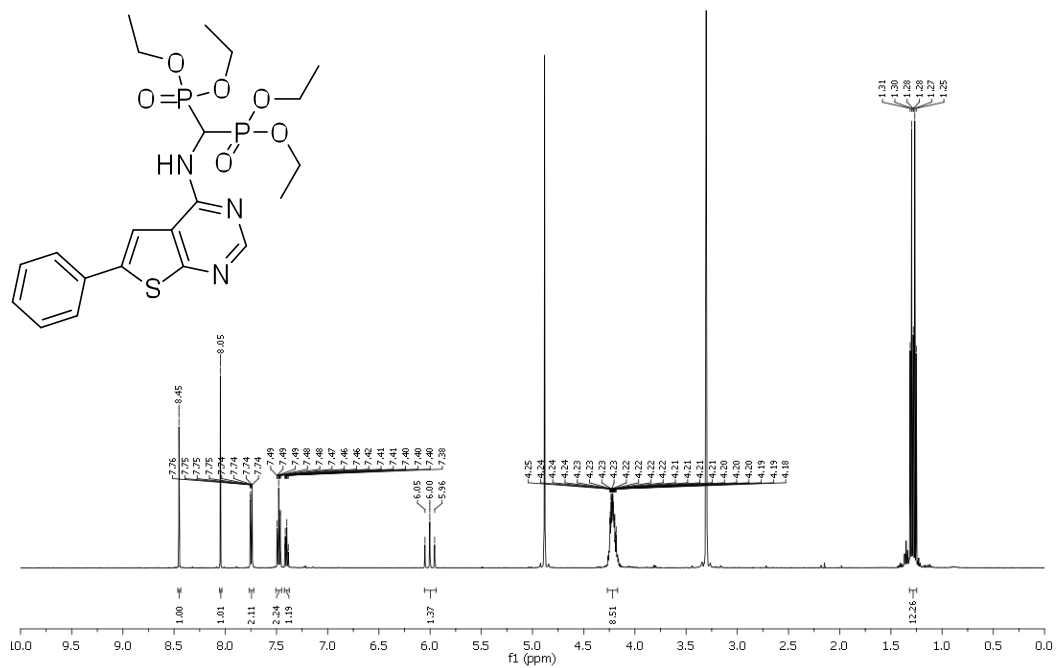


^{13}C NMR (125 MHz, CD_3OD)

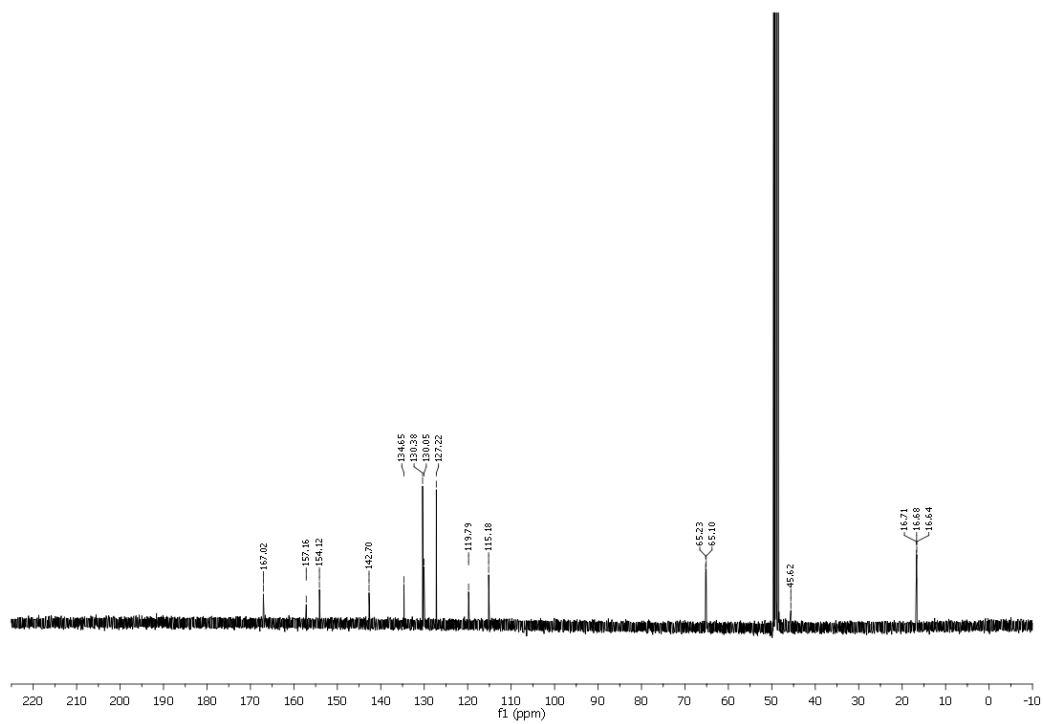


NMR Spectra of compound **36d**

^1H NMR (500 MHz, CD_3OD)

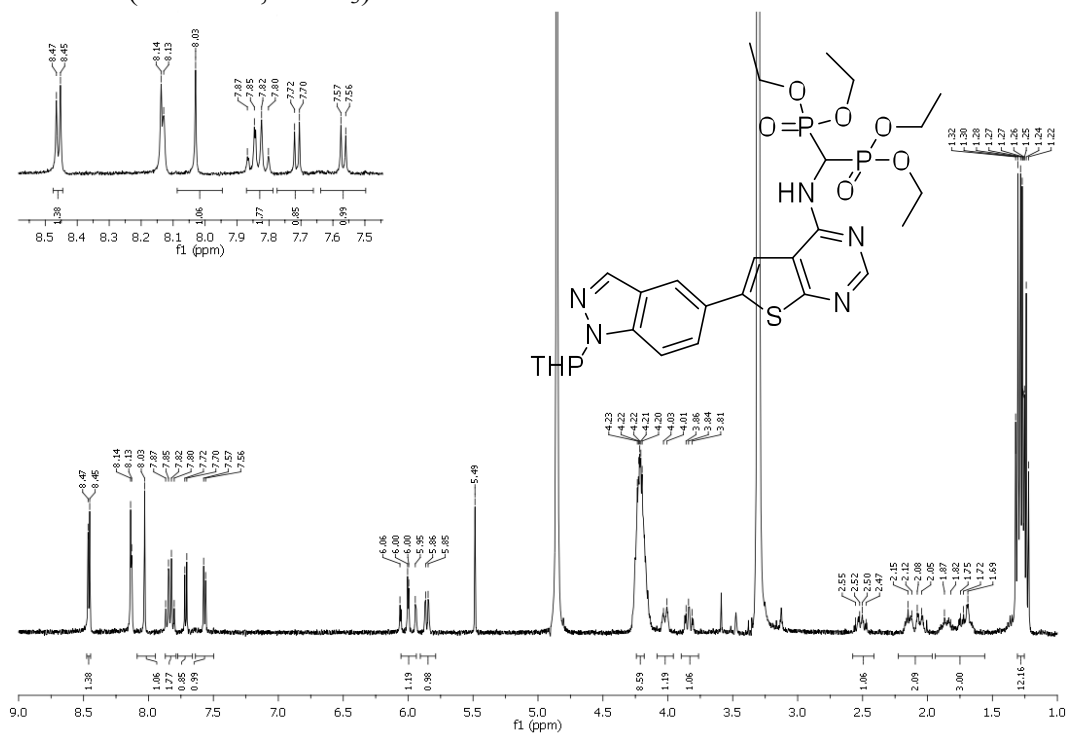


^{13}C NMR (125 MHz, CD_3OD)

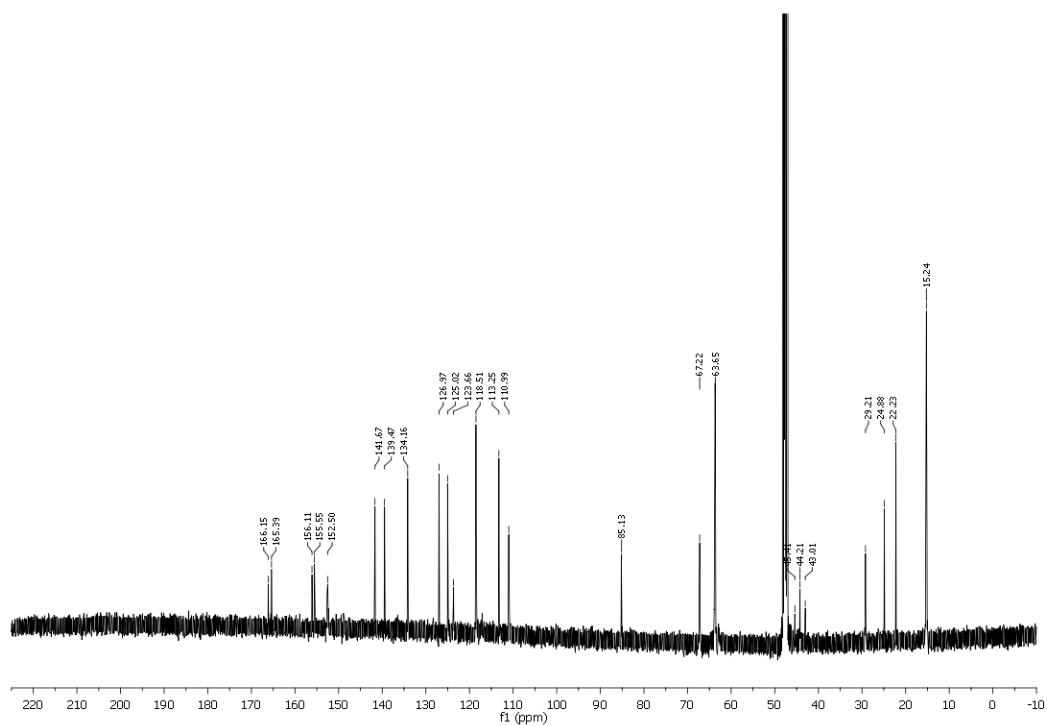


NMR Spectra of compound **36e**

^1H NMR (400 MHz, CDCl_3)

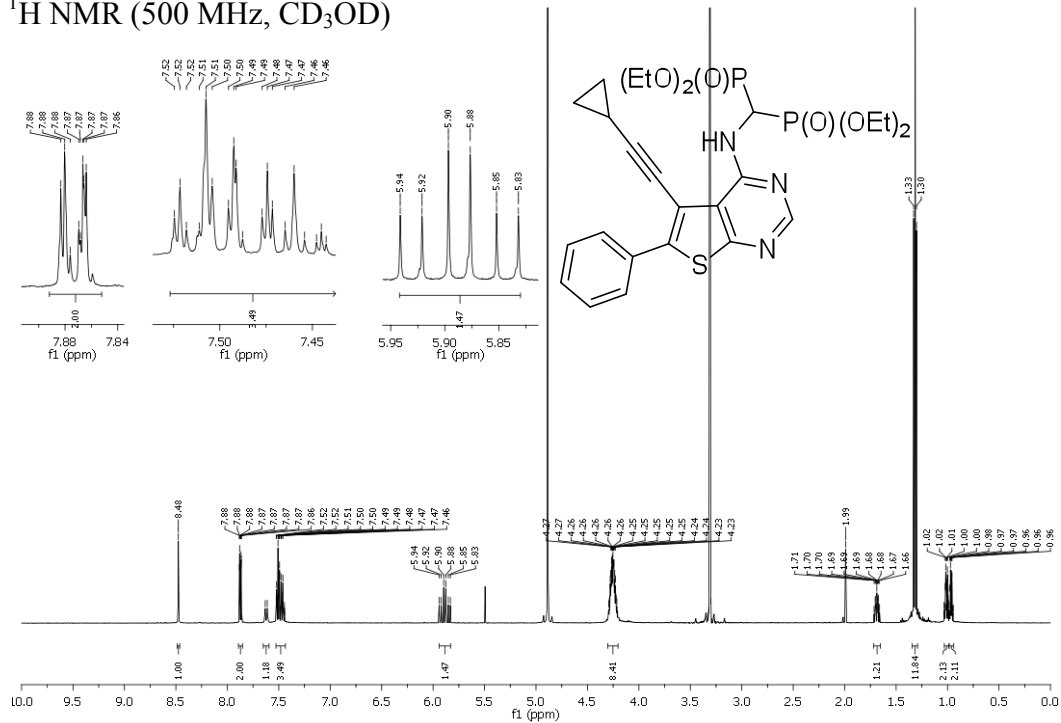


^{13}C NMR (125 MHz, CDCl_3)

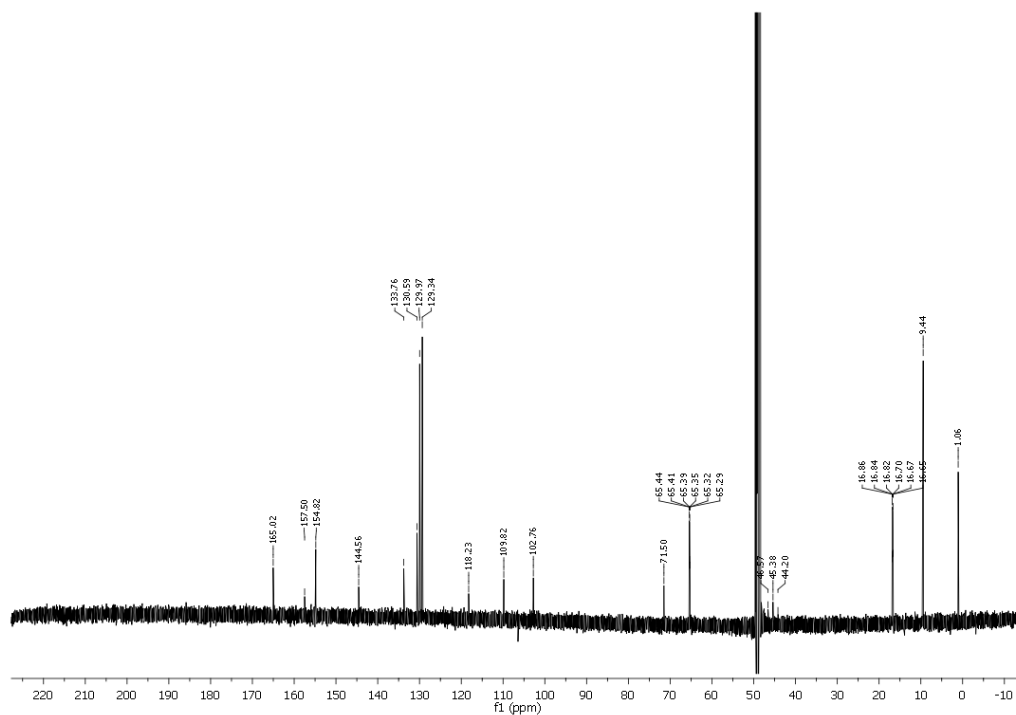


NMR Spectra of compound **36f**

¹H NMR (500 MHz, CD₃OD)

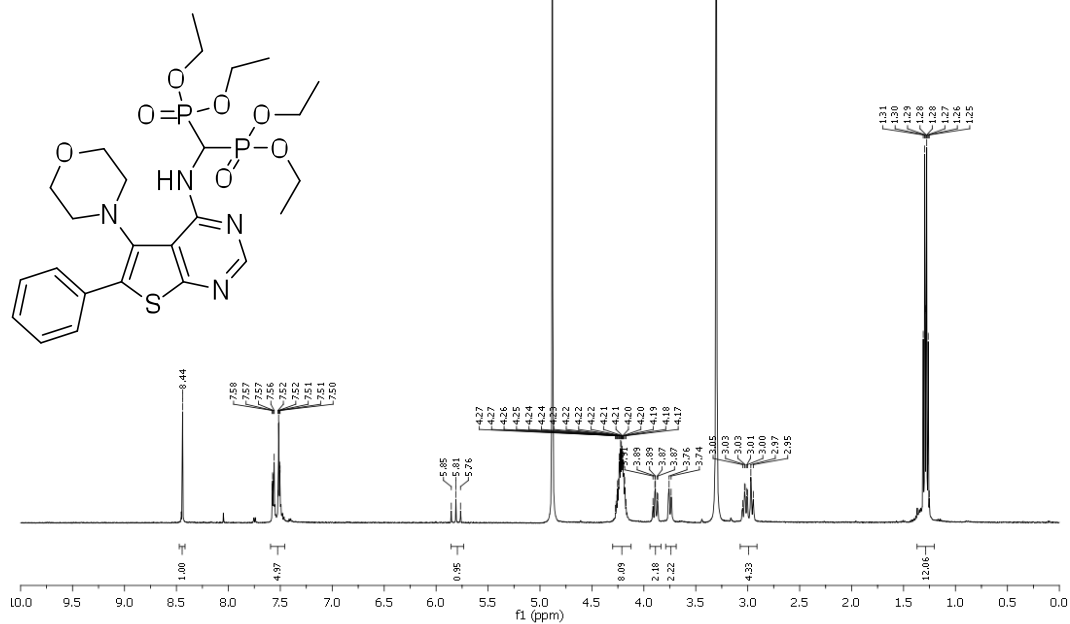


¹³C NMR (125 MHz, CD₃OD)

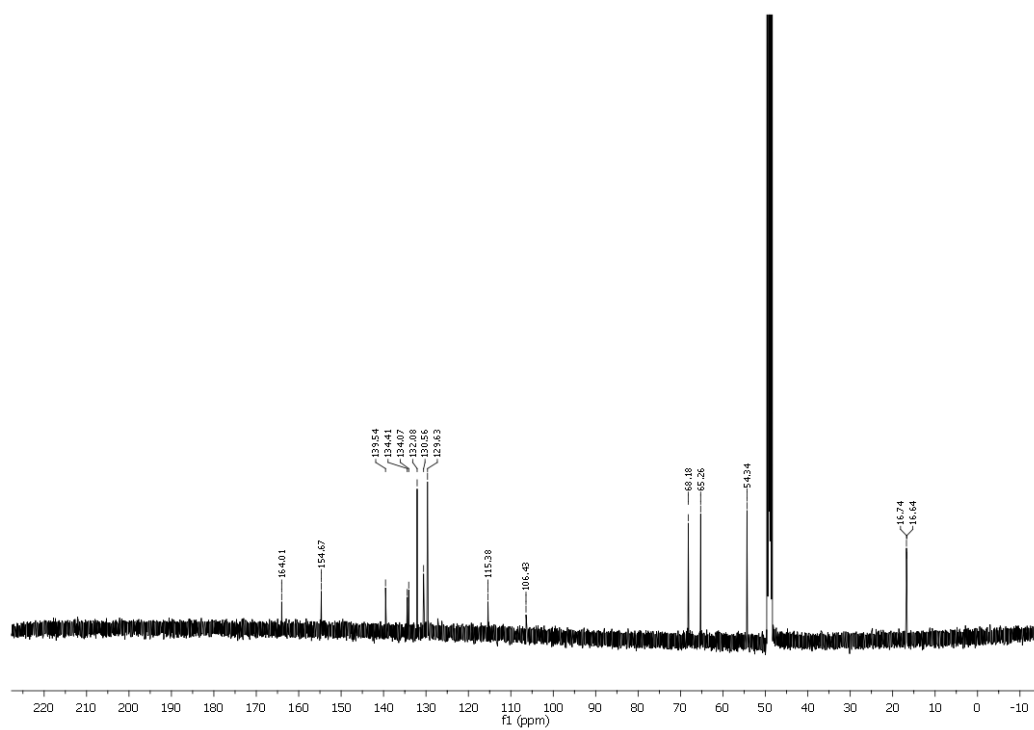


NMR Spectra of compound **36g**

^1H NMR (500 MHz, CD_3OD)

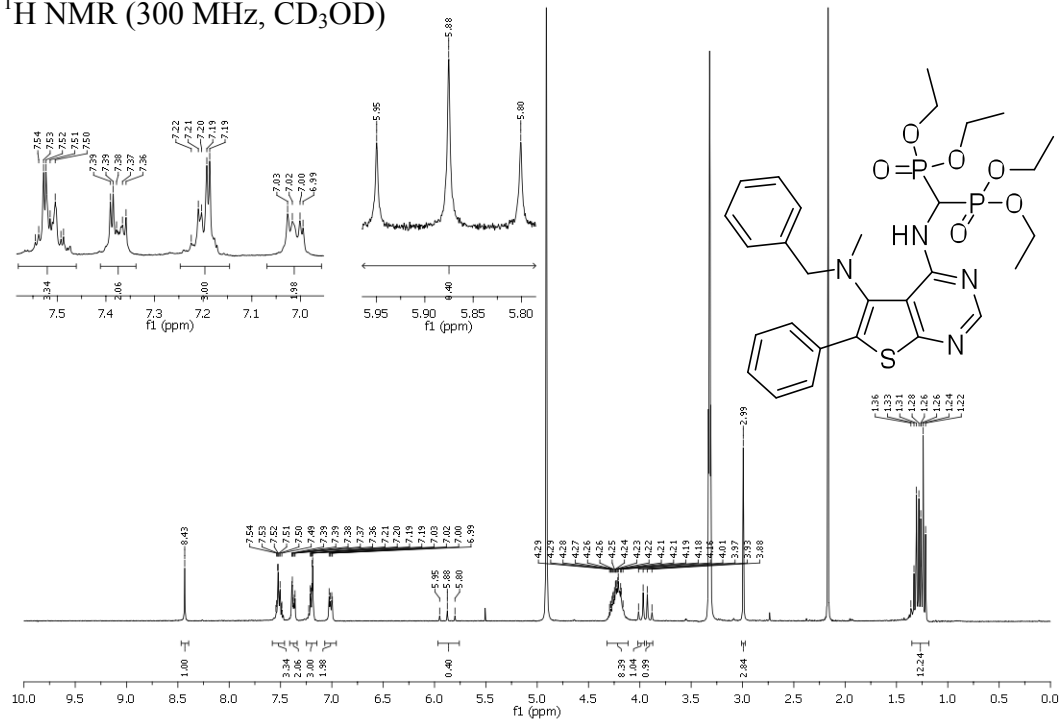


^{13}C NMR (125 MHz, CD_3OD)

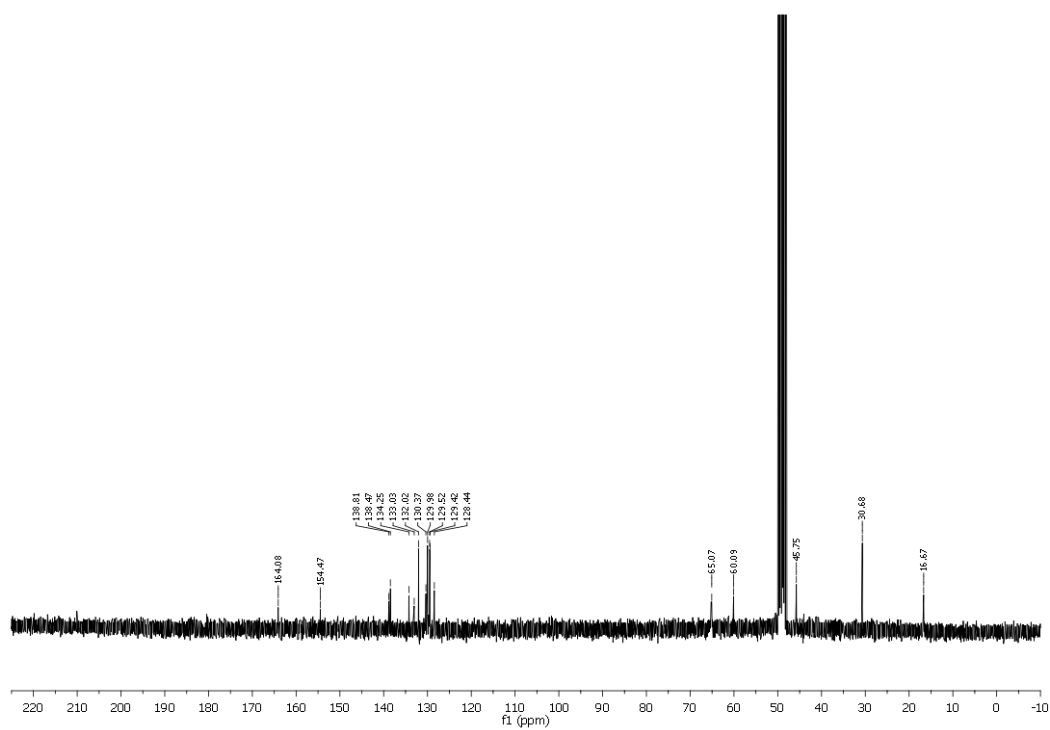


NMR Spectra of compound **36h**

^1H NMR (300 MHz, CD_3OD)

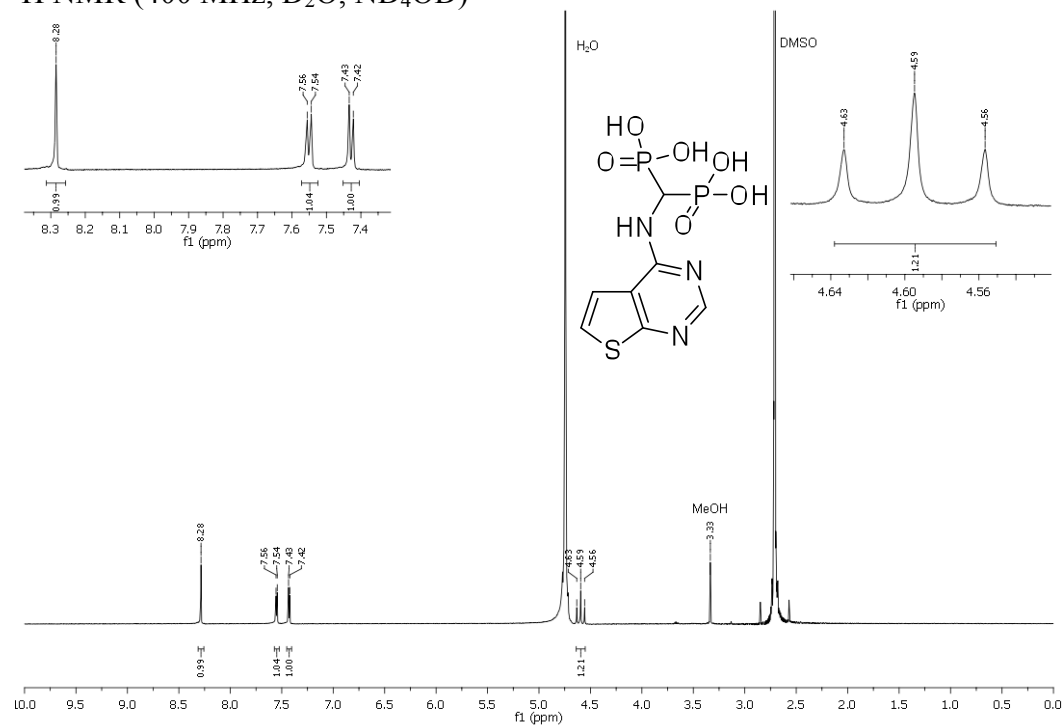


^{13}C NMR (75 MHz, CD_3OD)

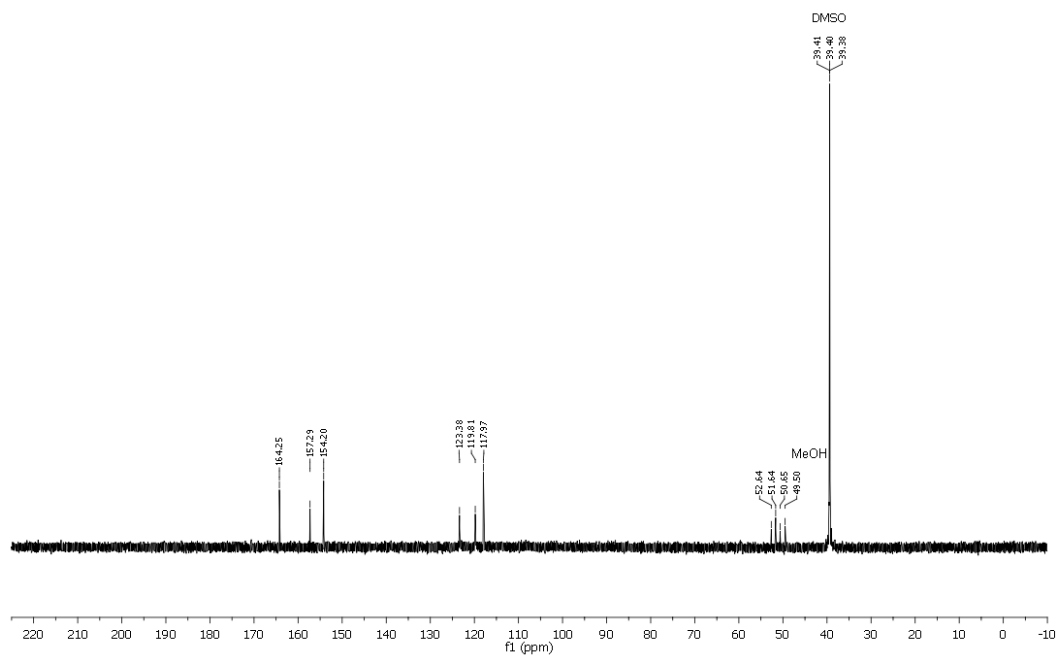


NMR Spectra of compound **37a**

^1H NMR (400 MHz, D_2O , ND_4OD)

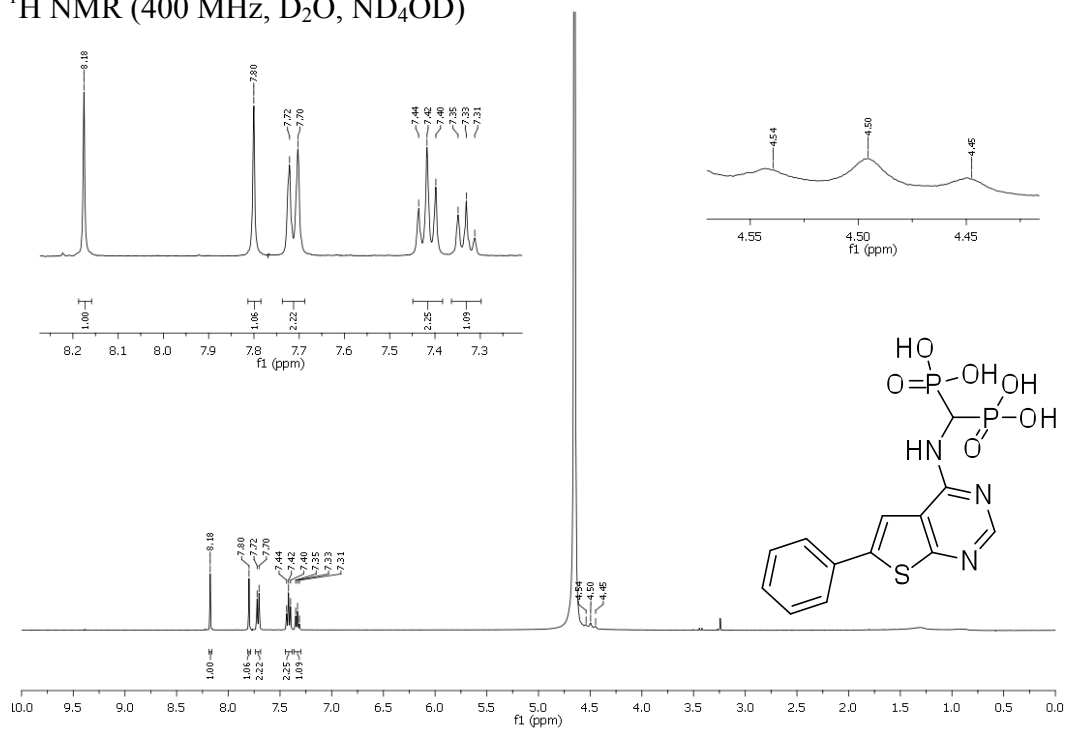


^{13}C NMR (125 MHz, D_2O , ND_4OD)

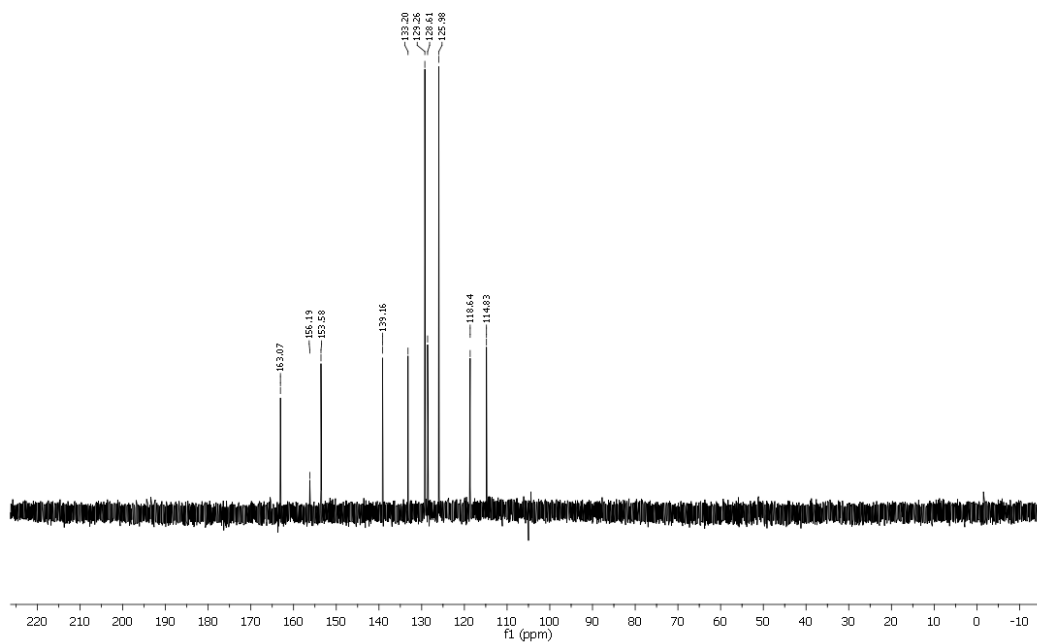


NMR Spectra of compound **37b**

^1H NMR (400 MHz, D_2O , ND_4OD)

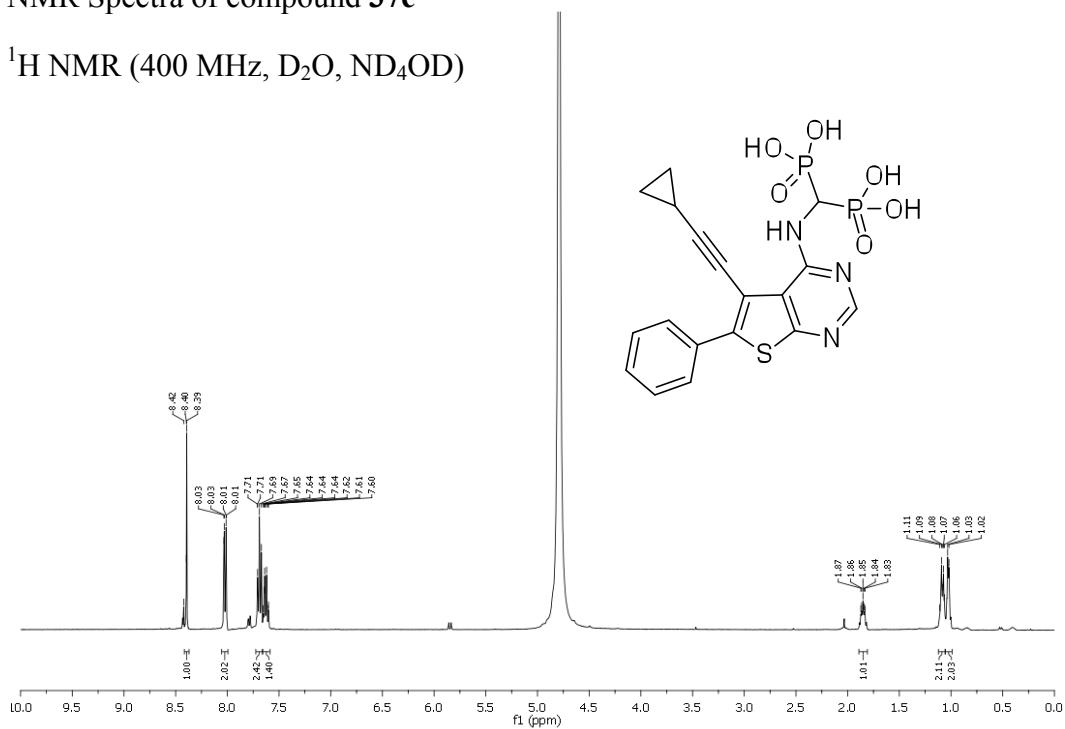


^{13}C NMR (125 MHz, D_2O , ND_4OD)

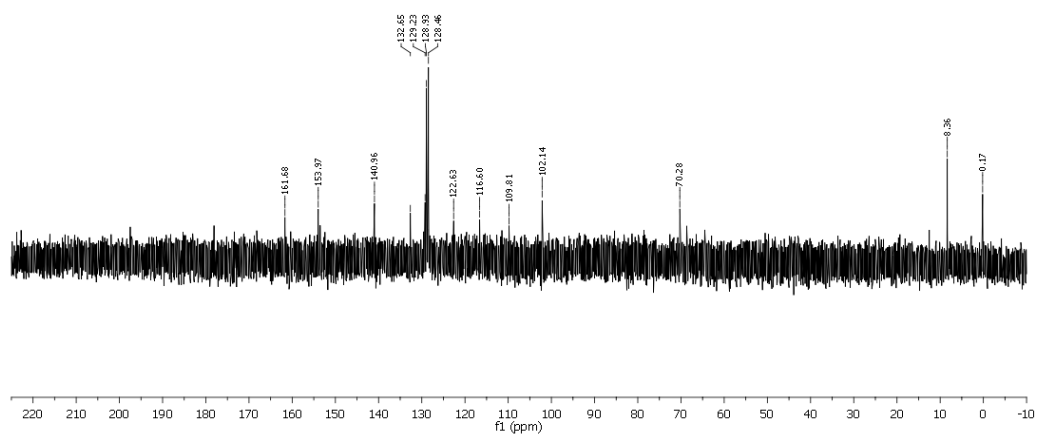


NMR Spectra of compound **37c**

^1H NMR (400 MHz, D_2O , ND_4OD)

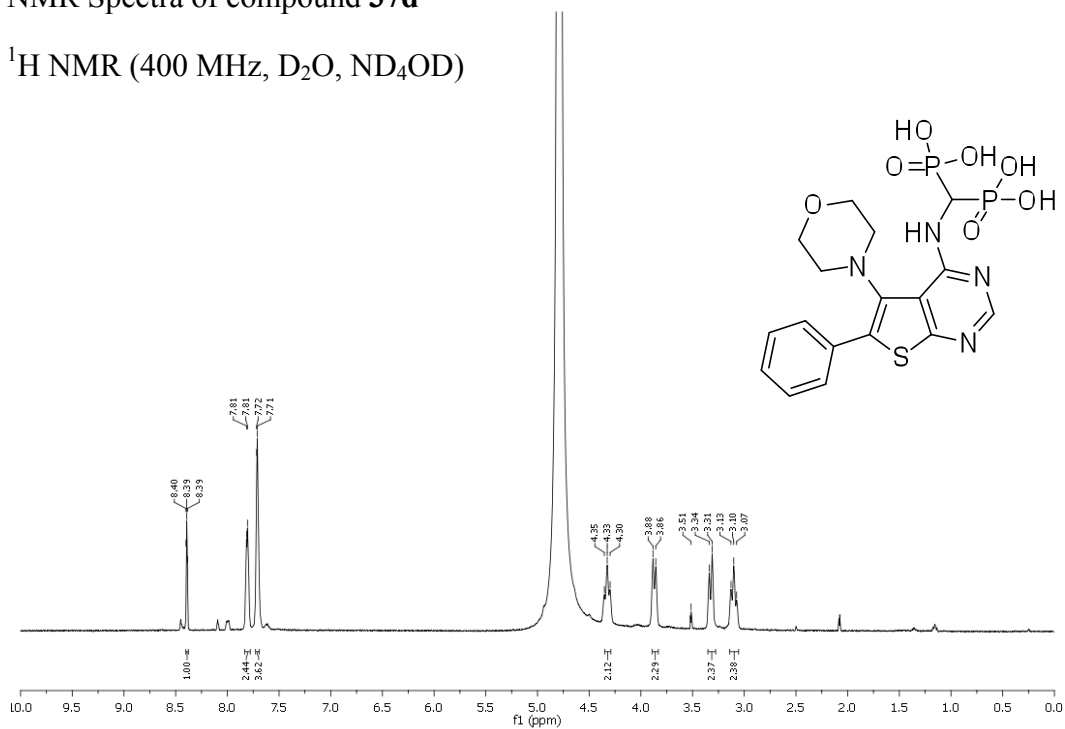


^{13}C NMR (75 MHz, D_2O , ND_4OD)

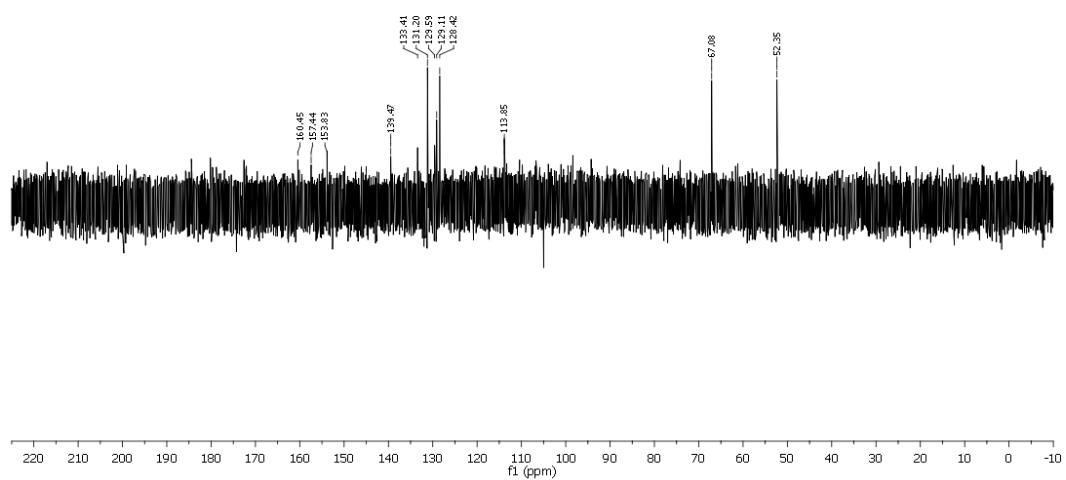


NMR Spectra of compound **37d**

^1H NMR (400 MHz, D_2O , ND_4OD)

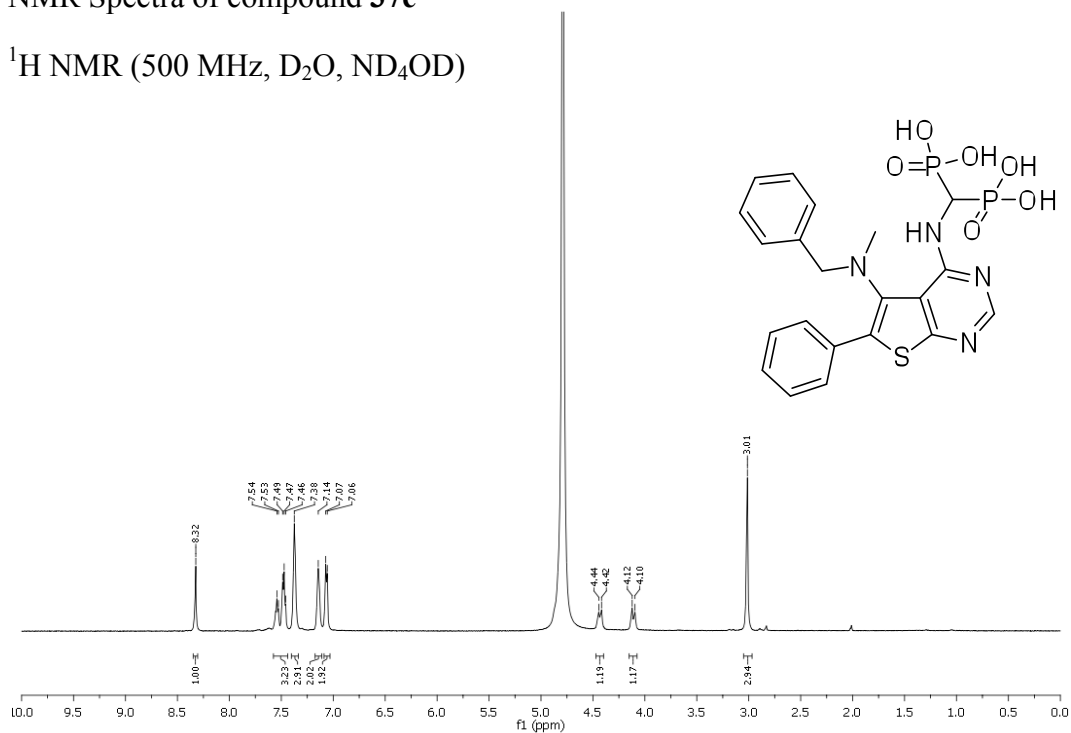


^{13}C NMR (126 MHz, D_2O , ND_4OD)

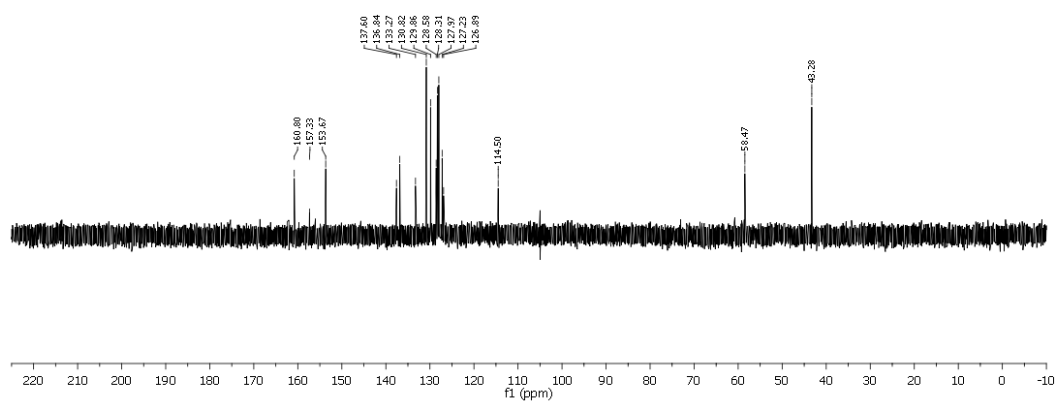


NMR Spectra of compound **37e**

^1H NMR (500 MHz, D_2O , ND_4OD)

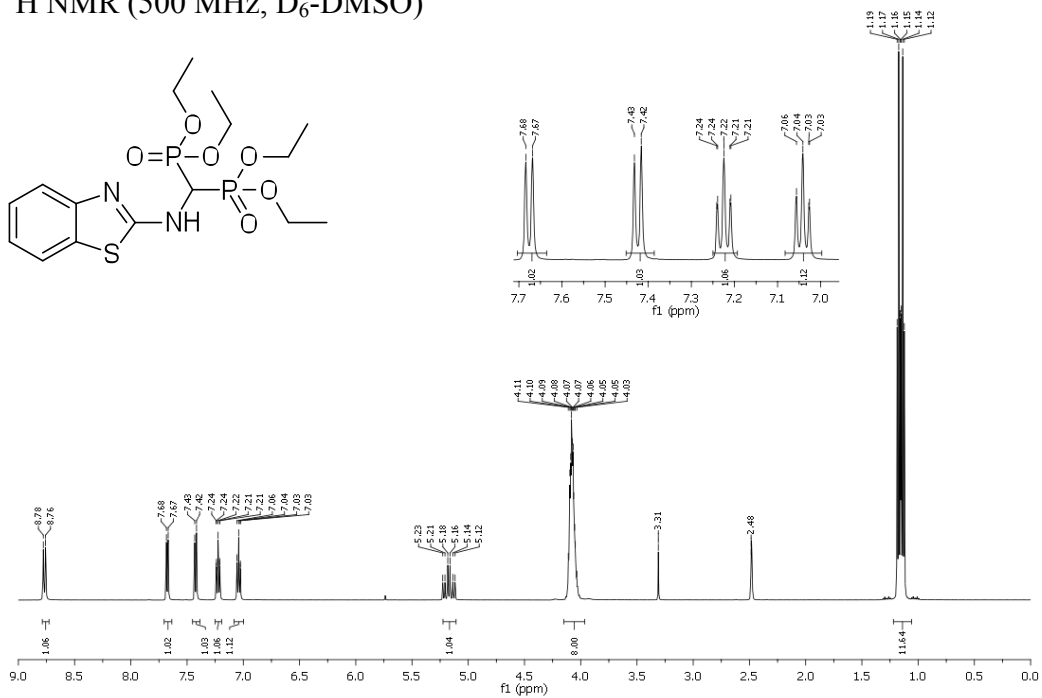
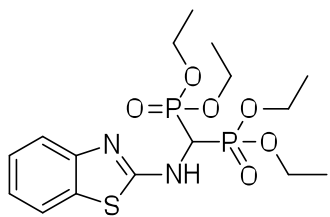


^{13}C NMR (125 MHz, D_2O , ND_4OD)

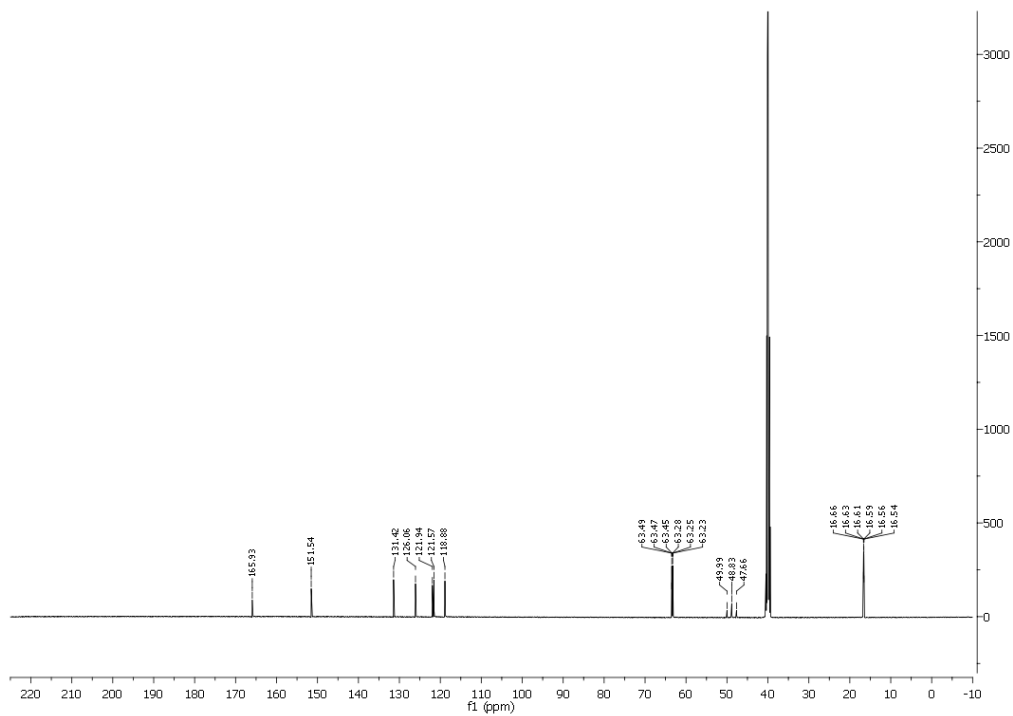


NMR Spectra of compound **39a**

^1H NMR (500 MHz, $\text{D}_6\text{-DMSO}$)

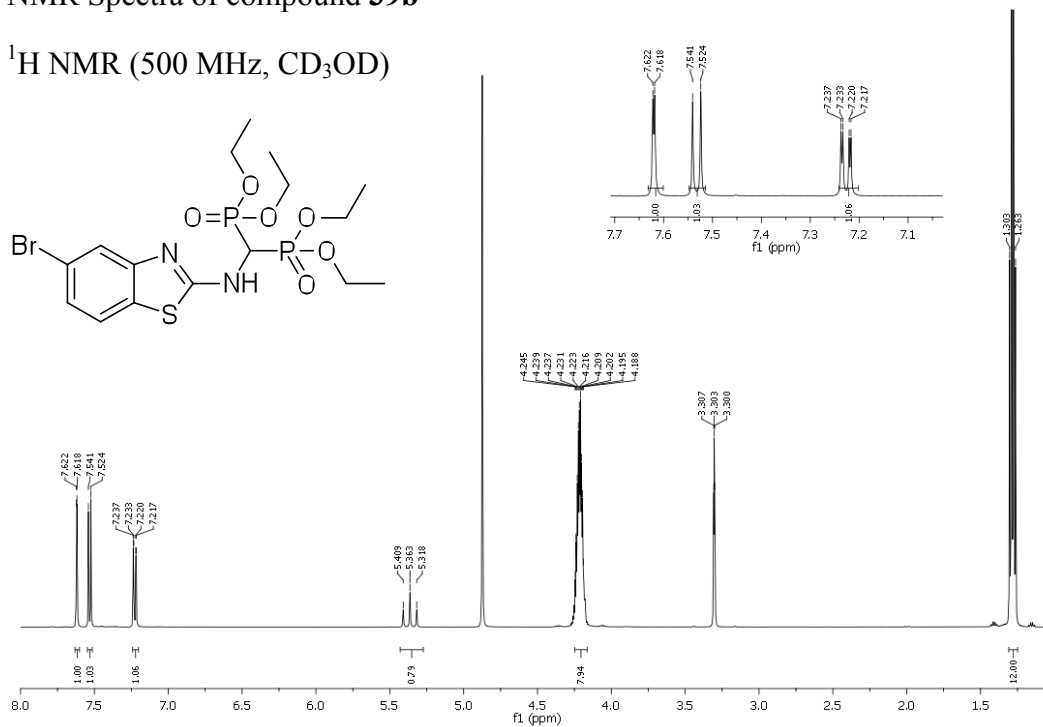
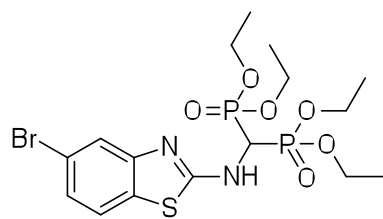


^{13}C NMR (125 MHz, $\text{D}_6\text{-DMSO}$)

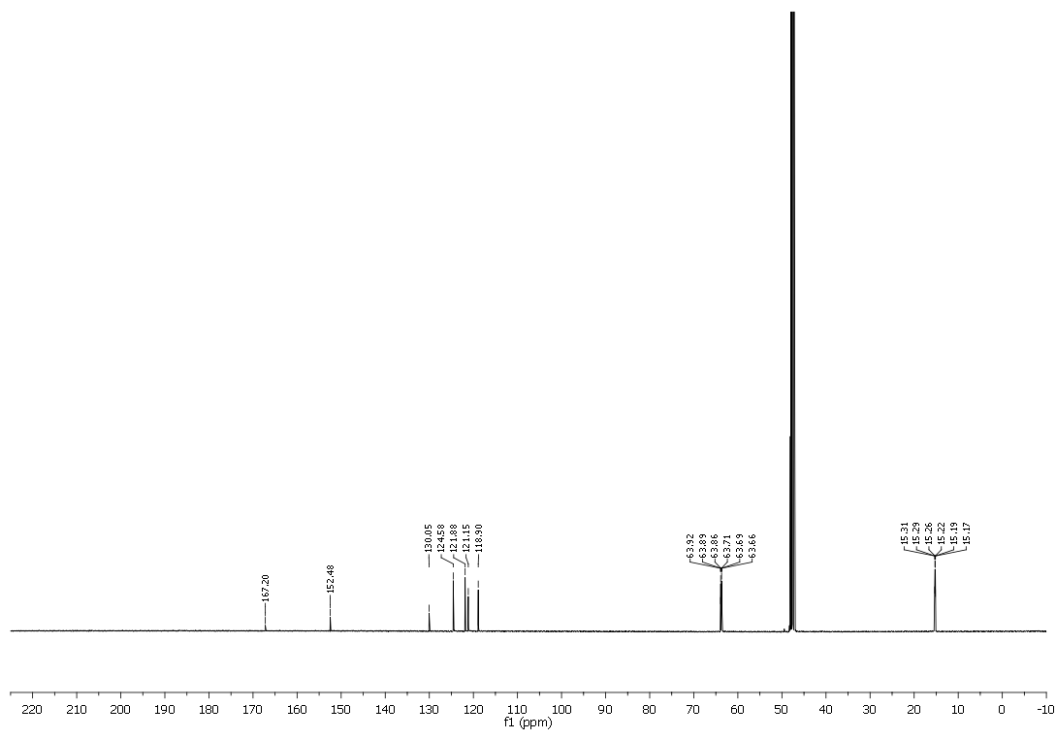


NMR Spectra of compound **39b**

^1H NMR (500 MHz, CD_3OD)

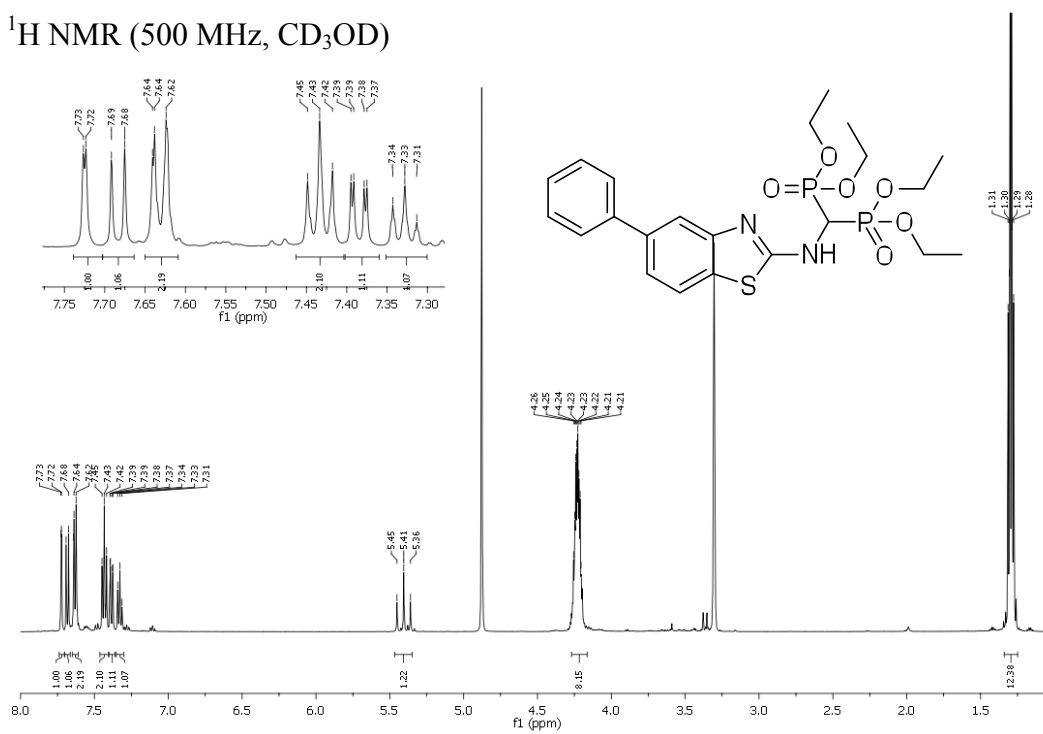


^{13}C NMR (125 MHz, CD_3OD)

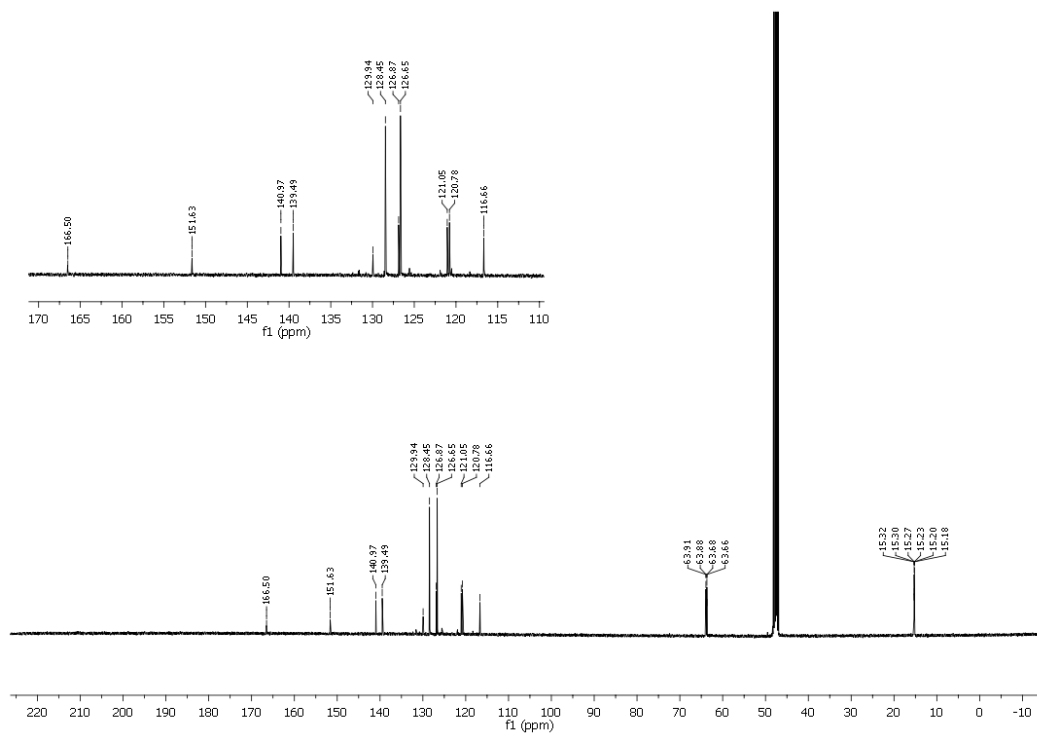


NMR Spectra of compound **39c**

^1H NMR (500 MHz, CD_3OD)

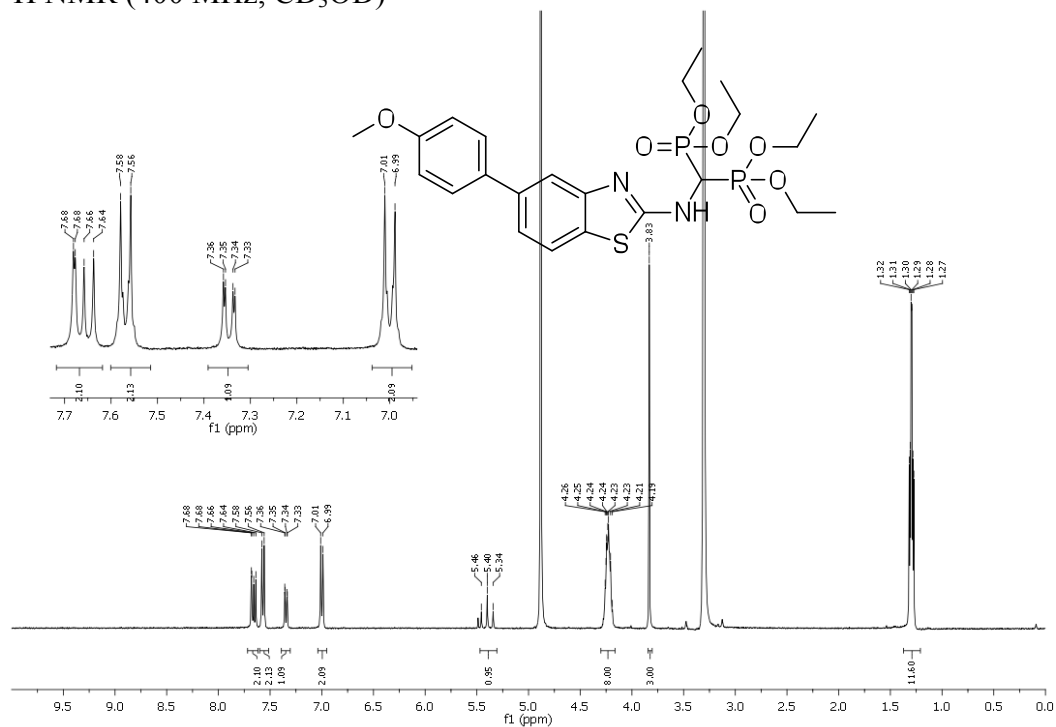


^{13}C NMR (125 MHz, CD_3OD)

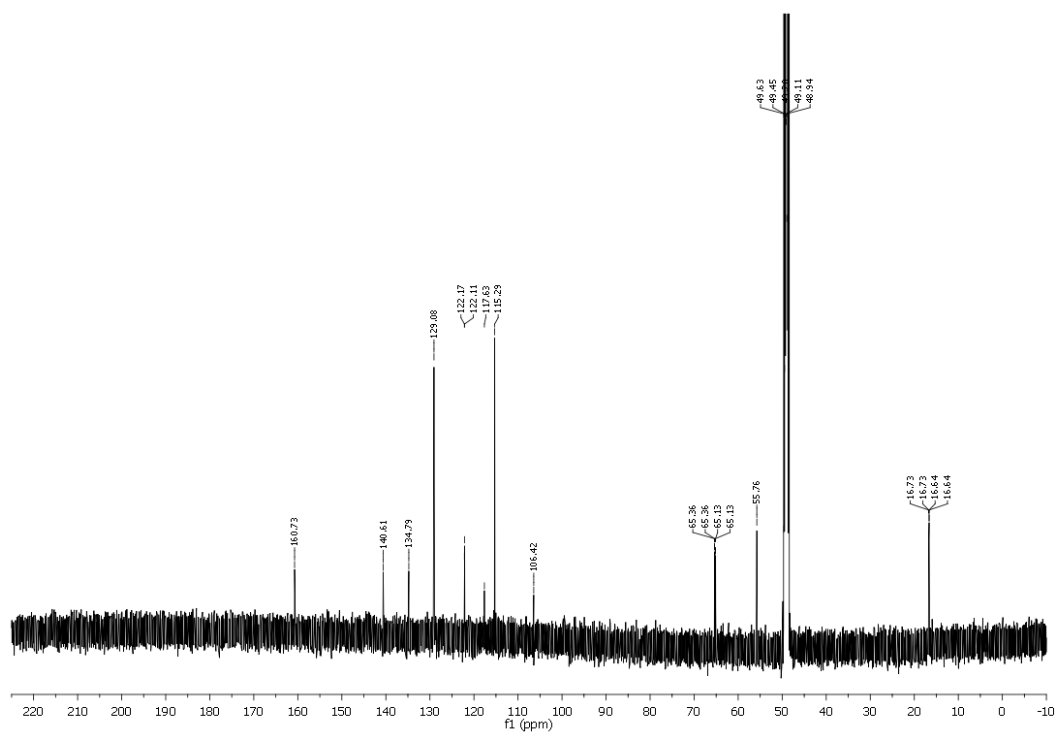


NMR Spectra of compound **39d**

^1H NMR (400 MHz, CD_3OD)

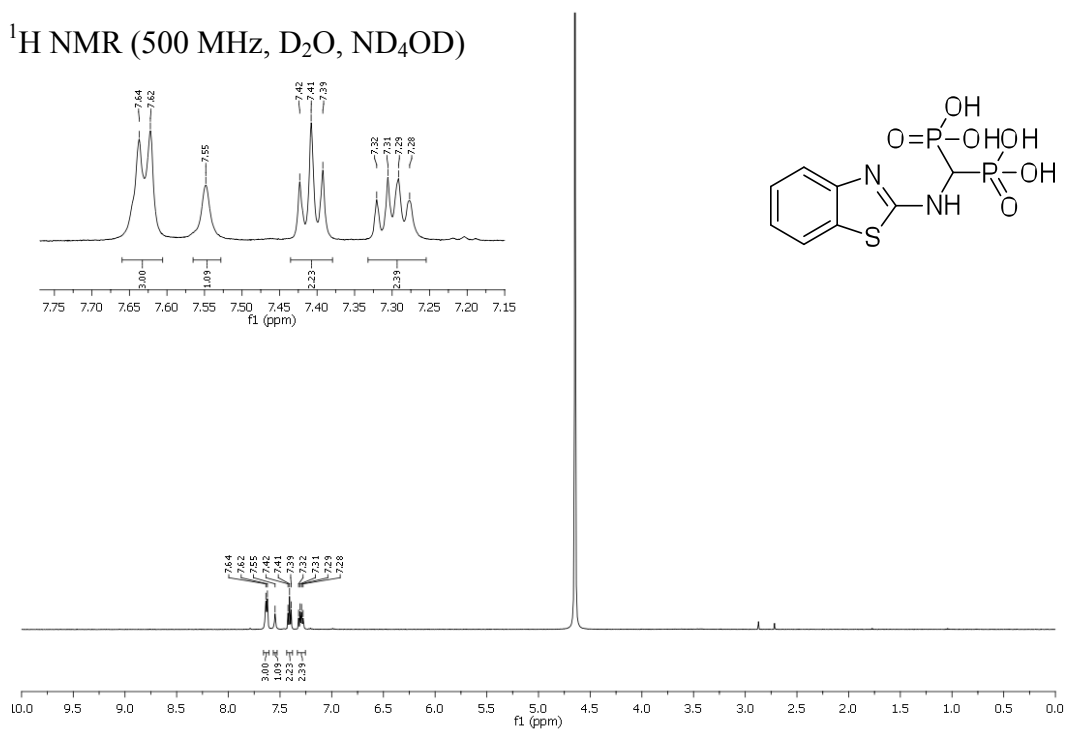


^{13}C NMR (125 MHz, CD_3OD)

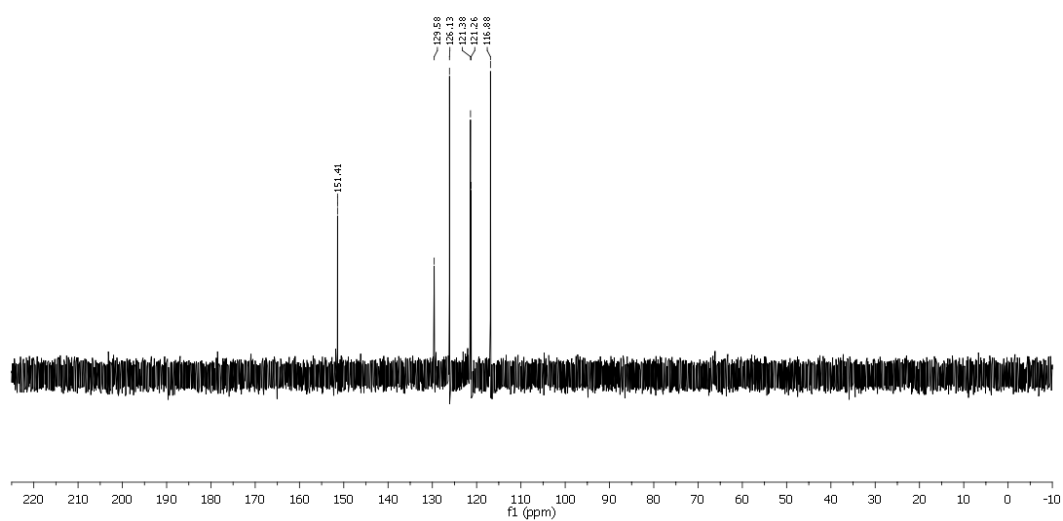


NMR Spectra of compound **40a**

^1H NMR (500 MHz, D_2O , ND_4OD)

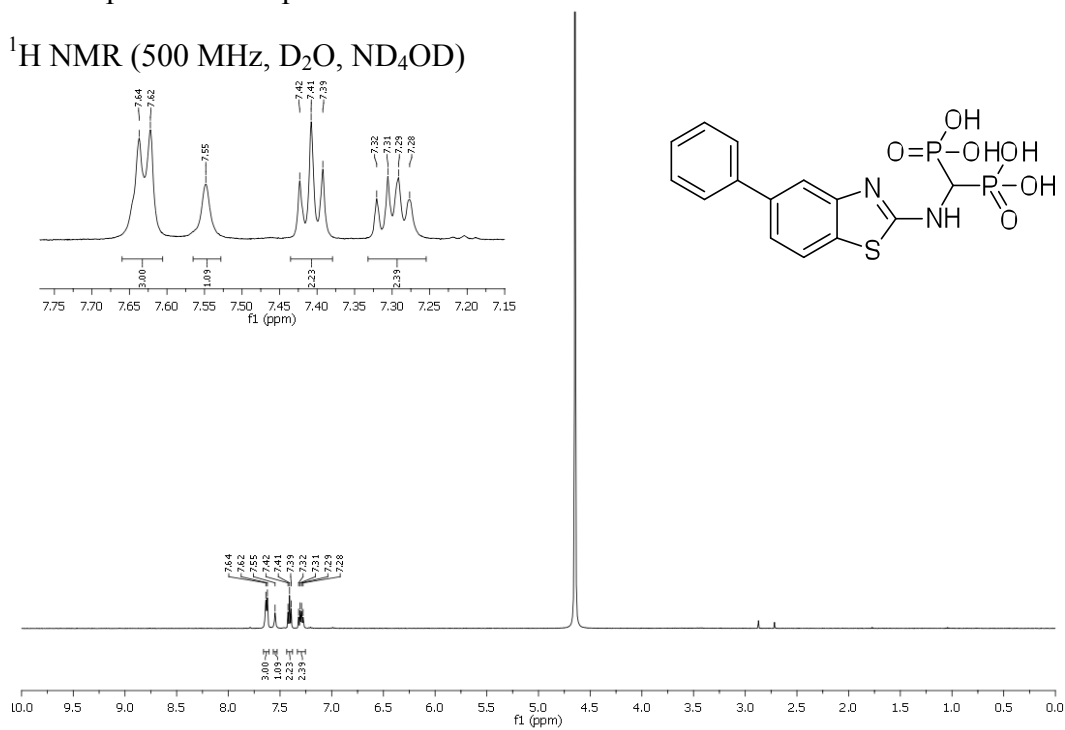


^{13}C NMR (125 MHz, D_2O , ND_4OD)

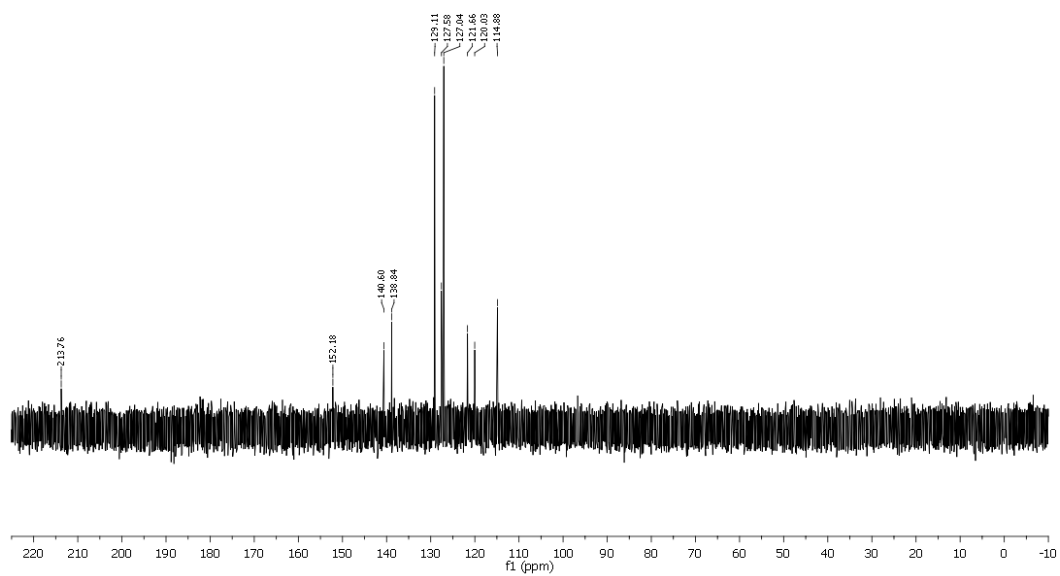


NMR Spectra of compound **40b**

^1H NMR (500 MHz, D_2O , ND_4OD)

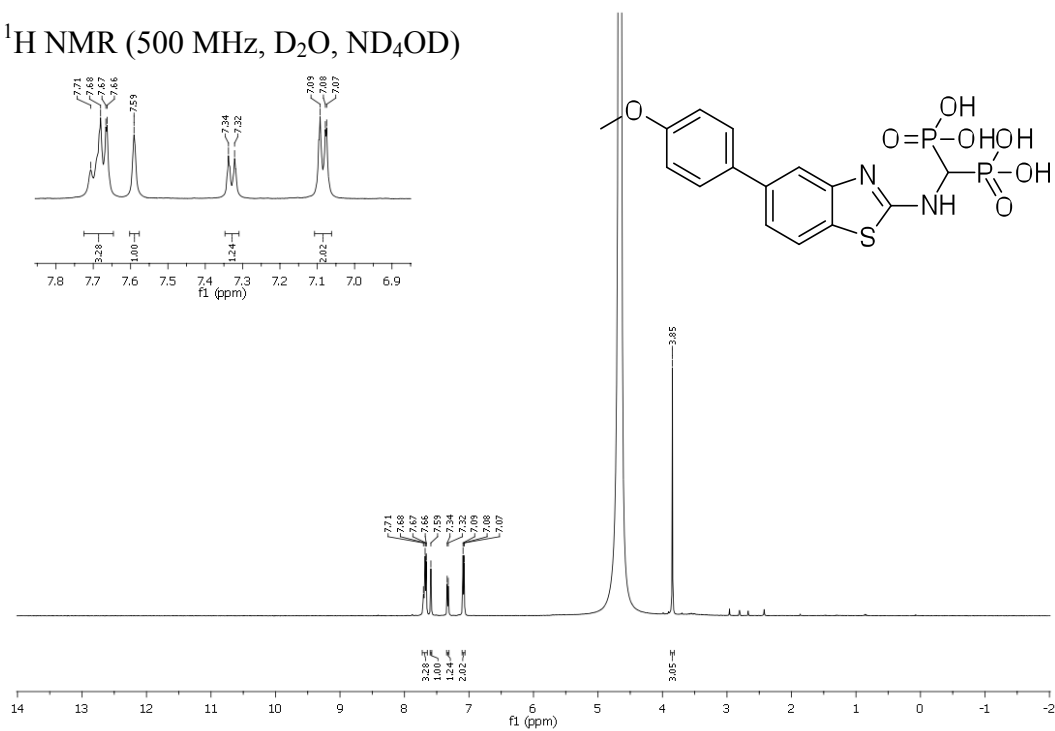


^{13}C NMR (125 MHz, D_2O , ND_4OD)



NMR Spectra of compound 40c

¹H NMR (500 MHz, D₂O, ND₄OD)



¹³C NMR (125 MHz, D₂O, ND₄OD)

